

UNIVERSITY OF CALGARY

Use of CO₂ in Vapex, Experimental and Modeling Study

by

Amin Badamchi Zadeh

A THESIS

SUBMITTED TO THE FACULTY OF GRADUATE STUDIES
IN PARTIAL FULFILMENT OF THE REQUIREMENTS FOR THE
DEGREE OF DOCTOR OF PHILOSOPHY

DEPARTMENT OF CHEMICAL AND PETROLEUM ENGINEERING

CALGARY, ALBERTA

FEBRUARY, 2013

© AMIN BADAMCHI ZADEH 2013

UNIVERSITY OF CALGARY
FACULTY OF GRADUATE STUDIES

The undersigned certify that they have read, and recommend to the Faculty of Graduate Studies for acceptance, a thesis entitled "Use of CO₂ in Vapex, Experimental and Modelling Study" submitted by AMIN BADAMCHI ZADEH in partial fulfilment of the requirements of the degree of DOCTOR OF PHILOSOPHY.



*Supervisor, Dr. Brij Maini
Department of Chemical and Petroleum Engineering*



*Co-Supervisor, Dr. Harvey W. Yarranton
Department of Chemical and Petroleum Engineering*



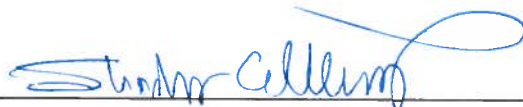
*Supervisory Committee, Dr. Anil Kumar Mehrotra
Department of Chemical and Petroleum Engineering*



*Dr. Pedro R. Pereira Almas
Department of Chemical and Petroleum Engineering*



*"Internal" External, Dr. Stephen R. Larter
Department of Geology and Geophysics*



External Examiner, Dr. Shawket Ghedan

27/11/2012

Date

Abstract

Employing CO₂ as the non-condensable gas in the Vapex process is an attractive option. The high solubility and viscosity reduction potential of CO₂ could provide improvement to Vapex performance. Mixtures of CO₂ and a hydrocarbon such as propane allow the solvent to be tailored to different reservoir conditions. To select the optimum solvent mixtures, data on the phase behavior and physical properties of the oil-solvent system are required.

The saturation pressure and solubility of propane in Athabasca bitumen as well as the liquid phase densities and viscosities, were measured at temperatures from 10 to 50°C.

The solubility of pure carbon dioxide in Athabasca bitumen was measured and compared with the literature data. Two liquid phases were observed at carbon dioxide contents above approximately 12 wt%. A correlation based on Henry's law was found to fit the saturation pressures at carbon dioxide contents below 12 wt%.

The saturation pressure and solubility of carbon dioxide and propane in Athabasca bitumen, as well as the liquid phase densities and viscosities, were measured for three ternary mixtures at temperatures from 10 to 25°C. Two liquid phases (carbon dioxide rich and bitumen rich) were observed at 13 wt% carbon dioxide and 19 wt% propane. Only liquid and vapour-liquid regions were observed for the other two mixtures: 13.5 wt% propane and 11.0 wt% carbon dioxide; 24.0 wt% propane and 6.2 wt% carbon dioxide.

Vapex physical model experiments were conducted using a fixed composition of the CO₂ and propane binary mixture as the solvent. The objective of this work was to evaluate the performance of this solvent in recovering Athabasca bitumen. In-line measurements of the density and viscosity of the produced oil were used to gain further insight into the mechanisms involved in the process.

An improved mathematical model was developed to predict the oil recovery performance of Vapex process. The compositional dependence of diffusion coefficient causes a strong non-linearity in the moving boundary diffusion equation of the Vapex mathematical model. Pseudo-concentration and pseudo-time terms were defined to resolve this non-linearity. The concentration profile ahead of solvent-bitumen interface was obtained analytically using the HIM “Heat Integral Method”. This results in a new correlation for the “average flow fraction of the heavy oil” in the flowing mixture, and drainage rate of heavy oil.

The new correlation for drainage rate of heavy oil has the same square-root relationship to most of the key reservoir parameters as the previous theories except that its relationship to kinematic viscosity is altered by the concentration dependence of the diffusion coefficient. The new mathematical model was tested against our Vapex experimental results at a pseudo steady state condition to back calculate the solvent apparent mass diffusion coefficient at the vapor chamber interface and its power law functionality to solvent concentration.

Acknowledgements

I would like to take this opportunity to express my gratitude, regards and sincere thanks to my supervisors, Dr. Brij Maini and Dr. Harvey Yarranton for their continuous guidance and support throughout my study at the University of Calgary. It has been a great pleasure and privilege to work under their supervision toward completion of this research.

I am very appreciative to Dr. Mehrotra and Dr. Svrcek for sharing their experience and expertise regarding to the solubility and property measurement of the solvent-bitumen system. Also I am very thankful to Dr. Marco Satyro for his technical inputs, helpful discussions, and great suggestions regarding the phase behaviour modeling.

I also wish to thank my colleagues in the Improved Heavy Oil Science and Technology (IHOST) and Asphaltene & Emulsion Research (AER). The technical support from Paul Stanislav during Vapex experiments and from Elaine Baydak, Florian Schoeggl and Dr. Kamran Akbarzadeh during PVT experiments and property measurements is highly acknowledged.

The phase behaviour software license from Computer Modeling Group (CMG) and Virtual Material Group (VMG) is highly appreciated. Financial support provided by AERI, Department of Chemical & Petroleum Engineering, and National Iranian Oil Company (NIOC) is greatly acknowledged.

Finally, I would like to appreciate my wonderful family for their understanding and patient and great emotional support throughout of this long study.

Dedication

To

My family,

My Mother,

And memory of my late Father.

Table of Contents

Approval Page.....	ii
Abstract.....	iii
Acknowledgements.....	v
Dedication.....	vii
Table of Contents.....	viii
List of Tables.....	xi
List of Figures and Illustrations.....	xiii
List of Symbols, Abbreviations and Nomenclature.....	xviii
CHAPTER 1 : INTRODUCTION.....	1
1.1 Heavy Oil Resources.....	1
1.2 Vapex Process.....	2
1.3 Research Objectives.....	4
1.4. Thesis Outline.....	6
CHAPTER 2 : LITERATURE REVIEW.....	8
2.1 Phase Behaviour of Bitumen and Solvent.....	12
2.2 Vapor Solvent for Bitumen Extraction.....	21
2.3 Viscosity of Heavy Oil and Solvent.....	22
2.4 Solvent Mass Diffusion Coefficient in Heavy oil.....	29
2.5 Gravity and Capillary Forces Interplay in Vapex.....	30
2.6 Vapex Process Mathematical Model.....	35
CHAPTER 3 : EXPERIMENTAL METHODS FOR PHASE BEHAVIOR AND PHYSICAL PROPERTIES.....	42
3.1 Materials.....	42
3.2 SARA Analysis.....	43
3.2.1. Extraction and Purification of Asphaltenes.....	44
3.2.2. Fractionation of Maltenes.....	45
Clay and Gel Activation.....	45
Chromatographic Procedure.....	46
Solvent Removal.....	48
3.3 High Temperature Gas Chromatography (HTSD) - Simulated Distillation (SimDist).....	51
3.4. Molecular Weight Measurements.....	53
3.4.1. Description and Operation of the Vapor Pressure Osmometer (VPO).....	54
3.5. Density Measurement.....	60
3.5.1. SARA Fraction Densities.....	60
3.5.2. Athabasca Bitumen Density Measurement at Elevated Pressure and Temperature.....	61
3.6. Athabasca Bitumen Viscosity Measurement.....	63
3.7. Phase Behavior Measurements.....	65

The phase behaviour measurements are described for mixtures of bitumen and propane. Variations in the procedure for bitumen/carbon dioxide and bitumen/propane/carbon dioxide mixtures are described afterwards.	65
3.7.1 Apparatus.....	65
3.7.2 Methodology for Mixtures of Propane and Bitumen	67
3.7.3 Methodology for Mixtures of Bitumen, Carbon Dioxide, and Propane	73
3.7.3.1. Solubility in Vapor-Liquid Region:	73
3.7.3.2. Phase Boundaries:	75
3.7.4. Carbon dioxide, Propane, and Bitumen.....	80
Cases 1 and 2	80
Case 382	
CHAPTER 4 : PROPERTIES AND PHASE BEHAVIOR OF MIXTURES OF BITUMEN, PROPANE, AND CARBON DIOXIDE	84
4.1. Bitumen Properties	84
4.1.1 Characterization.....	84
4.1.2 Density Data and Fitting.....	86
4.1.3 Viscosity Data and Fitting	89
4.2 Mixtures of Athabasca Bitumen and Propane	91
4.2.1. Saturation Pressure Correlation	94
4.2.2. Density and Viscosity Modeling	97
4.3 Mixtures of Athabasca Bitumen and Carbon Dioxide.....	102
4.3.1. Saturation Pressure Correlation	103
4.4. Mixtures of Bitumen, Propane, and Carbon Dioxide	108
4.4.1 Cases 1 and 2	109
4.4.2 Case 3	114
4.5 SUMMARY.....	116
CHAPTER 5 : EQUATION OF STATE MODELING.....	119
5.1. Peng - Robinson Equation of State	119
5.2. Athabasca Bitumen Characterization.....	122
5.3. Model Tuning for Mixtures of Athabasca Bitumen and Propane.....	126
5.3.1 Saturation Pressure	126
5.3.2 Density.....	128
5.3.3 Viscosity	129
5.4. Model Tuning for Mixtures of Athabasca Bitumen and Carbon Dioxide	133
5.6. Model Predictions for Athabasca bitumen/Carbon Dioxide/Propane Pseudo-Ternary Mixtures	135
5.6.1 Saturation Pressure	135
5.6.1.1 Propane and Carbon Dioxide Binary System.....	135
5.6.1.2 Bitumen, Propane, and Carbon Dioxide Pseudo-Ternary	136
5.6.2 Density.....	138
5.6.3 Viscosity	140
7. Summary	141
CHAPTER 6 : VAPEX PHYSICAL MODEL AND EXPERIMENTAL METHODS ..	142
6.1 Apparatus	142

6.2. Experimental Procedure.....	146
6.2.1. Solvent Preparation	146
6.2.2. Physical Model Preparation.....	147
6.2.3. Vapex Test.....	150
CHAPTER 7 : MATHEMATICAL MODEL OF THE VAPEX PROCESS.....	156
7.1 Introduction.....	156
7.2 Model Assumptions	157
7.3 Diffusion Model.....	159
7.3.1 Application of Fick’s Law	159
7.3.2 Linearization of Equation 7-6.....	164
7.3.3 Heat-Integral-Method (HIM) Solution of Convective-Diffusive P.D.E.	168
7.4. Fluid Flow and Movement of Interface	172
7.4.1 Fluid Flow Equation	172
7.4.2 Movement of the Interface	174
7.4.3 Dimensionless Flow and Interface Movement	177
7.4.4. Bitumen Flow Rate Equation	180
7.5. Model Solutions.....	183
7.5.1. Pseudo Steady State Condition.....	183
7.5.2. Transient Solution Procedure	186
CHAPTER 8 : RESULTS OF VAPEX EXPERIMENTS	189
8.1 Experimental Results	190
8.4 Phase Behaviour and Compositional Path	204
8.5 Solvent Mass Diffusion Coefficient	207
CHAPTER 9 : CONCLUSION AND RECOMMENDATION	214
9.1 Summary and Conclusions	214
9.2 Observation.....	217
9.3 Recommendations.....	218
REFERENCES	219

List of Tables

Table 2-1: Proved in situ reserves of bitumen in Alberta. (Berkawitz et al., 1975)	8
Table 2-2. Pseudo components of Athabasca bitumen. (after Bishnoi et. al. 1977).....	17
Table 2-3. Critical properties of Athabasca bitumen pseudo components using Kesler-Lee correlation, and binary interaction with carbon dioxide used by Sarkar and Mehrotra (1985).	18
Table 3-1: Comparison of composition measurements.	70
Table 3-2: Vapor pressure of pure propane compared with correlation values.....	72
Table 3-3: Saturation condition of carbon dioxide in Athabasca bitumen at 24.9°C.	75
Table 3-4: Phase regimes for 18wt% carbon dioxide in Athabasca bitumen.	79
Table 3-5: Composition of ternary mixtures of propane (C3), carbon dioxide (CO2), in Athabasca bitumen.....	83
Table 4-1. Properties and SARA Assay of Athabasca Bitumen at 22°C and 90 kPa.	85
Table 4-2. Athabasca Bitumen's SARA fractions Density (kg/m^3) compared to Literature.....	87
Table 4-3. Athabasca Bitumen Density.	88
Table 4-4: Effect of temperature on viscosity of Athabasca bitumen.	89
Table 4-5: Saturation pressure and liquid phase density (from cell volume) of mixtures of propane and Athabasca bitumen.....	91
Table 4-6: Viscosity and density of liquid mixtures of propane and Athabasca bitumen.	93
Table 4-7: Saturation condition of carbon dioxide in Athabasca bitumen at 24.9°C.	103
Table 4-8: Saturation conditions for two ternary mixture of propane, carbon dioxide, Athabasca bitumen.....	111
Table 4-9: Liquid phase density and viscosity for 13.5 wt% propane, 11.0 wt% carbon dioxide, 85.5 wt% Athabasca bitumen ternary mixture.....	112
Table 4-10: Liquid phase density and viscosity for 24.0 wt% propane, 6.2 wt% carbon dioxide, 69.8 wt% Athabasca bitumen ternary mixture.....	112

Table 4-11: Phase boundaries for 13.1 wt% propane, 19.2 wt% carbon dioxide, and 67.7 wt% Athabasca bitumen.....	116
Table 4-12: Propane, and carbon dioxide weight fraction in the vapour and liquid phases, for case 3 at 20°C, and 3950 kPa.	116
Table 5-1: Properties and composition of pseudo-components used to characterize Athabasca bitumen.....	125
Table 5-2: The final volume shift value obtained to match experimental density data for Propane and bitumen system.	128
Table 5-3. Propane Bitumen Experimental Viscosity and Regression Errors.	130
Table 7-1: Summary of the Vapex mathematical modeling equations.....	187
Table 8-2: Solvent composition, packed model properties, and Vapex test condition...	190
Table 8-3. Steady State Period of Vapex Experiments data.	209
Table 8-4. Solvent mass diffusion exponent d) calculated by Equation 7-79.	211
Table 8-5. Physical Model Properties in SI Units.....	211
Table 8-6. Solvent apparent mass diffusion coefficient at interface and N_{Ra}	212

List of Figures and Illustrations

Figure 1-1. Petroleum liquid classification based on viscosity and density.	1
Figure 1-2. Heavy Oil in-place and reserves world wide. (www.Total.com).....	2
Figure 1-3. Schematic of Vapex Process	4
Figure 2-1: Schematic of SAGD process. (after Duke du Plessis, 2004)	10
Figure 2-2: Mechanism involved in the Vapex process. (after Upreti et al., 2007).....	12
Figure 2-3: Effect of carbon dioxide, methane, and nitrogen solubility on Athabasca bitumen. (after Svrcek and Mehrotra 1982).....	15
Figure 2-4: Carbon Dioxide and Cold Lake Bitumen solubility and viscosity at 26°C, after Mehrotra et al. 1988.....	17
Figure 2-5: Carbon Dioxide solubility in Athabasca bitumen calculated by PR-EoS. (Mehrotra et al. 1985)	18
Figure 2-7: Two deriving mechanism in the compositional gravity drainage.(after DiCarlo et. al., 2007).....	32
Figure 2-8: Comparison of compositional drainage experimental saturation with simulation results. (Cuthiell et. al., 2006).....	33
Figure 3-1. Clay-Gel Adsorption Columns.....	47
Figure 3-2. Extraction Apparatus for Aromatics.	49
Figure 3-3. SARA fractions of the Athabasca bitumen.	50
Figure 3-4. Athabasca Maltene True Boiling Point Distribution curve from Sim.Dist. ASTM D2887 extended analysis.	53
Figure 3-5. Schematic of Vapor Pressure Osmometer (VPO).....	55
Figure 3-6. VPO calibration curve with sucrose octaacetate in toluene at 50°C.....	58
Figure 3-7. VPO molecular weight measurement for Athabasca maltenes in toluene at 50°C.	59
Figure 3-8. VPO molecular measurement for Athabasca bitumen in toluene at 50°C.	60
Figure 3-9. Anton Paar DMA 512P external cell density calibration result for water.	62
Figure 3-10. Anton Paar , DMA 512P external cell Density result for nitrogen.	62

Figure 3-12. Schematic of PVT cell, and experimental setup.	67
Figure 3-13: Continuous and step-wise pressure volume isotherms for 5.2 wt% propane in Athabasca bitumen at 60°C.....	71
Figure 3-14: LLV – VL phase boundaries at 20°C for 18wt% CO2 blend in Athabasca bitumen.....	77
Figure 3-15: Second liquid phase formation at 20°C and high pressure with 18wt% CO2 in bitumen.....	78
Figure 4-1: Athabasca maltene SimDist data and Athabasca bitumen true boiling point curve calculated from maltene data.	86
Figure 4-2. Effect of temperature and pressure on the density of Athabasca bitumen. The lines are the correlation, Equation 4-1.	88
Figure 4-3: Effect of temperature on the viscosity of Athabasca bitumen. The line is correlation, Equation 4-3.	90
Figure 4-4: Saturation pressure of propane in Athabasca bitumen (solid symbols - step-wise method; open symbols - continuous method).	95
Figure 4-5: Solubility of propane in Athabasca bitumen (solid symbols - step-wise method; open symbols - continuous method).	96
Figure 4-6: Effect of temperature on the density of mixtures of propane and Athabasca bitumen.....	99
Figure 4-7: Effect of temperature on viscosity of mixtures of propane and Athabasca bitumen.	101
Figure 4-8: Solid line is Athabasca bitumen propane saturated liquid mixture viscosity by the Shu (1984) viscosity correlation with empirical parameter from Equation 4-8.....	102
Figure 4-9: Saturation condition of carbon dioxide in several different crude oils (data from Simon 1965, and Quail 1988; lines are Equation 4-10).....	105
Figure 4-10: Saturation condition of carbon dioxide in Athabasca bitumen (solid symbols - Svrcek and Mehrotra 1982; open symbols - present work; lines are Equation 4-10).	106
Figure 4-11: Phase diagram of 18wt% carbon dioxide in Athabasca bitumen.....	107
Figure 4-12: Predicted versus measured solubility of carbon dioxide in Athabasca bitumen (Data from table 3-4 and prediction by Equation 4-10).....	108

Figure 4-13: Vapor liquid phase boundaries for two ternary mixtures of carbon dioxide, propane, and Athabasca bitumen (solid lines are predicted pressures).....	113
Figure 4-14: Liquid phase viscosity of two ternary mixture of propane, carbon dioxide, and Athabasca bitumen. Solid line are prediction by Lobe correlation. ...	114
Figure 4-15: Phase boundaries for 13.1 wt% propane, and 19.2 wt% carbon dioxide balanced with Athabasca bitumen in ternary mixture Case 3.	115
Figure 5-1: Athabasca Bitumen TBP curve, and VMGSim Extended TBP curve.	124
Figure 5-3: Measured (symbols) and modeled (lines) saturation pressures of mixtures of propane and Athabasca bitumen.	127
Figure 5-4: Measured (symbols) and modeled (lines) saturation liquid density of mixtures of propane and Athabasca bitumen (volume shifts from Table 5-2).	129
Figure 5-5: Modified Pedersen (1987) predicted viscosity for Athabasca bitumen and propane binary mixtures. Dashed lines are result before regression. Solid lines are prediction after adjusting b1-b5 coefficients by regression calculation in WinProp.	131
Figure 5-6: Comparison of viscosity models for Athabasca bitumen and propane saturated liquid mixtures.	132
Figure 5-7: Saturation pressures of Athabasca bitumen and carbon dioxide pseudo-binary mixtures. Solid symbols are from Svrcek and Mehrotra (1982); open symbols are from this work; dashed lines are EoS model; solid lines are from Henry's law correlation.	134
Figure 5-8: Measured (symbols) and modeled (lines) P-X two phase envelope for propane and carbon dioxide. Data from Reamer (1951). Model is PR EoS with $k_{ij} = 0.1315$	136
Figure 5-9: Measured (symbols), predicted (dashed lines, $k_{ij} = 0.135$), and tuned (solid lines, $k_{ij} = 0.2779$) saturation pressures for pseudo-ternaries Case 1 and Case 2 from table 3-5.	138
Figure 5-10: Measured (symbols) and predicted (lines) densities of the pseudo-ternaries, Case 1 and Case 2.	139
Figure 5-11: Measured (symbols) and predicted (Pederson lines, Lobe mixing rule dash line) viscosity for pseudo-ternaries, Case 1 and Case 2.	140
Figure 6-1: Simplified process flow diagram of the Vapex experimental apparatus.	143
Figure 6-2: Photograph of Vapex physical model (a, model components. b, partially assembled physical model top view).	143

Figure 6-3. Vapex Experimental Setup. (1- Isco Pump, 2 - Liquid solvent vessel, 3 - Vapor solvent vessel, 4 – Mass Flow meter, 5 – Injection well, 6 – Vapex physical model, 7 – Production well, 8 – High pressure separator, 9 – Free gas volume meter, 10 – Solution gas volume meter, 11 – Density meter, 12 – Viscosity meter, 13 – Water bath, 14 – Agilent GC.).....	144
Figure 6-4: Packing the Vapex physical model with 12-16 U.S. mesh glass bead.....	149
Figure 6-5: Discharging produced live oil through property measurement unit.	154
Figure 7-1: Vertical cross section of the Vapex process showing details at the interface of the heavy oil and solvent.	158
Figure 7-2: Normalized diffusion coefficient profile versus normalized concentration at different values of the power d.....	161
Figure 7-3: Athabasca bitumen – propane kinematic viscosity calculated by tuned PR EoS model in WinProp at 20°C, and fitted to Equation 7-11.	163
Figure 7-4: Relationship between interface position related and total bitumen produced.....	176
Figure 7-5: Material balance around a unit width element inside the penetration depth.	178
Figure 8-1: The cumulative injection and production data obtained from Run #1.....	192
Figure 8-2: The cumulative production and injection data obtained from Run #3.....	193
Figure 8-3: The cumulative injection and production data obtained from Run #4.....	194
Figure 8-4: Disassembling of the physical model at the end of the Vapex test #1.....	195
Figure 8-5: Comparing the dead oil flow rate of four Vapex tests.	196
Figure 8-6: Viscosity of the produced live oil sample during the Vapex test 1, 2, 3, and 4.....	198
Figure 8-7: Solvent volume fraction in the produced live oil during the several Vapex experiments.	199
Figure 8-8: Kinematic viscosity of the produced live oil samples during the Vapex experiments.	200
Figure 8-9: Composition of the solution gas during the Vapex experiments.	201
Figure 8-10: Vapor chamber composition during Vapex experiment 1,2, and 3.	202
Figure 8-11: comparing the cumulative bitumen production by different solvent composition.....	203

Figure 8-12: Compositional change during the Vapex experiment #1.	206
Figure 8-13: Compositional change during the Vapex experiment #3.	207
Figure 8-14. Athabasca bitumen – Binary solvent (carbon dioxide and propane) kinematic viscosity calculated by tuned PR EoS model in WinProp at Exp.1 T & P, and fitted to Equation 7-11.	209
Figure 8-15. Athabasca bitumen – Binary solvent (carbon dioxide and propane) kinematic viscosity calculated by tuned PR EoS model in WinProp at Exp. #4 T & P, and fitted to Equation 7-11.	210

List of Symbols, Abbreviations and Nomenclature

Symbol	Definition
A	Van Laar activity coefficient correlation constant.
a	Cubic EoS attractive term.
B	Van Laar activity coefficient correlation constant.
b	Co-volume,
C	Solvent concentration (volume fraction).
C_D	Dimensionless solvent volume fraction
C_{PD}	Pseudo concentration, dimension less.
D	Mass diffusion coefficient, L^2t^{-1}
d	Mass diffusion power, Equation 2-32
D_s	Mass diffusion coefficient at Vapex interface, L^2t^{-1}
f_b	Bitumen volume fraction in produced oil
g	Gravitational acceleration, Lt^{-2}
H	Height, L
H_{CO_2}	Carbon dioxide Henry coefficient, $ML^{-1}t^{-1}$
I(t)	Arbitrer Vapex interface location function.
K	Permeability, L^2
K_0	VPO constant
K_{ij}	Binary interaction coefficient.
m	Kinematic viscosity power, Equation 2-22
Mapp	Apparent molecular weight.
n	HIM-Polynomial function degree
N_B^{-1}	Reverse Bond number
N_{Pe}	Peclet number
N_{Ra}	Rayleigh number
N_s	Vapex dimensionless number, Equation 2-27
P_1	Solvent partial pressure, $ML^{-1}t^{-1}$
P_1^{sat}	Pure Solvent vapor pressure, $ML^{-1}t^{-1}$
Pc	Critical pressure, $ML^{-1}t^{-1}$
q	Vapex Oil Production rate per unite well-length, L^2t^{-1}
Q	Dimensionless oil rate
R	Universal gas constant.
r_i	Volume-shift value for component i,
r_t	Characteristic throat radius, L
T	Absolute temperature, T.
T_c	Critical temperature, T
t_p	Pseudo time, t^{-1}
t_{PD}	Dimension less pseudo time.
Tr	Reduced temperature.
U	Velocity of Interface, Lt^{-1}
V_{ci}	Critical volume of component i. L^3M^{-1}
w_i	Weight fraction of component i.
x	Compositional parameter, Equations 2-7 and 2-8

x_1	Solvent mole fraction.
X_D	Dimensionless horizontal distance.
Z_D	Dimensionless height.

Abbreviations	Definition
AAD	Average absolute deviation from MAE.
BC	Boundary condition
BPR	Back pressure regulator
CGE	Capillary gravity equilibrium
GC	Gas chromatography
HIM	Heat integral method
IC	Initial condition
MAE	Mean absolute error.
ODE	Ordinary differential equation
PDE	Partial differential equation
SARA	Saturate, Aromatic, Resin, and asphaltene.
SimDist	Simulated Distillation
VLE	Vapor-liquid equilibrium.
VLLE	Vapor-liquid-liquid-equilibrium.

Greek Symbols	Definition
ΔH_{vap}	Enthalpy of vaporization per unit mole, L^2t^{-1}
ΔV	Voltage change in VPO
$\Delta \rho$	Density difference, ML^{-3}
Γ	Dimensionless distance along Vapex interface.
λ	Viscosity correlation variable, Shu Equation and Pederson Equation.
$\alpha_{A(B)}$	Lobe viscosity mixing rule parameter.
δ	Penetration depth, L.
ε	Distance vertical from Vapex interface, L.
ε^*_D	Dimensionless distance vertical to Vapex interface.
η	Distance along Vapex interface, L.
φ	Porosity.
$\varphi_{A(B)}$	Volume fraction of component A(B) in Lobe correlation.
μ	Dynamic viscosity, $ML^{-1}t^{-1}$
θ	Vapex interface slope at each vertical location.
σ	Interfacial tension, $ML^{-2}t^{-2}$
ν	Kinematic viscosity, L^2t^{-1}
ω	Acentric factor.
γ_{C3}	Propane activity coefficient.
δ_D	Dimension less penetration depth.

CHAPTER 1 : INTRODUCTION

1.1 Heavy Oil Resources

Petroleum liquids are typically classified according to their viscosity and density (Ali and Thomas, 2000), Figure 1-1. Heavy oil is defined as having an API between 22.3 to 10° and a viscosity between 100 and 100000 mPa.s. Denser more viscous petroleum fluids are defined as bitumen. In situ heavy oil and oil sands are important energy resources, and can supply a significant energy demand of North America (Luhning, 2003). Approximately 36% of the world's heavy oil resources (~36%) are in Canada (www.Total.com), Figure 1-2. The primary oil recovery factors from tar-sand reserves are less than 5% due to the very high viscosity of the oil and often an enhanced oil recovery method is needed, even in the primary stage of production to increase oil mobility.

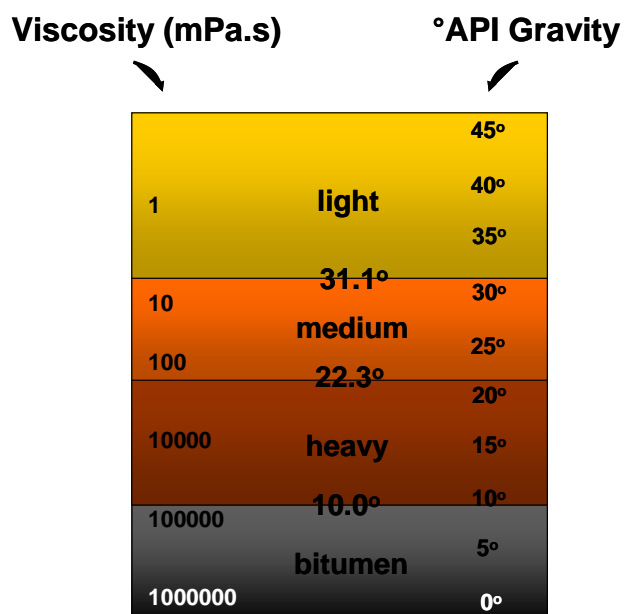


Figure 1-1. Petroleum liquid classification based on viscosity and density.

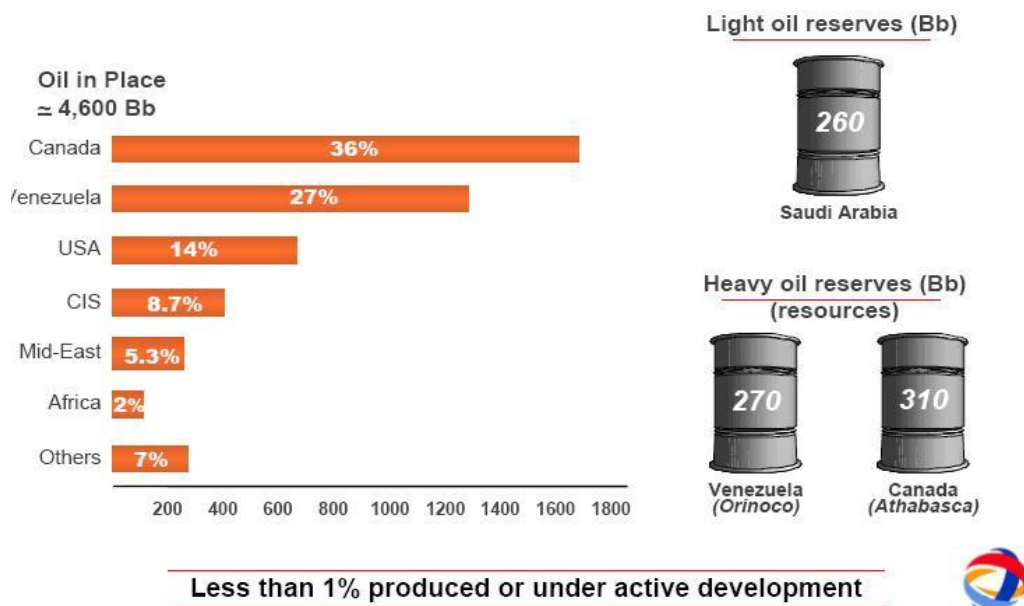


Figure 1-2. Heavy Oil in-place and reserves world wide. (www.Total.com)

1.2 Vapex Process

Solvent extraction is among several methods proposed for heavy oil and bitumen recovery and has received considerable attention in the last two decades (Butler and Mokrys, 1989; Dunn et al., 1989; Das, 1995; Jiang, 1997; Frauenfeld et al. 1998; Boustani, 2001; Chatzis, 2002; Karmaker, 2003; Talbi, 2005; Yazdani, 2007; Haidari, 2008). The Vapex process usually involves two horizontal wells, with an injection well located directly above the production well. The vaporized solvents are injected through the injection well and form a chamber of solvent vapour around the well, Figure 1-3. At the walls of the chamber, the solvent dissolves into a surface layer of the heavy oil and dramatically reduces its viscosity. The diluted oil layer is then mobile enough to drain down under the influence of gravity into the production well located near the bottom of

the formation. It is then pumped out to the surface and the vapour chamber grows laterally as more oil is drained out of the reservoir.

To date, most work on this process has focused on using light alkanes as the solvent. The most frequently considered solvents are mixtures of methane and propane (Jiang 1997). The economic viability of the process depends on maintaining a low solvent to oil ratio and is sensitive to the cost of natural gas and propane relative to the selling price of the produced oil.

However, Vapex may work even better when mixtures of CO₂ and propane are employed (Talbi, 2005). Currently, CO₂ is expensive but with environmental incentives to capture and sequester CO₂, costs are expected to drop. CO₂ is considered a better Vapex carrier gas than methane because it is more soluble in heavy oil and reduces the oil viscosity more (Svrcek and Mehrotra 1982). On the other hand, at typical heavy oil reservoir conditions (pressures of approximately 3.5MPa and temperatures of approximately 20 °C), the solubility and viscosity reduction by light alkanes, such as propane and butane, is much higher than with CO₂. Mixtures of CO₂ and a light alkane can achieve the desired reduction in viscosity while minimizing the required alkane volumes. Hence there is an incentive to evaluate mixtures of CO₂ and propane as a Vapex solvent.

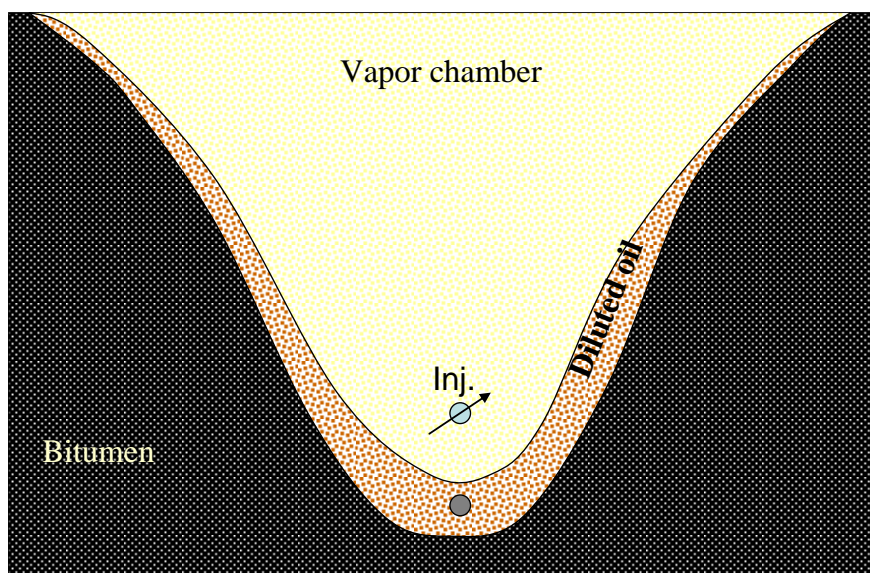


Figure 1-3. Schematic of Vapex Process

1.3 Research Objectives

The phase behaviour of CO₂-propane-bitumen mixtures can be more complex than that of methane-propane-bitumen mixtures. There is a greater possibility of more than one liquid phase being formed, which may cause adverse three-phase relative permeability effects. Formation of two liquid phases in CO₂-oil mixtures has been observed at high pressure and high mole fractions of CO₂ (Khan et al., 1992). Although the pressure in Vapex applications is usually much lower than that at which three phases were observed in the Khan et. al. study, the possibility of two liquid phases in the CO₂-propane-bitumen system at Vapex conditions cannot be ruled out *a priori*. Experimental data on the phase behavior are needed to determine the operating conditions that will avoid the formation of two liquid phases. Once the operating conditions are determined, it is also necessary to evaluate the performance of the CO₂/propane solvent mixture in physical model

experiments to determine if sufficient viscosity reduction and improved oil recovery rates occur in-situ.

Also, during the Vapex process, the bitumen viscosity is reduced substantially as more solvent transfers into it. According to the Stokes-Einstein equation, the mass diffusion coefficient in liquid phase is inversely proportional to the liquid viscosity. Therefore, the relationship between solvent mass diffusion and the solvent concentration in the diluted bitumen should be accounted for in the mathematical modelling of the Vapex process.

The objectives of this study are then to:

1. Develop a methodology to measure the gas solubility and liquid phase density and viscosity of propane and Athabasca bitumen mixtures and mixtures of propane, carbon dioxide and Athabasca bitumen using a conventional PVT cell at typical Canadian heavy oil reservoir temperatures of 10 to 50°C.
2. Develop analytical correlations to fit the measured phase behavior data.
3. Develop an equation of state (EoS) model to match the experimental PVT data.
4. Conduct a Vapex physical model experiment with CO₂-propane binary solvent blends at room temperature.
5. Develop an improved mathematical model including the effect of composition dependent mass diffusion on the oil production rate in the Vapex process.

1.4. Thesis Outline

This study is presented in nine chapters. The first chapter is an introduction to the Vapex process and statement of the problem. The second chapter provides an extensive literature review on the phase behaviour and experimental data for the bitumen, propane-heavy oil and non-condensable gas (e.g. methane, nitrogen, and CO₂) – heavy oil systems and equation of state modeling. It also includes a review of the Vapex process and solvent diffusion issues in this process.

Chapter 3 provides a detailed description of the experimental methodology and property measurement techniques for phase behaviour and physical properties of the Athabasca bitumen, binary mixtures of propane – bitumen, carbon dioxide – bitumen, and ternary mixture of carbon dioxide – propane – bitumen. The experimental data obtained in Chapter 3 are correlated and evaluated in Chapter 4. The bitumen characterization and equation of state modeling of experimental data from Chapter 3 are described in Chapter 5.

Chapter 6 describes the Vapex process physical experimental set up. It is an improved design where in-line measurements of the produced live oil density, viscosity and solvent volume fraction and composition in live oil and vapour chamber were measured during the experiments. Chapter 7 presents an improved mathematical model of the Vapex process where the compositional dependency of solvent mass diffusion and its effect in the Vapex process oil production rate are accounted for.

The Vapex experimental results are presented and discussed in Chapter 8. Finally, the conclusions of this study and recommendations for the future work are summarized in Chapter 9.

CHAPTER 2 : LITERATURE REVIEW

There are almost 143 billion m³ of bitumen (oilsands) reserves in Canada, mainly located in Alberta (Berkowitz et al., 1975). Table 1-1 shows that only very small fraction of these bitumen reserves are shallow enough to be recovered by surface mining. Almost 90% of bitumen reserves are in deep formation of Athabasca, Cold Lake, Peace River, and Wabasca fields.

The bitumen viscosity at reservoir condition varies widely but it is generally above 1000 Pa.s. Jacobs et al. (1980) reported huge viscosity reduction of Athabasca bitumen by increasing the temperature and by dissolving carbon dioxide at high pressure. Therefore, bitumen can be mobilized by both heating and dilution with a solvent.

Table 2-1: Proved in situ reserves of bitumen in Alberta. (Berkowitz et al., 1975)

	Depth Interval	Areal	In place Bitumen	
	m	10 ⁷ m ²	10 ⁹ bbl	10 ⁹ m ³
Athabasca	0-46	198	74.0	11.8
	46-610	2129	551.9	88
Cold Lake	305-610	1279	164.1	26.2
Peace River	305-762	478	50.4	8.0
Wabasca	76-762	714	53.8	8.5
		4798	894.2	142.5

Apart from cold production, bitumen recovery processes are generally classified as three types: thermal, non-thermal solvent dilution, and hybrid processes. The mobilized bitumen in any process cannot displace cold or undiluted high viscosity bitumen in the reservoir. However, it can drain to the bottom of the reservoir by natural gravity force,

provided it does not have to displace immobile bitumen in the process. Such gravity drainage also requires that sufficient density difference be present between the mobilized bitumen that is draining down and the fluid phase that is replacing it in the pore space. A vapor phase heat carrier (e.g. steam) or vaporized diluents can provide sufficient density difference to induce the gravity drainage of mobilized bitumen to a production well located at the bottom of the reservoir. The following is a list of recovery processes for bitumen:

- Thermal Process
 - Steam Assisted Gravity Drainage (SAGD)
 - Cyclic Steam Stimulation (CSS)
 - In situ Combustion, Toe to Heal Air Injection (THAI)
 - Electrical Heating
- Non –Thermal Solvent injection
 - Vapor Extraction (VAPEX)
- Hybrid Process
 - Expandable Solvent – Steam Assisted Gravity Drainage (ES-SAGD)
 - Solvent Aided Process (SAP)
 - Hot Solvent (n-Solve) Process

Figure 2-1 shows a schematic diagram of the SAGD process. Currently SAGD and CSS are the only commercially proven recovery processes (EUB 1998). In the SAGD process steam is injected into a horizontal well. The injected steam rises and contacts the bitumen. It condenses at steam–bitumen interface and heats up the bitumen and thereby

reduces its viscosity. The hot bitumen and condensed steam then drain down to the bottom producer well and are pumped to the surface. It is an energy intensive process and requires natural gas for steam generation. Also, the large water requirement and treatment of water for steam generation are issues with this process. The process typically requires three barrels of water converted to steam for each barrel of produced bitumen.

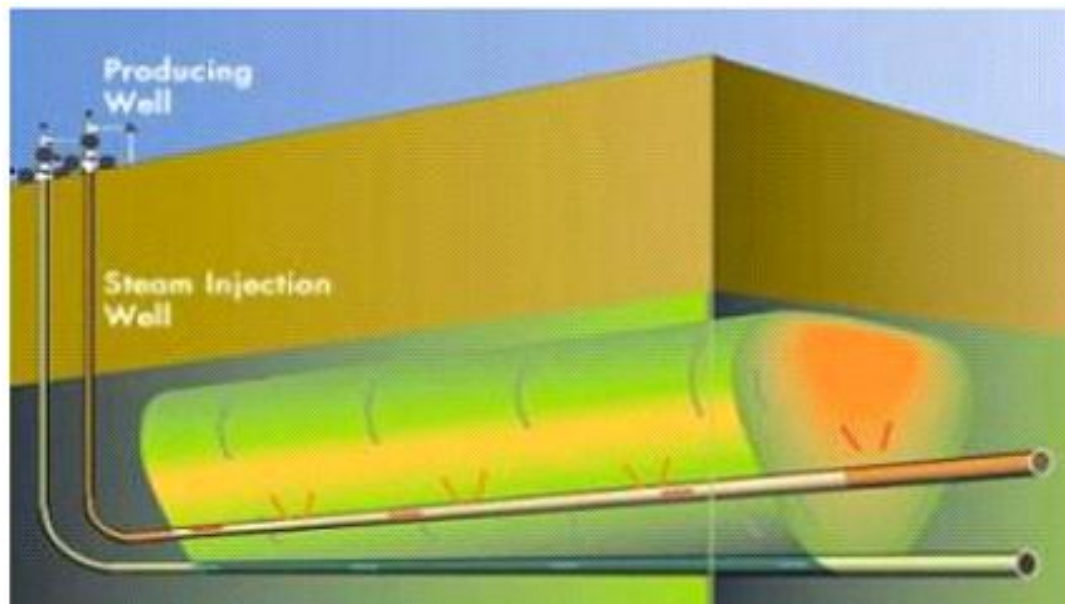


Figure 2-1: Schematic of SAGD process. (after Duke du Plessis, 2004)

The Vapex process is a vaporized solvent analog of the SAGD process. The Vapex process schematic is similar to Figure 2-1 where instead of steam a vaporized solvent is injected. The vaporized solvent contacts the bitumen and dilutes it by dissolution and diffusion. The viscosity of bitumen is reduced by mixing with the solvent. The solvent and bitumen mixture drains to the bottom production well where it can be pumped to surface.

The following are some advantages of Vapex Process (Karmaker and Maini, 2003):

- Low energy consumption
- Reduced green-house gas emission
- Minimum water handling and treatment
- Potential of in-situ upgrading of bitumen
- No heat loss, hence it can be used for reservoir with thin pay, or bottom water.

The solvent mass diffusion into the bitumen is one of the controlling factors in the Vapex process. Since mass diffusivity is smaller than thermal diffusivity, the recovery in Vapex is slower compared to thermal processes. Also, since heat can pass through shale barriers by conduction where solvent cannot, reservoir heterogeneity may be a bigger challenge for the Vapex process than thermal processes. The other potential disadvantages of the Vapex process are: the high cost of the solvent and the loss of the solvent which remains in the vapor chamber or in an overlying gas cap; and the possible loss of reservoir permeability due to asphaltene precipitation (Karmaker and Maini, 2003).

Figure 2-2 shows a schematic of Vapex process on a plane orthogonal to the horizontal wells. It illustrates the following factors involved in the Vapex process (Das et al., 1998):

- Phase behaviour of solvent and bitumen
 - Solubility
 - Swelling
 - Viscosity reduction
- Solvent diffusion and convective mixing of diluted oil with bitumen

- Gravity drainage
- Capillary force and imbibitions of the wetting phase into the vapour phase.

Each of these factors is discussed in the following sections.

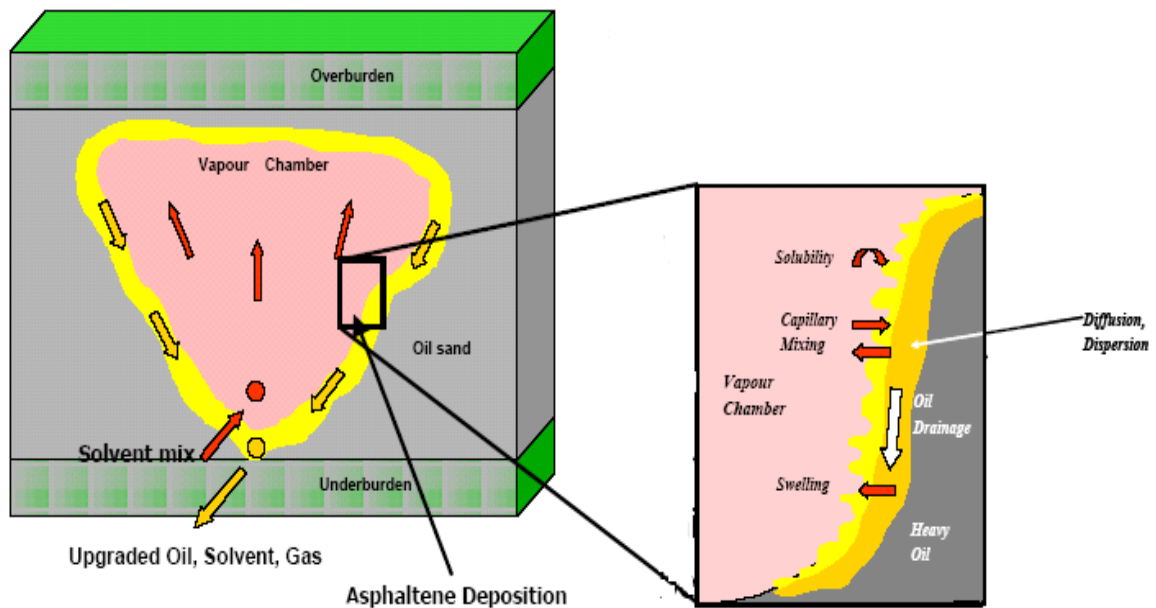


Figure 2-2: Mechanism involved in the Vapex process. (after Upreti et al., 2007)

2.1 Phase Behaviour of Bitumen and Solvent

Vapex is a gravity drainage process. During the Vapex process, compositional changes occur in both the oil and gas phases. The oil mobilization in the Vapex process occurs due to compositional changes in the oil phase by dissolution and diffusion of the solvent components into the oil phase. At the same time, the vapor phase composition also undergoes changes due to preferential dissolution of heavier gas components into the oil and vaporization of lighter oil components into the gas. Therefore, the phase behaviour of solvent and bitumen plays a critical role in the Vapex process. Data and models of the phase behaviour of bitumen, solvent, and their mixtures are required to design the best

solvent composition and operation conditions that will give the maximum solubility and viscosity reduction and results in optimum recovery of bitumen. It also helps to determine possible additional phases (a solid phase or a second hydrocarbon liquid phase) that bitumen and solvent mixture may form at the Vapex operating condition.

Bishnoi et. al. (1977) stated that thermodynamic properties like compressibility factors and phase compositions at equilibrium in hydrocarbon/hydrocarbon and hydrocarbon / non-hydrocarbon systems encountered in bitumen recovery processes are essential for modeling these processes. They reported density of Athabasca bitumen at 101.3 kPa and temperatures between 10 to 70°C. In their study the Athabasca bitumen was characterized with five pseudo components (see Table 2-2). The Peng-Robinson equation of state (1976) was used to calculate bitumen density at different temperatures. They also calculated carbon dioxide and methane solubility in Athabasca bitumen. There was no experimental data available at the time of their study to compare against the equation of state predicted solubility and density of carbon dioxide saturated bitumen. Nonetheless, their results correctly predicted higher solubility of carbon dioxide than methane in Athabasca bitumen.

Jacobs et al. (1980) measured the effect of temperature and pressure on the viscosity of Athabasca bitumen. The viscosity of bitumen decreased from 500 Pa.s. at 21.3°C to 0.07 Pa.s. at 130°C at atmospheric pressure. Their results showed small increase in viscosity of bitumen at higher pressure (6.9 MPa), but the effect of temperature was much stronger than pressure on bitumen viscosity. They also studied the effect of dissolved carbon

dioxide, methane, and nitrogen on the viscosity of Athabasca bitumen. Their experimental results show that carbon dioxide, in comparison to methane and nitrogen dramatically reduces the viscosity of bitumen, particularly at low temperatures (see Figure 2-3).

Svrcek and Mehrotra (1982) modified the experimental setup of Jacobs (1980) for viscosity measurements, to enable sampling of the saturated bitumen to determine the solubility of carbon dioxide, methane, and nitrogen in the saturated bitumen samples. The experimental solubility, viscosity and density data were in the temperature range of 25 to 100°C at pressures up to 10 MPa. It was observed that carbon dioxide has higher solubility in bitumen and causes tremendous reduction in viscosity. The solubility of nitrogen in bitumen was found to be very low, whereas that of methane was intermediate. Mehrotra and Svrcek (1982) developed an experimental method to measure the solubility of a synthetic combustion gas (17% CO₂, 1% CH₄, and 82% N₂) in Athabasca bitumen. The viscosity and density of the gas-saturated bitumen, the compositions of dissolved and equilibrium gases were also reported. Using the experimental data from Svrcek and Mehrotra (1982) for pure gas solubility in Athabasca bitumen, they developed empirical correlations that predict solubility of pure carbon dioxide, methane, and nitrogen gases, and the viscosity of saturated bitumen as function of pressure and temperature.

Mehrotra and Svrcek during 1980s reported extensive experimental data on the effect of carbon dioxide, methane, nitrogen, and ethane on different bitumen samples in Alberta (Athabasca (1982), Peace River (1985), Cold Lake (1988), Wabasca (1985), and

Marguerite Lake (1984)). Their experimental data confirms higher solubility of carbon dioxide in bitumen. The solubility of carbon dioxide in bitumen at any isothermal condition increases as the pressure increases.

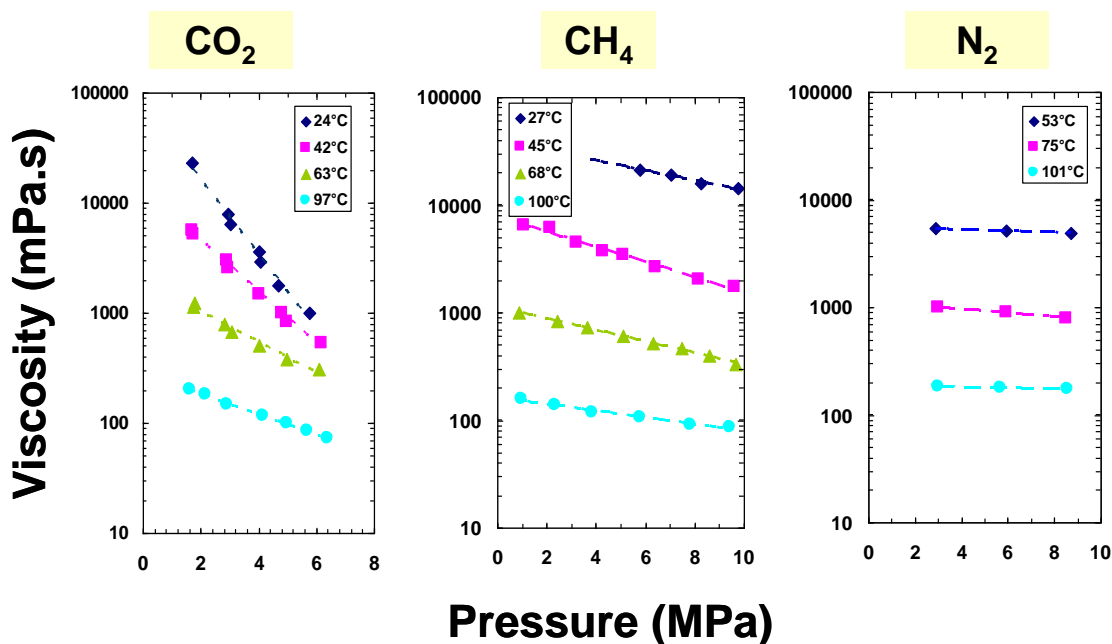


Figure 2-3: Effect of carbon dioxide, methane, and nitrogen solubility on Athabasca bitumen. (after Svrcek and Mehrotra 1982)

Figure 2-4 shows the solubility of carbon dioxide in Cold Lake bitumen at a temperature (~26°C) lower than critical temperature of carbon dioxide. It is interesting to note that as pressure increase the solubility of carbon dioxide in bitumen increases but, at certain pressures, its increase with pressure becomes very slow. This plateau is the point where a liquid phase rich in carbon dioxide forms and the V-L equilibrium becomes a L-L equilibrium condition. These results confirm the possibility of multiple liquid phase formation at low temperature and high pressure for carbon dioxide and bitumen system.

Mehrotra et al. (1985) used the Peng-Robinson (1978) equation of state and a flash calculation to estimate bitumen density and carbon dioxide and ethane solubility in Athabasca and Peace River Bitumen. The five pseudo component characterization of Bishnoi et al. was used in their study for Athabasca bitumen (see Table 2-2). It was found that results predicted using the Kesler-Lee (1976) critical property correlation for pseudo components (see Table 2-3) compared well with the experimental solubility data (Figure 2-5). They also extended the equation of state multi-phase flash calculation to low temperature and high pressure conditions. Their model also predicted VLL condition for the carbon dioxide and Athabasca bitumen at low temperature and high pressure similar to condition observed experimentally for the Cold Lake bitumen and carbon dioxide.

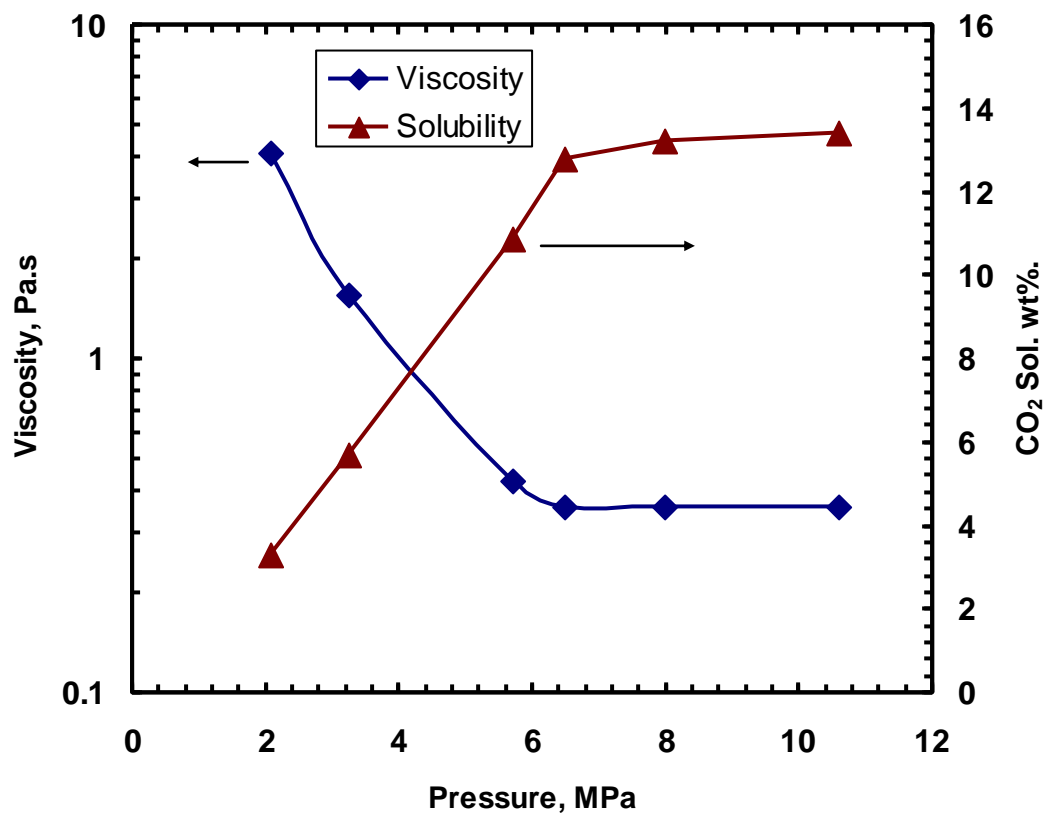


Figure 2-4: Carbon Dioxide and Cold Lake Bitumen solubility and viscosity at 26°C, after Mehrotra et al. 1988.

Table 2-2. Pseudo components of Athabasca bitumen. (after Bishnoi et. al. 1977)

	NBP ^o C	SG	MW	Wt%
HYP1	180	0.7939	142.6	1.8
HYP2	250	0.8291	192.8	5
HYP3	350	0.8955	290.1	1.8
HYP4	500	1.0599	508.5	71.4
HYP5	738	1.158	1092.8	20

Table 2-3. Critical properties of Athabasca bitumen pseudo components using Kesler-Lee correlation, and binary interaction with carbon dioxide used by Sarkar and Mehrotra (1985).

	Pc, kPa.	Tc, K	Acentric factor	K_{iCO_2}
HYP1	2582.27	535.443	0.61327	0.11
HYP2	1971.73	712.139	0.62193	0.11
HYP3	1949.01	820.302	0.79988	0.11
HYP4	1124.85	887.452	1.25751	0.12
HYP5	779.414	1165.73	1.29572	0.13

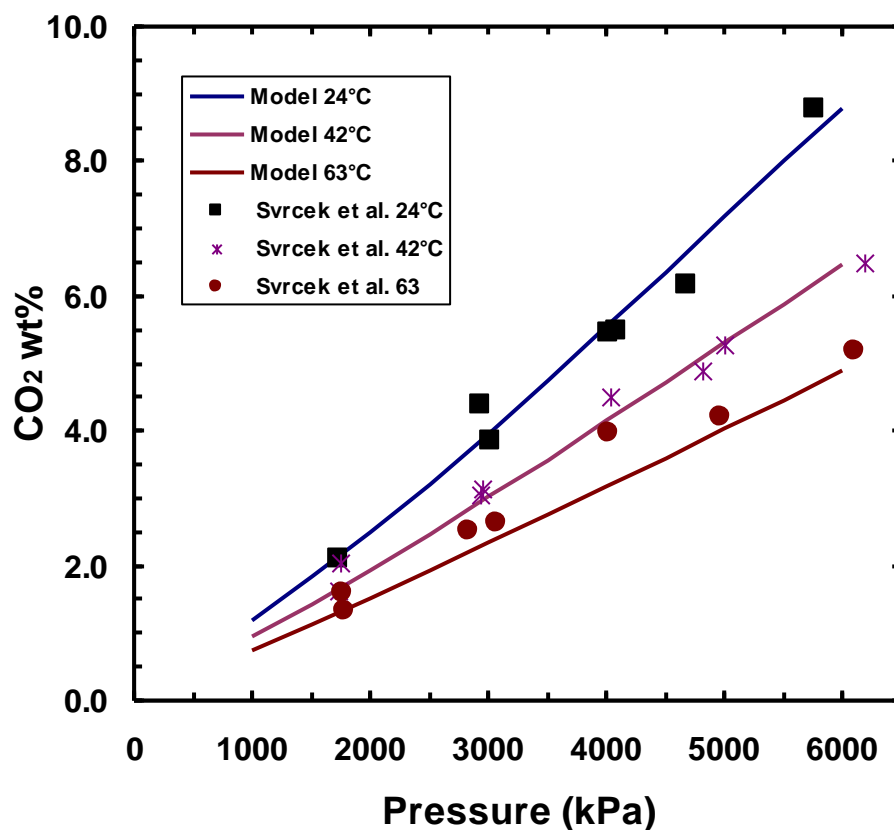


Figure 2-5: Carbon Dioxide solubility in Athabasca bitumen calculated by PR-EoS. (Mehrotra et al. 1985)

Simon et al. (1964) reported carbon dioxide solubility and viscosity data with 9 different oils. They also correlated the solubility and viscosity data for oil and carbon dioxide binary system using their experimental data. All of oils had vapor pressures of less than 1 atm at the experimental temperature of solubility study and the vapor phase composition was at least 99% carbon dioxide in equilibrium with the saturated oil (liquid phase). No multiple liquid phase (VLLE) condition was observed in their study.

Carbon dioxide can vaporize light alkanes (e.g. propane), form a binary vapor mixture, and became more efficient in viscosity reduction of the heavy oil. Figure 2-6 shows the pressure-composition diagram of the propane / carbon dioxide binary system, based on the experimental data from Reamer et al. (1951). They studied the influence of pressure and temperature on four mixtures of propane and carbon dioxide experimentally at pressure up to 69 MPa (10000 psia) and at eight temperatures between 277.59 and 344.26 K (40° to 160°F). In this temperature range, the compositions of coexisting liquid and gas phases were determined and presented in graphical (Figure 2-6) and tabular form.

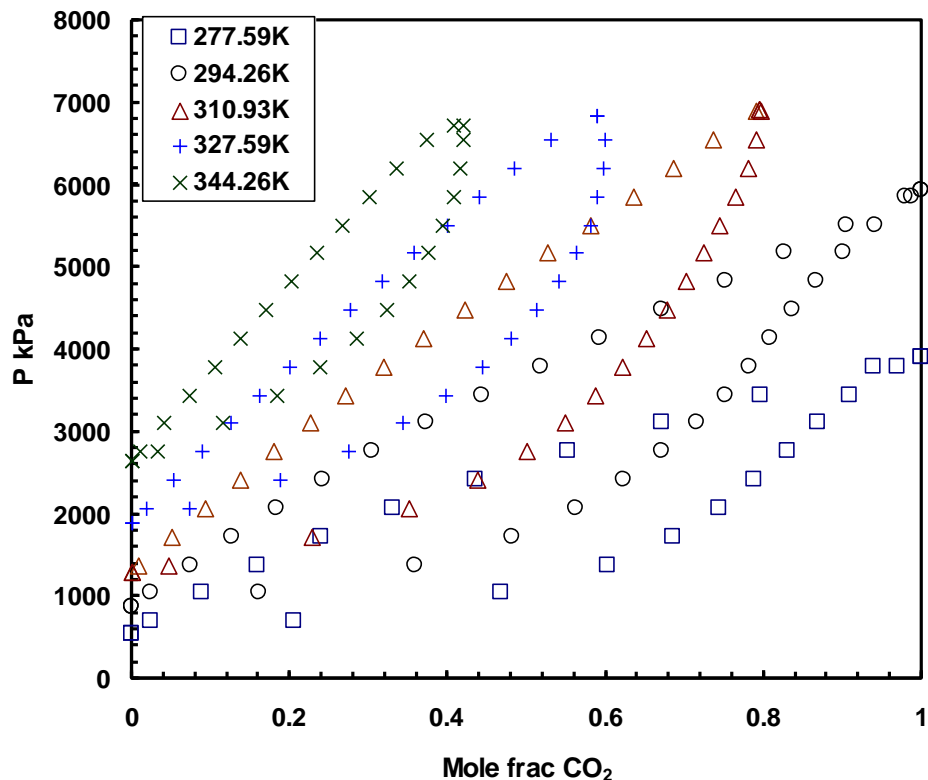


Figure 2-6: Pressure – composition diagram for the carbon dioxide – propane binary system. (Reamer 1951)

While there are considerable data in the literature for mixtures of carbon dioxide and crude oils, there are fewer data reported for mixtures of propane and heavy oils. Jacoby (1987) extracted bitumen from Athabasca oil sand with liquid or supercritical ethane, propane, and butane inside a PVT cell. The equilibrium viscosity and density of the extracted liquid phase were measured for different ratios of solvent to oil sand. He conducted similar experiments to investigate asphaltene precipitation from a heavy crude oil (13.5°API). Note that in these tests the extracted phases were not necessarily representative of the whole oil.

Frauenfeld et al. (2002) measured the solubility and viscosity of methane, ethane, propane, and carbon dioxide saturated Lloydminster Aberfeldy oil at 19°C and several pressures below the vapor pressure of the solvent. They also studied the solubility of ethane and propane in Cold Lake blended oil at 15°C and pressures below the vapor pressure of the solvent.

Freitag et al. (2005) measured the solubility, density and viscosity of the propane/Winter (Lloydminster) oil system at 28°C and 15°C. Using a semiautomatic PVT apparatus, they obtained self-consistent density and viscosity data. However, their propane solubility data were scattered. The precipitation of asphaltene and its effect on density and viscosity of saturated oil were reported at pressures above the vapor pressures of propane.

2.2 Vapor Solvent for Bitumen Extraction

Experimental studies of Vapex process have indicated that the performance of vapor extraction improves when propane, butane, or mixtures of propane-butane are used instead of ethane (Butler and Mokrys, 1993; Das and Butler, 1995; Yazdani, 2007; Badamchizadeh et al., 2008). Another variation of the basic process involves mixing the solvent with a non-condensable gas (CO₂, CH₄) to maintain the field operating pressure while the solvent vapor dilutes the oil. In this case, the mixture is selected to ensure it remains as vapor in the extraction chamber, and has a maximum solubility in the oil to ensure a sufficiently high extraction rate (Das and Butler, 1998; Talbi and Maini, 2003; Badamchizadeh et al., 2008).

Vapex experiments conducted with sand-packs in high-pressure stainless models show that CO₂-propane mixtures at operating pressures greater than 4.13 MPa perform better than methane-propane mixtures (Talbi and Maini, 2003). A complex solvent mixture containing 44.44% CO₂, 2.84% C₂, 19.67% C₃, 3.71% IC₄, 8.19% nC₄, and 21.15% C₅₊ (mole percentage) has been used to conduct a laboratory investigation with a 2-D physical model using Llançanelo crude (from an Argentinian field). The results indicate an excellent 82.9% recovery of the original oil in place at reservoir conditions of 9.4 MPa and 56°C (Cavallaro et al., 2005).

The use of CO₂ in the Vapex process can benefit the environment by sequestering CO₂ in underground formations. Furthermore, CO₂ has the advantage of being more soluble in heavy oil than methane. Thus, CO₂-solvent mixtures can be used in Vapex in order to obtain improved heavy oil recovery and to reduce CO₂ emissions.

2.3 Viscosity of Heavy Oil and Solvent

The high viscosity of bitumen at the oilsands reservoir condition is the main obstacle in bitumen recovery; hence, suitable steps to reduce bitumen viscosity are essential for oil recovery from oilsands reservoirs. In the Vapex process, the viscosity of bitumen is reduced as solvent diffuses and blends with the bitumen. Therefore, to correctly model the Vapex process performance, it is very important to have an accurate estimate of the bitumen-solvent mixture viscosity which is a function of its composition, temperature and pressure.

Svrcek and Mehrotra (1988) have shown that the following Walter's (1931) or ASTM two-parameter equation can correlate bitumen viscosity-temperature data.

$$\log(\log(\mu + 0.7)) = b_1 + b_2 \log(T) \quad (2-1)$$

where μ is viscosity in mPa.s., T is temperature in degree Kelvin. The value of b_1 and b_2 for their Athabasca bitumen sample was 10.010 and -3.74056. Later Mehrotra (1990) improved the double logarithmic term to $\log\log(\mu+0.8)$ in the aforementioned two parameter equation to better correlate bitumen and its fractions' viscosity with temperature. He introduced constant of 0.8 instead 0.7 in the double logarithmic term to prevent it from becoming negative at high temperatures for the light fractions of bitumen or for diluents like toluene. Then, he developed a simple viscosity mixing rule based on the two parameter viscosity-temperature correlation for the mixture viscosity of diluent-bitumen as follow:

$$\log(\mu_{mix} + 0.8) = \sum_{i=1}^{nc} x_i (M_i / M_{mix})^{0.5} 10^{(b_1)_i} T^{(b_2)_i} + \sum_{i=1}^{nc} \sum_{j=1}^{nc} x_i x_j (M_i M_j / M_{mix}^2)^{0.5} B_{ij} \quad (2-2)$$

where, μ_{mix} is the mixture viscosity in m.Pa.s., x_i is mole fraction of component i , M_i is molecular weight of component, M_{mix} is molar average molecular weight of mixture, and B_{ij} is an empirical viscosity binary interaction parameter. The variation of each component's viscosity with temperature was represented by two viscosity characterization parameter b_{1i} and b_{2i} . Mehrotra (1991) has shown that the viscosity calculated by Equation 2-2 was in reasonable agreement with the experimental data from different heavy oil and liquid solvent blends. This viscosity mixing model considers the

effect of temperature and composition on the viscosity of liquid mixture but neglects the pressure effects.

The viscosity of a liquid is also function of pressure but, in comparison to the effect of temperature and liquid diluents, the influence of pressure on the viscosity of bitumen is nominal. However, when gases are dissolved in the bitumen, the influence of pressure dependent gas solubility/concentration in saturated bitumen viscosity is quite significant. Svrcek and Mehrotra (1982, 1988; Mehrotra and Svrcek 1984, 1985a,b,c, 1988) published extensive experimental data on the effect of pressure and temperature on solubility of solvent gases in bitumen and mixture viscosity. Mehrotra (1988) developed correlations to predict the viscosity of bitumen saturated with nitrogen, carbon monoxide, methane, carbon dioxide, and ethane over wide temperature ranges.

The Lobe (1973) binary mixing rule has been found to provide accurate predictions of the viscosity of solvent diluted crude oils (Escobedo and Mansoori, 1997). The Lobe mixing rule is given by:

$$\nu_{mix} = \phi_A \nu_A \exp\{\phi_B \alpha_B\} + \phi_B \nu_B \exp\{\phi_A \alpha_A\} \quad (2-3)$$

$$\alpha_B = 0.27 \ln\left\{\frac{\nu_B}{\nu_A}\right\} + \left[1.3 \ln\left\{\frac{\nu_B}{\nu_A}\right\}\right]^{0.5} \quad (2-4)$$

$$\alpha_A = -1.7 \ln\left\{\frac{\nu_B}{\nu_A}\right\} \quad (2-5)$$

where ϕ is the volume fraction, ν is the kinematic viscosity, A is the lower viscosity component and B is the higher viscosity component. Escobedo and Mansoori successfully

predicted the viscosity of blends of aromatic solvents and crude oil with this mixing rule. For blends of crude oil with normal alkanes, such as n-pentane, n-heptane, and n-nonane, the predicted viscosity was in good agreement with experimental data up to the solvent content at the onset of asphaltene precipitation.

The Shu (1984) correlation was developed to calculate viscosity for the heavy oil and bitumen blended with light solvents. It is based on the Lederer (1933) equation for liquid mixture viscosity. The Shu equation for the mixture viscosity is:

$$\mu = \mu_{Bit}^{x_{Bit}} \times \mu_s^{x_s} \quad (2-6)$$

$$x_{Bit} = \frac{\alpha V_{Bit}}{\alpha V_{Bit} + V_s} \quad (2-7)$$

$$x_s = 1 - x_{Bit} \quad (2-8)$$

$$\alpha = \frac{17.04 \Delta \rho^{0.5237} \rho_{Bit}^{3.2745} \rho_s^{1.6316}}{\ln\left(\frac{\mu_{Bit}}{\mu_s}\right)} \quad (2-9)$$

where, μ is viscosity (mPa.s), V_{Bit} is volume fraction of bitumen in mixture, and V_s is volume fraction of light component (i.e. solvent) in the liquid mixture. The x_{Bit} and x_s are compositional parameters calculated with Equation 2-7 and 2-8. The variable α represents an empirical parameter having value between zero and unity. Equation 2-9 is an empirical estimate of α based on the best fit to the viscosity data of blends of 17 different crude oils and diluents. The Shu correlation is not valid at conditions where asphaltene precipitation occurs due to blending.

The Pedersen viscosity correlation (1987) was used to predict the viscosity of heavy oils. It uses the principle of corresponding states to calculate the viscosity of a component or mixture based on the viscosity of a reference substance at the same conditions of reduced pressure and temperature. The deviation from a direct corresponding state is accounted for by a “rotational coupling coefficient,” λ . The viscosity of the mixture is calculated according to the following formula:

$$\frac{\mu_{mix}(T, P)}{\mu_{ref}(T_{ref}, P_{ref})} = \left(\frac{T_{c,mix}}{T_{c,ref}} \right)^{-1/6} \left(\frac{P_{c,mix}}{P_{c,ref}} \right)^{2/3} \left(\frac{MW_{mix}}{MW_{ref}} \right)^{1/2} \left(\frac{\lambda_{mix}}{\lambda_{ref}} \right) \quad (2-10)$$

where, μ is viscosity (mPa.s), T_c is critical temperature (K), P_c is critical pressure (kPa), MW is molecular weight, and α is the rotational coupling coefficient. The subscript “mix” refers to the mixture property, and the subscript “ref” refers to the reference substance property. The reference substance for the Pedersen model is methane.

The mixture critical temperature and pressure are calculated using mixing rules that are a function of the component critical temperatures and pressures and mole fractions (Pedersen, et al. 1984). The molecular weight of the mixture is determined from:

$$MW_{mix} = b_1 \times (MW_w^{b_2} - MW_n^{b_2}) + MW_n \quad (2-11)$$

where, MW_w is the weight fraction averaged molecular weight, MW_n is the mole fraction averaged molecular weight, and b_1 and b_2 are coefficients. The rotational coupling coefficient is calculated as follows:

$$\lambda = 1 + b_3 \times \rho_r^{b_4} \times MW_{mix}^{b_5} \quad (2-12)$$

where, ρ_r is the reduced density of the reference substance and b_3 , b_4 , and b_5 are coefficients. The viscosity of a mixture calculated using the Pedersen model depends strongly on the critical pressures, critical temperatures and molecular weights of the components. The coefficients, b_1 to b_5 , can be adjusted to fit the measured data.

Yarranton and Satyro (2009) developed fluid density based viscosity correlation for hydrocarbons. It is based on general principle that the fluidity increases (or viscosity decreases) as fluid expands and there is greater distance between molecules. Yarranton and Satyro expressed fluidity as exponential function of fluid expansion relative to a compressed state, at which the molecules are too close to move in viscous flow. The correlation is formulated as a departure function from viscosity of gas as follows:

$$\mu - \mu_G = c_1(\exp(c_2\beta) - 1) \quad (2-13)$$

where μ and μ_G are the fluid and its dilute gas viscosity (mPa.s.), c_1 (mPa.s.) and c_2 (dimensionless) are fitting parameters. β is the correlating parameter between the fluidity and the fluid expansion as follows:

$$\beta = \frac{1}{\exp\left(\left(\frac{\rho^*}{\rho}\right)^n - 1\right) - 1} \quad (2-14)$$

where ρ is the fluid density (kg/m^3), ρ^* is the density of the fluid in the compressed state, and n is an empirical exponent which improves the predictions near the critical region.

The fluid density data is required in Equation 2-14. It can be calculated from any valid correlation or direct measured experimental data are required. Satyro and Yarranton (2010) eliminate the need of experimental density data, with densities calculated from Advanced Peng-Robinson EoS. They also correlate the density of the fluid at compressed state to the pressure and molecular weight of the component as follows:

$$\rho^* = \frac{\rho^o}{1 - c_4(1 - \exp(-c_3P))} \quad (2-15)$$

where P is the pressure (kPa), ρ^o is the compressed state density in a vacuum (kg/m³), c_3 (kPa⁻¹) and c_4 are adjustable parameters and defined as function of the component molecular weight.

The Expanded-Fluid viscosity correlation has two adjustable parameters per component, a compressed state density, ρ^o and an empirical parameter, c_2 that scales the viscosity response to fluid expansion. The inputs to the correlation are the fluid density and molecular weight, pressure, and the low pressure gas viscosity. The gas or liquid densities were determined using the Advanced Peng–Robinson equation of state and therefore the critical properties, acentric factor, and volume translation factor of the component are required as input instead of the density. The volumetric mixing rules for compressed state density, ρ^o , and parameter c_2 were proposed by Satyro and Yarranton (2010) to calculate the mixture viscosity. Motahhari et al. (2011) also proposed mass-based mixing rules to estimate mixture viscosity using Expanded-Fluid viscosity correlation.

2.4 Solvent Mass Diffusion Coefficient in Heavy oil

During vapor extraction, the diffusion of solvent gas in heavy oil or bitumen is the primary molecular phenomenon responsible for gas absorption and mixing of the solvent with heavy oil and bitumen. Thus, diffusion plays a very important role in Vapex (Das, 1996). For a Vapex modeling, accurate diffusion coefficient data are necessary to determine the rate of live oil production from the reservoir.

The diffusion coefficients of various solvents in heavy oil and bitumen have been experimentally determined by several researchers using a direct method involving the compositional analysis of liquid samples extracted at different times (Schmidt et al., 1982; Nguyen et al., 1998) and indirect methods based on property changes such as volume swelling and IFT change (Yang et al., 2005), pressure (Upreti et al. 2000 and 2002), and nuclear magnetic resonance (Wen et al. 2005). The experimentally measured diffusivities of solvent gases in heavy oil and bitumen from these studies are in the order of 10^{-9} to 10^{-11} m²/s.

While investigating the diffusion of toluene in heavy oil and bitumen, Oballa and Butler (1989) found a strong concentration dependence of diffusivity. Later, Upreti and Mehrotra (200, and 2002) experimentally determined the concentration-dependent diffusivity of gaseous carbon dioxide, methane, ethane, and nitrogen in Athabasca bitumen, in temperature range of 25-90 °C at 4 and 8 MPa pressure. Diffusivity correlations based on their results are provided by Upreti (2002). The results show that the diffusivity increases with temperature at a given gas concentration and pressure.

Hayduk and Chen (1971) proposed following correlation which relates the apparent diffusivity of gas and the viscosity of its mixture with heavy oil and bitumen:

$$D = \alpha\mu^{-\beta} \quad (2-16)$$

where D is apparent diffusivity (m^2/s), μ is mixture viscosity (Pa.s), α and β are two positive empirical parameters that depend on the solvent/solute pair. This correlation indicates that the diffusivity increases with decrease in the viscosity of mixture in a nonlinear fashion.

2.5 Gravity and Capillary Forces Interplay in Vapex

The oil displacement during a gravity drainage process by gas injection is due to the density difference between displaced wetting phase and displacing non-wetting phase. The amount of wetting phase (i.e. oil) recovered in this drainage process is a function of the interplay between capillary and gravitational forces, characterized by the inverse Bond number. The inverse Bond number is defined as the ratio of capillary forces to gravitational forces. The inverse Bond number can be defined in terms of the rock-fluid properties of the system as follows:

$$N_B^{-1} = \frac{\sigma/r_t}{\Delta\rho gH} \quad (2-17)$$

where, σ is the interfacial tension (IFT) between the two phases (N/m), r_t is a characteristic throat radius of the porous medium (m), $\Delta\rho$ is the difference between the

wetting-phase density (ρ_w) and the nonwetting-phase density (ρ_N) (kg/m^3), g is the gravitational acceleration (m/s^2), and H is the height over which the drainage takes place (m). An inverse Bond number larger than one indicates that the capillary force dominates and hence there will be no wetting-phase drainage or recovery.

In the Vapex process, the oil displacement during gas injection is due to compositional gravity drainage, where the injected gas and initial bitumen in place are not at thermodynamic equilibrium. There is no single Bond number that can be applied to compositional gravity drainage. Since the compositions of both the wetting and non-wetting phases change during the gravity drainage flow, different interfacial tension and density will be encountered at each equilibrium tie line.

Figure 2-7 shows two possible scenarios during compositional gravity drainage, condensing drive and vaporising drive. The wetting phase recovery is a function of inverse Bond number in the zone with compositional change. It is shown in the figure with a question mark (?). In the condensing drainage, the injected gas composition lies on the extension of tie line with lower IFT (i.e. smaller length). The condensing drainage will result in lower IFT at top and higher IFT near the bottom of the reservoir. The vaporizing drainage will be opposite of the condensing drainage, where the initial oil phase lies on the extension of tie line with lower IFT. The drainage mechanism in the Vapex process is more likely to be the condensing drainage.

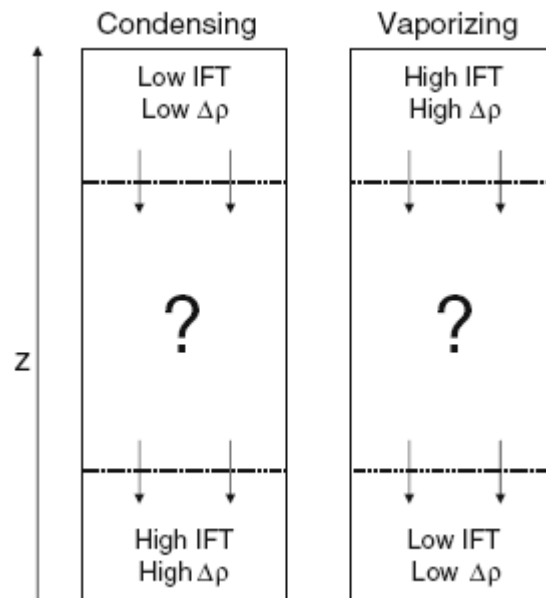


Figure 2-7: Two deriving mechanism in the compositional gravity drainage.(after DiCarlo et. al., 2007)

There have been few theoretical and experimental attempts to examine the process on the basis of non-equilibrium gravity drainage. This is surprising, given that, when gas is injected to facilitate such gravity drainage; it is unlikely to be at equilibrium with the oil in place. Jacquin et. al. (1989) performed compositional gravity drainage experiments for a ternary system of methane–butane–n-decane, from sandstone cores. His results showed improved recovery of the wetting phase when more butane is added to either the injected gas phase or to the oil in-place.

Cuthiell et al. (2006) developed a novel experimental method to investigate the capillary and gravitational forces interaction using CT scan imaging during a compositional drainage of heavy oil with n-butane. The experimental condition was set such that the

inverse Bond number was higher than 1; hence, it could not drain unless the composition of the oil phase and consequently the interfacial tension was reduced. Figure 2-8 is the CT scan image of the saturation of phases during compositional drainage, and it confirms a condensing drainage drive. The drainage process was modeled using numerical simulation. It was found that the capillary forces play a significant rule in the compositional process. The experimental saturation values during the compositional drainage process could not be matched by numerical simulation when the capillary effects were ignored.

DiCarlo et al. (2007a, b, c) studied the vertical compositional gravity drainage displacement experimentally and developed an analytical solution to the capillary – gravity equilibrium (CGE) for a simplified model of three component and two phase system. Their study shows that the equilibrium phase composition profile versus drainage length is different than the standard viscous forces dominated displacement.

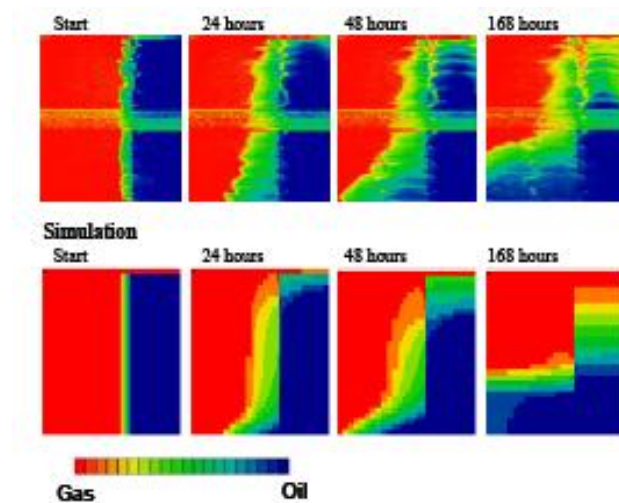


Figure 2-8: Comparison of compositional drainage experimental saturation with simulation results. (Cuthiell et. al., 2006)

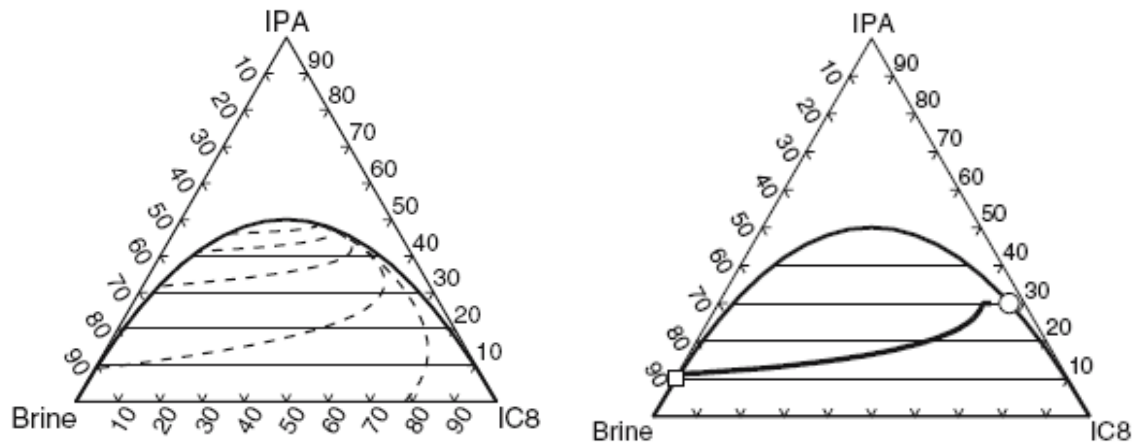


Figure 2-9: Lines of constant capillary pressure. Open circle is injected displacing fluid composition. Open square is the initial fluid composition. (DiCarlo 2007)

During the compositional gravity drainage with capillary and gravity equilibrium without diffusion, if the composition jumps between two ends of a tie line, the capillary pressure at the both sides of the jump must be equal. Thus the compositional change is always along a line between the lower left to upper right (see Figure 2-9). In the case of no diffusion, all component travel only with advected fluids and the phase composition jumps from one end of the tie line to the opposite end. The component diffusion between wetting and non-wetting phase during compositional drainage will smear the compositional jumps between the tie lines. The diffusion leads to higher oil recovery specially in case of condensing drive compositional drainage. The Vapex process is more likely condensing gas drive drainage. In case of condensing gas drive the diffusion lowers the IFT of the initial fluid, drops the capillary fringe, and results in greater oil recovery.

2.6 Vapex Process Mathematical Model

The theoretical analysis of heat transfer in the SAGD process (Butler 1985) was extended by Dunn et al. (1989) to mass transfer in the Vapex process, for modeling the oil rate. They assumed constant solvent diffusion coefficient (D_s), and interface velocity (U) in horizontal direction. Therefore, at steady state condition the continuity equation with Fick's law for solvent mass transfer will result in:

$$-U \times \frac{\partial C_D}{\partial \varepsilon} = D_s \frac{\partial^2 C_D}{\partial \varepsilon^2} \quad (2-18)$$

The initial and boundary conditions as shown in Figure 10 are:

$$C = 0 \text{ or } (C_D = C/C_s = 0) \quad @ t = 0, \varepsilon > 0 \quad (2-19)$$

$$C = C_s \text{ or } (C_D = C/C_s = 1) \quad @ t > 0, \varepsilon = 0 \quad (2-20a)$$

$$C = 0 \text{ or } (C_D = C/C_s = 0) \quad @ t > 0, \varepsilon \rightarrow \infty \quad (2-20b)$$

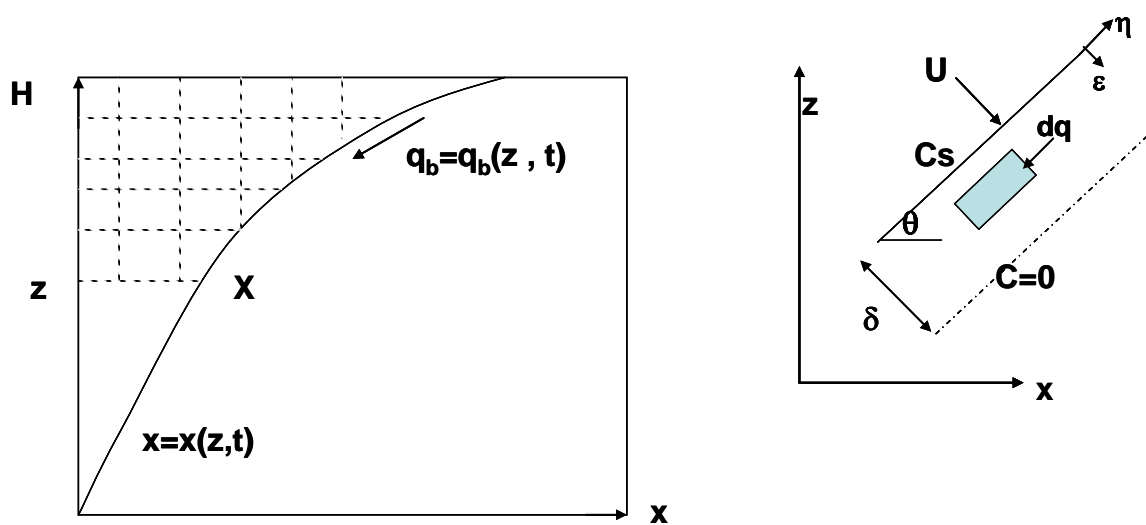


Figure 2-10: Vapex gravity drainage flow element.

The solution to the Equation 2-18 gives an exponential composition profile at the steady-state condition inside the penetration zone ($\delta=D/U$):

$$C_D = \frac{C}{C_s} = \exp\left(-\frac{U\varepsilon}{D}\right) \quad (2-21)$$

Dunn et al. assumed a power law functionality of mixture kinematic viscosity on the solvent volume fraction in bitumen:

$$\frac{\nu_s}{\nu} = C_D^m \quad (2-22)$$

Then oil rate for the Vapex process was obtained based on the Butler's approach for the oil rate in the SAGD processes per unit length of the well.

$$Q = \sqrt{\frac{2KgD\phi\Delta S_o H}{m\nu_s}} \quad (2-23)$$

Note that in the SAGD process there is no mixing between condensed steam and bitumen therefore the oil production rate is directly related to interface movement. In the Vapex process, there is some volume fraction of solvent in the produced oil. But the interface movement is a function of the amount of native bitumen production, not the mixed solvent and bitumen rate. Thus this neglect of the fractional flow of bitumen, during the development of Equation 2-23 by Dunn et al. is likely to introduce significant error.

Dunn et al. (1989) also performed Vapex experiments in a sand pack model with carbon dioxide and ethane. In order to match the experimental oil rate with Equation 2-23, they

found that a diffusion coefficient (D) almost 500 times larger than typically reported diffusivities in the literature for carbon dioxide and ethane were required.

Butler et al. (1989) developed a vapor solvent extraction mathematical model analog to the steam assisted gravity drainage model. Most importantly Butler introduced a general form of the solvent diffusion coefficient dependency on the concentration of the solvent in oil mixture. Equation 2-18 based on Butler model at steady state condition will be:

$$-U \times C_D = D_s \frac{\partial C_D}{\partial \varepsilon} \quad (2-24)$$

The general solvent concentration profile ahead of solvent–oil interface is then given by:

$$U\varepsilon = \int_{C_D}^1 \frac{DdC_D}{C_D} \quad (2-25)$$

Equation 2-25 includes the effect of diffusion coefficient dependence on the solvent concentration profile ahead of the vapor-oil interface in the Vapex process.

Butler et al. in their mathematical model correctly consider the dependency of the interface movement velocity to the amount of bitumen volume fraction in the produced oil. The steady state bitumen production rate in Butler's model is:

$$Q_b = \sqrt{2Kg\phi\Delta S_o H N_s} \quad (2-26)$$

where

$$N_s = \int_{C_{D\min}}^1 \frac{\Delta\rho D(1-C_s C_D)}{\mu} d \ln C_D = \int_{C_{D\min}}^1 \frac{D(1-C_s C_D)}{\nu} d \ln C_D \quad (2-27)$$

Equation 2-26 shows that the dimensionless N_s number in Vapex process is related to the volume fraction of bitumen, $C_B = I - C = I - C_s C_D$. Therefore in Butler's generalized model for steady state oil rate, it is necessary to know the functionality of the density difference ($\Delta\rho = \rho_{mix} - \rho_{vap} \sim \rho_{mix}$), diffusion coefficient (D), and viscosity (μ) to the volume fraction of solvent in the binary mixture.

Heidari et al. (2008) developed a mathematical model for the steam assisted gravity drainage process and improved the Pooladi-Darvish et al. (1996) model for the SAGD process. Pooladi-Darvish et al. used the heat integral method (HIM) to solve the unsteady-state heat transfer and temperature profile ahead of steam-bitumen interface in the heat penetration zone. This method uses an approximate polynomial distribution of temperature ahead of interface rather than exponential profile in the Butler's (1985) model for SAGD. The interface velocity vector (U) in the Heidari and Maini's approach (2008) is orthogonal to the interface and in the same direction as thermal diffusion, whereas in the Butler (1985) and Pooladi-Darvish et al. (1996) models it was considered in horizontal direction. Heidari et al. reported an improved match to the oil rate and SAGD experimental results after applying this correction in the direction of interface velocity vector.

Heidari and Maini (2008) then applied this approach to the mass transfer theoretical model of the Vapex process. They neglected the dependence of diffusion coefficient on solvent concentration in the oil mixture. The solution for Equation 2-18 in dimensionless form using the HIM becomes:

$$C_D = \left(1 - \frac{\varepsilon_D^*}{\delta_D}\right)^n \quad (2-28)$$

The steady-state dimensionless bitumen rate (Q_{bss}) based on Heidari model is given by:

$$Q_{bss} = \frac{q_{bss}}{\varphi \Delta S_o D} = \sqrt{\frac{2n}{mn+1} \cdot f_b \cdot N_{Ra}} \quad (2-29)$$

where, N_{Ra} is Rayleigh number, and f_b is the volume fraction of bitumen in produced oil mixture:

$$N_{Ra} = \frac{KHg}{\varphi \Delta S_o \nu_s D_s} \quad (2-30)$$

$$f_b = \left(1 - C_s \cdot \frac{mn}{nm+n+1}\right) \quad (2-31)$$

Heidari et al. used the experimental oil rate reported by Yazdani (2007) for Vapex physical models with different permeabilities and model heights to back calculate the solvent diffusivity in the oil with Equation 2-29. The calculated diffusivity was found to be in the expected range of $10^{-9} \text{m}^2/\text{sec}$. However, the diffusion coefficient was not same in all experiments and it increased (by as much as 40 - 50 times) with increasing height of the model. Heidari attributed this deficiency to the dependence of diffusion coefficient to the concentration of solvent in the oil mixture, which was neglected in his formulation.

Okazawa (2007) studied the effect of solvent diffusion coefficient dependence on solvent concentration in the oil mixture on the oil rate in Vapex process. He considered a power law functionality between solvent diffusion coefficient and concentration given by:

$$D = D_s C_D^d \quad (2-32)$$

where, D_s is the diffusion coefficient at the interface (i.e. $C_D = 1$). The functionality of diffusion coefficient to concentration introduces strong non-linearity in Equation 2-18 (Dunn et al., 1989) and Equation 2-24 (Butler et al., 1989) which now becomes:

$$-U \times \frac{\partial C_D}{\partial \varepsilon} = \frac{\partial}{\partial \varepsilon} \left(D_s \frac{\partial C_D}{\partial \varepsilon} \right) \quad (2-33)$$

Okazawa discussed the difficulty in deriving the steady-state concentration profile analytically from Equation 2-33. Okazawa assumed the following form of concentration profile in his analysis of the effect of concentration dependency of diffusion on the oil rate in Vapex process.

$$C_D = \left(1 - \frac{\varepsilon}{A/U} \right)^{\frac{1}{d}} = \left(1 - \frac{\varepsilon}{\delta} \right)^{\frac{1}{d}} \quad (2-34)$$

Figure 2-11 compares different concentration profiles within the Vapex process penetration zone from different mathematical models.

Okazawa assumed that the functionality of oil mixture's kinematic viscosity to solvent concentration was similar to the power law correlation of Dunn et al. (Equation 2-22). Then he followed the method used by Butler (1989) and obtained the following expression for the steady-state bitumen rate:

$$Q_b = f_b \times Q_{total} = \sqrt{\frac{2KgD_s \varphi \Delta S_o f_b H}{d \times \left(\frac{m}{d} + 1 \right) \nu_s}} \quad (2-26)$$

where, the bitumen volume fraction f_b is defined as:

$$f_b = \left(1 - C_s \cdot \frac{m+d}{m+d+1} \right) \quad (2-27)$$

An interesting observation in Okazawa's analyses is that the concentration profiles of solvent within the bitumen phase do not affect the basic correlations of the bitumen rate expressions to the key physical characteristics (e.g. permeability K , height H , and porosity ϕ). The square-root relationships originate from the inversely proportional impact of the interface advance rate on the thickness of the solvent-affected draining zone. In other words, the interface advance rate at any height must always be slower than the rate above it, because the lower location has to have a thicker draining zone in order to accommodate the flow which is increasing downward.

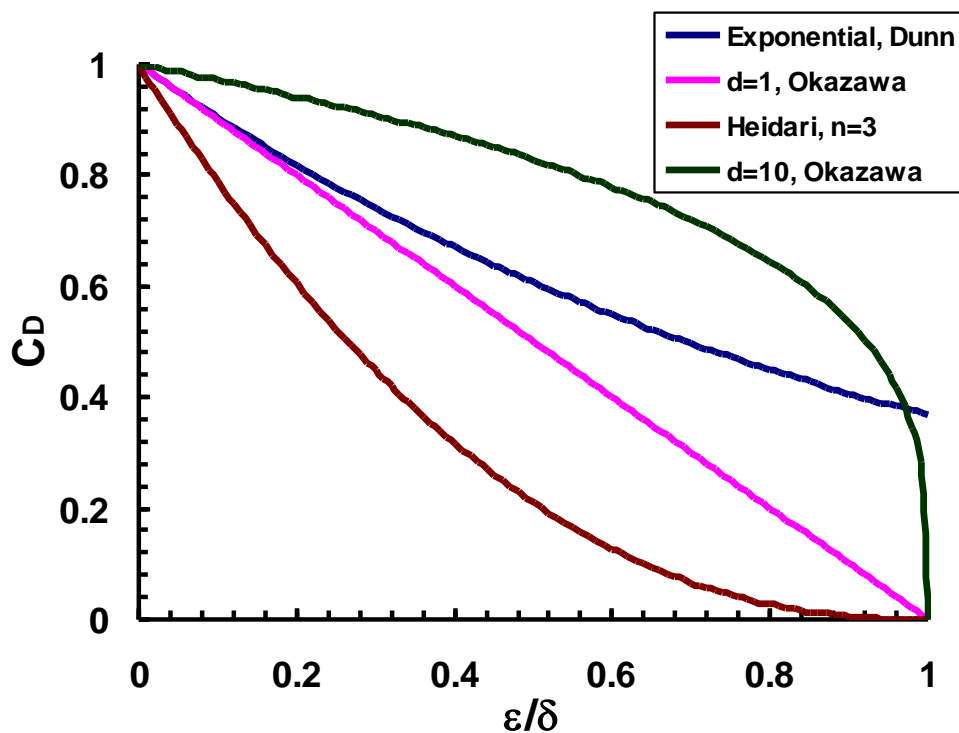


Figure 2-11: Solvent concentration profile ahead of Vapex interface by different theoretical method.

CHAPTER 3 : EXPERIMENTAL METHODS FOR PHASE BEHAVIOR AND PHYSICAL PROPERTIES

This chapter presents the experimental methods used to measure the properties of the Athabasca bitumen sample that was used during the course of this research. Characterization methods including SARA analysis and simulated distillation are discussed. The procedures for phase behaviour and property measurements for mixtures of bitumen, propane, and carbon dioxide are also presented. The high bitumen viscosity made equilibration challenging for these mixtures and the experimental modifications used to obtain the data are discussed.

3.1 Materials

The Athabasca bitumen was a coker feed sample obtained from Syncrude Canada Ltd. It was oil-sand bitumen that had been processed in the Syncrude plant to remove sand and water. Reagent grade solvents were used for asphaltene extraction and SARA fractionation, including n-pentane and n-heptane obtained from ConocoPhillips, toluene was supplied by Univar Calgary, and acetone purchased from VWR. Attapulugus clay was obtained from Engelhard Corporation, New Jersey and silica gel (grade 12, 28-200 mesh size) was obtained from Sigma Aldrich Co.

High purity solvents and chemicals were used for all molecular weight measurements performed with a vapour pressure osmometer. Toluene (99.96% purity) was obtained from VWR and sucrose octaacetate was obtained from Jupiter Instrument Co. The

propane (99.5 wt% purity) and the carbon dioxide (99.9wt% purity) used for PVT measurements was supplied by Praxair.

3.2 SARA Analysis

SARA fractionation is a technique for the separation of petroleum crudes into different fractions based on their solubility and adsorption properties. This method, referred to as Clay-Gel Absorption Chromatography (ASTM D 2007), is a procedure for classifying oil samples of initial boiling point of at least 260° C (500° F) into the following hydrocarbon types: saturates, aromatics, resins, asphaltene, and maltenes. The definitions of these fractions are:

- a) asphaltenes, or n-pentane insolubles – insoluble matter that precipitates from a solution of oil in n-pentane under the conditions specified.
- b) resins or polar compounds – material retained on adsorbent clay after percolation of the sample in n-pentane eluent under the conditions specified.
- c) aromatics – material that, on percolation, passes through a column of adsorbent clay in a n-pentane eluent but adsorbs on silica gel under the conditions specified.
- d) saturates – material that, on percolation in a n-pentane eluent, is not adsorbed on either the clay or silica gel under the conditions specified.
- e) maltenes – asphaltene-free bitumen including all of the saturates, aromatics, and resins.

SARA fractions were obtained from the Athabasca bitumen using the procedure outlined below. Simulated distillation assays were conducted for each fraction except the asphaltenes. The molecular weight and density were measured for each fraction.

3.2.1. Extraction and Purification of Asphaltenes

The first step of SARA fractionation is to precipitate asphaltenes from a crude oil with the addition of n-pentane. In the standard procedure (ASTM D2007), 40 volumes of n-pentane are added to one volume of bitumen. The mixture is sonicated using an ultrasonic bath for one hour and left to equilibrate for 24 hrs. The blend container is covered during this stage to prevent n-pentane vaporization at room temperature. The volume of the blend in the beaker is monitored, and in the event of any volume reduction (due to pentane vaporization), n-pentane is added to maintain a constant total volume. After equilibration, the mixture is filtered using a Watman's No.2 (8 μ m) filter paper. When 200cc (or 150 cc) of the blend is left in the bottom of the beaker, the filtration is stopped and 4 volumes of solvent are added, sonicated for one hour, and left to settle for 24 hrs. Then, the mixture is again filtered completely through filter paper. The filter cake is subsequently washed with n-pentane for 5 days until the washings are colourless. The solvent is recovered from the solvent-maltene (deasphalted oil) mixture using a rotary evaporator (Rotovap) at 40°C, 35kPa. The asphaltenes and maltenes are dried in a vacuum oven at 50° C until no change in weight is observed. These asphaltenes are referred to as nC5-asphaltenes since n-pentane was used for the extraction. The maltenes are further separated into saturates, aromatics and resins as discussed in the next section.

The same procedure was followed using n-heptane instead of n-pentane and the resulting asphaltenes are referred to as n-C7-asphaltenes. The n-C5 and n-C7-asphaltene contents of the Athabasca bitumen were 16.4 and 11.7 wt%, respectively. The n-C5-asphaltenes typically contain some resinous material that is insoluble in n-pentane but may be soluble in a higher n-alkane such as n-heptane.

Bitumen typically contains solids, such as sand and clay that cannot be dissolved in any solvent. The solid content of the bitumen was determined by dissolving the Athabasca bitumen in toluene and centrifuging for 6 min at 3500 rpm (900 relative centrifugal forces). The undissolved solids were recovered from the solution and dried.

3.2.2. Fractionation of Maltenes

The maltenes from the pentane extraction are used for fractionation into saturates, aromatics, and resins. The separation into these petroleum fractions is performed using the Clay-Gel Adsorption Chromatography method (ASTM D2007M). This technique is described in detail below.

Clay and Gel Activation

Approximately 200 g of Attapulugus clay is washed in a beaker with methylene chloride 2-3 times until the wash is colorless. The procedure is repeated with methanol and then with distilled water until the pH of the water is 6-7. The washed clay is evenly spread on a metal tray and dried in an oven overnight at 80°C under vacuum. Activation of the silica gel only requires heating. Approximately 200 g of silica gel is spread evenly on a

tray and dried in an oven overnight at 145°C. After this procedure the dried silica gel and clay are activated and ready for use in chromatography.

Chromatographic Procedure

The adsorption column consists of two identical glass sections assembled vertically as shown in Figure 3-1. 100 g of freshly activated Attapulugus clay is placed in the upper adsorption column. 200 g of activated silica gel is placed in the lower column. 50 g of Attapulugus clay is added on top of the gel. It is important that the adsorbents in each column be packed at a constant compaction level. A constant level of packing of the adsorbent is achieved with a minimum of ten taps with a soft rubber hammer at different points up and down the column. A piece of glass wool (of about 25 mm loose thickness) is placed over the top surface of the clay in the upper column to prevent agitation of the clay while charging the eluents. The two columns are assembled together (clay over gel) after lubricating the joint with hydrocarbon-insoluble grease.

5 g of maltene sample is weighed in a beaker, diluted with 25 mL of pentane and swirled to ensure a uniform sample. Prior to sample addition, 25 mL of pentane is added to the top of the clay portion of the assembled column with the help of a funnel and allowed to percolate into the clay. When all the pentane has entered the clay, the diluted sample is charged to the column. The sample beaker is washed 3-4 times with pentane and the washings are added to the column. After the entire sample has entered the clay, the walls of the column above the clay are washed free of the sample with pentane. After all the washings have entered the clay, pentane is added to maintain a liquid level well above the

clay bed until saturates are washed from the adsorbent. Approximately 280 ± 10 mL of pentane effluent is collected from the column in a graduated, 500 mL wide mouth conical flask. After the collection is finished, the flask is replaced with another flask for collection of aromatics and put away until the solvent is to be removed.

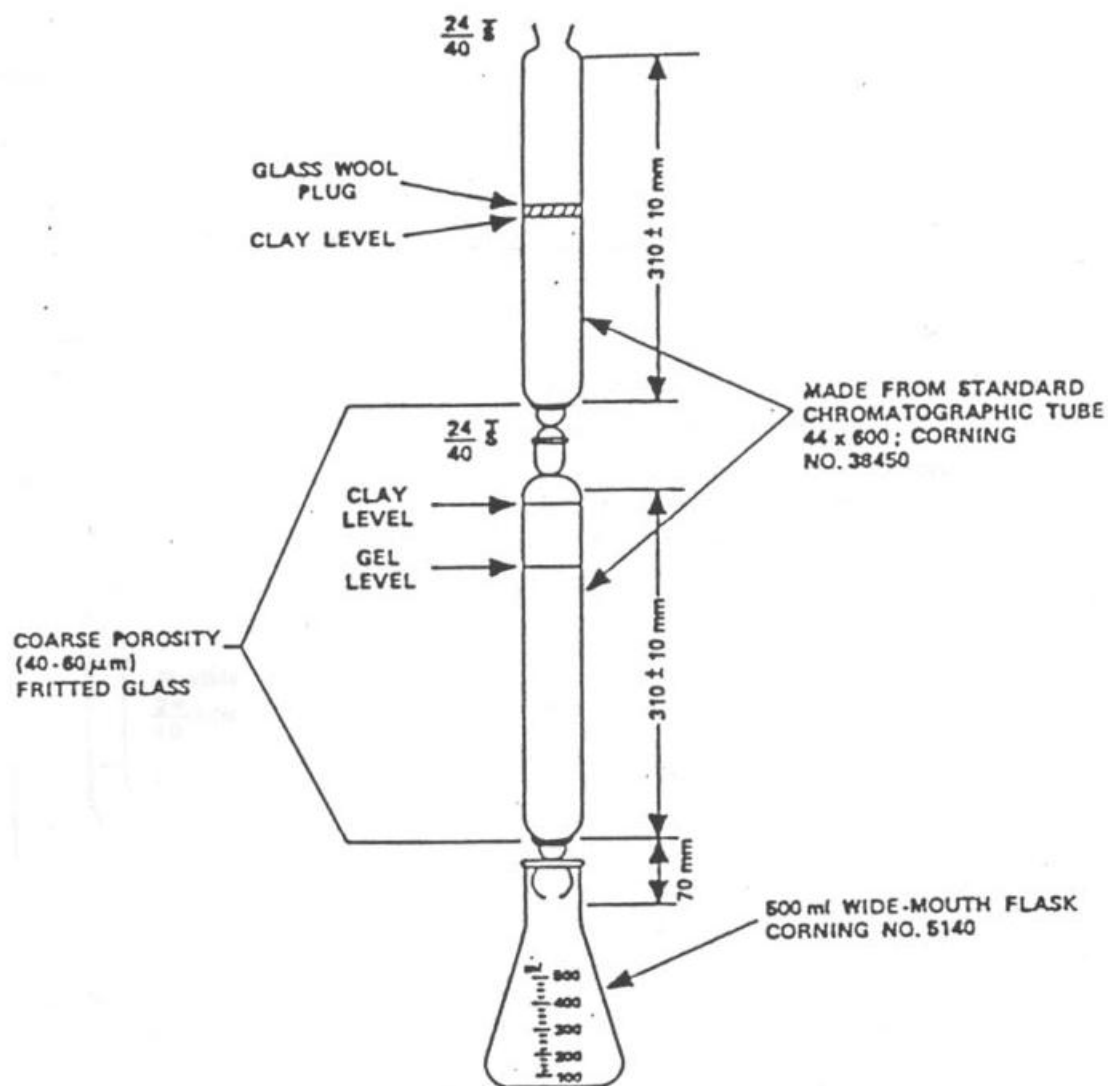


Figure 3-1. Clay-Gel Adsorption Columns

Immediately after all the pentane has eluted, a solvent mixture of pentane and toluene (50:50) in the amount of 1560 mL is added to the column through a separator funnel. The column is allowed to drain. At this point, resins are adsorbed on the clay in the upper column and aromatics are adsorbed on the gel in the lower column. The two column sections are disconnected carefully so that no sample or solvent is lost.

In order to extract the aromatics, the bottom section is placed in an extraction assembly. Toluene in the amount of 200 ± 10 mL is placed in a 500 mL 3-neck flask and refluxed at a rate of 8-10 mL/min for 2 hours as shown in Figure 3-2. The toluene reflux is measured by collecting the reflux flow for one minute in a graduated cylinder (the solution in the flask is later combined with the rest of the aromatic fraction).

To recover the resins, a solvent mixture of toluene and acetone (50:50) in the amount of 400 mL is charged slowly to the top clay column section. The effluent is collected in a separate flask. If the sample contains moisture, the effluent is collected in a 500 mL separator funnel, shaken well with approximately 10 g of anhydrous calcium chloride granules for 30 sec, allowed to settle and filtered through an 8μ size filter paper.

Solvent Removal

The saturate/pentane solution from the 500 mL wide mouth conical flask is transferred to a 500 mL round bottom flask. The conical flask is rinsed 3-4 times with pentane to remove all of the saturates from the round bottom flask. The solvent is evaporated using a Rotovap with the water bath set at a temperature of 35°C.

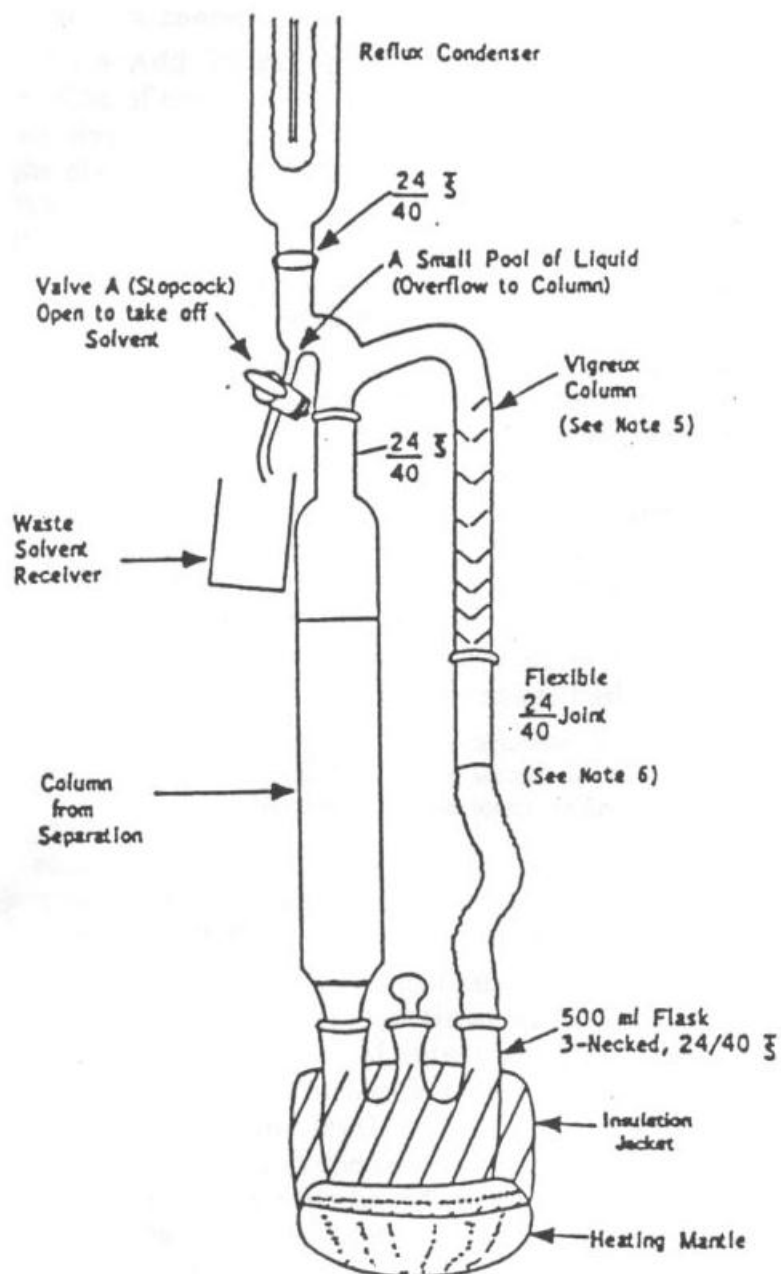


Figure 3-2. Extraction Apparatus for Aromatics.

Similarly, the resin/acetone/toluene and aromatic/pentane/toluene effluents are transferred to respective round bottom flasks and solvent is removed with the Rotovap with water bath temperature set at 65°C under vacuum. After solvent evaporation each fraction is transferred into glass vials. The fractions are dried in the fume hood until no change in weight is observed. Fig. 3-3 is a photograph of the saturate, aromatic, resins, and asphaltenes obtained for this study.



Figure 3-3. SARA fractions of the Athabasca bitumen.

3.3 High Temperature Gas Chromatography (HTSD) - Simulated Distillation (SimDist).

SimDist was reported early in the 1960s by Eggertsen et al. and Green et al. as a method of simulating the time-consuming laboratory-scale physical distillation "TBP" procedure by using GC. The SimDist technique is based on the fundamental assumption that individual nonpolar hydrocarbon component of a sample elute in the order of their boiling points from a GC column coated with nonpolar (hydrocarbon-like), stationary phase. The elution, or retention, time is dependent upon vapor pressure of the component and its affinity for the stationary phase. This varies with different types of hydrocarbons. For example, aromatic hydrocarbons and cycloalkanes (naphthenes) generally elute earlier than n-alkanes having the same boiling points. In SimDist, conditions are selected to give limited column efficiency and resolution unlike other chromatography techniques, which generally aim for highly efficient conditions that achieve high-resolution separation of components. The lower resolution analysis conditions provide distillation data that agree with physical distillation. SimDist became an ASTM standard method in 1973, with the designation D2887, "Boiling Range Distribution of Petroleum Fractions by GC". The current edition is designated D2887-97. This method applies to the determination of the boiling range distribution of petroleum products and fractions having a final boiling point (FBP) of 538 °C (1000 °F) or lower at atmospheric pressure.

HTSD is a relatively recent method which extends ASTM D2887 determination of the boiling range distribution of hydrocarbons to a FBP of about 750 °C (1382 °F). Technological advances in capillary GC columns and stationary phases together with

either programmed temperature vaporization (PTV) or on-column injection techniques, provide adequate separation from C5 to C120 normal paraffins and allows the characterization of petroleum products from about 36–750 °C (97–1382 °F). Under the special conditions of HTSD, elution of materials from the GC column occurs at up to 260–316 °C (500–600 °F) below their atmospheric equivalent boiling point (AEBP). For instance, the elution of C110 (AEBP of 735 °C or 1355 °F) occurs at a column temperature of about 427 °C (800 °F). Also under these conditions, little or no evidence of cracking is normally seen in HTSD. Precise yield correlations between HTSD and crude assay distillation (a procedure which uses methods ASTM D2892 and D5236.) have allowed HTSD to be successfully used in place of physical distillation procedures. SimDist methods are now becoming more widely used in characterizing hydrocarbons and heavy oil system.

For the purpose of this study, HTSD was performed on maltene fractions of the Athabasca bitumen to characterize bitumen fractions for equation of state modeling. This test was performed by the In-situe Combustion Research Laboratory at the Department of Chemical and Petroleum Engineering at the University of Calgary. Carbon disulphide (CS₂) was used as the carrier solvent. The test duration was 25 min. The tests were performed up to a maximum temperature of 629°C to prevent damage to the GC column. Figure 3-4 shows the resulting true boiling assay for the maltene sample.

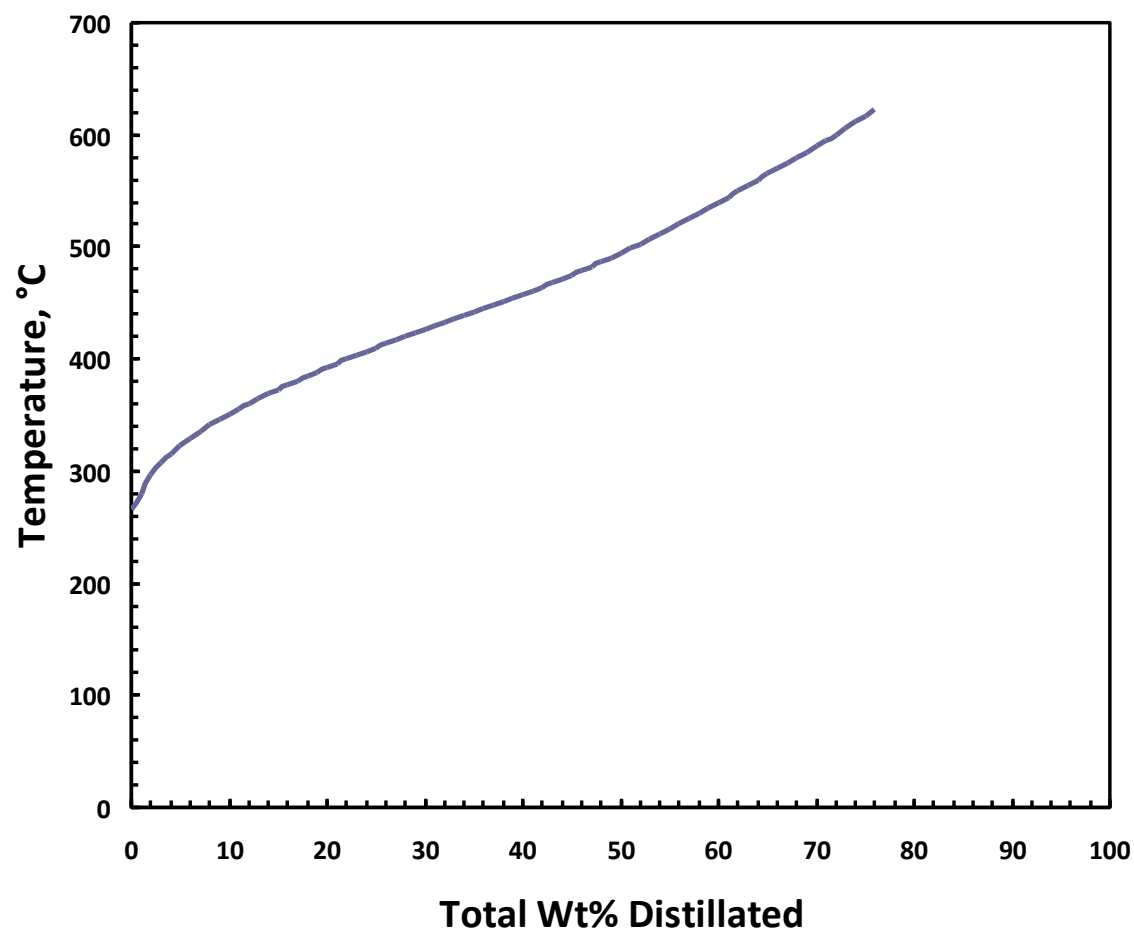


Figure 3-4. Athabasca Maltene True Boiling Point Distribution curve from Sim. Dist. ASTM D2887 extended analysis.

3.4. Molecular Weight Measurements

Several methods have been used for petroleum fractions molar mass determination. These can be divided into absolute methods that yield the absolute molar mass without the use of any standard and relative methods that require calibration with a material of known molecular weight. Molecular weight determination methods are also classified into those that give an average value (number or mass average) and those that give a

complete distribution. In the category of absolute methods, membrane osmometry, cryoscopy, eulliometry and light scattering measure the average molar mass while equilibrium ultracentrifuge measures the molecular weight distribution. In the category of relative methods, vapor pressure osmometry (VPO) measure the average molar mass and gel permeation chromatography (GPC) measures the molecular weight distribution. Among these methods, VPO and GPC have been extensively used because relative methods requiring calibration are generally easier and faster than absolute methods.

VPO on the other hand is a popular technique, as it appears to accurately measure the number-average molar mass under the correct set of temperature and solvent conditions. This technique was used to collect average molar mass data of Athabasca bitumen and maltene in ultra-pure toluene solvent, and at specific temperature and solute concentrations.

3.4.1. Description and Operation of the Vapor Pressure Osmometer (VPO)

Vapor Pressure Osmometry (VPO) is a technique based on the difference in vapor pressure between a pure solvent and a solution. The vapor pressure difference is manifested as a temperature difference, which can be measured very precisely with thermistors. When calibrated with a suitable standard material, the temperature difference can be converted to a molar concentration and thus to molecular weight. The theory is described in detail in the forthcoming section. A Model 833 VPO from Jupiter Instrument

Company was used. This osmometer has a detection limit of $5 \times 10^{-5} \text{ kmol/m}^3$ when used with toluene or chloroform.

A VPO consists of two thermistors in a temperature-controlled chamber containing saturated solvent vapor, as shown in Figure 3-5. Two thermistors are placed in the measuring chamber with their glass-enclosed, sensitive bead elements pointed up. Small pieces of fine stainless steel screen are formed into “caps” that are placed over the thermistors to hold a small volume of liquid on each bead. These thermistors are connected in an AC bridge. The voltage difference between the thermistors is measured with a synchronous detector system.

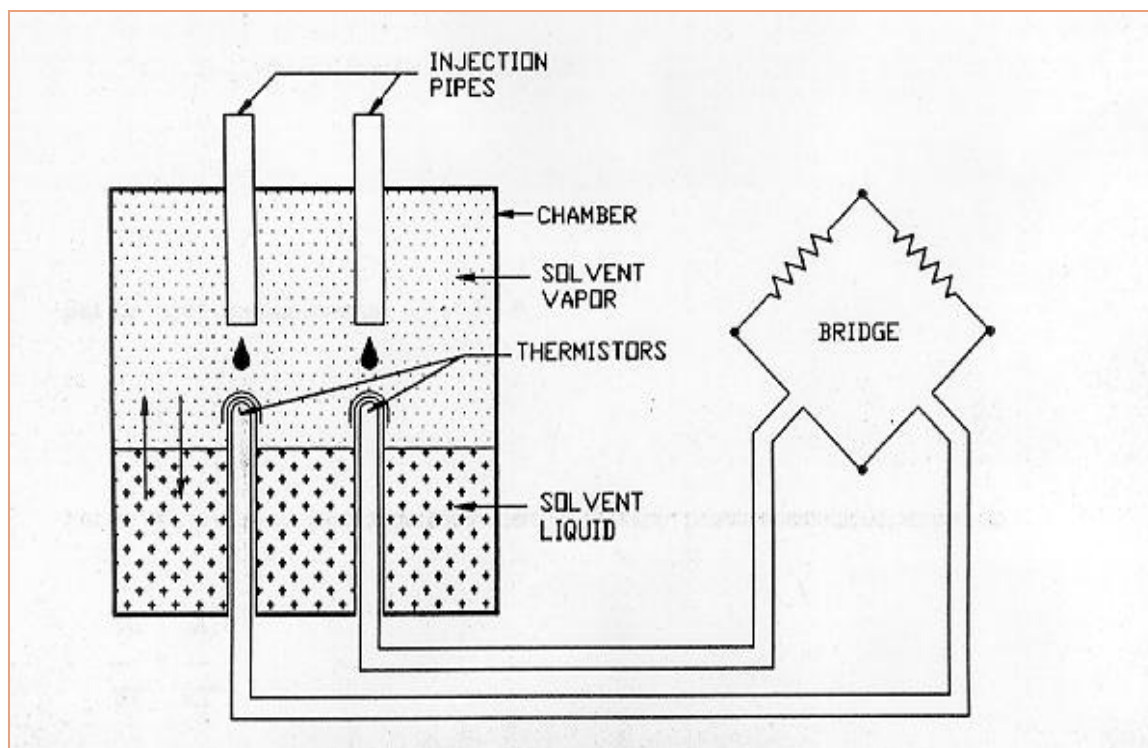


Figure 3-5. Schematic of Vapor Pressure Osmometer (VPO)

The chamber contains a reservoir of pure solvent and two wicks to provide a saturated solvent atmosphere around the thermistors. Temperature is controlled by a closed loop control system to maintain a stable, uniform chamber temperature. Under these conditions, if pure solvent is placed on both thermistors, they will be at the same temperature and the bridge can be adjusted to zero to establish a “reference” condition.

If the pure solvent on one thermistor is then replaced by a solution, condensation into the solution from the saturated solvent atmosphere will proceed due to lower vapor pressure of the solution. But solvent condensation releases heat, so this process will warm the thermistor. In principle, condensation will continue until the thermistor temperature is raised enough to bring the solvent vapor pressure of the solution up to that of pure solvent at the surrounding chamber temperature. Thus a temperature difference will be attained between the two thermistors, which is directly related to the vapor pressure of the solution. If the solute concentration is known, this temperature difference can be used to calculate the molecular weight of the solute as follows (Peramanu et al., 1999):

$$\frac{\Delta V}{C_2} = \frac{K_0}{M_{app}} = K_0 \left(\frac{1}{M_2} + A_2 C_2 + A_3 C_2^2 + \dots \right) \quad (3-1)$$

where M_{app} is the apparent molecular weight of the solute and A_i are the coefficients. Most solutes form nearly ideal solutions with the solvent at low concentrations and it is sufficient to include only the first power of concentration in Equation 3-1. Hence,

experimental data can be fit to a straight line for extrapolation to a zero concentration as follows:

$$\frac{\Delta V}{C_2} = \frac{K_0}{M_{app}} = K_0 \left(\frac{1}{M_2} + A_2 C_2 \right) \quad (3-2)$$

Note that a plot of $\Delta V/C_2$ versus C_2 gives a straight line with a slope of $K_0 A_2$ and an intercept of K_0/M_2 . For an ideal system, a plot of $\Delta V/C_2$ versus C_2 gives a line of a constant value of K_0/M_2 .

The VPO was first calibrated using sucrose octaacetate ($M = 678.6$ kg/kmol) in ultra pure toluene at 50°C . The calibration curves are shown in Figure 3-6, where the VPO response, $\Delta V/C_o$ is plotted versus the concentration of sucrose, C_o . A straight line was obtained and the instrument constant was calculated from the intercept. The value of 4313 mV-litre/mol was found for the constant.

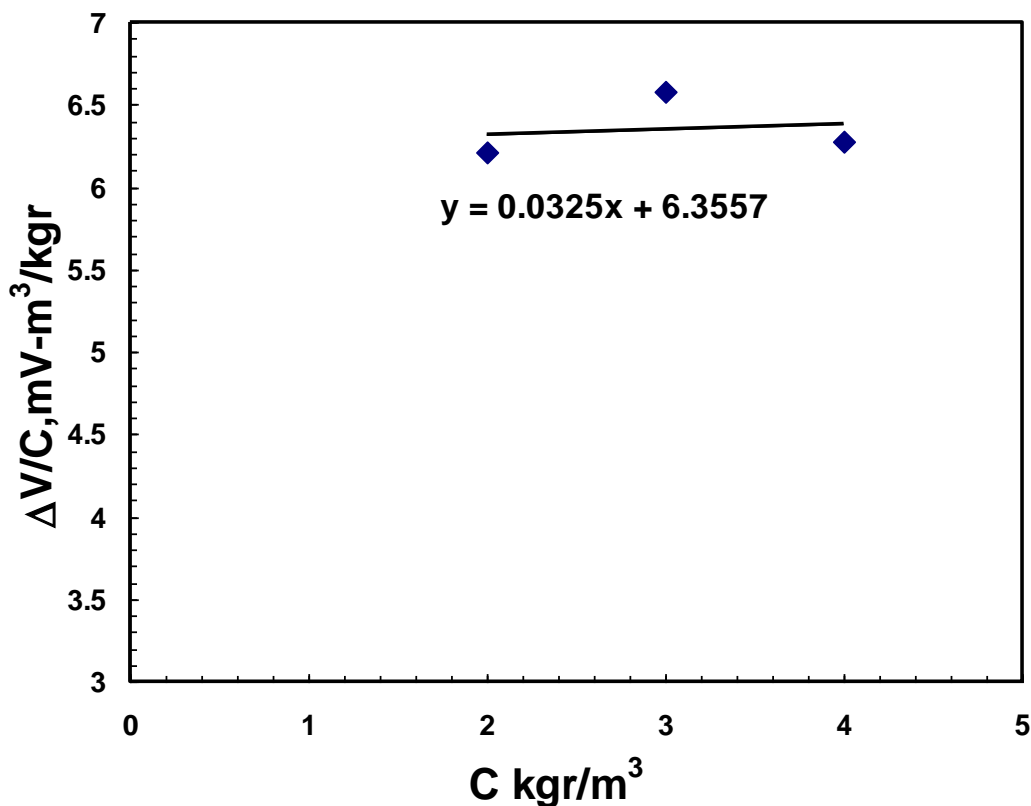


Figure 3-6. VPO calibration curve with sucrose octaacetate in toluene at 50°C.

Once the instrument constant, K_0 , was obtained apparent molecular weight for the Athabasca bitumen, and maltenes fraction were measured. With a nearly constant VPO response, as shown in Fig. 3-6, 3-7, and 3-8 a truncated form of Equation 3-2 was used to calculate the apparent molar mass, for bitumen, and maltenes.

$$M = \frac{K_0 C_s}{\Delta V} \quad (3-3)$$

The Athabasca bitumen molecular weight was determined to be 552 kg/kmol which compares well with the literature value of 557 g/mol (Peramanu et al, 1999). The measured molecular weight for the maltenes was 510 kg/kmol.

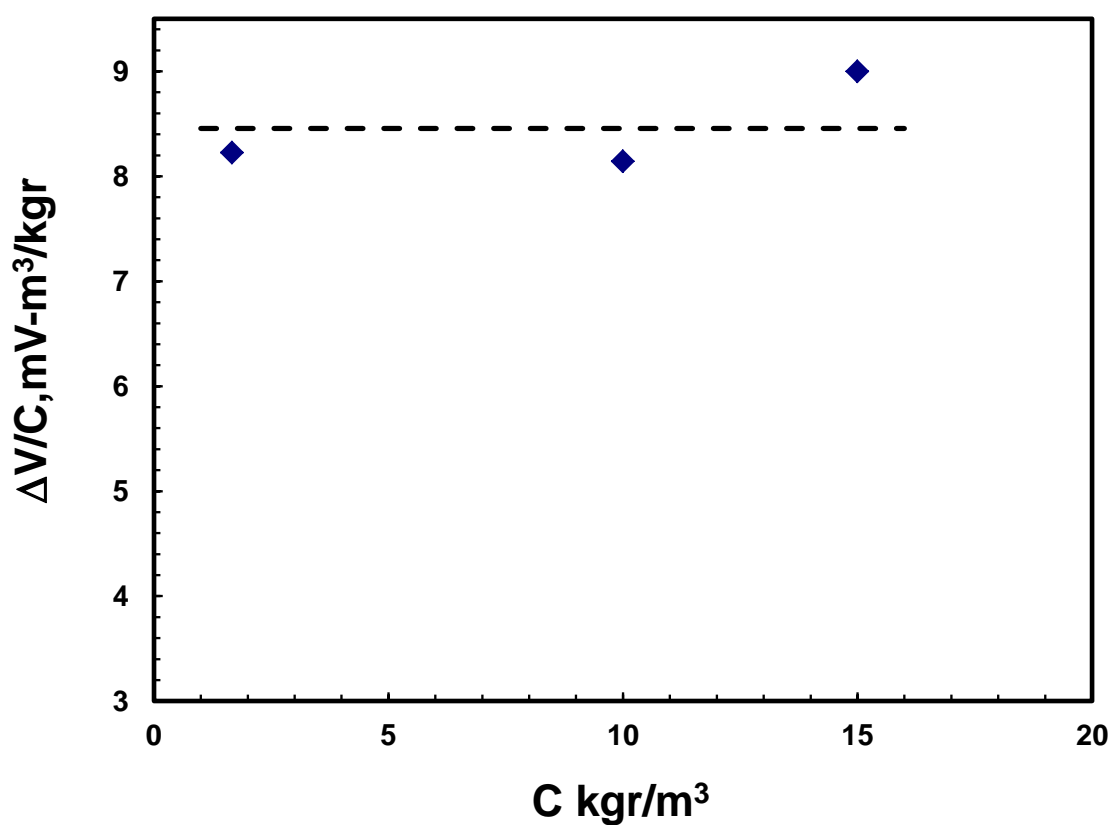


Figure 3-7. VPO molecular weight measurement for Athabasca maltenes in toluene at 50°C.

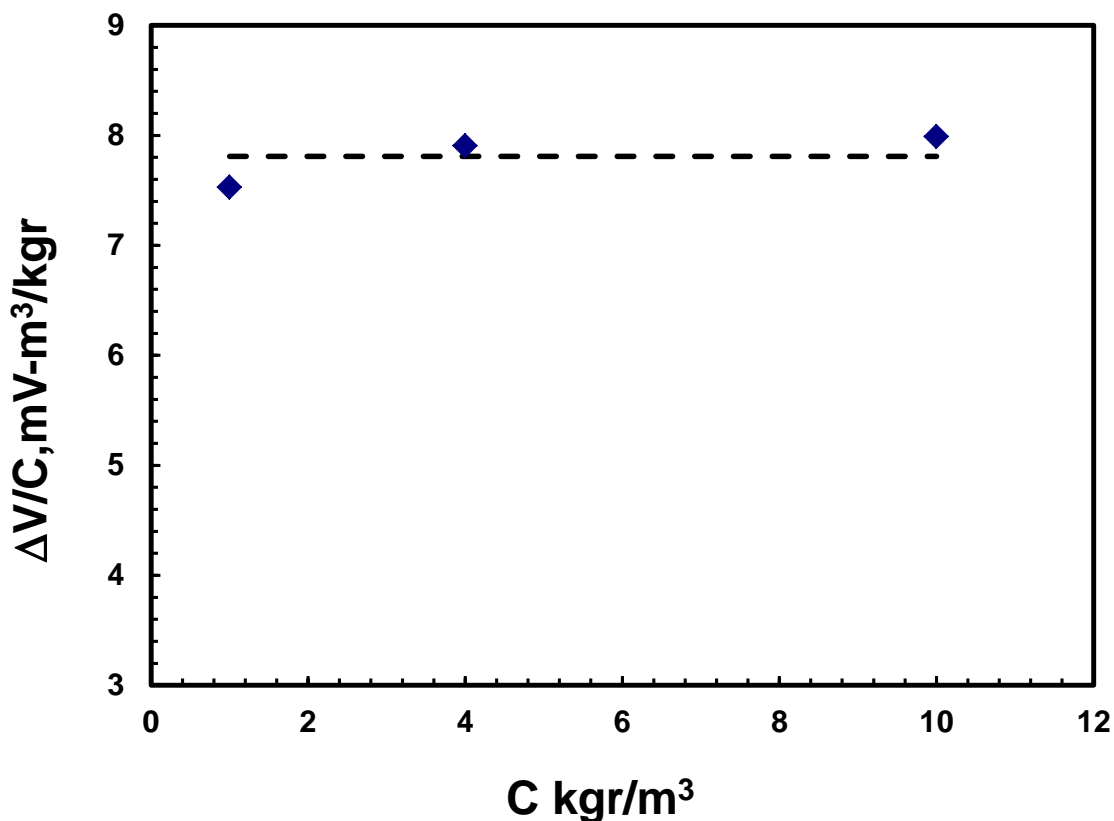


Figure 3-8. VPO molecular measurement for Athabasca bitumen in toluene at 50°C.

3.5. Density Measurement

3.5.1. SARA Fraction Densities

Densities of SARA fractions were measured with an Anton Paar DMA 46 density meter calibrated with demineralised water and air, resulting in measurements accurate to within $\pm 0.5 \text{ kg/m}^3$. The density measurements were made at room conditions, 22°C and 90 kPa.

The density of saturates, and aromatics can be measured directly; however, densities were calculated indirectly from the densities of mixtures of each SARA fractions in toluene.

The density is determined indirectly from a plot of the inverse mixture density (specific volume) versus each SARA mass fraction, as follows:

$$\frac{1}{\rho_M} = \frac{1}{\rho_T} + \left(\frac{1}{\rho_A} - \frac{1}{\rho_T} \right) w \quad (3-4)$$

$$\rho_A = \frac{1}{S + I} \quad (3-5)$$

where ρ_M , ρ_T and ρ_A are the mixture, toluene and average densities (kg/m^3) respectively, and w is the weight fraction of each SARA fraction. S and I are the slope and intercept of the inverse mixture density (specific volume) plot versus weight fraction, respectively.

3.5.2. Athabasca Bitumen Density Measurement at Elevated Pressure and Temperature

An Anton Paar DMA 5000 density meter equipped with a DMA 512P external high pressure unit was employed to measure the density of the liquids. The external unit was calibrated using nitrogen and distilled water for pressures from 779 to 6900 kPag (100 to 1000 psig) and temperatures between 10 and 50°C. The density measurements are precise to $\pm 0.5 \text{ kg/m}^3$. The detail procedure to calibrate Anton Paar DMA 512P external cell is explained in the Anton Paar user manual. Fig. 3-9 and 3-10 shows the accuracy of the calibration and compares the measured density with literature data for densities of water, and predicted densities for N_2 using the Peng Robinson equation of state.

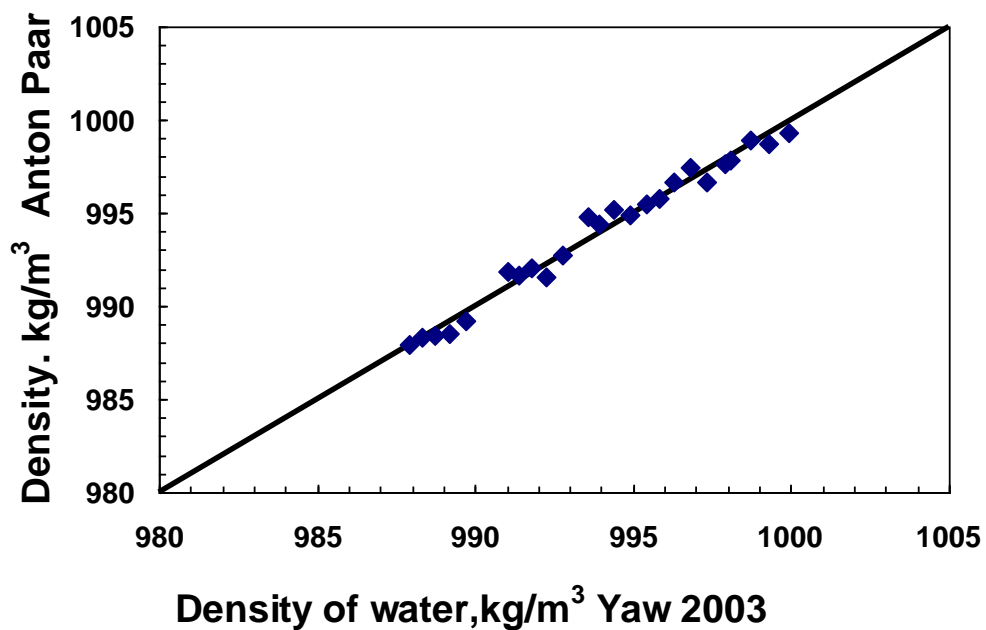


Figure 3-9. Anton Paar DMA 512P external cell density calibration result for water.

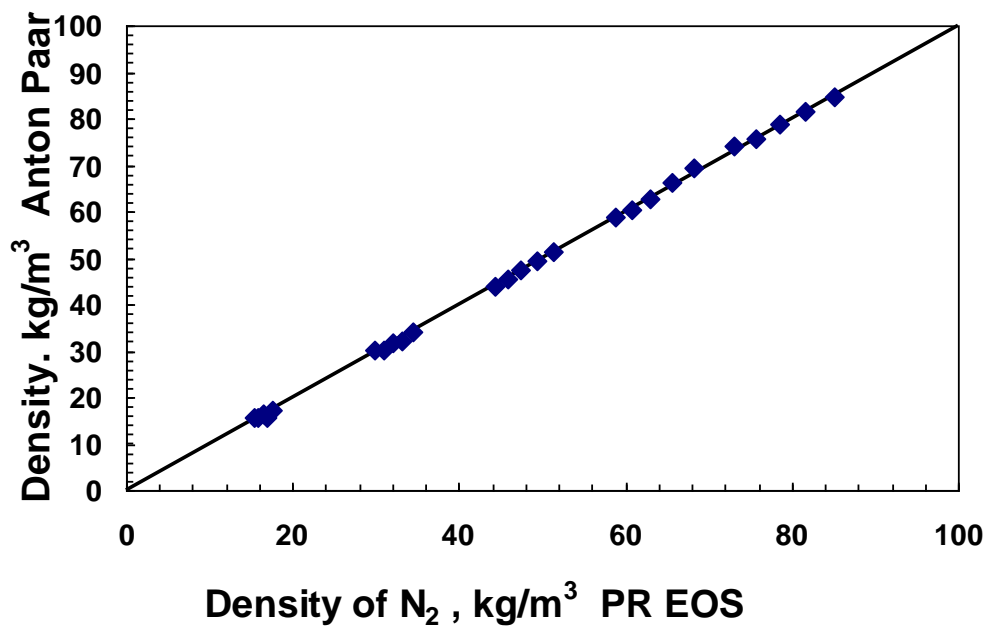


Figure 3-10. Anton Paar , DMA 512P external cell Density result for nitrogen.

The calibrated Anton Paar DMA 512P external density meter was used to measure the density of the Athabasca bitumen at temperatures between 10-50°C, and three different pressures of 90, 1468, 3536kPa. The bitumen was preheated and displaced directly to the density meter. The pressure was controlled to within ± 7 kPa with the pump. The temperature was controlled within ± 0.1 °C, by circulating water around the density meter cell.

3.6. Athabasca Bitumen Viscosity Measurement

A ViscoPro2000 Cambridge viscometer was used to measure the viscosity of the liquid phases in this study. Figure 3-11 shows a detail schematic of the ViscoPro2000 measurement cell. The viscosity measurement is based on a simple electromagnetic concept. Two coils move a piston back and forth magnetically at a constant force. Proprietary circuitry analyzes the piston's two-way travel time to measure the absolute viscosity.

In a flowing system, a deflector, positioned over the piston, moves fluid into the measurement chamber. This feature, coupled with the constant piston motion, keeps the sample fresh and mechanically scrubs the chamber. A built-in temperature detector (RTD) senses actual temperature in the measurement chamber.

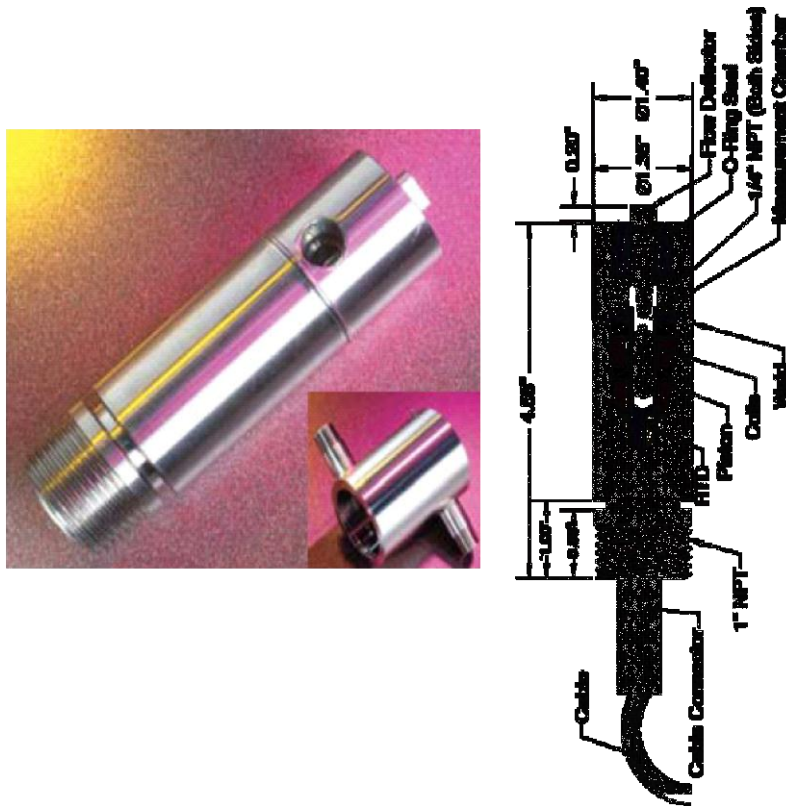


Figure 3-11. Cambridge in-line viscometer ViscoPro 2000 flow through measurement cell. Courtesy of www.Cambridgeviscosity.com.

The sensor comes with a removable jacket which can be plumbed with a separate flow line for temperature control of sample material. In this study the temperature of this device was controlled to within $\pm 0.1^{\circ}\text{C}$ using an external water bath, which circulated the bath water through the external shell. In addition for viscosity measurement over a wide temperatures range (i.e. -15 to 190°C), the viscometer was placed in an air bath, and the temperature was controlled to within $\pm 0.1^{\circ}\text{C}$.

Measurements can be made in 13 different viscosity ranges within an overall span of 0.2 to 20,000 mPa.sec. For each range of measurement a specific piston was required. The piston in this study was for 5-100 mPa.s. Hence viscometer was calibrated in the 5-100 mPa.s range and is precise to ± 2 mPa.s. The recommended flow rate over the sensor head is 0.5 to 1.0 ft/sec. The maximum operating limits of the viscometer are 6900 kPa abs and 190°C.

3.7. Phase Behavior Measurements

The phase behaviour measurements are described for mixtures of bitumen and propane. Variations in the procedure for bitumen/carbon dioxide and bitumen/propane/carbon dioxide mixtures are described afterwards.

3.7.1 Apparatus

The experiments were carried out in a DB Robinson Jefri PVT cell, shown schematically in Figure 3-12. The main component of the apparatus is a transparent sapphire cylinder enclosed in pressurized hydraulic fluid. The cell is equipped with a magnetic mixer and a floating piston. A cell window provides a view of the total cell volume. The volume of the fluid inside the cell was determined from fluid level measurements obtained with a calibrated cathetometer sited through the cell window. The cathetometer is precise to $\pm 0.1 \cdot 10^{-7} \text{ m}^3$. The maximum capacity of the PVT cell is 100 cm^3 . It can operate up to 69 MPag and at temperatures from -15°C to 200°C. The cell is contained in an air bath and the temperature was controlled to within $\pm 0.1^\circ\text{C}$.

The PVT cell was equipped with in-line viscosity and density meters. The temperature of these devices was controlled to within $\pm 0.1^\circ\text{C}$ using an external water bath, which circulated the bath water through their external shells. A ViscoPro2000 Cambridge Viscometer was used to measure the viscosity of the liquid phases displaced from the PVT cell. The operating limits of the viscometer are 6,900 kPa abs and 190°C . It was calibrated in the 5 to 100 mPa.s range and is precise to ± 0.2 mPa.s. An Anton Paar DMA 5000 density meter equipped with a DMA 512P external high pressure unit was employed to measure the density of the displaced liquids. The external unit was calibrated using nitrogen and water for pressures from 690 to 6,900 kPag (100 to 1,000 psig) and temperatures between 10 and 50°C . The density measurements are precise to ± 0.5 kg/m³.

A pycnometer (11 ± 0.1 cm³ at 20°C) was used to take a sample of saturated liquid and measure its density. A Jefri 10 litre gasometer was used to measure the amount of the gas dissolved in the sample. An Agilent Micro GC 3000 was employed for compositional analysis of the vapour phase. This GC was also connected to the gasometer to analyze the composition of the gas that was dissolved in heavy oil.

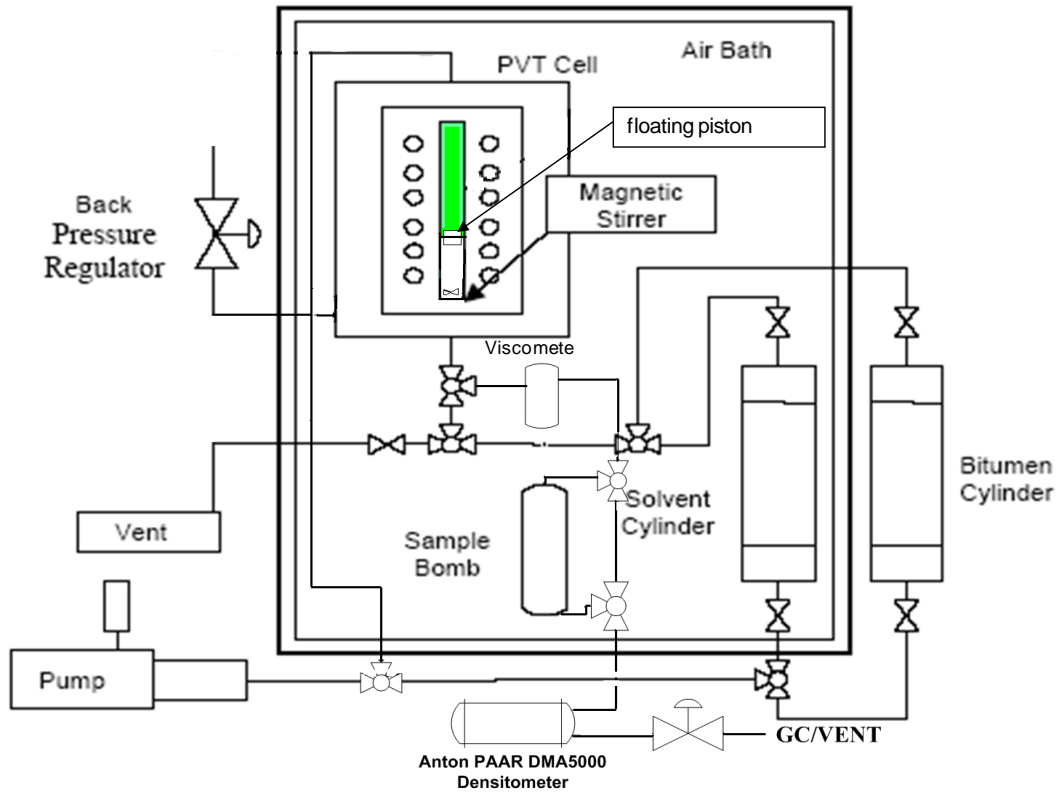


Figure 3-12. Schematic of PVT cell, and experimental setup.

3.7.2 Methodology for Mixtures of Propane and Bitumen

Measurements were taken for Athabasca bitumen alone and for mixtures of bitumen and propane. For some calculations, the density and viscosity of liquid propane were required and were determined from the following correlations (Yaw, 2003):

$$\log(\rho_{C_3}) = \log(221.51) - \log(0.27744) \left(1 - \frac{T}{369.82}\right)^{0.287} \quad (3-6)$$

$$\log(\mu_{C_3}) = -3.1759 + \frac{297.12}{T} + 0.0095452T - 0.000018781T^2 \quad (3-7)$$

where ρ is density in kg/m^3 , μ is viscosity in $\text{mPa}\cdot\text{s}$, T is temperature in K , and subscript $C3$ indicates propane. Correlations for the density and viscosity of the Athabasca bitumen sample are described in Chapter 4.

The diffusion and dissolution of propane from the vapor phase into the bitumen was very slow requiring weeks or months to reach equilibrium even when the PVT cell was rocked. In order to accelerate the dissolution process we first mixed the fluids in the liquid phase region. To begin an experiment, a known amount of liquid propane was injected into the cell just above its saturation pressure. The mass was determined from the volume measurement and the propane density (Equation 3-6). Then, a known volume of bitumen was added to the cell at 50°C while the pressure was maintained so that all of the system was in the liquid phase. The volumes were determined from two independent measurements: 1) from the pump displacements; 2) from the cathetometer readings. The mixture was stirred during fluid injection to the PVT cell and for 2 hours after injection to enhance mixing. The mixer was turned off during volume measurements, and was used to accelerate equilibration at a given test condition.

For a given composition, the saturation pressure was determined at several temperatures through constant composition expansion test (CCE). After the saturation measurements, the pressure was increased to bring the system back to a single liquid phase. The liquid was then displaced to the in-line viscometer and density meter where the viscosity and density were measured at the previously obtained bubble point conditions. During this

displacement a sample at one saturation condition was recovered in the pycnometer for density and composition measurements.

The composition measurements for each trial are presented in Table 3-1. The pump and cathetometer readings were taken when the fluids were injected into the cell. The pycnometer based composition was determined from mass measurements on a sample before and after degassing. The gasometer based composition is based on the volume of gas recovered and the measured mass of bitumen in the sample. The measurements are all within 5% (± 0.5 to 1 wt%) of each other. The pycnometer and gasometer are expected to be less accurate than the other measurements because the samples may have contacted residual bitumen in the dead volume between the PVT cell and the pycnometer. Also, these samples would not be representative if a second liquid phase existed in the PVT cell, for example at high propane contents. The pump displacement measurements are expected to be less accurate than the cathetometer measurements because the pump pressure is not constant during the injection. All compositions reported below are based on cathetometer measurements.

The constant composition expansion (CCE) was performed to measure the saturation pressure. The first step was to identify the approximate pressure and volume at the bubble point. Starting from a high pressure, well above the bubble point, the pressure was gradually decreased by expanding the cell volume at a rate of approximately 3 cm³/h. The volume inside the cell was measured at constant time intervals. The specific volume was determined from the volume measurements and the known mass of fluid in the cell. Then,

pressure was plotted versus specific volume as shown in Figure 3-13. Pressure decreases significantly in the liquid phase region but very little or not at all once a vapor phase appears. Hence, the bubble point is identified by the change in slope of a pressure-specific volume plot. The continuous expansion method is only approximate because there is insufficient time for the system to equilibrate. The fluid tends to remain supersaturated during the continuous expansion and the bubble point cannot be determined accurately.

Table 3-1: Comparison of composition measurements.

Trial	Propane Content, wt%			
	Pump	Cathetometer	Pycnometer	Gasometer
1	5.0	5.2	4.7	4.8
2	10.2	10.1	-	-
3	10.4	11.0	-	-
5	15.6	15.2	-	-
4	15.6	15.6	-	15.3
6	22.5	21.4	23.4	23.1
7	25.2	25.5	-	-
8	25.5	26.1	-	24.1

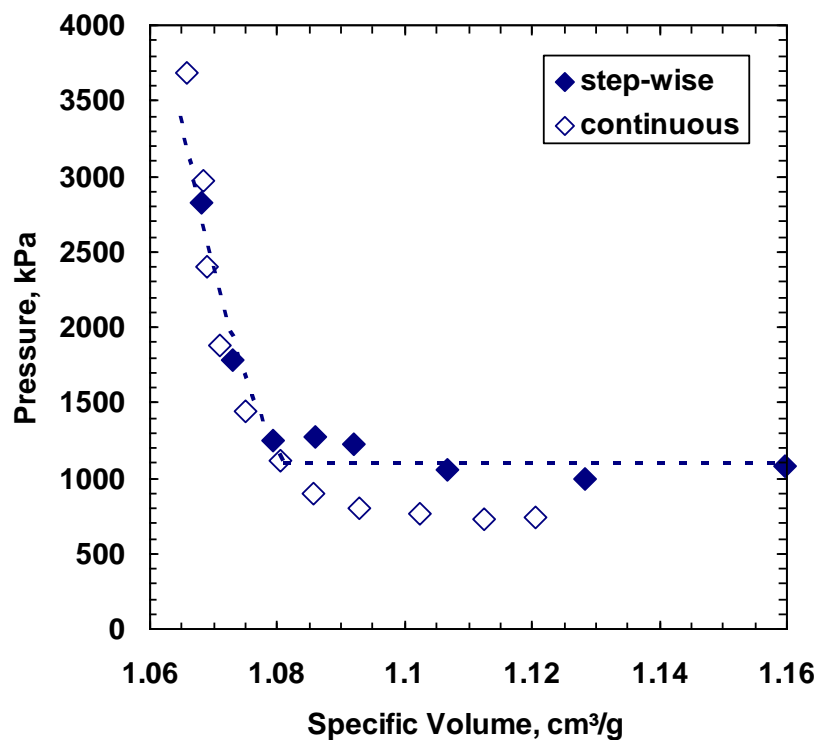


Figure 3-13: Continuous and step-wise pressure volume isotherms for 5.2 wt% propane in Athabasca bitumen at 60°C.

In order to obtain a more accurate saturation pressure, the fluid was compressed and re-equilibrated at a pressure well above the bubble point. The pressure was again decreased but with a step-wise volume expansion. After each step, sufficient time was allowed until the pressure was stable for 4 to 5 hours. In general, 12 hours was sufficient in the single liquid phase region. The amount of time needed to reach equilibrium increased to as much as 48 hours as the saturation pressure was approached. Figure 3-13 shows the results for a continuous and step-wise expansion test for 5.2 wt% propane at 60°C. In this

case, the solubility of the propane in bitumen at the test temperature and measured saturation pressure is simply the initial composition of the fluid in the cell.

Unfortunately, there was no means to check the accuracy of the propane-bitumen saturation pressure data directly. In order to test the saturation pressure measurement method, the vapor pressure of pure propane was measured at several conditions and compared with values obtained from a correlation (Perry, 7th Ed), Equation 3-8.

$$\ln(P_{C3}^{vap}) = 59.078 - \frac{3492.6}{T} - 6.0669 \ln(T) + 1.0919E - 5 \times T^2 \quad (3-8)$$

where, T is in the range of 85 - 369.0 K, and P is propane vapor pressure in Pa. The saturation pressures measured by the step-wise method are within 0.7% of the correlated values. Table 3-2 shows that the continuous tests are less accurate even in case of a pure and less viscous component like propane.

Table 3-2: Vapor pressure of pure propane compared with correlation values.

Method	Temperature (°C)	Measured Pv (kPa)	Perry, 7 th Ed. Pv (kPa)	Relative Error (%)
step-wise	9.9	640	636	0.7
continuous	10.0	634	638	0.6
continuous	21.0	835	860	2.9
step-wise	21.0	855	860	0.6
continuous	49.8	1617	1708	5.3
step-wise	50.1	1730	1717	0.7

3.7.3 Methodology for Mixtures of Bitumen, Carbon Dioxide, and Propane

Measurements were taken for two fluid systems: 1) bitumen and carbon dioxide, 2) bitumen, carbon dioxide, and propane. The methodology for each fluid system is described below. For some calculations, the density or viscosity of the liquid solvent was required and was determined from the following correlations (Yaw, 2003):

$$\rho_{CO_2} = 463.82 + 0.2616 \times \left(- \left(1 - \frac{T}{304.19} \right)^{0.2903} \right) \quad (3-9)$$

$$\log(\mu_{CO_2}) = -19.492 + \frac{1594.8}{T} + 0.0793T - 0.00012025T^2 \quad (3-10)$$

where ρ is density in kg/m³, μ is viscosity in mPa.s, T is temperature in K, and subscript CO_2 indicate carbon dioxide. Equations 3-6 and 3-7 were used for liquid propane properties. Correlations for the density and viscosity of propane were provided in Section 3.7.2 and are provided for the Athabasca bitumen sample in Chapter 4.

3.7.3.1. Solubility in Vapor-Liquid Region:

The solubility of CO₂ in Athabasca bitumen was measured at 25°C and pressures of 3.96 and 6.02 MPa. An excess volume of carbon dioxide vapor phase was charged to cell at a known temperature and pressure. Then, a given volume of bitumen at 50°C was introduced to the cell against a constant back pressure. After bitumen injection, the air bath temperature was set to the desired test temperature, and the desired pressure in the vapour-liquid region was set using the hydraulic pump. The cell was rocked to enhance the mixing between bitumen and CO₂. As the CO₂ dissolved in the bitumen, the vapor phase volume decreased and hydraulic pump displacements were required to maintain the

pressure. The system was assumed to have reached equilibrium when the pressure without further pump displacement was constant for 24 hours.

After equilibration, the saturated bitumen was displaced to the pycnometer and density meter at the test temperature and pressure. Once measuring the mass of the pycnometer, the carbon-dioxide saturated bitumen was opened to the gasometer cylinder and the amount of gas released was measured at room pressure and temperature. The solubility is then the mass of the released gas divided by the mass of the sample. The compositions based on the pycnometer and gasometer measurements are given in Table 3-3. Theoretically, the two methods should result same value for the CO₂ solubility in the bitumen. However each method has potential for experimental error.

Pycnometer Method: The mass of dissolved gas is the difference between the mass of live oil and the amount of dead oil recovered at atmospheric condition in the lab. Once the pycnometer full of live oil sample from experimental condition is brought to room temperature and pressure in the gasometer, the dissolved CO₂ flushes-out of bitumen into the gasometer. The released CO₂ carries some bitumen in the form of bitumen-CO₂ foam to the gasometer liquid trap. Therefore, to determine the dead oil mass, the mass of bitumen left in the gasometer liquid trap, connection lines, and pycnometer were all measured. The mass of bitumen left in the gasometer connection lines was obtained by cleaning the line with toluene. There could be an accumulation of error from all the mass measurements.

Gasometer Method: The CO₂ solubility from the gasometer was calculated from the measured volume of released gas at room temperature and pressure. There could be a

small error due to the volume of gas in the gasometer's connection lines (dead-volume). Therefore the average of the two measurements was used for any results discussed below.

Table 3-3: Saturation condition of carbon dioxide in Athabasca bitumen at 24.9°C.

Pressure (kPa)	Carbon dioxide wt%	
	pycnometer	gasometer
6017	12.0	11.1
6017	11.1	10.1
6017	10.3	9.9
3953	6.6	5.4
3957	5.6	5.6

3.7.3.2. Phase Boundaries:

The phase boundaries were investigated for a global composition of 18 wt% carbon dioxide in bitumen – carbon dioxide binary mixture. A known amount of carbon dioxide was injected to the cell at 20°C, just above its saturation pressure. The mass was determined from the volume measurement and the carbon dioxide density (Equation 3-9). Then, a known volume of bitumen was added to the cell at the same temperature and pressure. The volumes were determined from two independent measurements: 1) from the pump displacements, and 2) from the cathetometer readings. The composition was determined from an average of the two readings.

This binary mixture exhibited liquid-liquid-vapor phase behavior. The L-L/L-L-V/L-V phase boundaries were identified at several temperatures, 10, 20 and 25°C. At each

temperature, the mixture was compressed to a pressure well above the L-L-V boundary. For all the temperatures, two liquid phases were observed at these high pressures. A stepwise method was used to delineate the phase boundaries. The pressure was decreased stepwise by expanding the cell volume. After each step, sufficient time was allowed until the pressure was stable for 4 to 5 hours. Then the volume of each phase was measured with the cathetometer. Figures 3-14 and 3-15 show the phase volumes at each pressure steps for test at 20°C.

The phase regimes were also investigated at one supercritical carbon dioxide temperature, 40°C and pressures up to 11 MPa. The volumes of each phase at each condition are provided in Table 3-7. The dense liquid phase composition was determined when only V-L phases were present. The mass of carbon dioxide in the dense liquid phase was determined from the difference between the initial mass of carbon dioxide and the mass of carbon dioxide in the second phase (vapour). The latter mass was calculated from the volume of the phase (measured with the cathetometer) and its density. Peng - Robinson EoS was used for vapour phase density, assuming pure carbon dioxide is only component in this phases. The mass of bitumen was known and so the composition can be calculated. Compositions based on the initial mass of carbon dioxide from cathetometer and pump displacement measurements are given in Table 3-7. There is uncertainty in both the cathetometer and the pump displacement measurement; the cathetometer because there may be a volume change upon mixing carbon dioxide and bitumen and the pump displacement because the pump pressure was not constant during the injection. Therefore, an average composition was used in all cases.

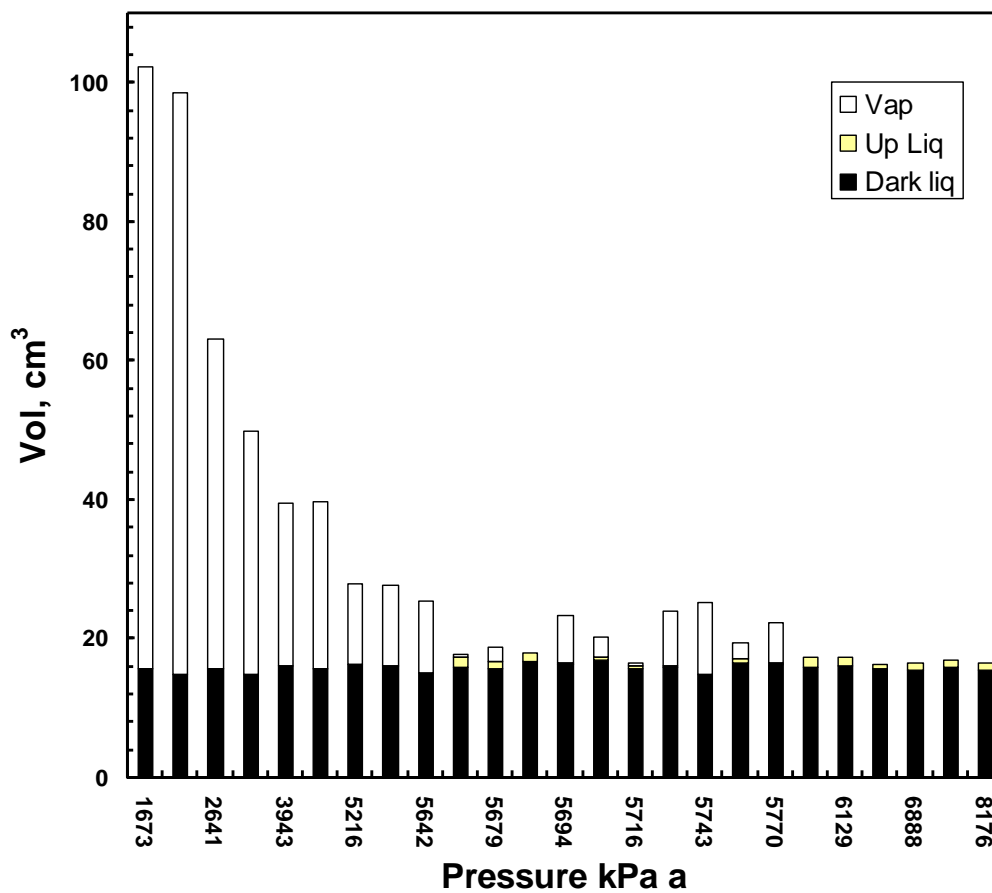


Figure 3-14: LLV – VL phase boundaries at 20°C for 18wt% CO₂ blend in Athabasca bitumen.

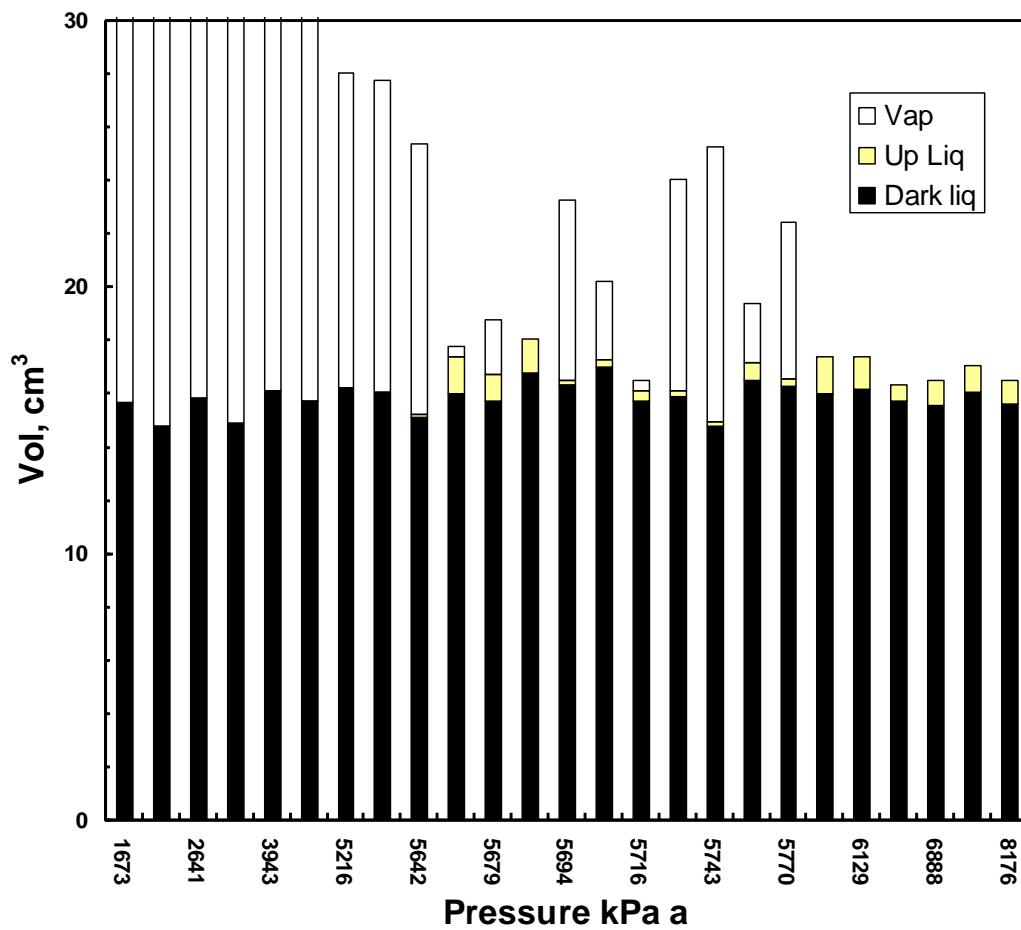


Figure 3-15: Second liquid phase formation at 20°C and high pressure with 18wt% CO₂ in bitumen.

Table 3-4: Phase regimes for 18wt% carbon dioxide in Athabasca bitumen.

Temperature (°C)	Pressure (kPa)	Total Cell Vol cm3	Lower Liquid (vol fr)	Upper Liquid (vol fr)	Vapour (vol fr)	Lower Liquid Composition	
						cathetometer (wt% CO2)	pump (wt% CO2)
9.8	5339	17.05	0.965	0.035	0	-	-
10.0	4562	16.99	0.964	0.036	0	-	-
20.3	8176	16.53	0.946	0.054	0	-	-
19.9	7252	17.06	0.941	0.059	0	-	-
20.2	6888	16.51	0.943	0.057	0	-	-
20.0	6355	16.37	0.963	0.037	0	-	-
20.0	6129	17.40	0.930	0.070	0	-	-
19.9	5993	17.39	0.923	0.077	0	-	-
25.5	6988	16.92	0.963	0.037	0	-	-
25.4	6468	17.08	0.948	0.052	0	-	-
25.2	6437	17.20	0.944	0.056	0	-	-
9.7	4549	17.69	0.922	0.042	0.037	-	-
10.0	4536	17.61	0.933	0.028	0.039	-	-
20.1	5770	22.43	0.727	0.011	0.262	-	-
20.0	5758	19.41	0.850	0.037	0.113	-	-
20.0	5743	25.31	0.585	0.006	0.409	-	-
20.1	5719	24.04	0.663	0.008	0.329	-	-
19.8	5716	16.54	0.952	0.025	0.023	-	-
19.9	5694	20.23	0.841	0.015	0.144	-	-
19.9	5694	23.31	0.701	0.007	0.291	-	-
19.8	5679	18.82	0.836	0.055	0.109	-	-
19.9	5675	17.81	0.901	0.077	0.022	-	-
20.0	5642	25.38	0.596	0.004	0.400	-	-
22.1	5762	24.66	0.613	0.006	0.381	-	-
25.0	6455	18.56	0.882	0.020	0.097	-	-
25.0	6438	17.47	0.932	0.052	0.016	-	-
25.1	6424	19.97	0.813	0.006	0.180	-	-
9.9	4521	22.81	0.711	0	0.289	13.70	11.68
9.7	3250	41.91	0.374	0	0.626	7.27	4.76
9.8	2464	56.34	0.277	0	0.723	6.32	3.74
10.0	1523	95.26	0.155	0	0.845	4.70	1.99
20.1	5228	27.77	0.579	0	0.421	8.71	6.32
20.0	5216	28.04	0.580	0	0.420	8.67	6.28
20.0	3943	39.67	0.406	0	0.594	6.18	3.59
20.1	3140	49.98	0.299	0	0.701	5.01	2.32
19.8	2641	63.14	0.251	0	0.749	3.70	0.90
20.1	1699	98.59	0.150	0	0.850	2.76	-
19.9	1673	102.33	0.153	0	0.847	2.45	-
25.0	3987	39.42	0.403	0	0.597	6.55	3.98
25.0	3924	39.34	0.401	0	0.599	6.83	4.29
24.9	2150	78.72	0.196	0	0.804	3.40	0.58
24.8	1639	103.47	0.147	0	0.853	2.95	0.08
39.6	10950	16.85	0.980	0	0.020	17.02	15.24
39.6	9639	17.30	0.943	0	0.057	15.35	13.46
39.2	9244	18.09	0.921	0	0.079	14.32	12.35
39.7	4738	36.03	0.445	0	0.555	7.00	4.48
39.6	2417	76.02	0.210	0	0.790	3.20	0.36

3.7.4. Carbon dioxide, Propane, and Bitumen

Three different ternary mixtures were examined: 1) at a composition where only liquid and vapour-liquid regions are expected to form; 2) at a composition in a region where a second dense (asphaltene- rich) phase is expected to form; and, 3) at a composition in a region where a second carbon dioxide-rich liquid phase is expected to form.

Cases 1 and 2

In Cases 1 and 2, a known amount of liquid propane was injected into the cell just above its saturation pressure. The mass was determined from the volume measurement and the propane density. Then, a known volume of bitumen was added to the cell at 50°C while the pressure was maintained so that all of the system was in the liquid phase. Liquid carbon dioxide was then added to the mixture of propane and bitumen already in the cell to make up the desired composition. The mixture was stirred during fluid injection to the PVT cell and for 2 hours after injection to enhance mixing.

No secondary liquid phase was observed and the step-wise method described in Section 3.7.2. was used to find the bubble point pressure at temperatures from 10 to 25°C. Starting from a pressure well above the bubble point, the pressure was gradually decreased by expanding the cell volume at near 3 cm³/h rate. The approximation saturation pressure was determined from the change in slope of a pressure-volume plot. In order to obtain a more accurate saturation pressure, the fluid was compressed and re-equilibrated at a pressure well above the bubble point. The pressure was again decreased, but with a step-wise volume expansion. After each step, sufficient time was allowed until

the pressure was stable for 4 to 5 hours. In general, 4 hours was sufficient in the single liquid phase region. The amount of time needed to reach equilibrium increased to as much as 48 hours as the saturation pressure was approached.

After the saturation pressure measurements, the pressure was increased to bring the system to the liquid phase region. The liquid phase was transferred to the viscometer and density meter. Then the density and viscosity were measured at saturation pressure for each temperature. A sample was also transferred to the pycnometer to determine the composition, and check the density at one condition.

The composition measurements for Case 1 and Case 2 are reported in Table 3-5. The propane compositions from the pump displacement and cathetometer measurements are within 0.5% of each other (± 0.2 to 0.8 wt%). There is less agreement in the carbon dioxide measurements (± 2 wt%). The discrepancy may result from bitumen in the dead volume during the carbon dioxide injection or excess volume changes upon mixing propane, carbon dioxide and bitumen. An average of the pump displacement and cathetometer measurements is used in all of the following results. The pycnometer and gasometer measurements are in reasonable agreement with the propane compositions, but show slightly lower values for carbon dioxide.

It is likely that the samples obtained in the pycnometer were not completely representative, either due to bitumen contamination from the dead volume between the

PVT cell and the pycnometer, or because a second liquid phase was present in the system.

Case 3

Liquid propane was displaced into the PVT cell and the pressure increased to just above the saturation pressure of carbon dioxide. Then, liquid carbon dioxide was displaced into the cell. The composition of liquid solvent was determined from the volume measurements and the pure component densities. The volumes were determined from pump displacements and cathetometer readings. In this case also, there was a discrepancy between the two measurements.

A bubblepoint test was conducted for the solvent mixture and compared with a PR-EoS calculation. The cathetometer-based composition of the solvent (40 wt% propane and 60 wt% carbon dioxide) provided the best match with the measured saturation pressure, which was 3,295 kPa at 10°C. The predicted pressure was 3,248 kPa; within 1.5% of the experimental measurement. Therefore, only the cathetometer measurements were used for this experiment. After the bubble point test, a known volume of bitumen was displaced to the cell at a pressure just above the saturation pressure of the solvent. The final composition is reported in Table 3-5.

Table 3-5: Composition of ternary mixtures of propane (C3), carbon dioxide (CO2), in Athabasca bitumen.

Case	Composition, wt%							
	pump		cathetometer		pycnometer		Gasometer	
	C3	CO ₂	C3	CO ₂	C3	CO ₂	C3	CO ₂
1	13.6	11.5	13.4	10.4	11.8	8.4	12.8	9.1
2	23.6	7.2	24.4	5.2	23.4	4.6	23.4	4.6
3	-	-	13.1	19.2	-	-	-	-

The ternary mixture exhibited liquid-liquid-vapour phase behaviour. Both the L1-L2/L1-L2-V and L1-L2-V/L1-V phase boundaries were identified at several temperatures between 10 and 25°C. At each temperature, the mixture was compressed to a pressure well above the L1-L2-V boundary. For all the temperatures, two liquid phases were observed at these high pressures. The step-wise method was then used to find the L1-L2-V boundary. The pressure was further reduced step-wise to find the pressure at which the upper liquid phase disappeared (L1-V boundary). Then saturated liquid (L1) phase was displaced to the viscometer and density meter at constant temperature and nearly constant pressure and a sample was recovered in the pycnometer. Finally, a sample of the vapour-phase was recovered and its composition was measured with the gas chromatograph.

CHAPTER 4 : PROPERTIES AND PHASE BEHAVIOR OF MIXTURES OF BITUMEN, PROPANE, AND CARBON DIOXIDE

This chapter presents characterization, density, and viscosity data for Athabasca bitumen. Saturation pressure, density, and viscosity data are provided for mixtures of the bitumen with propane and carbon dioxide at typical Canadian heavy oil reservoir temperatures from 10 to 50°C. Analytical correlations developed to fit the experimental results are also presented.

4.1. Bitumen Properties

4.1.1 Characterization

The molecular weight, density, and SARA analysis in weight percent of Athabasca bitumen is compared with literature values in Table 4-1. The molecular weight and density are within 0.5% of the literature values. There is more variation in the SARA analysis which could result from differences in the samples or differences in the procedure. The split between resins and aromatics in SARA analysis is notoriously dependent on operators (Yarranton, 2009). Note that the saturate and asphaltene content measurements are more consistent (less than 2 wt% variation).

The Simdist true boiling point distillation curves for bitumen and maltene fraction are summarized in Figure 4-1. The maltene wt% in bitumen was known from SARA analysis (Table 4-1); therefore, the distillation curve for the bitumen was calculated from the

maltene assay. The bitumen TB curve will be used later to characterize Athabasca bitumen as several pseudo-components.

Table 4-1. Properties and SARA Assay of Athabasca Bitumen at 22°C and 90 kPa.

	This work	Literature*
Molecular Weight (kg/kmol)	552	557
Density (kg/m ³) @20°C	1007.34	1013.97
Saturate (wt %)	19.51	17.27
Aromatics(wt %)	46.97	39.7
Resins(wt %)	17.10	25.75
C5 - Asphaltene (wt %)	16.41	17.28
C7 - Asphaltene (wt %)	11.71	na
Solids (wt %)	0.3	na

* Peramanu et. al. 1999

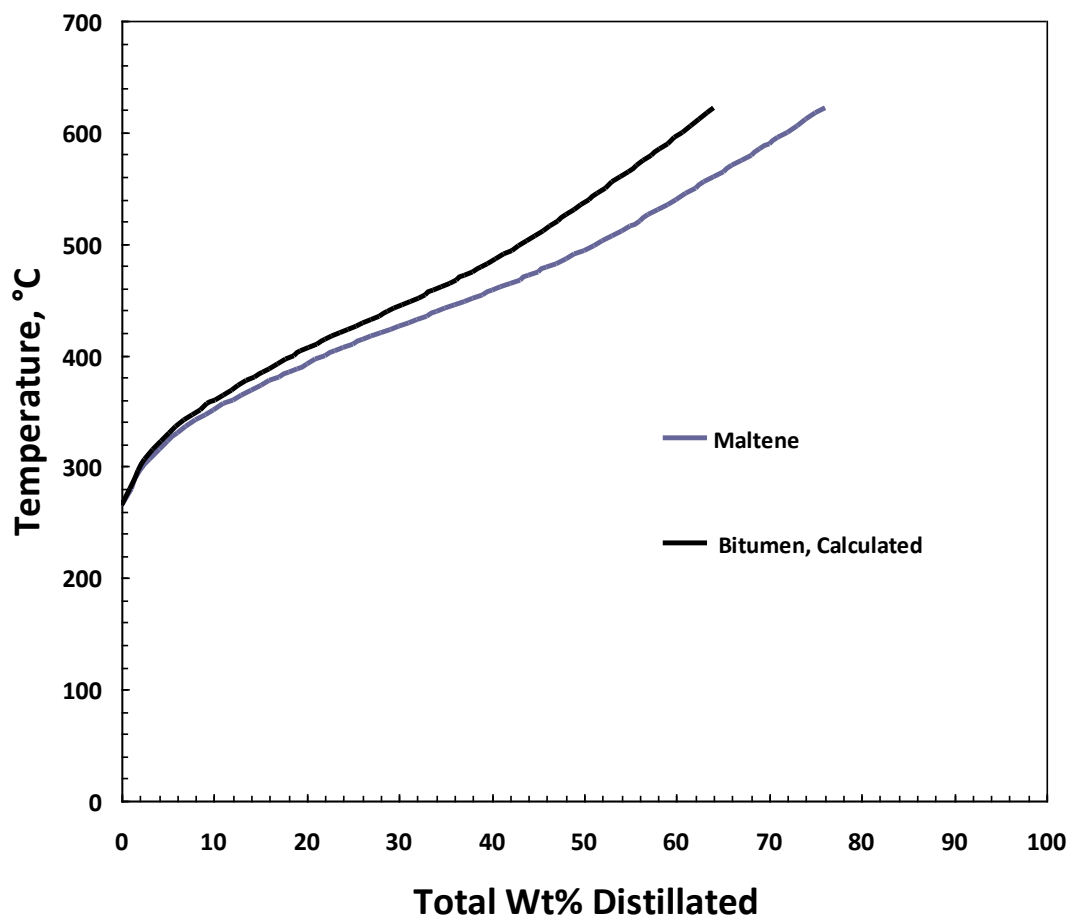


Figure 4-1: Athabasca maltene SimDist data and Athabasca bitumen true boiling point curve calculated from maltene data.

4.1.2 Density Data and Fitting

Measured densities for SARA fractions of Athabasca bitumen are compared to the average values reported for the Western Canadian oils and International oils (Sabbagh et al., 2006) in Table 4-2. The measurements are within 15 kg/m³ of the literature values with the exception of the aromatics which deviate by 34 kg/m³. The deviation may be a result of the different split between resins and aromatics in the SARA assay.

Table 4-2. Athabasca Bitumen's SARA fractions Density (kg/m³) compared to Literature.

	This work	Literature*
Saturate	885	880
Aromatics	1015	981
Resins	1027	1040
Asphaltene	1190	1185
Bitumen	1025	na

* O. Sabbagh 2006.

Bitumen densities at 90, 1468, and 3536 kPa over a range of temperatures from 10 to 50°C are reported in Table 4-3 and shown in Figure 4-2. The data are similar to those reported by Bishnoi et al. 1977, for a different Athabasca bitumen, also shown in Figure 4-2. The data were fitted with the following correlation:

$$\rho_{bit} = (1020.0 - 0.6317(T - 273.15)) \exp\left\{ (2.521 \cdot 10^{-9}(T - 273.15) + 6.8072 \cdot 10^{-7})P \right\} \quad (4-1)$$

where, ρ_{bit} is the bitumen density in kg/m³, P is pressure in kPa, and T is absolute temperature, K. The exponential term is a temperature dependent compressibility. The correlation fits the data to within ± 0.4 kg/m³. Note this correlation is specific to Athabasca bitumen sample used during the course of this research. It was developed to aid in calculating the mass of bitumen in the PVT cell. However, this correlation format can be used for other bitumen's density prediction if it is fitted to the experimental data.

Table 4-3. Athabasca Bitumen Density.

Temperature (°C)	Density (kg/m ³)		
	90 kPa	1470 kPa	3540 kPa
10	1014	1015	1016
20	1007	1008	1010
30	1001	1002	1004
40	995	996	997
50	989	990	991

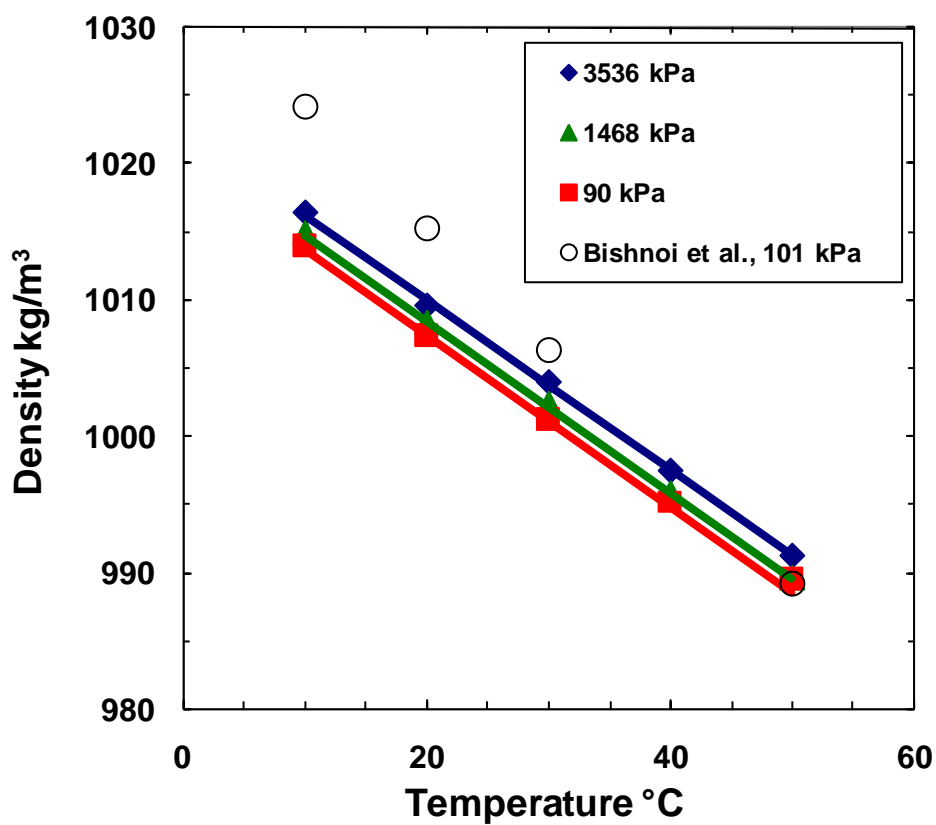


Figure 4-2. Effect of temperature and pressure on the density of Athabasca bitumen. The lines are the correlation, Equation 4-1.

4.1.3 Viscosity Data and Fitting

The viscosity of the Athabasca bitumen was measured at atmospheric pressure for temperatures from 115 to 147°C, Table 4-4. The data are compared with viscosities reported by Svrcek and Mehrotra (1982) for another Athabasca bitumen sample in Figure 4-3. The sample in this work is less viscous but both samples show the same trend with temperature.

Table 4-4: Effect of temperature on viscosity of Athabasca bitumen.

Temperature (°C)	Viscosity (mPa.s)
103.9	148
109.1	116
115.4	89.1
117.9	79.3
123.1	65.5
127.2	57.5
131.0	49.0
135.9	41.5
139.0	36.3
141.7	33.9
144.2	31.0
144.8	30.3
144.9	29.3
147.6	27.9

The Svrcek and Mehrotra data were fitted with the following correlation:

$$\log(\log(\mu_{bit})) = -3.70015 \log(T) + 9.90602 \quad (4-2)$$

where, μ_{bit} is the bitumen viscosity. The fit was accurate to within $\pm 15\%$.

The data from this work were fitted with the same slope:

$$\log(\log(\mu_{bit})) = -3.70015 \log(T) + 9.87056 \quad (4-3)$$

In this case the fit was accurate to $\pm 5\%$, demonstrating good consistency between the two sets of measurements.

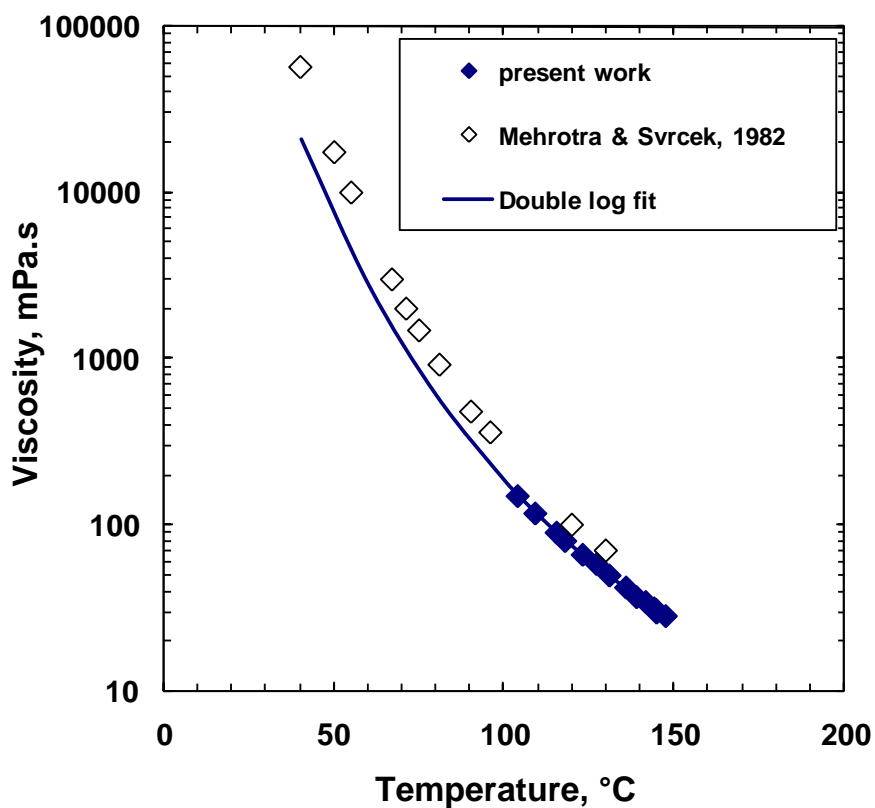


Figure 4-3: Effect of temperature on the viscosity of Athabasca bitumen. The line is correlation, Equation 4-3.

4.2 Mixtures of Athabasca Bitumen and Propane

The phase behaviour and properties of mixtures of propane and bitumen were investigated using the step-wise method at temperatures from 10 to 50°C and propane fractions of 5.2, 11.0, 15.4, 15.6, and 25.5 wt%. Continuous method tests were performed for propane compositions of 21.1 and 26.1 wt% propane. Vapour and liquid phases were established and no multiple liquid phases were expected. The saturation pressure data and liquid phase densities from these experiments are provided in Table 4-5. Density and viscosity data were obtained from samples taken at many of these compositions as well as at a propane composition of 10.1 wt%. The density and viscosity measurements are given in Table 4-6.

Table 4-5: Saturation pressure and liquid phase density (from cell volume) of mixtures of propane and Athabasca bitumen.

Method	Composition (wt% propane)	Temperature (°C)	Pressure (kPa)	Liquid Density (kg/m ³)
Step Wise	5.2	20.2	530	953
		40.0	789	940
		60.4	1082	927
Step Wise	10.9	10.0	478	916
		20.1	624	-
		29.9	741	894
		40.0	892	881
		50.0	1171	879
Step Wise	15.4	10.1	589	872
		50.1	1365	845

Table 4-5				
Step Wise	15.6	10.0	600	873
		19.9	718	868
		29.9	941	849
		39.7	1130	848
		50.1	1344	844
Continuous	21.4	10.3	676	-
		15.4	761	-
		19.8	830	-
		25.1	928	-
		29.8	1002	-
		35.3	1158	-
		39.9	1252	-
		45.4	1354	-
		44.9	1354	-
		49.6	1555	-
Step Wise	25.4	10.1	632	823
		20.1	831	819
		20.1	829	815
		30.0	1016	806
		39.9	1290	800
		50.0	1537	791
Continuous	26.1	10.8	733	-
		15.7	815	-
		20.7	912	-
		30.0	1115	-
		40.0	1268	-
		49.2	1624	-

Table 4-6: Viscosity and density of liquid mixtures of propane and Athabasca bitumen.

Composition	Temperature	Pressure	Viscosity	Density ^{Anton Paar}	Density ^{Pycnometer}
(wt% propane)	(°C)	(kPa)	(mPa.s)	(kg/m ³)	(kg/m ³)
5.2	79.1	4934	87.4	949	-
5.2	83.5	4920	72.0	941	-
5.2	84.6	4905	68.6	938	-
5.2	84.5	4422	69.1	950	-
5.2	90.5	4892	54.4	944	-
5.2	74.5	4893	110	942	-
5.2	60.5	4887	219	948	-
5.2	60.2	4890	223	949	-
5.2	60.2	2853	218	949	-
10.1	49.8	1406	74.8	-	-
10.1	50.0	3564	80.5	-	-
10.1	47.0	3564	94.7	-	-
10.1	59.4	3564	51.3	-	-
10.1	69.0	3564	32.9	-	-
10.1	78.8	3564	21.7	-	-
10.1	88.0	3564	15.2	-	-
10.1	50.4	3564	64.3	-	-
10.1	10.0	3943	-	935	-
10.1	20.0	3943	-	929	-
10.1	30.0	3943	-	922	-
10.1	40.0	3943	-	915	917
10.1	50.0	3943	-	909	-
15.6	11.2	1551	211	912	-
15.6	20.3	1565	122	906	907
15.6	30.5	1551	69.9	898	-
15.6	40.1	1585	44.7	893	-
15.6	49.9	1694	34.0	883	-
21.4	10.8	863	70.4	846	853
21.4	15.5	1034	48.5	-	-
21.4	20.4	1062	35.6	-	-
21.4	25.1	1055	32.7	-	-
21.4	30.0	1130	24.8	-	-
21.4	34.8	1289	21.0	-	-
21.4	40.0	1399	17.2	-	-
21.4	45.0	1544	14.4	-	-

Table 4-6 Cont.

21.4	50.0	1668	12.2	-	-
26.1	10.7	904	42.0	847	844
26.1	20.7	1120	26.4	-	-
26.1	29.9	1261	18.0	-	-
26.1	40.2	1444	12.3	-	-
26.1	49.6	1786	8.6	-	-

4.2.1. Saturation Pressure Correlation

The saturation pressures of propane in the Athabasca bitumen are shown in Figures 4-4 and 4-5. As the propane content approaches approximately 20 wt% (76 mol %), the saturation pressure approaches the vapour pressure of pure propane. A regular solution model (Akbarzadeh et. al. 2005) predicts the onset of asphaltene precipitation in propane diluted bitumen to occur at a propane content of 23 wt% (~79 mol%). Hence, it is likely that a second liquid phase appears when the saturation pressure reaches the vapour pressure of propane. In other words, liquid-liquid and vapour-liquid-liquid phase regimes are expected at propane contents above approximately 20 wt%.

The saturation pressure data was fitted starting from the following equality of fugacity between the liquid and vapour phases:

$$x_{C_3}\gamma_{C_3}P_{V_{C_3}} = y_{C_3}\phi_{C_3}^*P \quad (4-4)$$

where, P_V is the vapour pressure in kPa and γ_{C_3} is the activity coefficient of propane in the bitumen. If the vapour phase is pure propane, the expression simplifies as follows:

$$x_{C_3}\gamma_{C_3}P_{V_{C_3}} = P \quad (4-5)$$

The correlation was fitted to the data as shown in Figures 4-4 and 4-5. The best fit value of the activity coefficient was 1.158, which fit the saturation pressures with an average relative deviation of 5.1%. The agreement was very good except for the 5.2 wt% propane data. It is possible that the measurements failed to reach equilibrium because the viscosity was highest at this composition.

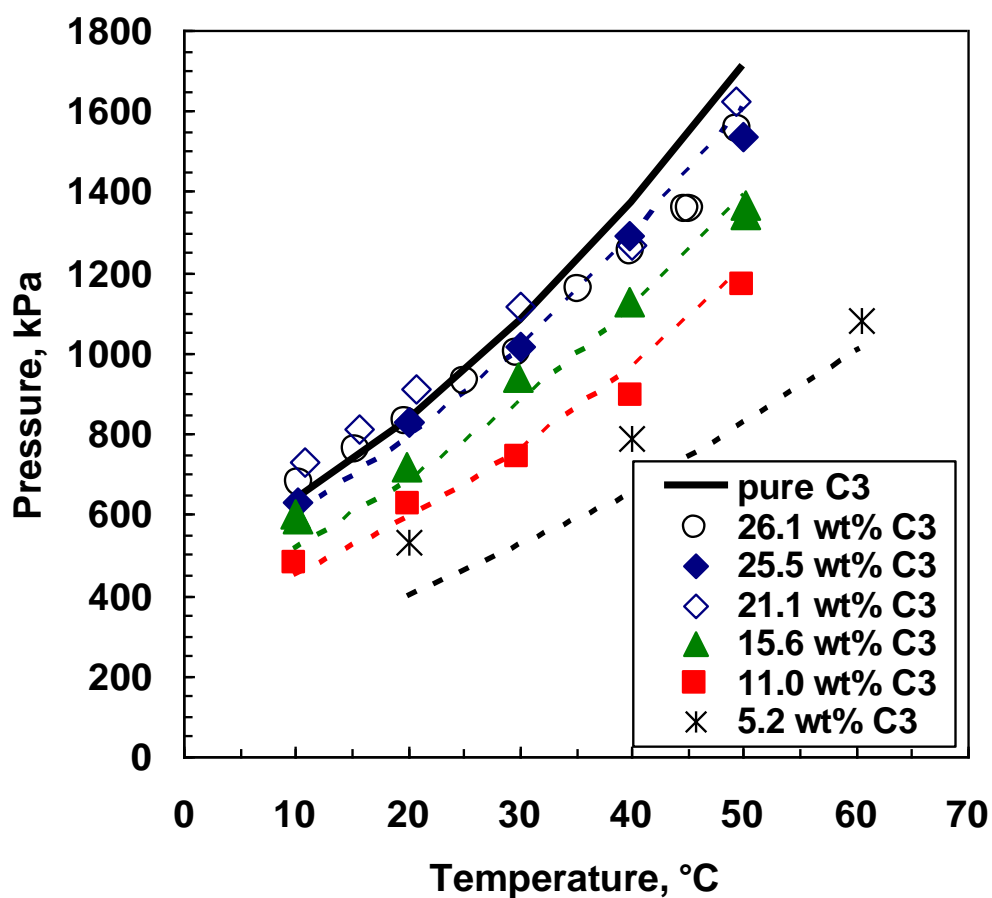


Figure 4-4: Saturation pressure of propane in Athabasca bitumen (solid symbols - step-wise method; open symbols - continuous method).

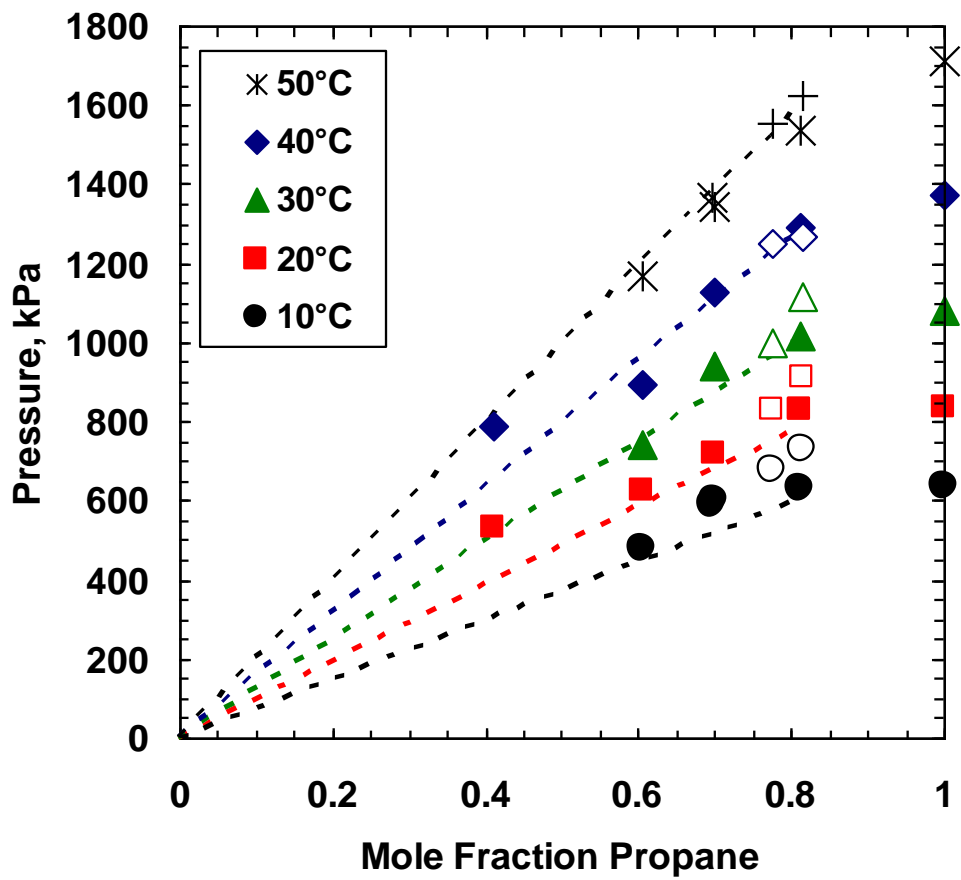


Figure 4-5: Solubility of propane in Athabasca bitumen (solid symbols - step-wise method; open symbols - continuous method).

Note that the activity coefficient in reality depends on composition, temperature and pressure. The van Laar form of the activity coefficient (Smith, 4th Ed, 1987, pp 378) is given by:

$$\ln \gamma_{C_3} = \frac{A}{\left(1 + \frac{Ax_{C_3}}{Bx_{bit}}\right)} \quad (4-6)$$

where, A and B are constants. The best fit for the data was found when A = 0.1469 and A/B went to zero; that is, no compositional dependence and a constant γ_{C_3} of 1.158. Physically, there must be a non-zero value of A/B and the result simply demonstrates that this value is too small to be distinguished with our data. Since A/B is proportional to the ratio of the molecular cross-sections, the result suggests that the average effective cross-section for the molecules in bitumen is much larger than for propane. Data at higher mole fractions of propane would be required to determine the value of A/B.

While the form of Equation (4-5) is expected to apply to heavy oils in general, the fitted activity coefficient applies to the Athabasca bitumen sample. Data from other heavy oils are required to test if the activity coefficient varies with other heavy oils. Also note, the correlation is valid only in the vapour-liquid region.

4.2.2. Density and Viscosity Modeling

The densities listed in Table 4-5 were determined from the measured volume in the PVT cell at the saturation point (no vapour phase present). The densities in Table 4-6 were measured with the Anton Parr density meter and the pycnometer. The density meter and

pycnometer measurements are in good agreement with each other but are consistently 30 to 40 kg/m³ higher than the cell volume based densities at the same temperature and pressure. It is possible that bitumen in the dead volume between the PVT cell and the density meter altered the density of the samples in the density meter and pycnometer. Another possibility is that there is volume change upon mixing propane and bitumen. The densities based on the cell volume were determined assuming no excess volume but the excess volumes for mixing hydrocarbons may not be negligible.

The densities based on the cell volume are plotted in Figure 4-6. The change in density with temperature was also predicted from the density of pure propane and pure bitumen assuming no excess volume, as follows:

$$\rho_{mix} = \frac{1}{\sum w_i / \rho_i} \quad (4-7)$$

The agreement with the data is within experimental error except at 25.5 wt% propane. The discrepancy could be due to neglecting excess volume in Equation 4-7, which may not be true at higher concentration or temperature. It is also likely that a second liquid phase had formed at this condition.

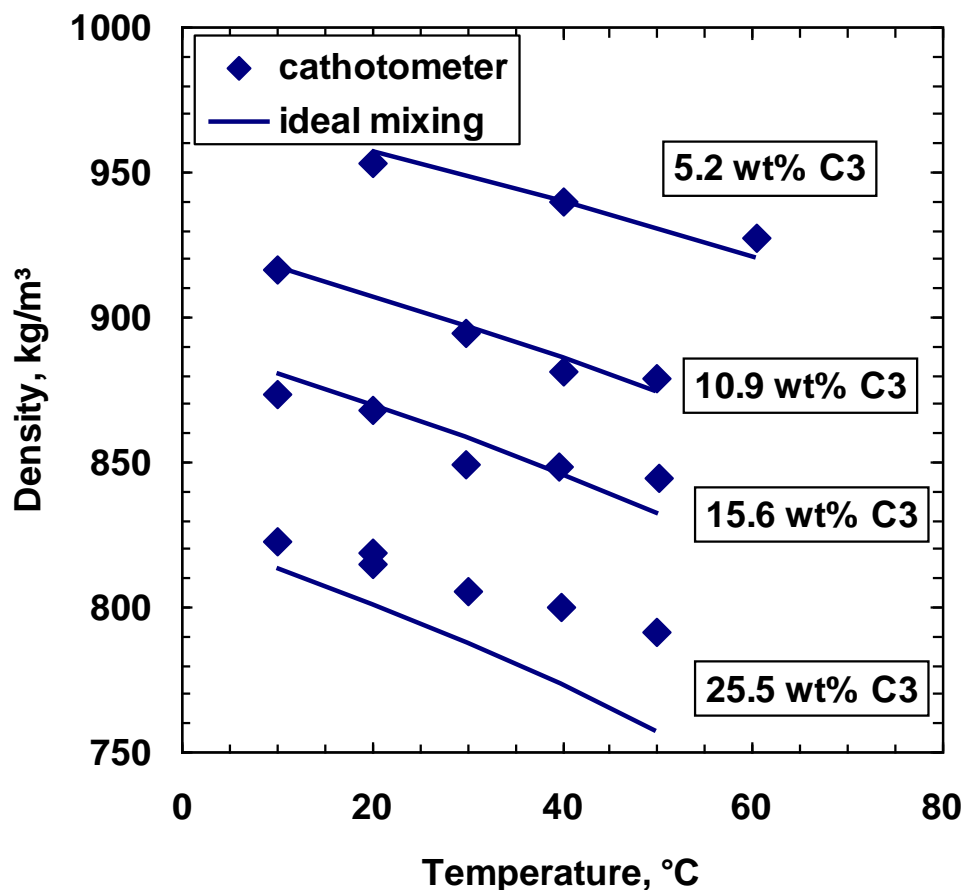


Figure 4-6: Effect of temperature on the density of mixtures of propane and Athabasca bitumen.

Viscosities of saturated liquid mixtures of propane and bitumen are shown on Figure 4-7. The Lobe (1973) binary mixing rule has been found to provide accurate predictions of the viscosity of solvent diluted crude oils (Escobedo, 1997). The Lobe mixing rule was given by Equations 2-3 to 2-5. The Lobe mixing rule gave acceptable predictions of the mixture viscosities, as shown on Figure 4-7. The correlation fits all but three data points within an order of magnitude. The predictions are poorest at low temperatures and

propane contents above 21 wt%. Again, it is likely that a second liquid phase had formed at the high propane contents.

The Athabasca bitumen and propane viscosity data were also examined with the Shu (1984) correlation, given in Equations 2-6 to 2-9. Unlike the Lobe mixing rule, the Shu correlation in its original form was not able to calculate the bitumen and propane liquid mixtures viscosity. In this study, the constant coefficients in Equation 2-9 were adjusted to fit the experimental viscosity data for 10.9 wt% and 15.6 wt% propane in bitumen. The modified correlation for the Shu correlation empirical parameter α is given by:

$$\alpha = \frac{0.000375 \Delta \rho^{-8.56653} \rho_{Bit}^{4.567001} \rho_s^{-5.27094}}{\ln\left(\frac{\mu_{Bit}}{\mu_s}\right)} \quad (4-8)$$

Figure 4-8 shows modified Shu correlation based viscosity predictions for 10.9 wt% and 15.6 wt% along with other composition of propane in binary mixture with bitumen.

The viscosity data highlights one of the difficulties in the application of the Vapex process in Athabasca Reservoirs. At the reservoir temperature, which is typically around 10°C, the diluted oil viscosity with 21.4 wt% propane is an order of magnitude higher than what is typically achieved in thermal recovery processes. A much higher mass fraction of propane would be needed for reducing the viscosity of diluted oil to the same level as in thermal processes. However, this would make the propane concentration higher than the threshold at which asphaltene precipitation becomes a serious concern. Moreover, with a higher concentration of propane, there is also a possibility of forming a

second propane-rich liquid phase which can dramatically increase propane consumption without a proportionate increase in the net oil rate. One option for overcoming these problems is to operate at a higher temperature by introducing some form of reservoir heating. Another option is to find better solvents (e.g. mixture of propane and carbon dioxide) that would mitigate some of these problems and this will be discussed in the next chapter.

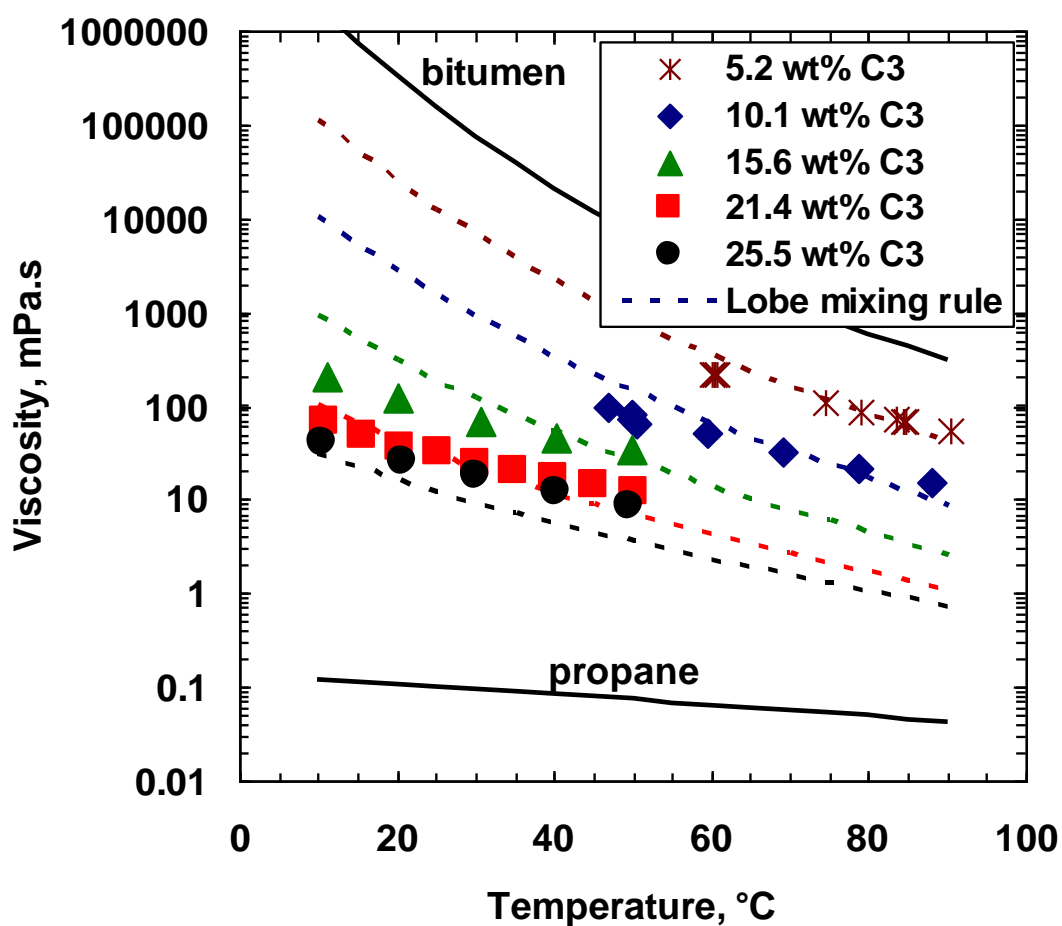


Figure 4-7: Effect of temperature on viscosity of mixtures of propane and Athabasca bitumen.

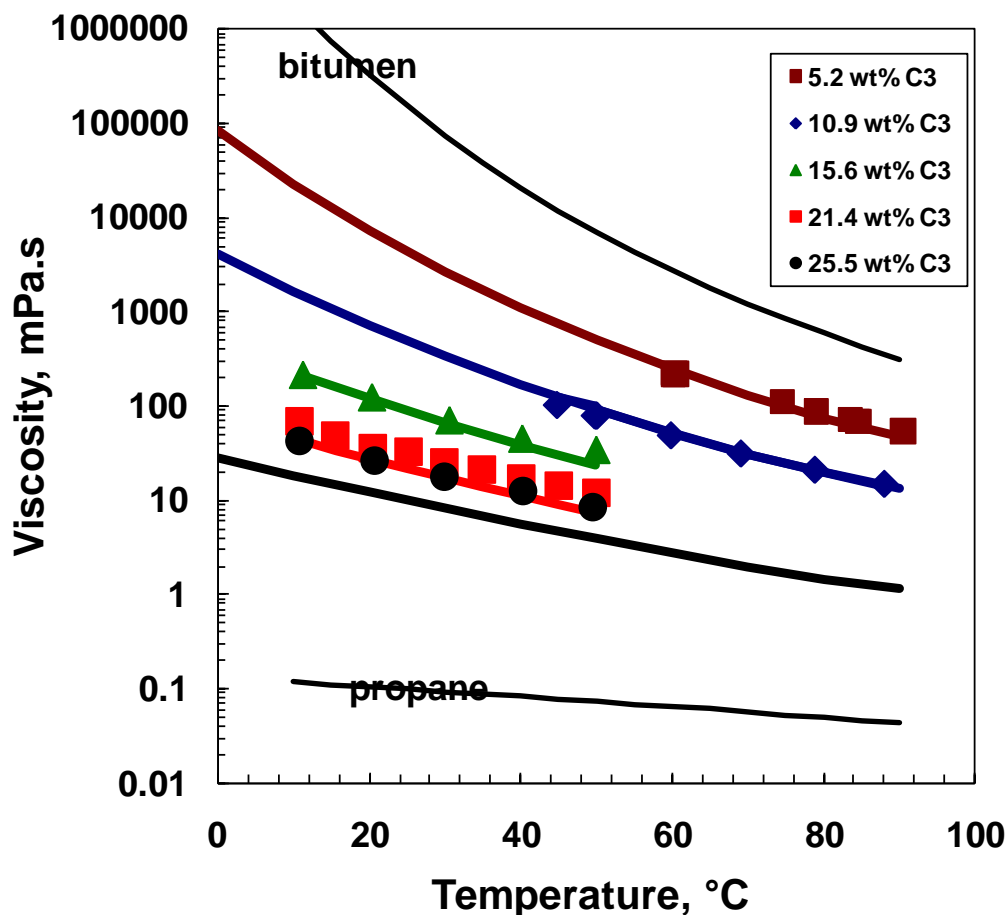


Figure 4-8: Solid line is Athabasca bitumen propane saturated liquid mixture viscosity by the Shu (1984) viscosity correlation with empirical parameter from Equation 4-8.

4.3 Mixtures of Athabasca Bitumen and Carbon Dioxide

There is considerable published data on mixtures of carbon dioxide and crude oils. Therefore, only a limited number of measurements were made in order to verify the data collected in this thesis against literature data. The solubility of CO₂ in Athabasca bitumen was measured at 25°C and pressures of 3.96 and 6.02 MPa, Table 4-7. The phase boundaries for 18 wt% carbon dioxide in bitumen are reported in Table 3-4 (chapter 3).

Note that mixtures of carbon dioxide and bitumen can form two liquid phases at temperatures below the carbon dioxide critical point.

Table 4-7: Saturation condition of carbon dioxide in Athabasca bitumen at 24.9°C.

Pressure (kPa)	Carbon Dioxide (wt%)
6017	11.6
6017	10.6
6017	10.1
3953	6.1
3957	5.6

4.3.1. Saturation Pressure Correlation

Saturation pressures for carbon dioxide in 10 different crude oils have been reported at temperatures from 28 to 120°C (Simon, et al. 1965, and Quail et al. 1988). Some of this data is reproduced in Figure 4-8. All of the data was fitted with a Henry's law type model starting with the following equality between the fugacity of carbon dioxide in the two phases:

$$x_{CO_2} H_{CO_2}^o = y_{CO_2} \phi_{CO_2}^* P \quad (4-9)$$

where x and y are the mole fractions in the liquid and vapour phases respectively, H^o is Henry's constant for carbon dioxide (CO₂) in bitumen in kPa, ϕ^* is the fugacity coefficient, and P is pressure in kPa. If the vapor phase in equilibrium with saturated bitumen is pure carbon dioxide, Equation 4-9 can be simplified as follows:

$$x_{CO_2} H_{CO_2}^o = P \quad (4-10)$$

where, $H_{CO_2} = H^{\circ}_{CO_2}/\phi_{CO_2}$ is a modified constant including the fugacity coefficient. An expression for the modified Henry's constant of the following form was found to fit the data:

$$\ln H_{CO_2} = \ln A + \frac{B}{T} + \frac{CP}{RT} \quad (4-11)$$

where A , B , and C are fitting parameters. The best fit values were $A = 135500$ kPa, $B = -872.1$ K, and $C = 0.1464$ m³/kmol which fit the saturation pressures with an average relative error of 1.7%. The correlation is compared with the data in Figure 4-9. The correlation is valid in the vapour-liquid region below the critical point and in two-phase regions above the critical temperature.

Saturation pressures for carbon dioxide in Athabasca bitumen were reported by Svrcek et. al. (1985), and are shown in Figure 4-10 along with data from the present work from Table 4-7. Note that above 11 wt% carbon dioxide, the saturation pressure does not change as the carbon dioxide content increases indicating that another liquid phase may have formed. Figure 4-10 also shows the predictions using Equation 4-9, which predicted the saturation pressures at less than 11 wt% carbon dioxide with an average absolute error of 5.4%.

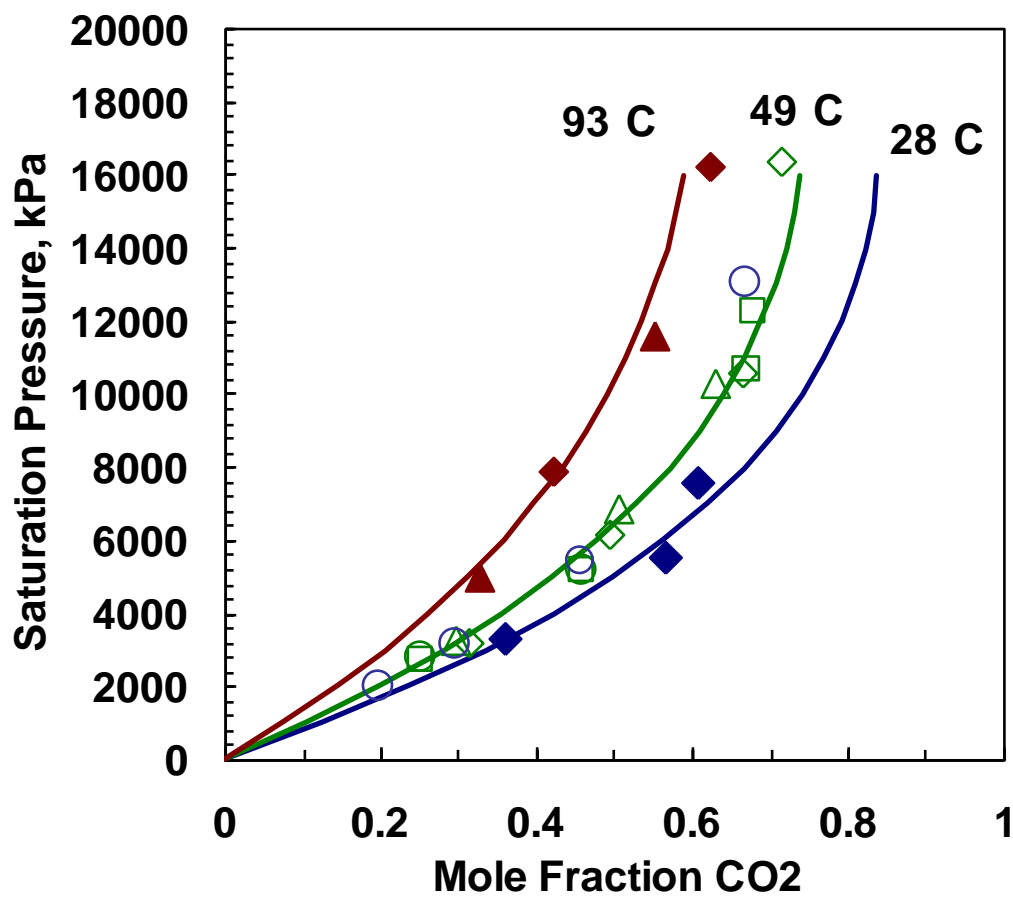


Figure 4-9: Saturation condition of carbon dioxide in several different crude oils (data from Simon 1965, and Quail 1988; lines are Equation 4-10)

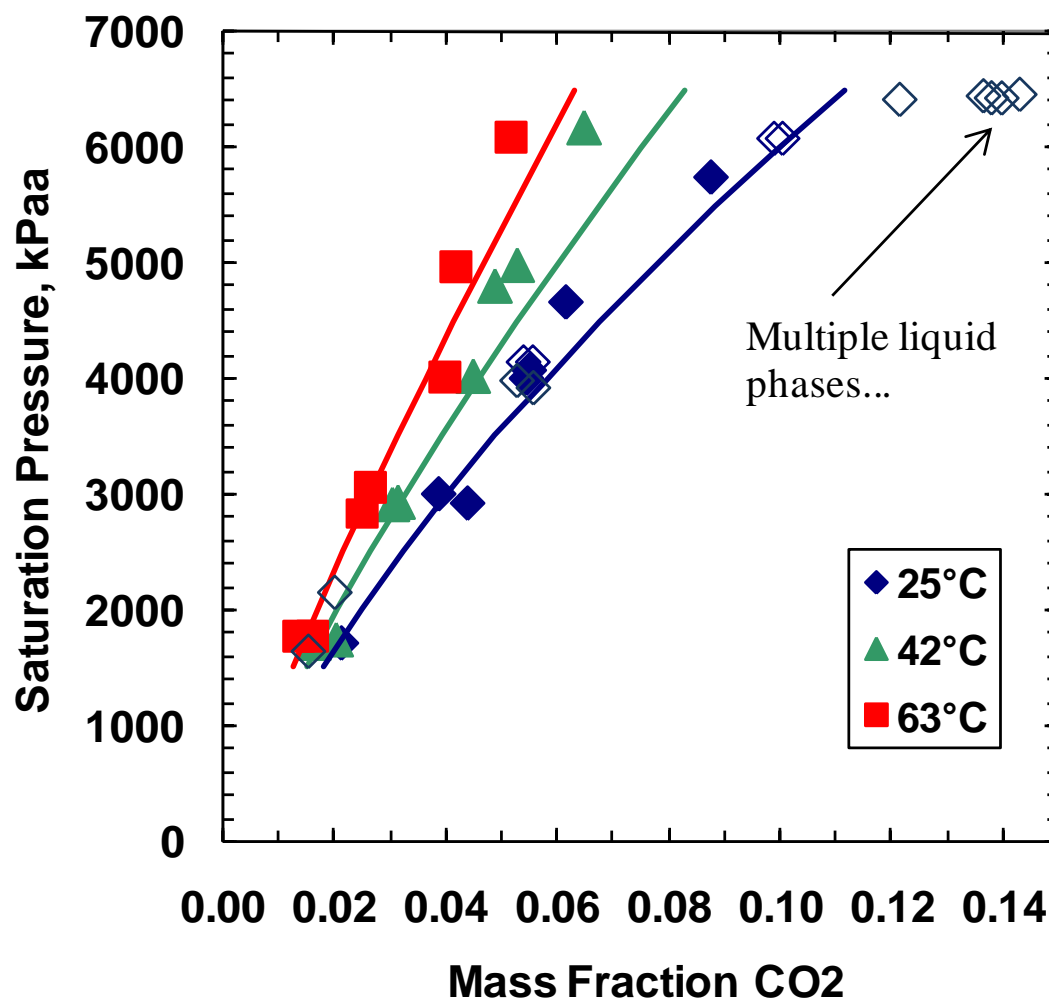


Figure 4-10: Saturation condition of carbon dioxide in Athabasca bitumen (solid symbols - Svrcek and Mehrotra 1982; open symbols - present work; lines are Equation 4-10).

Figure 4-11 shows the phases observed for 18 wt% (73 mol%) carbon dioxide in Athabasca bitumen. Below the critical point of pure CO₂, there is a transition from liquid-liquid to vapour-liquid-liquid to vapour-liquid phase regimes as the pressure is reduced at constant temperature. The VLL region is narrow and spanning, at most, 800 kPa at any

given temperature. Since the light liquid phase and vapor phase are mostly pure carbon dioxide, therefore VLL - VL transition pressure doesn't change much (i.e. very narrow) at each temperature, but overall density of the system is changing during this phase transition. Above the critical point, two phases were observed at all measured temperatures and pressures; however, we did not detect a third asphaltene-rich phase in our experiments. Figure 4-12 confirms that the Henry's law correlation applies in the vapour-liquid region and the two-phase regions above the critical point.

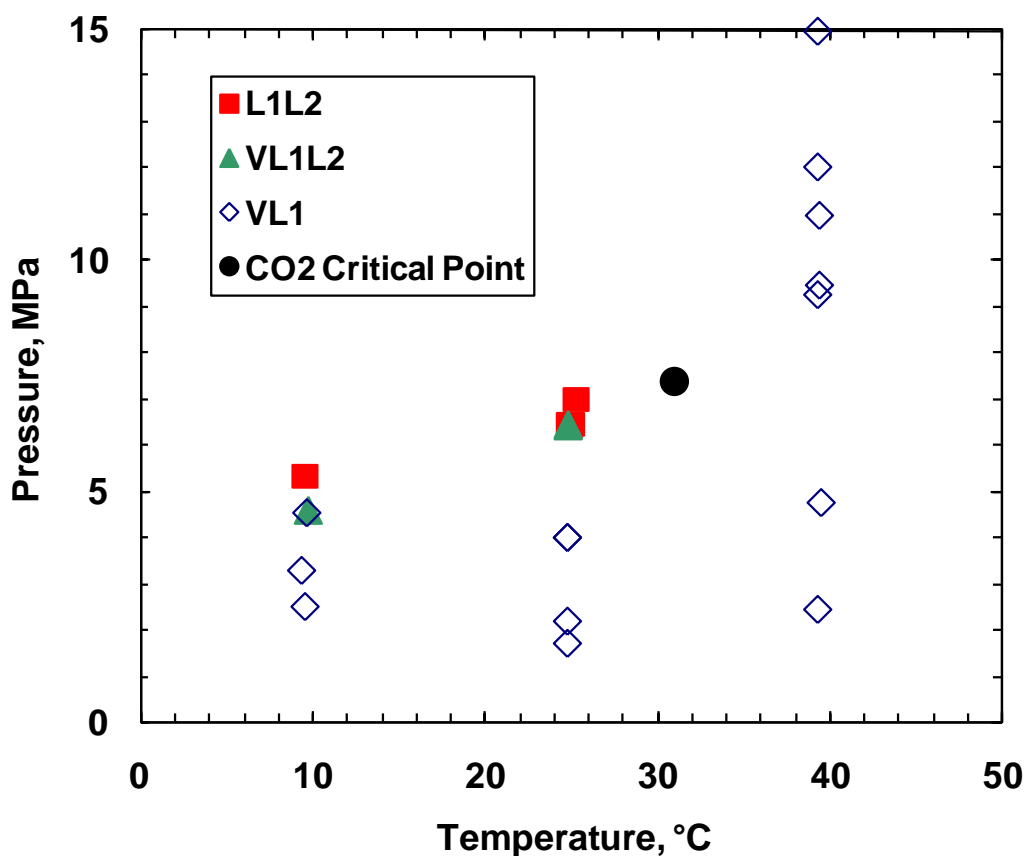


Figure 4-11: Phase diagram of 18wt% carbon dioxide in Athabasca bitumen.

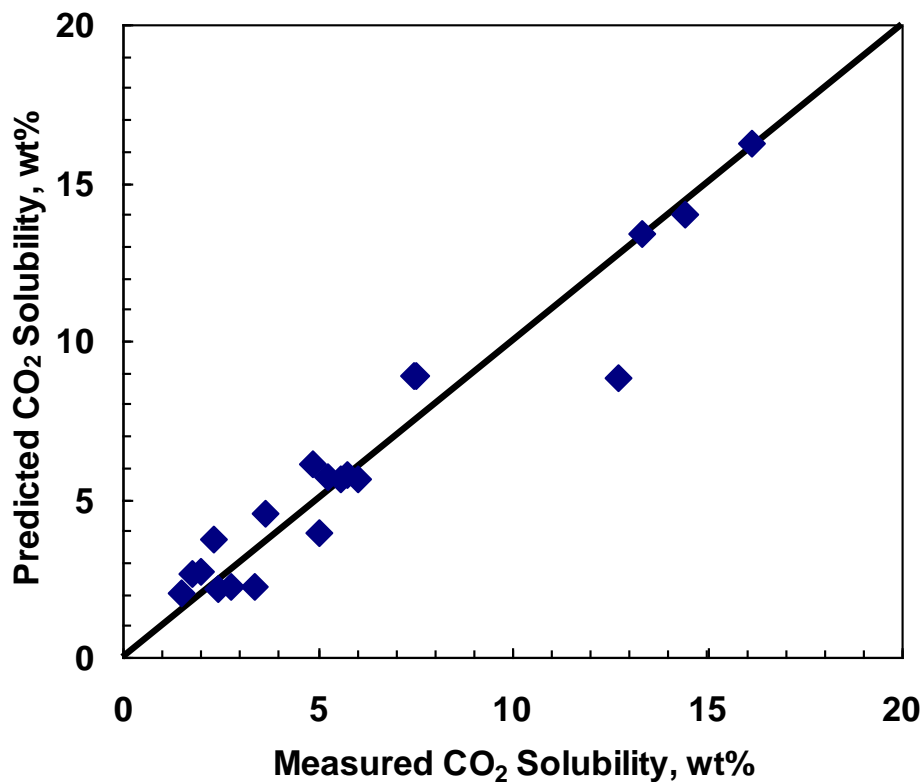


Figure 4-12: Predicted versus measured solubility of carbon dioxide in Athabasca bitumen (Data from table 3-4 and prediction by Equation 4-10).

4.4. Mixtures of Bitumen, Propane, and Carbon Dioxide

The following three ternary systems were evaluated:

1. 11.0 wt% carbon dioxide, 13.5 wt% propane
2. 6.2 wt% carbon dioxide, 24.0 wt% propane
3. 13.1 wt% carbon dioxide, 19.2 wt% propane.

In Cases 1 and 2, only liquid and vapour-liquid regimes were directly observed. However, as noted in Section 4.2, a second dense (asphaltene-rich) phase formed at propane contents greater than 20 wt% in Athabasca bitumen. Hence, another dense phase may be expected in Case 2, but was not observed by means of this experimental setup. In Case 3, multiple phase regimes were observed and this system will be discussed separately.

4.4.1 Cases 1 and 2

The saturation pressures for Cases 1 and 2 are given in Table 4-8 and were of the order of 3500 kPa and 2000 kPa, respectively. The saturation pressures were predicted assuming only one liquid phase was present and using Equation 4-4 for the propane partial pressure and Equation 4-10 for the carbon dioxide partial pressure. It was assumed that the vapour consisted of an ideal mixture of propane and carbon dioxide. The predicted pressure is then given by:

$$P = 1.157x_{C_3}P_{v_{C_3}} + x_{CO_2}H_{CO_2} \quad (4-12)$$

The predicted saturation pressures are compared with the data on Figure 4-13. The predicted saturation pressures are within 10% of the measured saturation pressures.

The densities and viscosities of the liquid phases are given in Tables 4-8 to 4-10. The densities were within 2% of the densities calculated assuming no volume change upon mixing. The viscosities were predicted in a two step calculation. First, the viscosity of the carbon dioxide and propane mixture (solvent) was determined from Lobe mixing rule (Equations 2-6 to 2-9). The viscosity of the ternary mixture was determined from the

solvent and bitumen properties using Lobe correlation again. The predicted viscosities are plotted on Figure 4-14 and are within a factor of 2 of the measured values. The predictions are very good considering that the only inputs are the density and viscosity of bitumen, pure propane, and pure carbon dioxide. To put this into perspective, at 10°C, the viscosity of bitumen is $1.79 \cdot 10^6$ mPa.s compared with 0.089 and 0.11 mPa.s for propane and carbon dioxide, respectively.

Note that while a second dense liquid phase was expected for the Case 2 ternary mixture, no evidence of this phase was observed either visually or through deviations between the data and predictions for saturation pressure and viscosity. It is possible that the amount of this phase was too small to have a noticeable effect on the measured data.

Table 4-8: Saturation conditions for two ternary mixture of propane, carbon dioxide, Athabasca bitumen.

Composition, wt%		Method	Temperature (°C)	Pressure (kPa)	Liquid Density (kg/m ³)			
C3	CO2							
13.5	11.0	Step Wise	10.0	1838	823			
			15.0	1961	827			
			19.9	2113	821			
			25.2	2304	814			
			10.2	1798	830			
		Continuous	14.9	1959	829			
			19.9	2110	821			
			24.8	2299	823			
			24.0	6.2	Step Wise	10.0	3189	890
						10.3	3126	898
15.1	3443	884						
20.2	4001	867						
25.1	4252	882						
20.2	3796	868						
Continuous	10.0	3226				897		
	10.2	3132	899					
	15.1	3447	891					
	20.1	3927	860					
	20.2	3800	888					
	25.2	4226	867					

Table 4-9: Liquid phase density and viscosity for 13.5 wt% propane, 11.0 wt% carbon dioxide, 85.5 wt% Athabasca bitumen ternary mixture.

Temperature (°C)	Pressure (kPa)	Viscosity (mPa.s)	Density ^a (kg/m ³)	Density ^b (kg/m ³)
10.3	3309	49.4	-	-
11.3	4585	46.9	920.4	-
11.4	4656	42.5	918.0	-
15.6	3573	36.9	-	-
16.0	4692	33.1	912.3	-
16.0	4602	35.9	915.4	-
20.2	3998	28.8	-	-
20.5	4212	28.7	906.8	-
20.6	5110	27.7	907.6	-
20.6	4584	28.7	907.7	-
20.7	4696	27.5	907.7	898.4
25.2	4354	22.4	-	-
25.7	4618	23.9	904.6	-
25.7	4657	21.9	903.9	-

a - Anton Paar, b - Pycnometer

Table 4-10: Liquid phase density and viscosity for 24.0 wt% propane, 6.2 wt% carbon dioxide, 69.8 wt% Athabasca bitumen ternary mixture.

Temperature (°C)	Pressure (kPa)	Viscosity (mPa.s)	Density ^a (kg/m ³)	Density ^b (kg/m ³)
10.3	2716	23.7	856.4	-
10.3	2716	21.9	856.3	-
11.0	2716	23.7	855.0	-
11.8	2716	22.4	851.9	-
15.2	2717	11.6	851.7	-
16.6	2723	17.6	851.4	-
20.1	2723	13.9	847.1	843.9
20.3	2716	15.6	847.6	-
20.5	2723	13.7	845.3	-
24.8	2716	11.7	839.9	-
25.0	2716	11.6	840.3	-
10.3	2716	23.7	856.4	-

a - Anton Paar, b - Pycnometer

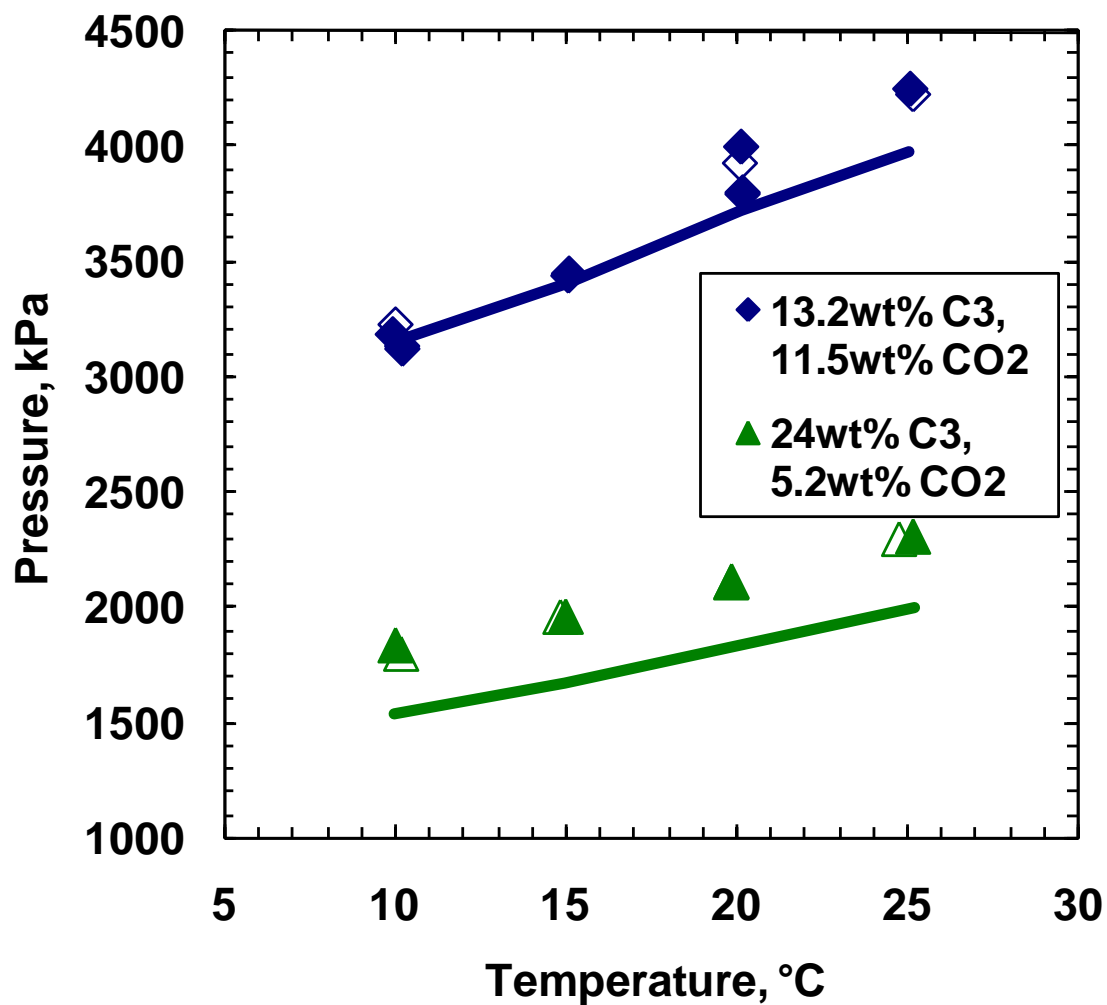


Figure 4-13: Vapor liquid phase boundaries for two ternary mixtures of carbon dioxide, propane, and Athabasca bitumen (solid lines are predicted pressures).

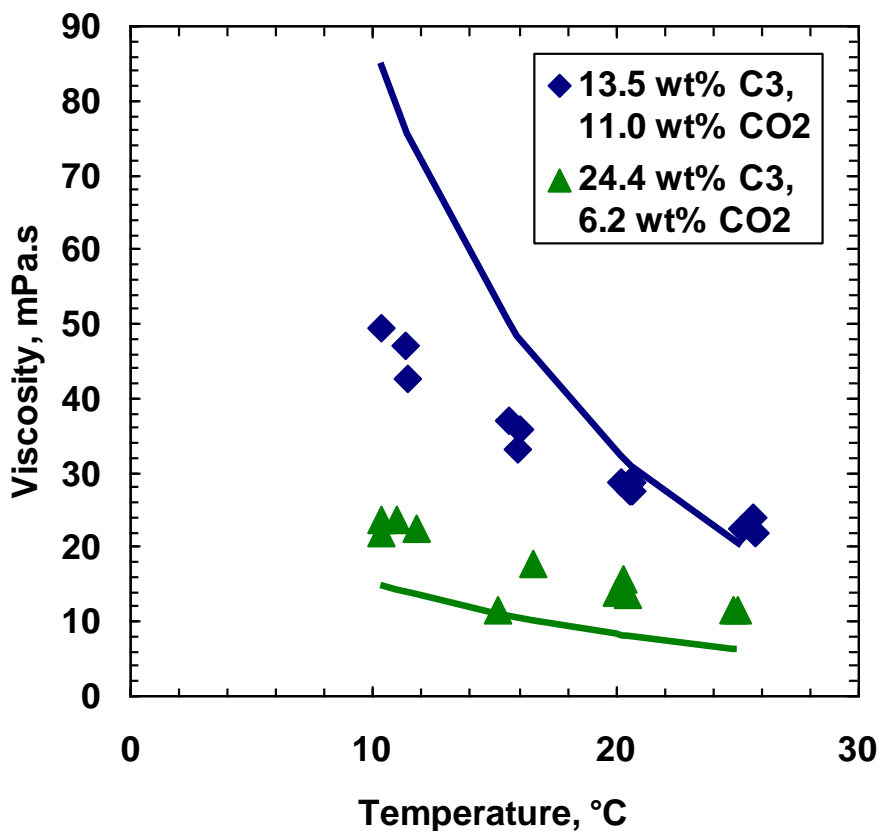


Figure 4-14: Liquid phase viscosity of two ternary mixture of propane, carbon dioxide, and Athabasca bitumen. Solid line are prediction by Lobe correlation.

4.4.2 Case 3

Figure 4-15 shows the phases observed for the 13 wt% carbon dioxide, 19 wt% propane systems. With the high carbon dioxide content, two liquid phases were observed at higher pressures. A narrow (approximately 500 kPa) VLL region was detected with a VL region at lower pressures. Not surprisingly, the addition of propane reduced the amount of carbon dioxide required to form multiple liquid phases. The vapour phase appeared at pressures of the order of 3500 kPa, Table 4-11. Shelton and Yarborough (1977) detected

a third dense phase at high carbon dioxide contents in a crude oil. While it was not observed in these experiments, it is likely that an asphaltene-rich phase is also formed at the high a content of propane and carbon dioxide (32 wt% combined).

A liquid and a vapour sample were obtained in the vapour-liquid region at a pressure of 3950 kPa and a temperature of 20°C. The compositions of both phases and the physical properties of the liquid phase are reported in Table 4-12. At these conditions there is sufficient solubility of the propane and carbon dioxide to reduce the viscosity to 39 mPa.s.

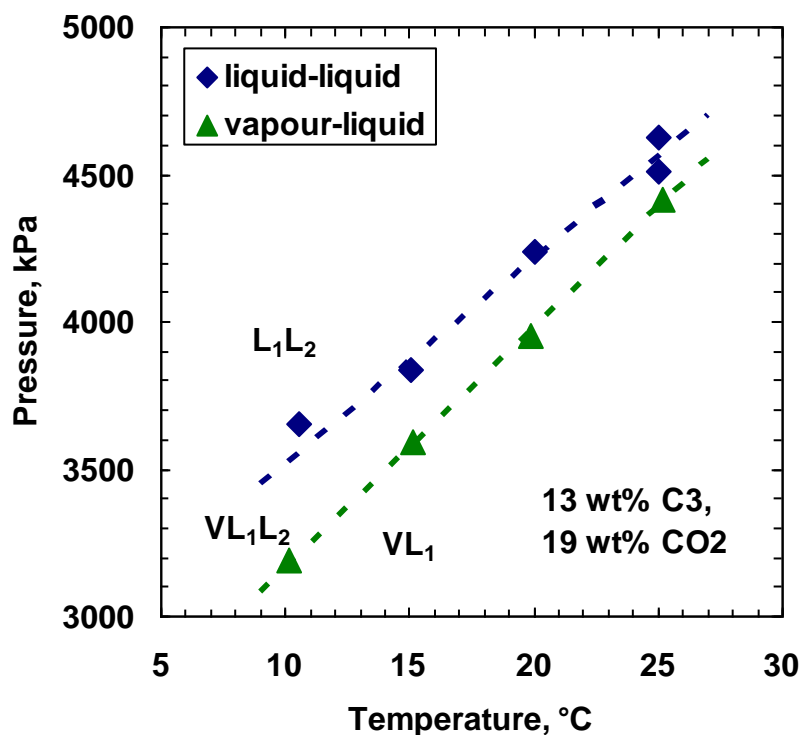


Figure 4-15: Phase boundaries for 13.1 wt% propane, and 19.2 wt% carbon dioxide balanced with Athabasca bitumen in ternary mixture Case 3.

Table 4-11: Phase boundaries for 13.1 wt% propane, 19.2 wt% carbon dioxide, and 67.7 wt% Athabasca bitumen.

LL to VLL		VLL to VL	
Temperature (°C)	Pressure (kPa)	Temperature (°C)	Pressure (kPa)
10.5	3651	10.1	3189
14.9	3760	15.1	3594
15.0	3835	19.9	3950
20.0	4237	25.2	4412
25.0	4512		
25.1	4628		

Table 4-12: Propane, and carbon dioxide weight fraction in the vapour and liquid phases, for case 3 at 20°C, and 3950 kPa.

Property	Liquid	Vapour
Propane, wt%	12	21
Carbon Dioxide, wt%	9	79
Viscosity, mPa.s	39	-
Density, kg/m ³	913	-

4.5 SUMMARY

In summary, mixtures of propane and Athabasca bitumen formed liquid or vapour-liquid phase regimes at compositions of up to approximately 20 wt% propane. Saturation pressure, density and viscosity data all indicate that a second dense phase appears at propane content above 20 wt%, however, visual confirmation was not possible. The

saturation pressures data were fitted with a modified form of Raoult's law. The density of the liquid phase at different temperatures and pressures was predicted from the propane and bitumen densities assuming no volume change upon mixing. The viscosity of the liquid phase was predicted from the propane and bitumen viscosities using the Lobe and Shu mixing rules.

The expected viscosity reduction at the reservoir temperature in Athabasca bitumen by dilution with propane under conditions that minimize the risk of asphaltene precipitation and the formation of a second liquid phase is modest compared to what can be achieved in thermal recovery processes.

Mixtures of propane and carbon dioxide may provide a more broadly applicable solvent because the ratio of carbon dioxide to propane can be adjusted to achieve a desired saturation pressure appropriate for a given reservoir temperature and pressure.

Binary mixtures of propane and bitumen form a second dense asphaltene-rich phase at propane contents above approximately 20 wt%. Binary mixtures of carbon dioxide and bitumen form a second carbon dioxide rich liquid phase at carbon dioxide contents above approximately 11 wt%. Multiple liquid phases were also observed in a ternary mixture of 13.1 wt% propane, 19.2 wt% carbon dioxide, and bitumen. Only liquid and vapour liquid regions were observed for two other ternary mixtures: 13.5 wt% propane and 11.0 wt% carbon dioxide; 24 wt% propane and 6.2 wt% carbon dioxide. A second dense phase was expected but not observed for the latter mixture but may have been too small to detect.

The saturation pressures for the binary and ternary mixtures could be predicted with correlations based on vapour pressure for propane and Henry's law for carbon dioxide. The viscosity of the liquid phase could be predicted with the Lobe mixing rule.

The formation of a second liquid phase would make the use of such solvents in Vapex more complex. It is likely that the carbon dioxide rich liquid phase will simply drain into the production well without extracting substantial oil components, thereby increasing the solvent consumption. Moreover, the presence of a second liquid phase draining with the diluted oil would reduce the total liquid rate due to relative permeability effects. Therefore it would be advisable to operate at conditions that do not give multiple liquid phases.

The experimental results also suggest that the mixed carbon dioxide and propane solvent is less likely to precipitate asphaltenes than pure propane. Although, this aspect was not fully examined in this work, it is something that should be further investigated and may turn out to be a significant advantage of using carbon dioxide in Vapex.

CHAPTER 5 : EQUATION OF STATE MODELING

In this chapter, an oil characterization and equation of state model are developed to describe the phase behaviour of mixtures of carbon dioxide, propane, and Athabasca bitumen. The model is tuned to fit the experimental phase behaviour data for pseudo-binary and pseudo-ternary mixtures of these components that were reported in Chapters 3 and 4. Solubility data for carbon dioxide and Athabasca bitumen reported by Svrcek 1982 are also used.

5.1. Peng - Robinson Equation of State

The Peng-Robinson equation of state (PR EoS) parameters were modified using the CMG WinProp software to improve the equation of state model prediction against the experimental solubility and phase property data. The PR-EoS (1978) is given by:

$$P = \frac{RT}{v - b} - \frac{a}{v(v + b) + b(v - b)} \quad (5-1)$$

where P is pressure, T is temperature, v is the molar volume, R is the universal gas constant, and a and b are the EoS parameters. The PR-EoS parameters for a pure component are defined as follows:

$$a_i = 0.45724 \frac{R^2 T_{ci}^2}{P_{ci}} \left[1 + c_i (1 - T_{ri}^{0.5}) \right]^2 \quad (5-2)$$

$$b_i = 0.07780 \frac{RT_{ci}}{P_{ci}} \quad (5-3)$$

where

$$c_i = 0.3796 + 1.485\omega_i - 0.1644\omega_i^2 + 0.01667\omega_i^3 \quad (5-4)$$

and T_r , T_c , P_c and ω are the reduced temperature, the critical temperature, the critical pressure, and the acentric factor, respectively.

The mixing rules used to determine the PR-EoS parameters for a mixture of components are given by:

$$a = \sum_i \sum_j x_i x_j a_{ij} \quad (5-5)$$

$$b = \sum_i x_i b_i \quad (5-6)$$

where

$$a_{ij} = (1 - k_{ij})(a_i a_j)^{0.5} \quad (5-7)$$

and k_{ij} is the binary interaction parameter between components i and j .

It is usually impractical to tune binary interaction parameters for every pair of components in a mixture, particularly for the ill-defined pseudo-components used in oil characterization. Instead, the binary interaction can be correlated to either the critical volume or temperature of the components. In this work, the Li et al. (1985) correlation based on the method of Chueh and Prausnitz (1967) was employed:

$$k_{ij} = 1 - \left(2 \frac{\sqrt{V_{ci}^{1/3} V_{cj}^{1/3}}}{V_{ci}^{1/3} + V_{cj}^{1/3}} \right)^\theta \quad (5-8)$$

where, V_{ci} , is the critical molar volume (m^3/kgmol) of the component i , and θ is the dimensionless binary interaction exponent. When necessary the interaction parameters are fine tuned by adjusting the exponent in Equation 5-8.

Volume Translation

While cubic EoS can provide accurate predictions of vapour-liquid equilibrium, the predicted liquid phase densities are not accurate. Peneloux et al. (1982) reported that the calculated liquid densities can be improved by shifting the calculated liquid density with a constant volume as follows:

$$v_{mix}^t = v_{EoS} - \sum_{i=1}^{nc} x_i r_i \quad (5-9)$$

where, v^t is the translated molar volume of mixture, v_{EoS} molar volume from the cubic equation of state, r_i is volume shift value for each component, and x_i is mole fraction of each component. The volume shift does not affect the fugacity and equilibrium pressure calculated from a cubic EoS but improves the liquid phase density prediction. In WinProp the volume shift is zero by default. The correlation of Jhaveri and Youngren (1988) can be applied to calculate volume shift parameter for any component. Also the volume shift value can be changed in the regression calculation to match experimental liquid density.

Viscosity Modeling

Equations of state do not provide viscosity predictions. However, viscosity models can be coupled with an equation of state. In this work, the Pedersen viscosity correlation (1987) was used to predict the viscosity of heavy oils. The viscosity of a mixture calculated using the Pedersen model depends strongly on the critical pressures, critical temperatures and molecular weights of the components. The coefficients, b_1 to b_5 , (Equation 2-11 and 2-12) can be tuned to fit measured data.

Two different versions of the Pedersen correlation are available in WinProp. The Modified Pedersen (1987) uses a modification to the methane viscosity equation as described in Pedersen and Fredenslund (1987). This modification showed improved results for heavy oil mixture viscosities and was used in this thesis.

5.2. Athabasca Bitumen Characterization

Since bitumen is an ill-defined mixture of literally millions of different chemical species, it is impossible to model it as a collection of pure components. Instead, the bitumen is represented as a mixture of pseudo-components where each pseudo-component represents a boiling point interval. The properties of each pseudo-component are determined from correlations based on the boiling point and constrained by other known properties such as the average density and molecular weight of the bitumen.

In this work the Athabasca bitumen was initially characterized using an ASTM D2887 simulated distillation curve, Figure 5-1, constrained with a bulk liquid density of 1010 kg/m³ (at 15.56°C and 101.325 kPa, i.e. specific gravity of 1.01) and an average molecular weight of 552 g/mol. The distillation curve (a distribution of normal boiling points) was then split into series of pseudo-components using the oil characterization routine from the VMGSim process simulator. Details of splitting a distribution curve into pseudo-components are provided in VMGSim user manual but are summarized below.

Step 1: The experimental distillation curve was extrapolated over the residue fraction of the bitumen.

Step 2: The distillation curve was divided into 28 pseudo-components representing boiling point intervals of equal ΔT (the Refining Method). The average boiling points of the pseudo-components ranged from 265.7 °C to 865.6°C, Figure 5-1.

Step 3: A pressure-temperature two phase envelope was predicted using the PR-EoS with the full number of pseudo components. The pseudo-components were lumped to reduce the number of pseudo-components to 5, 4, and 3. Then, P-T two phase envelopes were generated for each characterization and compared with the full characterization phase envelope. Figure 5-2 shows that bitumen can be represented with 4 pseudo components within reasonable error. The critical temperature of bitumen with full characterization (28-pseudo components, $T_c = 772.3^\circ\text{C}$) and with reduced to 4 lumped pseudo components ($T_c = 768.8^\circ\text{C}$) are similar. The critical pressure with 4 lumped component ($P_c = 2052 \text{ kPa}$) is just 150 kPa (only 0.5 %) less than full characterization critical pressure ($P_c = 2192 \text{ kPa}$).

Table 5-1 shows the properties and composition of the 4 pseudo-components obtained from this characterization procedure for the Athabasca bitumen.

After creating the pseudo-components, the model was tuned in three steps:

1. adjust the binary interaction parameters to match saturation pressure data for the pseudo-binaries of bitumen/propane and bitumen/carbon dioxide

2. adjust the volume translation parameters to match the density of the bitumen\propane mixtures (an existing correlation was used for bitumen/carbon dioxide mixtures)
3. adjust the viscosity correlation parameters to match viscosity data for the pseudo-binaries

After tuning, the model was tested on the data for the two pseudo-ternary mixtures of bitumen, propane and carbon dioxide. The model tuning and testing are presented below.

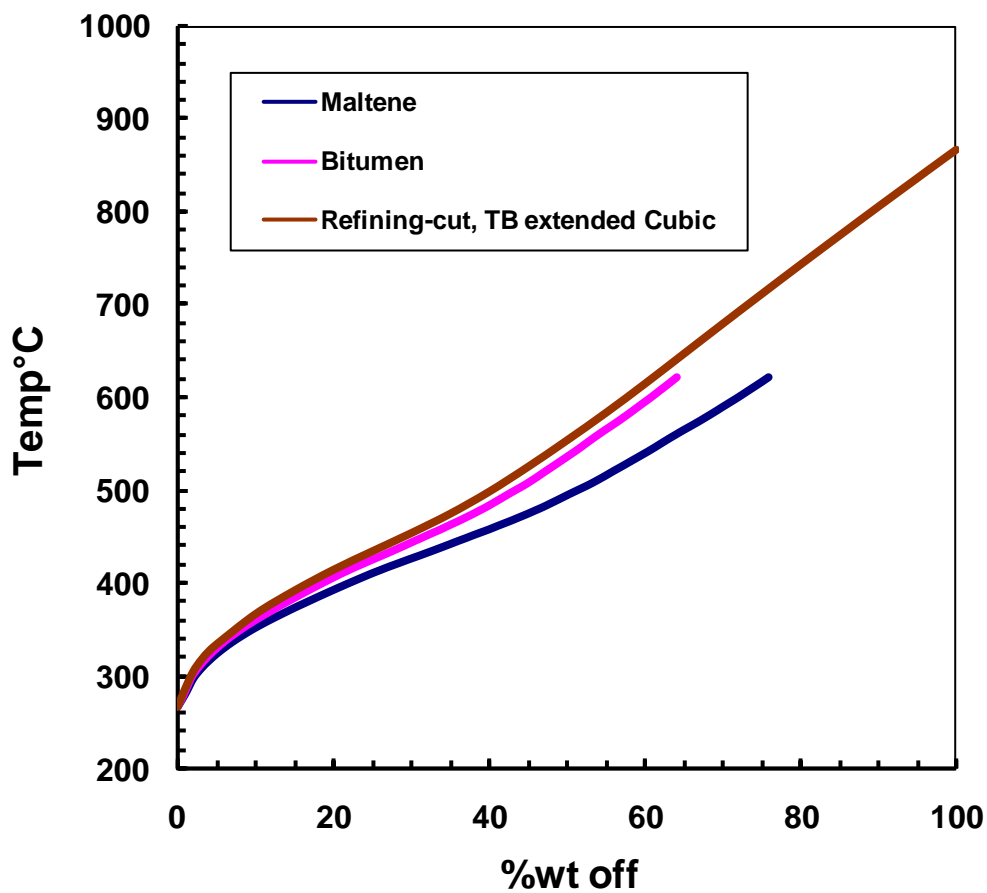


Figure 5-1: Athabasca Bitumen TBP curve, and VMGSim Extended TBP curve.

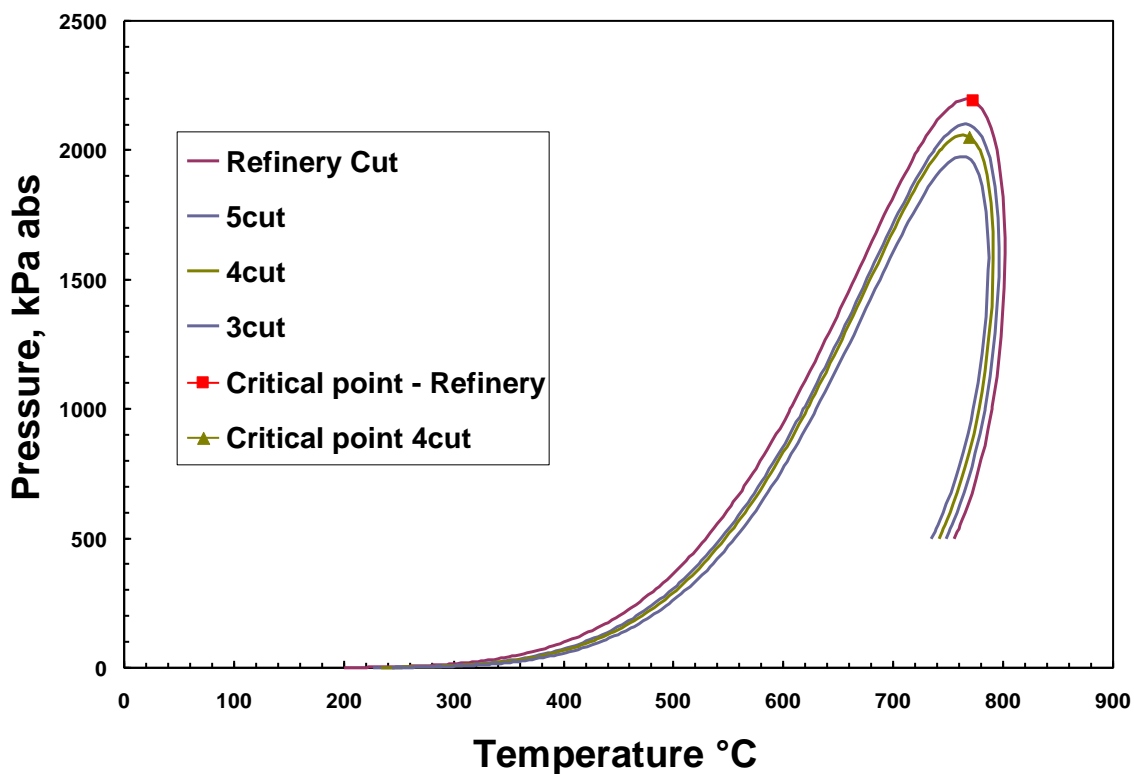


Figure 5-2: Effect of the number of pseudo-components on the predicted P-T two phase envelope for Athabasca bitumen (PR EoS with refinery cuts).

Table 5-1: Properties and composition of pseudo-components used to characterize Athabasca bitumen.

	HYP1	HYP2	HYP3	HYP4
Sg	931.19	977.33	1034.74	1096.73
MW	350.99	483.27	694.30	951.13
NBP [C]	372.12	472.88	612.23	781.08
Pc [kPa]	1700.07	1390.67	1072.87	803.86
Tc [K]	843.38	936.29	1061.89	1214.58
Vc [m3/kmol]	0.9376	1.1859	1.5467	2.0048
Acentric factor	0.7435	0.9736	1.1858	1.4108
Mole Fraction	0.3625	0.2763	0.2036	0.1576
Vol Fraction	0.2500	0.2500	0.2500	0.2500
Mass Fraction	0.2305	0.2419	0.2561	0.2715

5.3. Model Tuning for Mixtures of Athabasca Bitumen and Propane

Propane properties are available in WinProp's component library. The WinProp regression subroutine was used to tune PR-EoS parameters to match the experimental data presented in Chapter 4. First the saturation pressure data for Athabasca bitumen and propane were matched. Then the predicted density of this binary system was tuned. In the final step, the WinProp viscosity correlation was adjusted to match to the experimental data. The details of this tuning process are explained in the following sections.

5.3.1 Saturation Pressure

The saturation conditions for different compositions of propane in bitumen are reported in Table 4-5 (Chapter 4). The EoS model was tuned to match the saturation pressures at all reported temperatures for 10.9 wt% and 15.6 wt% propane in bitumen. Then, the predicted pressures from the tuned EoS model were compared with the data at the other compositions (5.2 and 25.5 wt% propane).

An exponent of 0.46 for the binary interaction parameter correlation, Eq. 5-8, provided the best fit to the saturation pressures, Figure 5-3. The predicted saturation pressures for all different composition of propane in bitumen were within mean average error of 6.7% for the whole temperature range. The average absolute deviation (AAD) in the absolute error for all the experimental data is 4.45%. The equation of state model saturation pressure prediction is very close to the activity model developed in the previous chapter for bitumen and propane system (Equation 4-5). The maximum error of 20% is for

5.2wt% saturation pressure at 20°C where due to high viscosity of the system there is lower confidence in the measured saturation pressures at this composition.

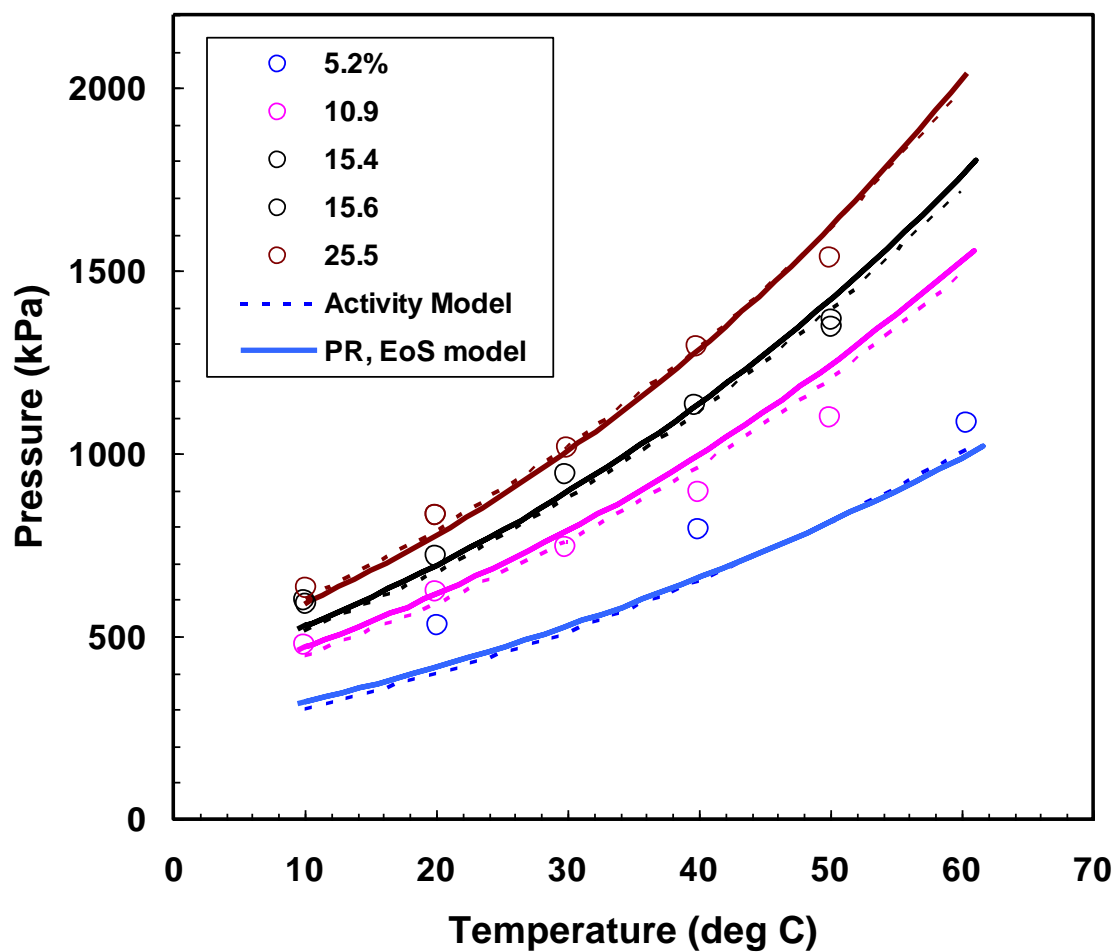


Figure 5-3: Measured (symbols) and modeled (lines) saturation pressures of mixtures of propane and Athabasca bitumen.

5.3.2 Density

The volume shift parameters for propane and all of the pseudo-components were adjusted by a similar magnitude to match the measured density of the mixtures, Table 5-2. The tuned densities are compared with the measured densities in Figure 5-4. The equation of state model predicts the liquid density with mean absolute error (MAE) of 1.14%. The AAD in the absolute error for all experimental density data is 0.52%.

Table 5-2: The final volume shift value obtained to match experimental density data for Propane and bitumen system.

Vshift	Lower Bound	Upper Bound	Initial Value	Final Value	% Change
HYP4	-1.54E-01	9.52E-02	5.13E-02	-2.04E-02	-139.67
HYP3	-1.54E-01	2.00E-01	7.83E-02	-3.11E-02	-139.67
HyP2	-1.54E-01	2.00E-01	1.15E-01	-4.55E-02	-139.67
HYP1	-1.54E-01	2.00E-01	1.56E-01	-6.19E-02	-139.67
C3	-1.73E-01	2.67E-02	-7.33E-02	-1.73E-01	-136.42

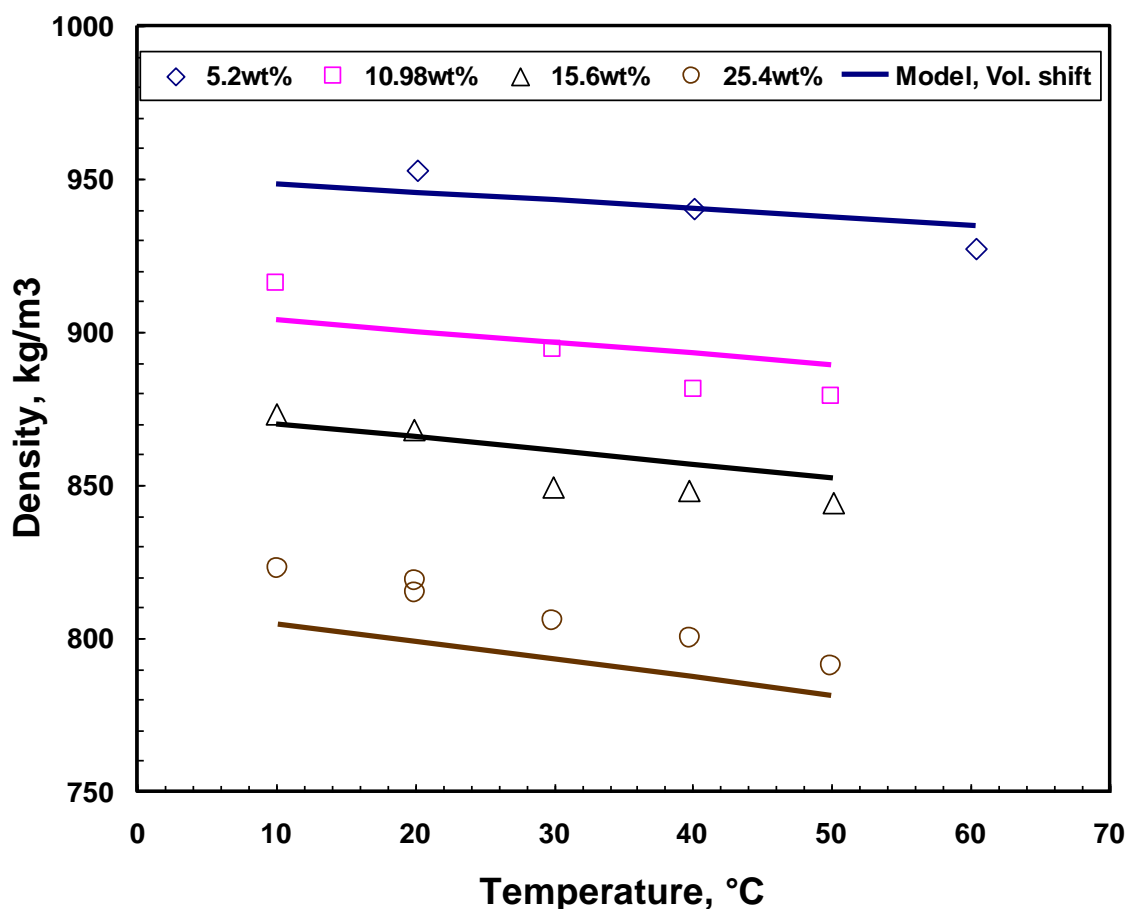


Figure 5-4: Measured (symbols) and modeled (lines) saturation liquid density of mixtures of propane and Athabasca bitumen (volume shifts from Table 5-2).

5.3.3 Viscosity

The b_1 to b_5 coefficients in the Pedersen correlation (Equation 2-11 and 2-12) were selected as regression calculation parameters to match the experimental viscosity for the Athabasca bitumen and propane. Figure 5-5 shows the effect of regression calculation on improving Pedersen correlation viscosity prediction for this binary system. Pure propane and Athabasca bitumen viscosity in this figure are from Equation 3-7 and 4-3. The

experimental data for the highest and lowest temperature at each concentration of propane was used in the regression calculation. The viscosity values for the rest of the temperature and pressure conditions were predicted and compared to the experimental data in Figure 5-5. The mean absolute error for the experimental data that was used in the regression calculation was 24.2%, where the average absolute deviation in all the error was 15%.

Table 5-3. Propane Bitumen Experimental Viscosity and Regression Errors.

Propane wt Frac	Temp °C	Pressure kPa	Experimental data	Before regression	After regression	ERROR reduction	ERROR after
0.2581	10.65	904	4.20E+01	5.83E+00	2.09E+01	3.59E-01	5.02E-01
0.2581	49.58	1786	8.59E+00	2.56E+00	8.20E+00	6.57E-01	4.54E-02
0.1009	50	3564	8.05E+01	6.68E+01	7.56E+01	1.10E-01	6.03E-02
0.1009	88.03	3564	1.50E+01	1.63E+01	2.29E+01	-4.36E-01	5.23E-01
0.1564	30.49	1551	6.99E+01	2.29E+01	4.77E+01	3.55E-01	3.18E-01
0.1564	50	1694	3.40E+01	1.18E+01	2.53E+01	3.97E-01	2.56E-01
0.0524	60.23	4890	2.23E+02	5.52E+02	1.90E+02	1.33E+00	1.46E-01
0.0524	90.5	4891.6	5.44E+01	1.11E+02	5.89E+01	9.62E-01	8.40E-02

ERROR Reduction = ERROR before regression - ERROR after regression

ERROR = (experimental - calculated) / experimental

MAE 2.42E-01
AAD 0.157782

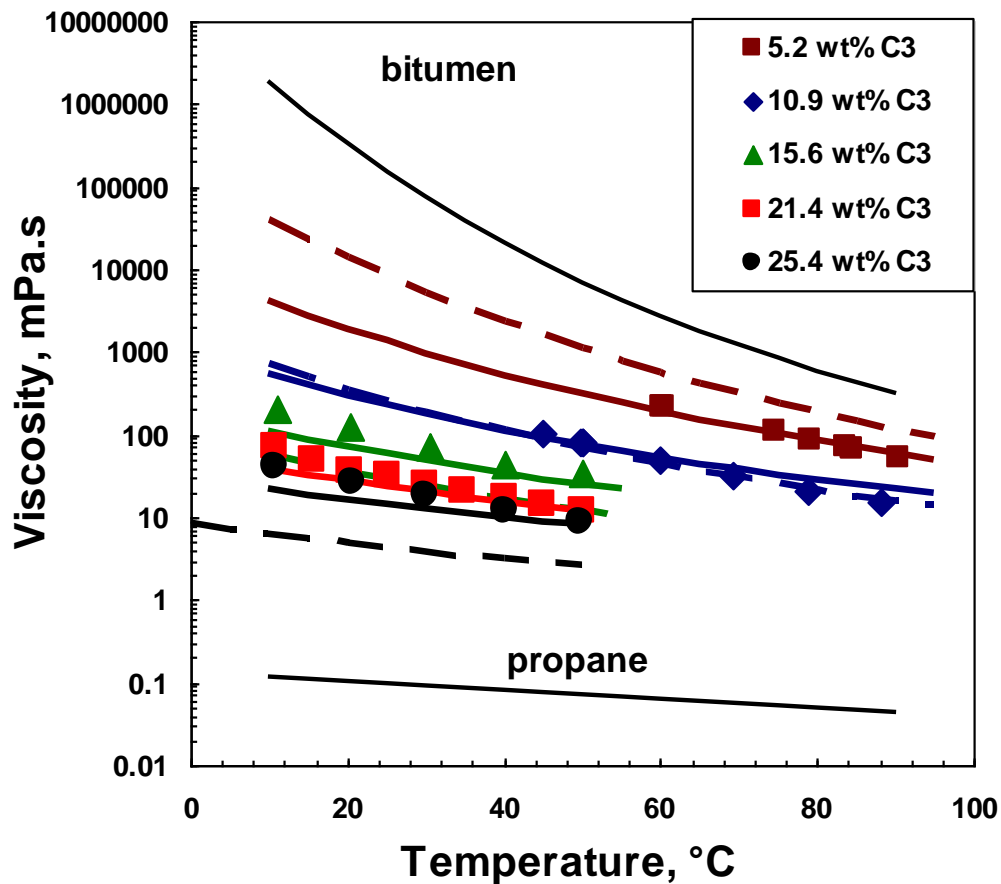


Figure 5-5: Modified Pedersen (1987) predicted viscosity for Athabasca bitumen and propane binary mixtures. Dashed lines are result before regression. Solid lines are prediction after adjusting b1-b5 coefficients by regression calculation in WinProp.

Recall that the viscosity data were also modeled with the Lobe and Shu analytical correlations in Chapter 4. Figure 5-6 compares the viscosities calculated with the different methods for Athabasca bitumen and propane saturated liquid mixtures. The modified Shu correlation gives the best match to the experimental data but this correlation is not available in most commercial thermodynamic or reservoir simulation

software. The tuned Pedersen correlation, which is available in the software, provided acceptable results for the conditions in this study. However, the comparison with the Shu correlation in the Figure 5-6 suggests that the modify Pedersen correlation may have significant errors as the temperature and propane content decrease.

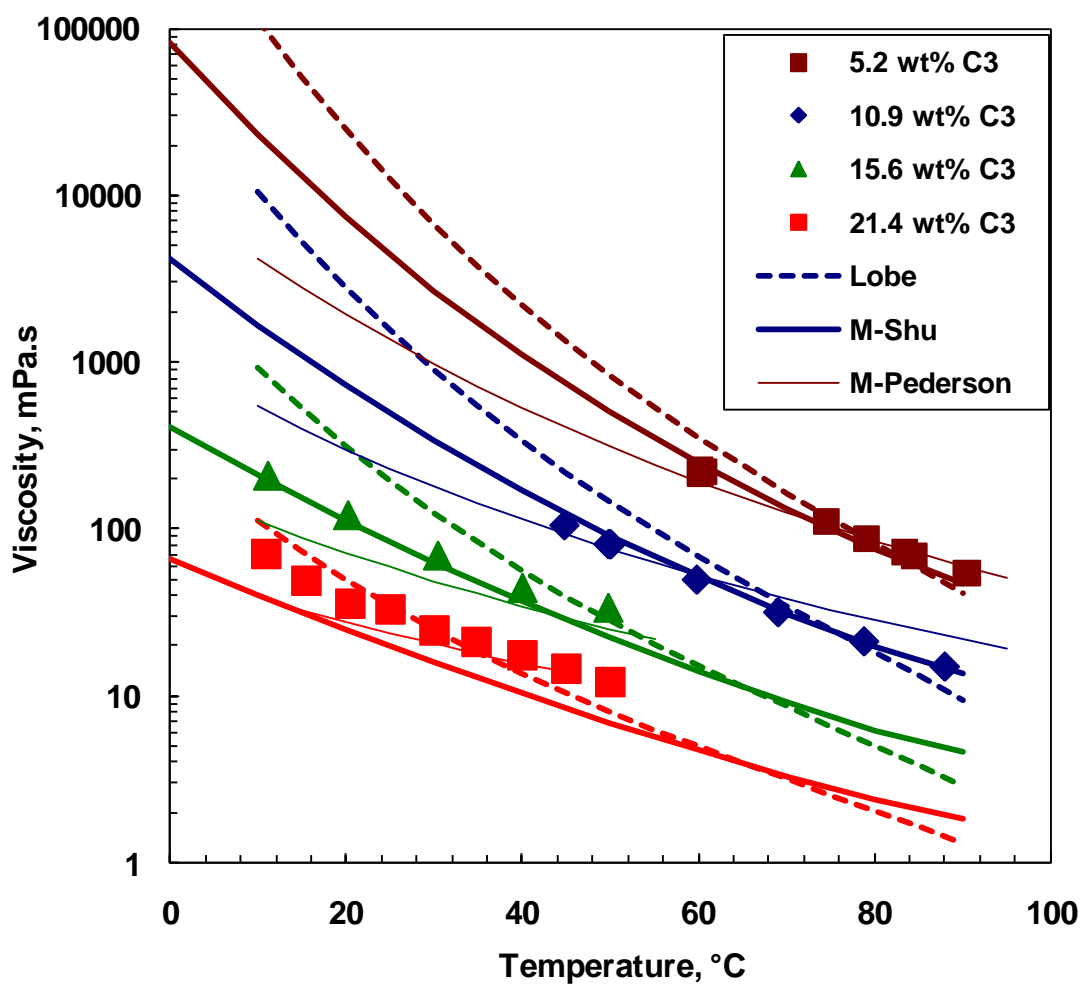


Figure 5-6: Comparison of viscosity models for Athabasca bitumen and propane saturated liquid mixtures.

5.4. Model Tuning for Mixtures of Athabasca Bitumen and Carbon Dioxide

The modified PR-EoS model obtained from bitumen and propane was extended to calculate the bitumen – carbon dioxide binary system experimental saturation pressures reported by Svrcek and Mehrotra (1982) along with the saturation pressure data obtained during this study. The binary interaction parameter between carbon dioxide and bitumen fractions was adjusted to further improve calculated saturation pressures against experimental data. The binary interaction of 0.092 was found to give the best fit, Figure 5-7. The mean absolute error for all the saturation data at 25, 42, and 63°C was 8.1 %, with average absolute deviation of 5.2% from mean absolute error. Figure 5-7 also compares the EoS model results with the Henry's law correlation presented in Chapter 4 (Equation 4-17). The general Henry's law correlation provides a slightly better fit than the EoS model with mean absolute error of 5.4%.

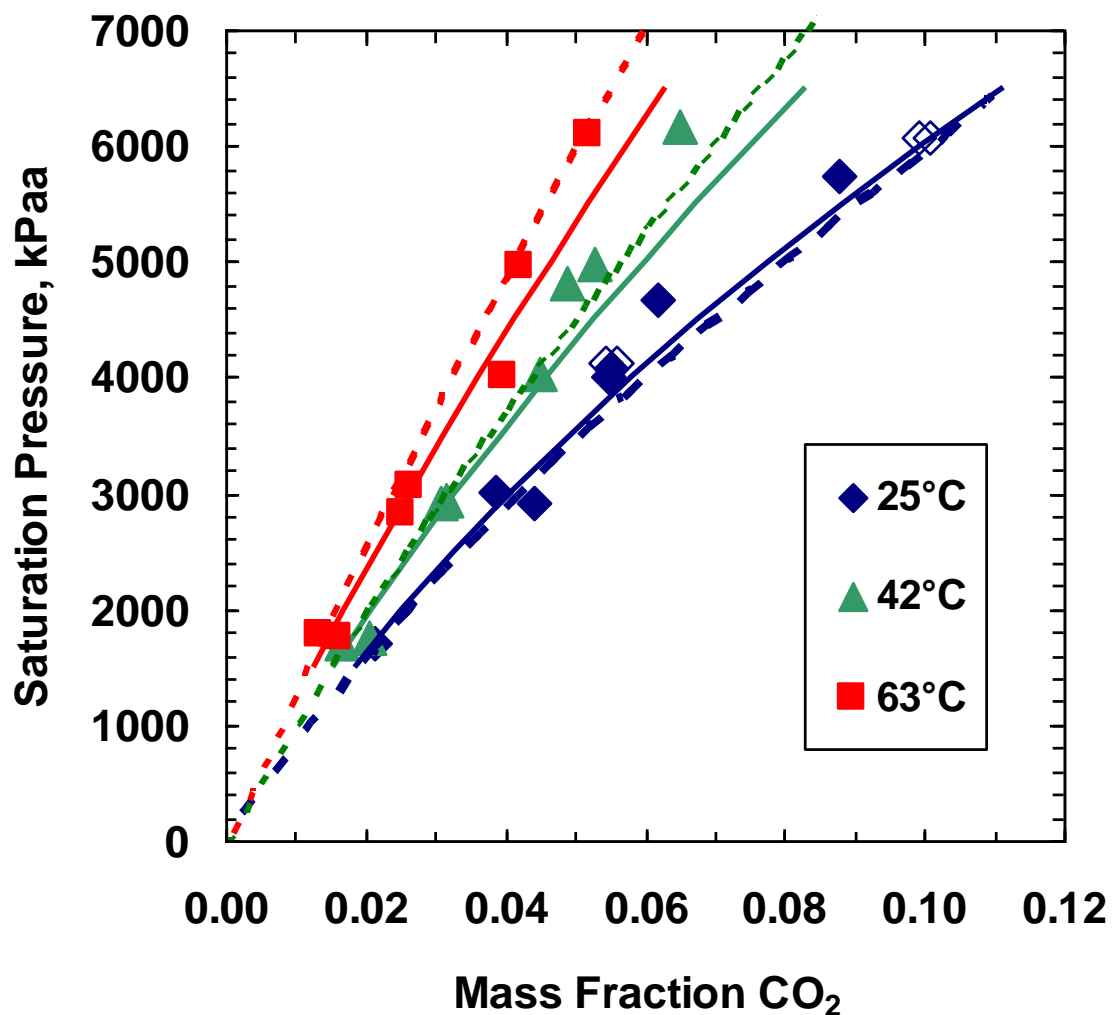


Figure 5-7: Saturation pressures of Athabasca bitumen and carbon dioxide pseudo-binary mixtures. Solid symbols are from Svrcek and Mehrotra (1982); open symbols are from this work; dashed lines are EoS model; solid lines are from Henry's law correlation.

5.6. Model Predictions for Athabasca bitumen/Carbon Dioxide/Propane Pseudo-Ternary Mixtures

5.6.1 Saturation Pressure

Before testing the EoS model on the pseudo-ternary mixture, it is necessary to estimate the binary interaction parameter between propane and carbon dioxide.

5.6.1.1 Propane and Carbon Dioxide Binary System

There are extensive data available for the binary mixture of propane and carbon dioxide in the chemical equilibrium data book DECHEMA. The volumetric and phase behaviour of the propane – carbon dioxide binary system was reported by Reamer et al. (1951). The binary interaction coefficient between propane and carbon dioxide was adjusted to 0.135 to match the experimental data. Figure 5-8 shows the modeled P-X two phase envelope.

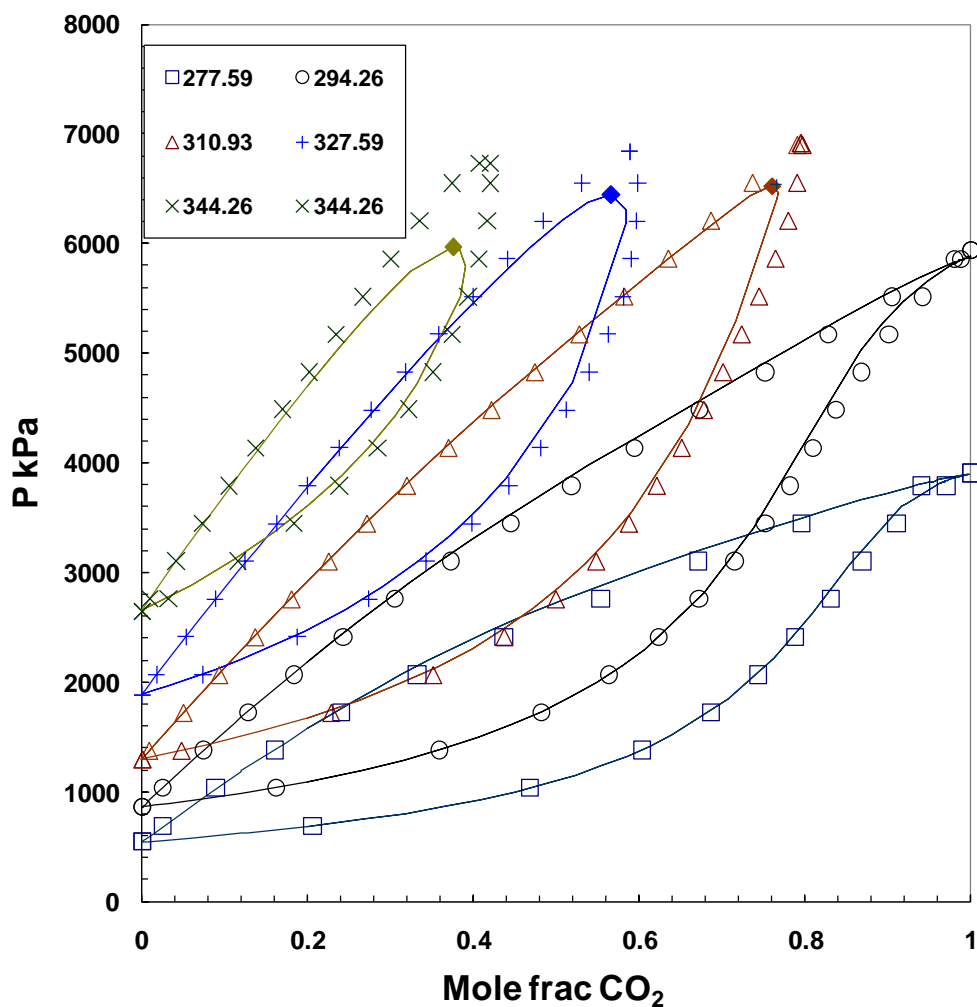


Figure 5-8: Measured (symbols) and modeled (lines) P-X two phase envelope for propane and carbon dioxide. Data from Reamer (1951). Model is PR EoS with $k_{ij} = 0.1315$.

5.6.1.2 Bitumen, Propane, and Carbon Dioxide Pseudo-Ternary

The PR-EoS model obtained so far has successfully predicted the binary systems of propane-Bitumen, carbon dioxide-bitumen, and propane-carbon dioxide. Ideally it was expected that the EoS model to predict the vapour – liquid equilibrium data for the ternary system of propane-carbon dioxide-bitumen without further tuning of binary

interaction parameters. The predicted saturation pressures for the two ternary mixtures (Case 1: 11.0 wt% carbon dioxide, 13.5 wt% propane; Case 2, 6.2 wt% carbon dioxide, 24.0 wt% propane) are shown in Figure 5-9. It is clear that the propane-carbon dioxide binary interaction of 0.135 was not useful for bitumen-propane-carbon dioxide ternary system. The interaction of propane-carbon dioxide seems to be different with presence of large molecules of bitumen fractions.

The model was further tuned by adjusting the binary interaction between propane and carbon dioxide to a value of 0.2779, Figure 5-9. This binary interaction was obtained by matching the saturation pressure for Case 1 at 10 and 25 °C with 3.8% error. Then, the resulting saturation pressures for other conditions in Case 1 and Case 2 were predicted and compared with experimental data, Figure 5-9. The new binary interaction parameter between CO₂ and propane can predict all the experimental data for Cases 1 and 2 with a mean absolute error of 1.87% and an average deviation relative to the mean error for all the data of 1.5%. This further confirms the workflow that was pursued to develop equation of state fluid model for the propane-carbon dioxide-bitumen: 1) characterize the bitumen based on a SimDist extended analysis; 2).tune the equation of state parameters for the binary systems. The tuned model could then predict the saturation properties of ternary mixtures.

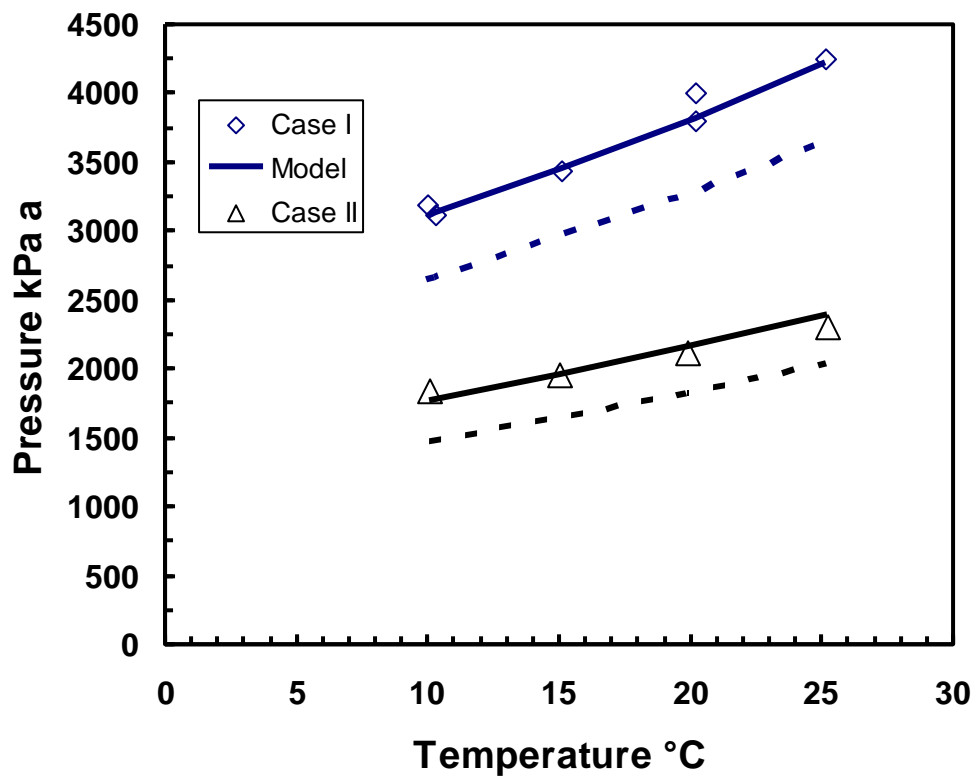


Figure 5-9: Measured (symbols), predicted (dashed lines, $k_{ij} = 0.135$), and tuned (solid lines, $k_{ij} = 0.2779$) saturation pressures for pseudo-ternaries Case 1 and Case 2 from table 3-5.

5.6.2 Density

The volume shift parameters for bitumen/propane from Table 5-2 and the Jhaveri and Youngren (1988) volume shift correlation for carbon dioxide were used without modification. Figure 5-10 shows the density predicted by equation of state model for ternary system Cases 1 and 2. The mean absolute error of predicted liquid density for all experimental data was 1.25%, whereas the average absolute deviation from mean error was 0.62%. Therefore two parameter Peng-Robinson cubic equation of state liquid density

prediction is substantially improved by introducing the third parameter (i.e. volume shift) to the cubic equation of state.

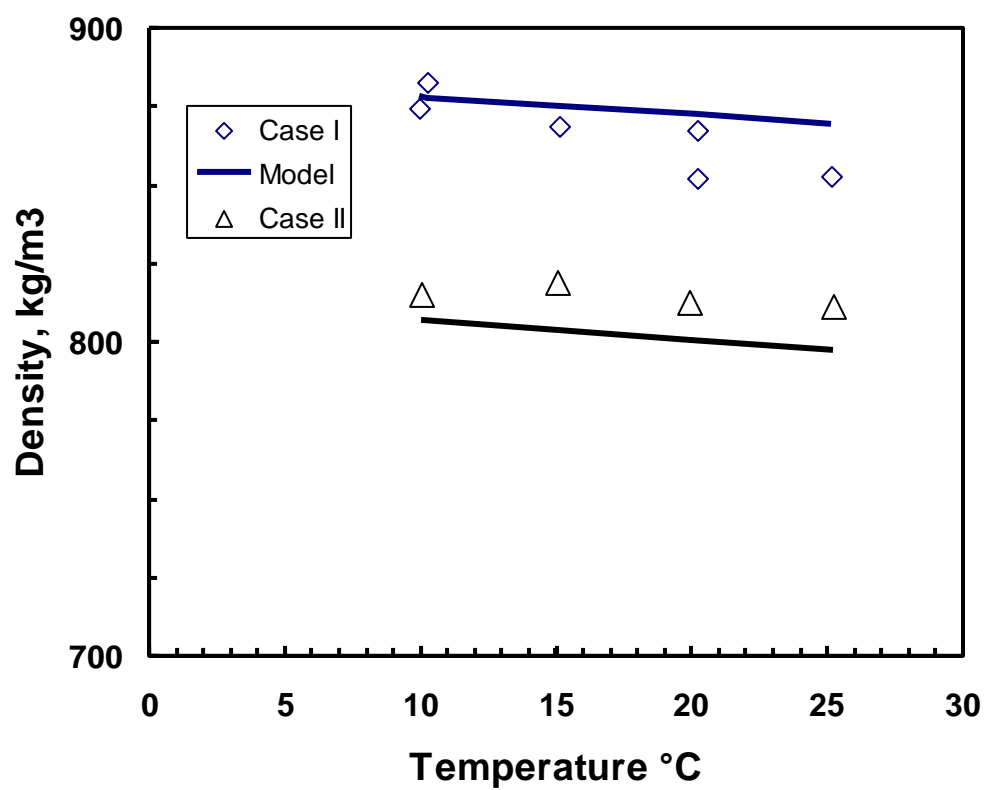


Figure 5-10: Measured (symbols) and predicted (lines) densities of the pseudo-ternaries, Case 1 and Case 2.

5.6.3 Viscosity

The modified Pedersen correlation parameters were obtained from propane – bitumen binary system (Figure 5-5). It was used without further modification to predict the viscosity of the propane – carbon dioxide – bitumen ternary mixtures, Figure 5-11. The modified Pederson viscosity correlation could predict the ternary system viscosity within one order of magnitude of the experimental data for Case 1 and 2. The prediction at temperature above 20 degree was better than at lower temperatures. The mean absolute error was 21%, where the relative absolute deviation from mean absolute error was 8%. The Lobe mixing rule at lower concentration of CO₂ (Case 2) predicts the ternary mixture viscosity better than higher concentration of CO₂ in ternary system.

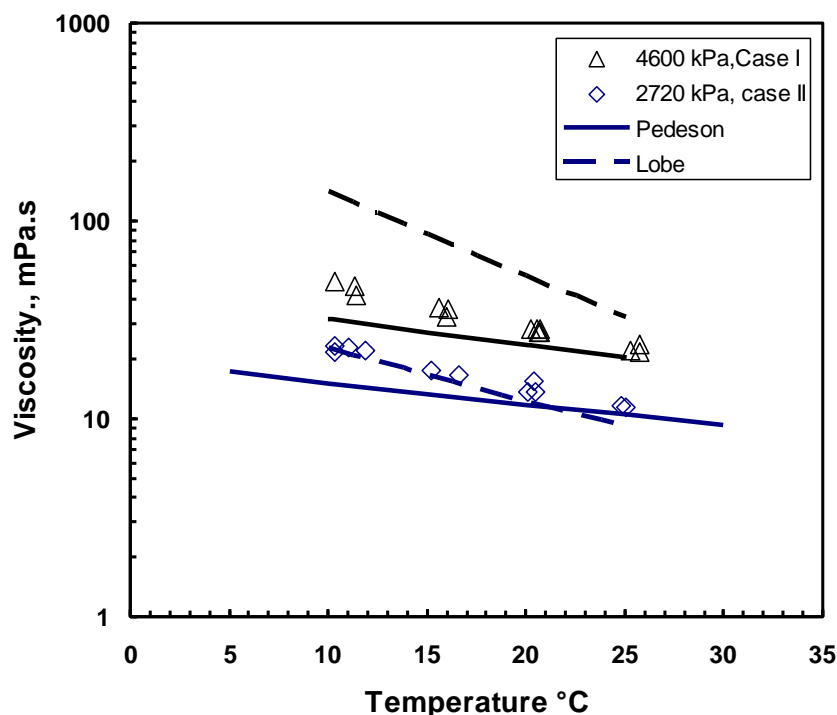


Figure 5-11: Measured (symbols) and predicted (Pederson lines, Lobe mixing rule dash line) viscosity for pseudo-ternaries, Case 1 and Case 2.

7. Summary

A methodology was developed to characterize Athabasca bitumen into pseudo components. The SimDist analysis of asphaltene free fraction of Athabasca bitumen was converted to normal boiling point distribution of bitumen. The pseudo component critical properties and molecular weight obtained from characterization process were sufficient to model bitumen and solvent blends, using Peng-Robinson equation of state.

The binary interaction parameter in the Peng-Robinson equation of state was adjusted to improve the saturation pressure and solubility prediction for ternary mixture of propane, carbon dioxide, and bitumen.

It was confirmed that the two parameter cubic equation of state required a third parameter (i.e. volume-shift) to better predict liquid density. The volume shift parameter was adjusted to improve cubic equation of state calculated liquid density against experimental data.

Pederson (1987) viscosity correlation coefficients were modified to improve liquid viscosity prediction for propane, carbon dioxide, and bitumen mixtures.

CHAPTER 6 : VAPEX PHYSICAL MODEL AND EXPERIMENTAL METHODS

This chapter presents the apparatus and procedures used to evaluate the Vapex process at the lab scale. The physical model was designed to represent a vertical slice of the reservoir pattern perpendicular to the well pair. It was made in the form of an annulus between two coaxial pipes and packed with glass beads. The Vapex solvent preparation, physical model packing and saturation, Vapex experiment procedures, and produced live oil properties measurements are described in the following sections.

6.1 Apparatus

Figures 6-1, 6-2 and 6-3 show a simplified process flow diagram and photographs of the experimental apparatus. The apparatus is comprised of the following major units:

- Solvent injection unit
- Vapex physical model
- Live oil production, sampling and properties measurement unit
- Ambient condition separator and gas gathering unit
- Compositional analysis unit

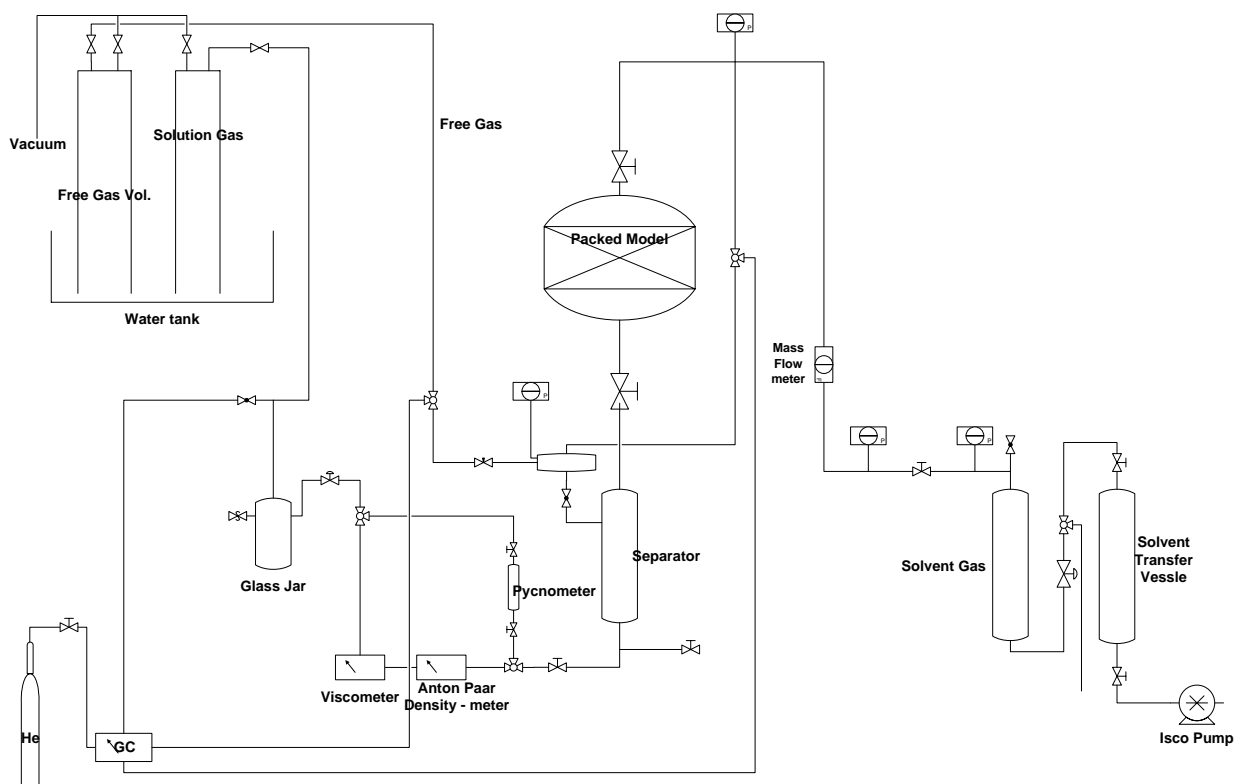


Figure 6-1: Simplified process flow diagram of the Vapex experimental apparatus.

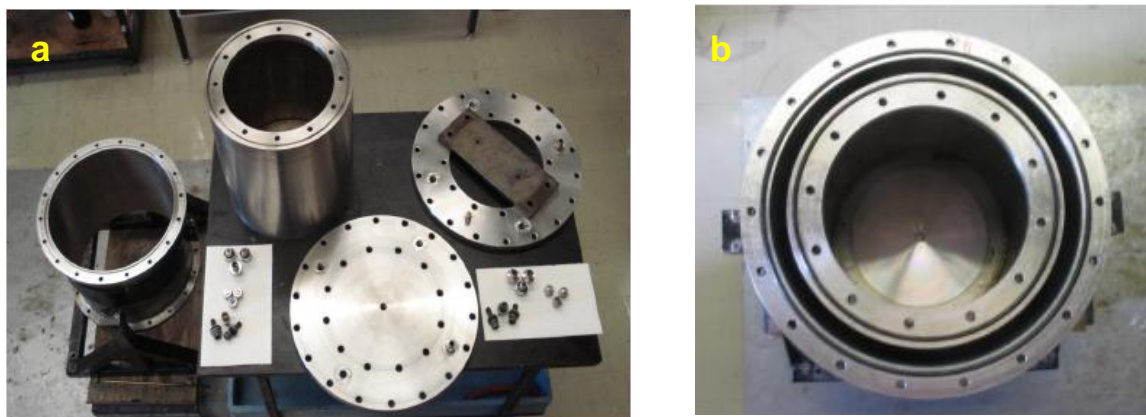


Figure 6-2: Photograph of Vapex physical model (a, model components. b, partially assembled physical model top view).

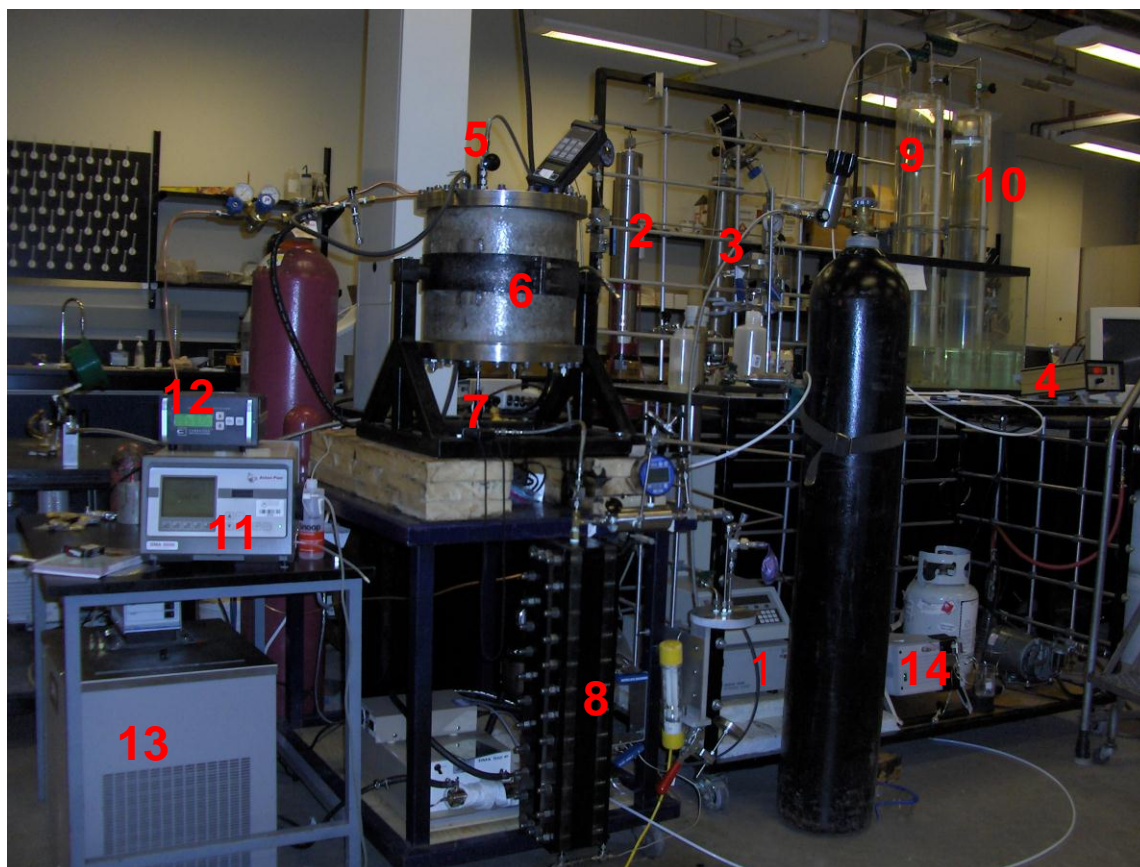


Figure 6-3. Vapex Experimental Setup. (1- Isco Pump, 2 - Liquid solvent vessel, 3 - Vapor solvent vessel, 4 – Mass Flow meter, 5 – Injection well, 6 – Vapex physical model, 7 – Production well, 8 – High pressure separator, 9 – Free gas volume meter, 10 – Solution gas volume meter, 11 – Density meter, 12 – Viscosity meter, 13 – Water bath, 14 – Agilent GC.)

The solvent injection unit consisted of a positive displacement pump (ISCO model 500D), a 1.2 litre high pressure transfer vessel for liquid solvent, a back pressure regulator, a five litre capacity high pressure container for vapour solvent, a pressure regulator, and a mass flow meter (Brooks Analog Thermal Mass Flow Meter model 5860E).

The Vapex physical model was a vertical slice type model built in cylindrical geometry using the annular space between two co-axial pipes. The co-axial pipes were flanged into two stainless steel discs on the top and bottom, which served to seal the ends of the annulus. The annulus was packed with 12-16 U.S. Mesh glass beads. The annular cavity of the model was 12 in (30.48 cm) high, 12.1 in (30.73 cm) OD, 10.71 in (27.2 cm) ID with total volume of 4.90 Liters.

The fluid production and property measurement unit consisted of a high pressure vessel with a calibrated sight glass to separate the produced live-oil and vapor at the test pressure and temperature. The property measurement section was equipped with a stainless steel pycnometer ($11\text{e-}6\text{ m}^3$ at 20°C), an in-line viscometer, and a digital density-meter. A ViscoPro2000 Cambridge viscometer was used to measure the viscosity of the produced live-oil while an Anton Paar DMA 5000 density meter equipped with a DMA 512P external high pressure unit was employed to measure its density. These measurements were performed in-line while the live oil was displaced from the high pressure separator to the low pressure sample collection unit. A back pressure regulating valve was used to keep the pressure at test condition during the displacement of the produced live oil out of separator through the property measurement and into the sampling section.

The atmospheric separator and gas gathering unit included a 1 litre glass jar and two inverted plastic cylinders placed in water reservoir, and a vacuum pump to raise the water

level in the plastic cylinders. The cylinders were used to collect and monitor produced gas: one for the free gas and the other for the solution gas (the gas produced during the live oil discharge to glass jar at ambient conditions). In both plastic cylinders, the gas volume was measured as the volume of water displaced by gas. Each 1 cm height in the cylinders represented 153.3 mL and 102.6 mL for the free gas and solution gas, respectively.

Also a JEFRI 10 Litre gasometer was used to measure the amount of the gas dissolved in the pycnometer sample of produced live oil. An Agilent micro GC 3000 was employed for compositional analysis of the vapour phase. As shown in the process flow diagram, Figure 6-1, it was possible to take a sample or connect to the GC in-line at several points in order to examine the composition of the vapour solvent, the free gas, and the solution gas.

6.2. Experimental Procedure

An improved experimental set-up and a modified experimental procedure were developed with the aim of obtaining a better understanding of the produced live oil properties and the performance of the Vapex process. The experiments involved three steps: 1) Vapex solvent preparation; 2) physical model packing and saturation; 3) the Vapex test.

6.2.1. Solvent Preparation

The solvent mixtures of propane and carbon dioxide were prepared in high pressure transfer vessels. The vessels were filled at pressures well above the saturation pressure of

the more volatile component (carbon dioxide) so that all displacements were in the liquid state. The pressure was maintained using a back pressure regulating valve connected to the transfer fluid (i.e. hydraulic oil) side of the sealing piston in the vessel. The volume of the high pressure liquid solvent vessel was 1.2 L which limited the mass of solvent mixture that could be prepared. The volume of each component needed to make 1.2 L of the mixture (e.g. 59 wt% CO₂ and 41 wt% propane) was calculated from the component densities. The densities of carbon dioxide, propane and their liquid mixtures were calculated using VMG thermo software.

The specified volume of the lighter liquid (propane) was first injected into the transfer vessel using a positive displacement syringe pump. The pump volume displacements were cross-checked with the volume of hydraulic oil that came out of the transfer vessel through the BPR to ensure that the measured volume of liquid propane was correct. Then, the required volume of liquid carbon dioxide was added in the same way. After finishing this process, the high pressure transfer vessel was isolated and at least one day was allowed for these liquid mixtures to blend through natural convection and also by turning the vessel up-side down every three to four hours. After blending, a sample from the liquid mixture was taken at high pressure and expanded to a single phase vapour. Then, the composition was analyzed with an Agilent 6890N GC equipped with TCD detector.

6.2.2. Physical Model Preparation

The first step in model preparation was assembling the pieces and a leak test to make sure the sealing o-rings in the top and bottom flanges were working properly. Nitrogen gas at

room temperature and 4570 kPa pressure was injected into the model and, if there was no obvious sign of leak, the model was isolated and kept under pressure overnight to see whether the pressure would hold. Once the model was leak free, it was slowly depressurized to ambient pressure and then packed with 12-16 U.S. mesh glass beads. In order to have homogeneous packing, the glass beads were poured into the model from four openings at the top while the model was being vibrated with a pneumatic shaker (see Figure 6-4). Then, the filling ports were sealed and the model was vacuumed from the injection well at top to remove air out of the model. Carbon dioxide at 34.5 kPa gauge (5 psig) was injected from the production well at bottom and then the model was depressurized to ambient conditions. The vacuum was applied once again, and this process repeated for two or three times. Finally, the model was evacuated to a high vacuum and water was imbibed into the model from the bottom production well. The weight of water used to saturate the model was monitored to determine the pore volume.

The next step was to saturate the model with Athabasca bitumen. The Athabasca bitumen supply vessel was put under 103.4 kPag (15 psig) nitrogen pressure and connected to the four ports on top of the water saturated model. The whole set-up was placed inside a large Blue-M oven. The temperature was set at 40 °C to reduce the bitumen viscosity. During this bitumen injection into the model, water was produced from the production port at the bottom.

The bitumen was first injected from an inlet at the top that was at the opposite side of the bottom production well. After producing about 20% pore volume of water, two other

inlets were opened on top to the right and left sides of the bottom production well. After approximately 75% pore volume of water was displaced, the fourth inlet, directly above the production well, was opened. The displaced water was collected in a large graduated cylinder and its weight was monitored until bitumen breakthrough.

After bitumen breakthrough, bitumen production was continued to see if any more water was produced. However, due the high viscosity of the bitumen, the displacement was piston-like and there was no measurable amount of water production after breakthrough. The initial bitumen saturation was determined from the produced water volume.



Figure 6-4: Packing the Vapex physical model with 12-16 U.S. mesh glass bead.

The model is now ready for the Vapex test. The inlets at the top and the production well were all closed and 24 hours were allowed for the saturated model to reach room temperature. It was then moved and assembled into the Vapex experimental set up.

6.2.3. Vapex Test

The high pressure liquid solvent vessel filled with liquid mixture of propane and carbon dioxide, and the oil saturated packed model were placed and connected to the Vapex set-up. Then all the connections, the high pressure separator and the vapor solvent vessel were tested again for any leaks with nitrogen at 4.6 MPa, which was well above the Vapex experiment pressure. Once the set-up was leak free, the nitrogen filled compartments were brought to ambient conditions except for the property measurement unit (i.e. density-meter, viscometer, and pycnometer) which was kept at the experimental pressure.

Then, the injection side of the set-up was pressurized and filled with the vapor solvent mixture at the test pressure, while the production side was left at the ambient conditions. The solvent mixture was displaced from high pressure liquid solvent vessel to the high pressure vapor solvent vessel using the ISCO syringe pump. A back pressure regulator was used to maintain the pressure in the liquid solvent vessel above the bubble point pressure, while the pressure in the vapor solvent vessel was below the dew point pressure of the mixture. With this method, the solvent was moved from the liquid phase to the vapour phase at a fixed composition.

In order to supply the heat of vaporization for the liquid mixture and avoid a temperature decrease in the vapor solvent vessel, the liquid solvent was displaced at a constant low flow rate (1-2 cm³/min) so that a constant temperature could be maintained with a heat tape around the vapour transfer vessel. The amount of heating was just enough to prevent a temperature drop in the vapor solvent supply vessel and was adjusted proportionally to the rate of liquid solvent withdrawal from high pressure liquid solvent transfer vessel. With this procedure, a supply of constant composition gaseous solvent at room temperature and test pressure was provided to the injection well.

The next step was to start the Vapex experiment by opening the injection well. Since the packed model was saturated with Athabasca bitumen at the ambient conditions, approximately five minutes were allowed for the model to be pressurized, and then the production well was opened. Due to the high pressure of the solvent vapour, the high permeability of the glass beads, and possibly also due to the wall effects, the breakthrough of the vapour solvent happened very quickly (in less than one minute). During early time, several drops of water and bitumen were produced by a displacement process driven by the pressure difference between the top and the bottom. However, the pressure in the separator vessel and the production side of the model increased very quickly to the injection pressure and then only gravity was left as the driving force.

Once the pressure was nearly equal on both sides of the model, live oil and some free gas were produced by gravity drainage. The free gas flow rate was controlled with a fine needle valve. The composition of the free gas was analyzed during the experiment using

the micro GC. The level of the produced live-oil in the separator was recorded with time to obtain the rate of live-oil production. The flow rate of the syringe pump was adjusted to supply just enough solvent to the vaporizing vessel to stabilize the pressure and avoid over-pressurizing the vapour solvent vessel (e.g. 0.07 cm³/min).

After the live oil level had built up in the separator, the live oil was displaced out of the separator to a glass jar at ambient conditions through the property measurement and sampling unit. During this discharge, the pressure in the property measurement and sampling unit was maintained with the BPR. The back pressure regulating valve was adjusted in a way that we did not cause any pressure change in the high pressure separator. The BPR pressure was set approximately 69-138 kPa lower than the separator to make live oil move out of separator to the density-viscosity measurement unit. During the discharge, the free gas production line was closed but the production well was left open and solvent vapor along with live oil were entering the separator. The level of the oil in the separator was monitored during the discharge as well. Therefore, any volume discharged out of the separator was occupied by the produced live oil and free gas. Since the composition of free gas and its temperature and pressure were known, the moles of the free gas produced during discharge could be calculated.

The live oil was discharged from the separator through a three way valve (see Figure 6-5) that allowed it to either flow through the sampling pycnometer or through the density-viscosity measurement unit to reach the BPR, whose output was discharged to the glass jar at ambient condition. The live oil was first passed through the pycnometer. After a

volume of oil 3-4 times of the pycnometer volume was displaced, the pycnometer was isolated at the test conditions and the live oil was redirected to the density and viscosity measurement unit, where the density of the live oil and its viscosity were measured. Once the level in the separator became low enough (down to 1 cm), the discharge was stopped and the live oil sample was isolated inside the density meter and viscometer.

The sample of live oil captured in the pycnometer was moved to Jeffri Gasometer to measure the GOR and the composition of the solution gas. The density of the live oil in the pycnometer was determined. The live oil density was also measured using the in-line Anton Paar density meter. Since the viscometer was calibrated between 5 and 100 mPa.s and often the produced oil viscosity was above this range, the temperature of the produced oil left in the density-meter and viscometer was increased by circulating warm water through their shell. A profile of the viscosity of the live oil versus temperature was measured. The viscosity at the experimental conditions was estimated by extrapolating this profile.

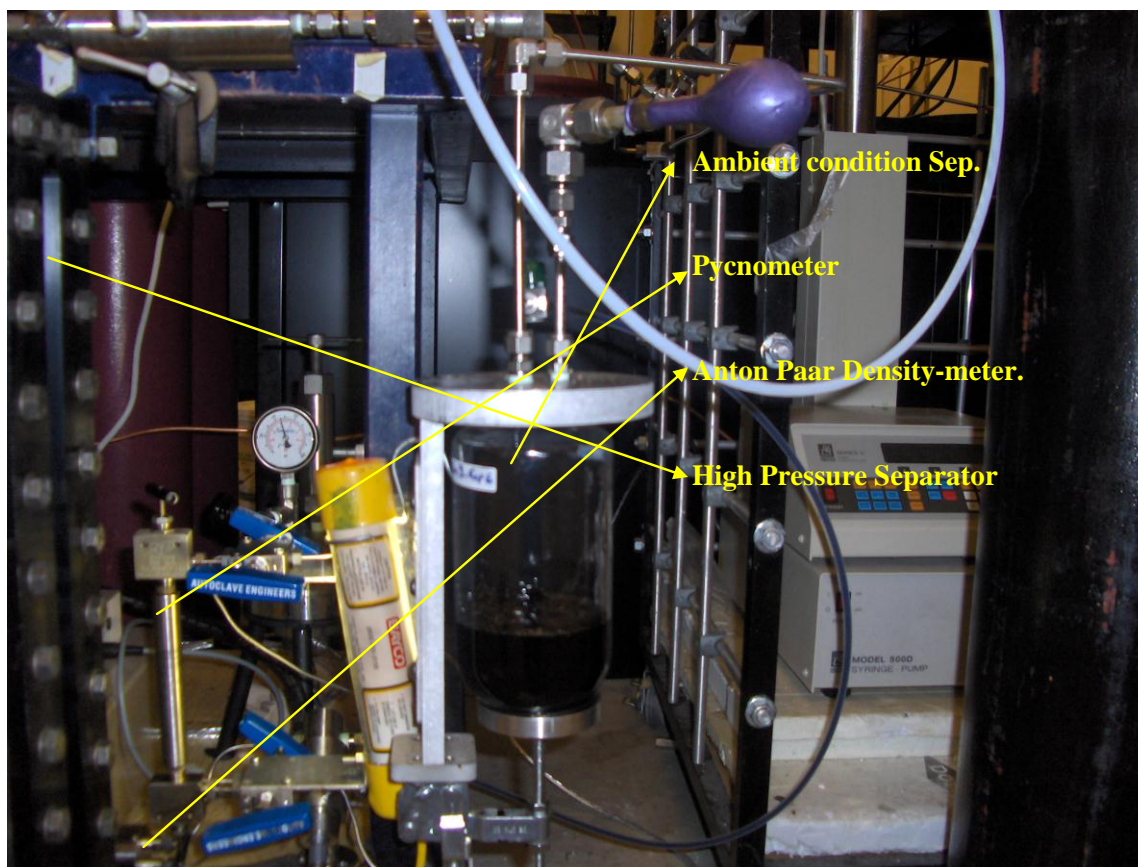


Figure 6-5: Discharging produced live oil through property measurement unit.

During the sample discharge from the separator, the amount of the gas coming out of produced live oil (the solution gas) was measured in the solution gas container by monitoring the level of the water in plastic cylinder. When the solution gas stopped coming out from the oil, the jar containing the sample was weighed and then left open under a fume hood. These jars were mildly heated to expedite the solution gas release and the amount of the gas vaporized was calculated from the change in mass of the jar sample.

Once the discharge process finished, the free gas valve was opened and monitoring of the live oil and free gas production rate continued. These cycles of production and sample discharge were continued until the end of the test and the start of the blow-down process. Each run was continued until the oil recovery was above 30% or the liquid solvent in the transfer vessel was depleted. Then, the final sample was discharged and after removing of the all the produced oil from the separator, the injection line was closed and the model was depleted to ambient conditions (blow down). The amount of vapour produced and its composition during this process were monitored. After reaching to ambient conditions, the physical model was opened to examine the depletion pattern left from the Vapex process. Finally the physical model was cleaned and prepared for the next test.

CHAPTER 7 : MATHEMATICAL MODEL OF THE VAPEX PROCESS

This chapter describes the development of a semi-analytical gravity drainage model for the Vapex process. The mathematical model developed in this chapter is applicable to the sideway expansion stage of the Vapex process.

7.1 Introduction

The previously developed models for the Vapex (Dunn et al. 1989, Heidari 2008) assumed that the diffusion coefficient of solvent in heavy oil is constant. These models are similar to the theoretical analysis of heavy oil production from in situ steam heating and steam assisted gravity drainage (i.e. SAGD). These theoretical gravity drainage models substitute a mass transfer effect (at isothermal conditions) for the heat transfer effect in previously developed mathematical models for the SAGD process.

Okazawa (2009) recently addressed the dependency of the mass transfer coefficient on concentration due to extreme viscosity reduction with solvent dissolution into bitumen. Neglecting the concentration dependence of diffusivity is a serious issue with the current analytical models. Unlike the heat transfer gravity drainage process, where the functionality of the heat transfer coefficient on temperature is weak, the molecular diffusivity of solvents in the Vapex process can change dramatically. Okazawa (2009) pointed out the difficulty of obtaining an analytical solution due to the strong non-linearity in the moving boundary partial differential equation caused by the functionality

of diffusion coefficient on concentration. He was able to obtain an approximate solution by assuming a concentration profile ahead of the solvent/bitumen interface.

We introduce a new analytical solution for the moving boundary diffusion equation of the Vapex mathematical model. The non-linearity caused by diffusion coefficient is resolved by introducing newly defined pseudo-concentration and pseudo-time terms.

7.2 Model Assumptions

Figure 7-1 shows Vapex process. Many different mechanisms are involved in the Vapex process and each has a different degree of influence on the drainage rate (Das 1998). The major mechanism of the process is the gravity drainage caused by density difference between the liquid heavy oil and the injected vapour solvent. The drainage flow of the heavy oil is boosted by the viscosity reduction due to the penetration of the injected solvent into the oil. Therefore in this study we focused on modeling how vapour solvent penetrates into the oil and its impact on the fluid flow.

In the proposed model, the diffusion coefficient is defined as a function of the solvent concentration. The diluted oil viscosity is also a function of the solvent concentration in the oil phase. The liquid phase is considered incompressible and the oil swelling due to solvent dissolution is neglected. It is assumed that the temperature and pressure in the vapour chamber are constant and that the solvent and bitumen at the interface are in equilibrium.

The interfaces between the vapour chamber and the saturated (diluted) heavy oil and between the diluted oil and undiluted heavy oil are both sharp (Butler 1989, Dunn 1989). Hence the effect of capillary force is neglected. As result of this assumption, the only phase behind the solvent – oil interface is solvent vapour and the oil phase flows ahead of this interface. Therefore the mathematical model is a moving boundary diffusion equation.

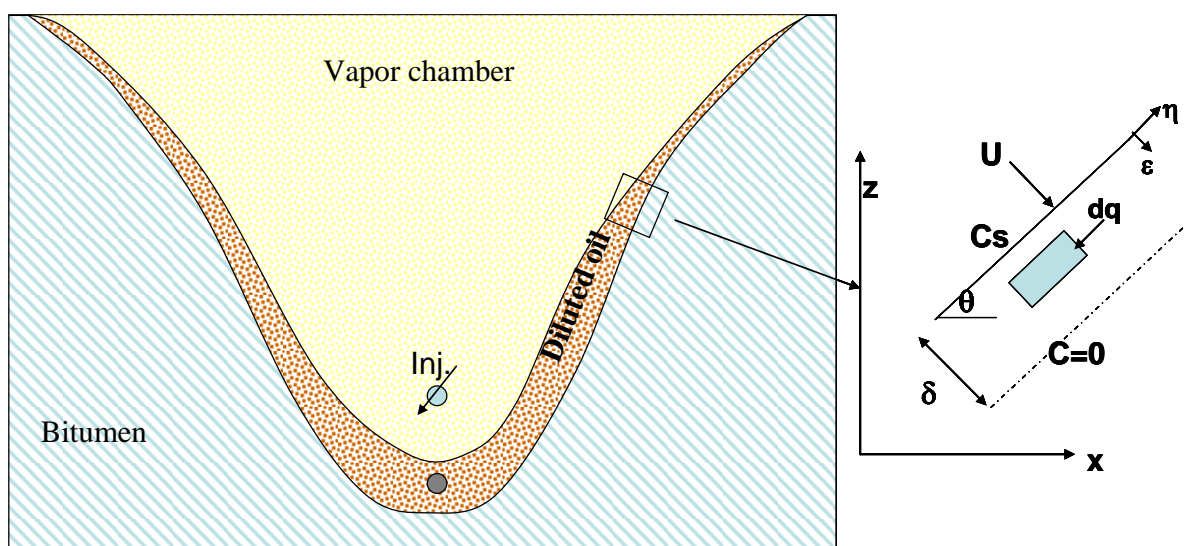


Figure 7-1: Vertical cross section of the Vapex process showing details at the interface of the heavy oil and solvent.

We assume no-flow boundary conditions for the top and the bottom (i.e. overburden, and underburden), and the vapour chamber expands laterally. Solvent vapour penetrates ahead of interface into the oil phase in the direction normal to the interface (i.e. one dimensional diffusion). Diluted oil drains parallel to the interface. In the drainage zone, the concentration of the solvent changes rapidly from equilibrium concentration to a

minimum amount in a very thin layer. The thickness of this layer is called penetration depth δ (see Figure 7-1).

The solvent concentration change ahead of interface is modeled as 1-D mass transfer process according to Fick's first law. The combination of mass transfer ahead of interface and diluted oil drainage dictates the movement of the interface. This sideways interface mobility also plays a role as a pseudo-convective term, which has impact on dispersive mass transfer into the oil zone. The rate at which diluted oil drains parallel to interface is strongly coupled with the compositional profile of solvent ahead of interface. Hence, the mathematical model of the Vapex process must account for mass diffusion, dispersion, fluid flow, and the dependence of fluid physical properties (density, viscosity, and diffusion coefficient) on concentration. In the following section, the modeling of mass transfer, fluid flow, and the moving boundary condition are explained in more detail.

7.3 Diffusion Model

7.3.1 Application of Fick's Law

In the proposed model, the solvent penetrates into oil in the direction normal to interface according to the Fick's first law. A material balance across a differential distance, $d\varepsilon$, in the diluted oil zone (see Figure 7-1), is given by:

$$\frac{\partial}{\partial \varepsilon} \left(D \frac{\partial C}{\partial \varepsilon} \right) = \frac{\partial C}{\partial t} \quad (7-1)$$

where D is diffusion coefficient m^2/sec and C is the solvent volume fraction in the diluted oil m^3/m^3 . The model is assumed to be semi-infinite since the penetration depth of mass transfer into the bitumen zone compared to the physical dimension of the system is small.

Therefore, the initial and boundary conditions are:

$$C = 0 \quad @ t = 0, 0 \leq \varepsilon \quad (7-2)$$

$$C = C_s \quad @ t > 0, \varepsilon = I(t) \text{ interface} \quad (7-3)$$

$$C = 0 \quad @ t > 0, \varepsilon \geq (I(t) + \delta) \quad (7-4)$$

where $I(t)$ represents the location of the interface at any time, C_s is the solvent concentration in bitumen at interface, and δ is the penetration depth. The highest concentration of the solvent in the bitumen (C_s) is at the interface between the solvent and the bitumen where the bitumen is saturated with solvent at the process pressure and temperature. Hence, the normalized concentration, C_D , is defined as:

$$C_D = \frac{C}{C_s} \quad (7-5)$$

Equation 7-1 can then be written as:

$$\frac{\partial}{\partial \varepsilon} \left(D \frac{\partial C_D}{\partial \varepsilon} \right) = \frac{\partial C_D}{\partial t} \quad (7-6)$$

The initial and boundaries conditions become:

$$C_D = 0 \quad @ t = 0, \varepsilon \geq 0 \quad (7-7)$$

$$C_D = 1 \quad @ t > 0, \varepsilon = I(t) \text{ interface} \quad (7-8)$$

$$C_D = 0 \quad @ t > 0, \varepsilon \geq (I(t) + \delta) \quad (7-9)$$

The location of the interface is determined by material balance and involves solving Equation 7-6 coupled with the fluid flow equation.

The mass diffusion coefficient (D) is a known function of concentration. The functional dependence of D on C_D can be complex. Here it was assumed to be a simple power law relationship, as proposed by Okazawa (2009):

$$\frac{D}{D_s} = C_D^d \quad (7-10)$$

where D_s is the diffusion coefficient at the interface (i.e. $C_D = 1$). Figure 7-2 shows normalized diffusion coefficient versus normalized concentration for different values of the power d .

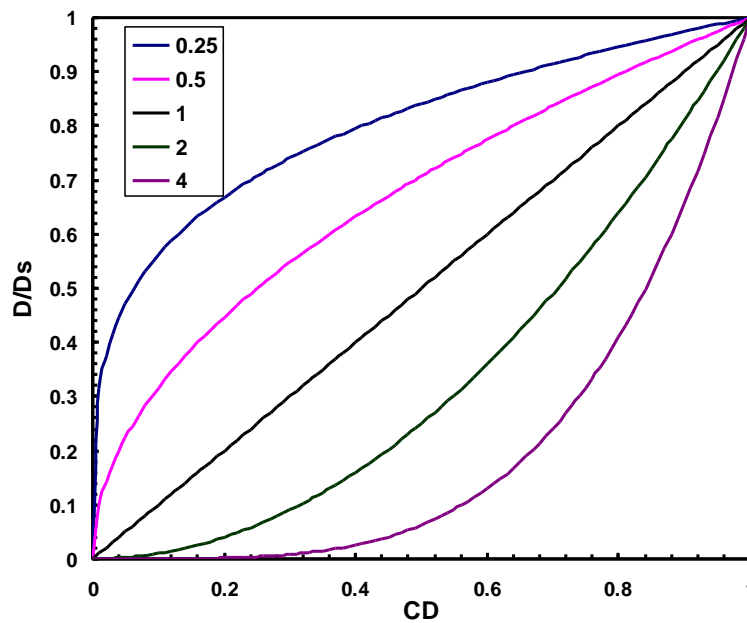


Figure 7-2: Normalized diffusion coefficient profile versus normalized concentration at different values of the power d .

Butler (1985b) proposed a power law correlation for the effect of temperature on bitumen viscosity in SAGD modeling. An analogous relationship was assumed for the effect of solvent concentration on the kinematic viscosity of the mixture:

$$\frac{\nu_s}{\nu} = C_D^m \quad (7-11)$$

where, ν_s is the kinematic viscosity at the interface. Figure 7-3 confirms that kinematic viscosity of Athabasca bitumen/propane mixtures at 20°C can be approximately fitted to a power-law type function represented by Equation 7-11. The equation of state model developed during the course of this study was used to calculate propane/bitumen binary mixture dynamic viscosity and liquid density. Then kinematic viscosity for propane – bitumen binary mixtures (solid symbols in Figure 7-3) are calculated values obtained from the equation of state model and the solid line represents the power law correlation, Equation 7-11.

Note, Equation 7-11 predicts that, as the solvent concentration goes to zero, the kinematic viscosity of the bitumen goes to infinity; that is, bitumen is immobile at zero solvent concentration. In reality, bitumen has a finite viscosity at reservoir temperature. However, Equation 7-11 is justified because the mobility of the saturated bitumen at interface is much higher than bitumen itself; therefore the contribution to the fluid flow is only from solvent diluted bitumen.

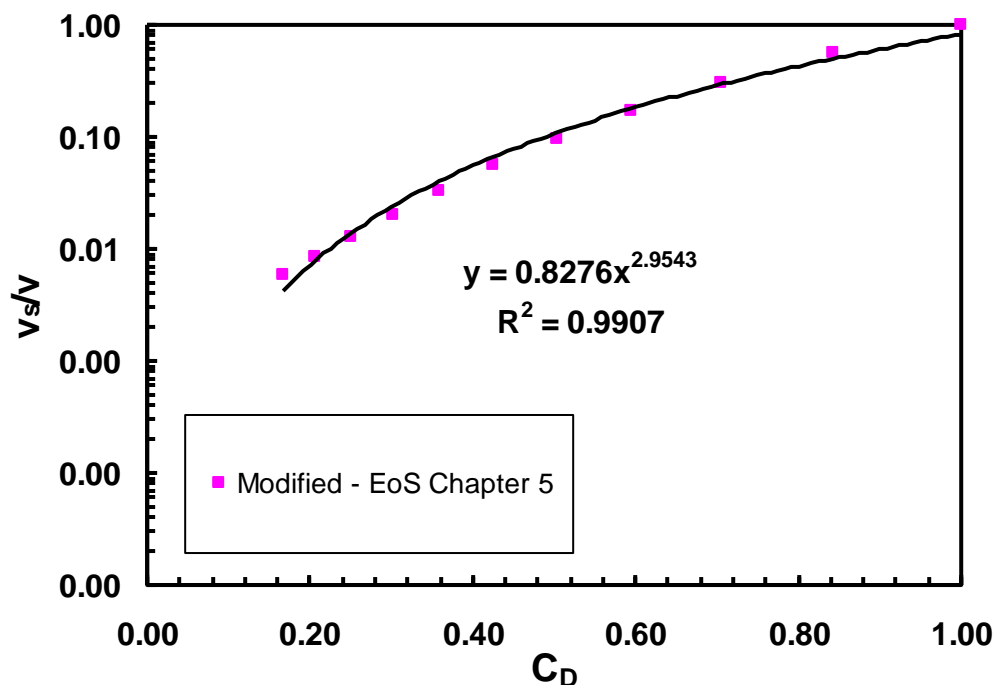


Figure 7-3: Athabasca bitumen – propane kinematic viscosity calculated by tuned PR EoS model in WinProp at 20°C, and fitted to Equation 7-11.

Equation 7-11 and Equation 7-10 can be used to eliminate the concentration and obtain the following expression for the diffusivity coefficient:

$$D = \left(D_s v_s^{d/m} \right) \times v^{-d/m} \quad (7-12)$$

The first term in Equation 7-12 is a constant for any given solvent in the Vapex process at fixed operating pressure and temperature, since it depends only on the saturation conditions. If the power functionality of diffusivity and viscosity in Equations 7-10 and 7-11 is equal ($d = m$), then the diffusion coefficient will be inversely proportional to

kinematic viscosity. This satisfies the Stokes – Einstein equation (Bird et. al., 2002, chapter 17). Therefore, the power – law correlation assumed in Equations 7-10 and 7-11 is consistent with Stokes' law.

7.3.2 Linearization of Equation 7-6.

The power law relationship between the diffusion coefficient and concentration introduces a strong non-linearity to Equation 7-6. This non-linearity can be eliminated by defining the pseudo normalized concentration, C_{PD} , and pseudo time, t_p , as follows:

$$C_{PD} = (d+1) \times \int_0^{C_D} C_D^d dC_D \quad (7-13)$$

$$t_p = \int_0^t \frac{D}{D_s} dt \quad (7-14)$$

Equation 7-14 can also be written as:

$$t_p = \int_0^t \left(\frac{v_s}{v} \right)^{d/m} dt \quad (7-15)$$

From Equation 7-13, we can obtain the following derivatives, using the chain rule:

$$\begin{aligned} \frac{\partial C_{PD}}{\partial \varepsilon} &= \frac{\partial C_{PD}}{\partial C_D} \cdot \frac{\partial C_D}{\partial \varepsilon} = (d+1) \times C_D^d \times \frac{\partial C_D}{\partial \varepsilon} \\ \Rightarrow \frac{\partial C_D}{\partial \varepsilon} &= \frac{1}{(d+1) \times C_D^d} \cdot \frac{\partial C_{PD}}{\partial \varepsilon} \end{aligned} \quad (7-16)$$

$$\begin{aligned} \frac{\partial C_{PD}}{\partial t} &= \frac{\partial C_{PD}}{\partial C_D} \cdot \frac{\partial C_D}{\partial t} = (d+1) \times C_D^d \times \frac{\partial C_D}{\partial t} \\ \Rightarrow \frac{\partial C_D}{\partial t} &= \frac{1}{(d+1) \times C_D^d} \cdot \frac{\partial C_{PD}}{\partial t} \end{aligned} \quad (7-17)$$

Equations 7-16 and 7-17 are substituted into Equation 7-6 to obtain:

$$\frac{\partial}{\partial \varepsilon} \left(D_s \cdot C_D^d \cdot \frac{1}{(d+1) \times C_D^d} \cdot \frac{\partial C_{PD}}{\partial \varepsilon} \right) = \frac{1}{(d+1) \times C_D^d} \cdot \frac{\partial C_{PD}}{\partial t} \quad (7-18a)$$

which with some algebraic manipulation and the use of Equation 7-10, Equation 7-18a is rearranged to obtain:

$$\frac{\partial}{\partial \varepsilon} \left(\frac{\partial C_{PD}}{\partial \varepsilon} \right) = \frac{1}{D} \cdot \frac{\partial C_{PD}}{\partial t} \quad (7-18b)$$

Equation 7-18b is still a non-linear partial differential equation. The time term is replaced with pseudo-time to eliminate this non-linearity. From Equation 7-14 and the chain rule, the following expression is derived:

$$\frac{\partial C_{PD}}{\partial t} = \frac{\partial C_{PD}}{\partial t_p} \cdot \frac{\partial t_p}{\partial t} = \frac{\partial C_{PD}}{\partial t_p} \cdot \left(\frac{v_s}{v} \right)^{d/m} \quad (7-19)$$

Equations 7-19 and 7-10 are substituted into Equation 7-18b to obtain:

$$\begin{aligned} \frac{\partial}{\partial \varepsilon} \left(\frac{\partial C_{PD}}{\partial \varepsilon} \right) &= \frac{1}{D_s \times \left(\frac{v_s}{v} \right)^{d/m}} \times \left(\frac{v_s}{v} \right)^{d/m} \times \frac{\partial C_{PD}}{\partial t_p} \\ &\Rightarrow \frac{\partial}{\partial \varepsilon} \left(\frac{\partial C_{PD}}{\partial \varepsilon} \right) = \frac{1}{D_s} \cdot \frac{\partial C_{PD}}{\partial t_p} \end{aligned} \quad (7-20)$$

Since D_s is a constant value throughout the Vapex process Equation 7-20 is a linear P.D.E.

The initial and boundary conditions defined by Equations 7-7 to 7-9 are written in-term of pseudo normalized concentration C_{PD} , and pseudo time t_p , as follows:

$$\text{I.C. } C_{PD} = 0 \quad @ \ t_p = 0, 0 \leq \varepsilon \quad (7-21)$$

$$\text{B.C. \#1: } C_{PD} = 1 \quad @ \ t_p > 0, \varepsilon = I(t_p) \text{ interface} \quad (7-22)$$

$$\text{B.C. \#2: } C_{PD} = 0 \quad @ \ t_p > 0, \varepsilon \geq (I(t_p) + \delta) \quad (7-23)$$

where $I(t_p)$, is the interface location at any pseudo time; it is the pseudo time form of Equation 7-15 and is given by:

$$I(t_p) = \int_0^{t_p} U \cdot di \quad (7-24)$$

where U is the velocity of interface m/sec, and i is the variable of integration.

The first boundary (Equation 7-22) is a moving boundary and its location is not known prior to complete solution for the diffusion and fluid flow problem. The unknown location of the interface is avoided by introducing a new coordinate system, ε^* , that travels with interface:

$$\varepsilon^* = \varepsilon - \int_0^{t_p} U \times di \quad (7-25)$$

Therefore, C_{PD} will be a function defined at the surface of ε^* at time t_p , where ε^* is a function of ε and t_p . Hence, applying the chain rule to $C_{PD}(\varepsilon^*(\varepsilon, t_p), t_p)$ gives:

$$\frac{\partial C_{PD}}{\partial \varepsilon} = \frac{\partial C_{PD}}{\partial \varepsilon^*} \cdot \frac{\partial \varepsilon^*}{\partial \varepsilon} + \frac{\partial C_{PD}}{\partial t_p} \cdot \frac{\partial t_p}{\partial \varepsilon} = \frac{\partial C_{PD}}{\partial \varepsilon^*} \times (1) + \frac{\partial C_{PD}}{\partial t_p} \times (0) = \frac{\partial C_{PD}}{\partial \varepsilon^*} \quad (7-26)$$

$$\frac{\partial C_{PD}}{\partial t_p} = \frac{\partial C_{PD}}{\partial \varepsilon^*} \cdot \frac{\partial \varepsilon^*}{\partial t_p} + \frac{\partial C_{PD}}{\partial t_p} \cdot \frac{\partial t_p}{\partial t_p} = \frac{\partial C_{PD}}{\partial \varepsilon^*} \times (-U) + \frac{\partial C_{PD}}{\partial t_p} \times (1) \quad (7-27)$$

Equations 7-26 and 7-27 are substituted into Equation 7-20 to obtain:

$$\boxed{\frac{\partial^2 C_{PD}}{\partial \varepsilon^{*2}} + \frac{U}{D_s} \times \frac{\partial C_{PD}}{\partial \varepsilon^*} = \frac{1}{D_s} \times \frac{\partial C_{PD}}{\partial t_p}} \quad (7-28)$$

Equation 7-28 is a convective-diffusive P.D.E. The convective term, $\frac{U}{D_s} \cdot \frac{\partial C_{PD}}{\partial \varepsilon^*}$, is the result of the new coordinate that travels with interface. This term acts as convective flow of mass in the direction opposite to ε^* (i.e. diffusion direction). It smears the steepness of the concentration gradient that is created by the diffusive term.

Although Equation 7-28 expresses several different mechanisms that occur in the Vapex process (diffusive, convective, and transient terms), it does not reveal the relative importance of each term. It is a common practice to evaluate the role of each term in the dimensionless form of Equation 7-28. Also a dimensionless solution will be widely applicable. The following dimensionless variables, normalized with respect to total drainage height available in Vapex process (i.e. H), apply to Equation 7-28:

$$\varepsilon_D^* = \frac{\varepsilon^*}{H} \quad (7-29)$$

$$t_{pD} = \frac{D_s t_p}{H^2} \quad (7-30)$$

The dimensionless form of Equation 7-28 is then given by:

$$\boxed{\frac{\partial^2 C_{PD}}{\partial \varepsilon_D^{*2}} + \frac{U \times H}{D_s} \times \frac{\partial C_{PD}}{\partial \varepsilon_D^*} = \frac{\partial C_{PD}}{\partial t_{pD}}} \quad (7-31)$$

where the convective term coefficient is the Peclet number N_{Pe} :

$$N_{Pe} = \frac{UH}{D_s} \quad (7-32)$$

The Peclet number represents the importance of convective mass transfer to diffusive mass transfer. The initial and boundary conditions in dimensionless form are:

$$\text{I.C. } C_{PD} = 0 \quad @ \ t_p = 0, \ \varepsilon_D^* \geq 0 \quad (7-32a)$$

$$\text{B.C. \#1: } C_{PD} = 1 \quad @ \ t_p > 0, \ \varepsilon_D^* = 0 \quad (7-32b)$$

$$\text{B.C. \#2: } C_{PD} = 0 \quad @ \ t_p > 0, \ \varepsilon_D^* \geq \delta_D \quad (7-32c)$$

7.3.3 Heat-Integral-Method (HIM) Solution of Convective-Diffusive P.D.E.

The integral method has been used to approximate the solution of diffusive dominated non-linear problems. Pooladi Darvish (1996) and Heidari (2008) employed this method to analytically model the temperature distribution for the SAGD process. Later, Heidari (2008) applied the same method to solve the concentration distribution in Vapex modeling.

In H.I.M., a particular form, such as a polynomial, is assumed for the concentration profile arising from mass diffusion into an unknown thickness called the penetration depth. The penetration depth corresponds to the boundary layer thickness in hydrodynamics. The coefficients of the polynomial function are found using the actual as well as auxiliary boundary conditions. The latter are defined using the definition of mass penetration depth, so there is no effect of mass transfer beyond the penetration depth. Having obtained the equation for concentration distribution, the mass transfer equation is integrated over the appropriate interval, and the two equations are combined to obtain an ordinary differential equation for the unknown penetration depth. Upon solving this ODE, the concentration penetration depth (i.e. δ in Figure 7-1) is obtained, which can

then be used to find other parameters in particular the concentration distribution. Note that the H.I.M. provides only an approximate solution because the assumed function describing the concentration distribution is forced to satisfy only the integrated form of the original equation.

We assumed the maximum penetration depth of solvent to be equal to δ . The normalized δ with respect to the maximum height available for drainage, i.e. H (model height), is:

$$\delta_D = \frac{\delta}{H} \quad (7-33)$$

The penetration depth is much smaller than the height and there is no effect of mass transfer beyond this depth. Therefore boundary and initial condition for Equation 7-31 are:

$$\text{I.C. } C_{PD} = 0 \quad @ \ t_p = 0, \ \varepsilon_D^* \geq 0 \quad (7-34)$$

$$\text{B.C. \#1: } C_{PD} = 1 \quad @ \ t_p > 0, \ \varepsilon_D^* = 0 \quad (7-35)$$

$$\text{B.C. \#2: } C_{PD} = 0 \quad @ \ t_p > 0, \ \varepsilon_D^* \geq \delta_D \quad (7-36)$$

Also since it assumed that there is no effect of mass transfer beyond the penetration depth, we can define the following auxiliary boundary conditions:

$$\text{B.C. \#3: } \frac{\partial C_{PD}}{\partial \varepsilon^*} = 0 \quad @ \ t_p > 0, \ \varepsilon_D^* \geq \delta_D \quad (7-37a)$$

$$\text{B.C. \#4: } \frac{\partial^2 C_{PD}}{\partial \varepsilon^{*2}} = 0 \quad @ \ t_p > 0, \ \varepsilon_D^* \geq \delta_D \quad (7-37b)$$

The higher order derivatives will also be equal to zero.

Let us assume that the unsteady state distribution of normalized solvent concentration ahead of interface is a 3rd order polynomial:

$$C_{PD} = A(t_{pD}) + B(t_{pD})\varepsilon_D^* + C(t_{pD})\varepsilon_D^{*2} + D(t_{pD})\varepsilon_D^{*3} \quad (7-38)$$

The initial and boundary conditions (i.e Equation 7-34 to 7-37) are employed to obtain the following:

$$C_{PD}(0, t_{pD}) = A(t_{pD}) = 1 \quad (7-39a)$$

$$C_{PD}(\delta_D, t_{pD}) = 0 = 1 + B(t_{pD})\delta_D + C(t_{pD})\delta_D^2 + D(t_{pD})\delta_D^3 \quad (7-39b)$$

$$\frac{\partial C_{PD}(\delta_D, t_{pD})}{\partial \varepsilon_D^*} = 0 = B(t_{pD}) + 2C(t_{pD})\delta_D + 3D(t_{pD})\delta_D^2 \quad (7-39c)$$

$$\frac{\partial^2 C_{PD}(\delta_D, t_{pD})}{\partial \varepsilon_D^{*2}} = 0 = 2C(t_{pD})\delta_D + 6D(t_{pD})\delta_D \quad (7-39d)$$

Equations 7-39b-d are used to solve for the three unknown coefficients B, C, and D:

$$B(t_{pD}) = -\frac{3}{\delta_D} \quad (7-40)$$

$$C(t_{pD}) = \frac{3}{\delta_D^2} \quad (7-41)$$

$$D(t_{pD}) = -\frac{1}{\delta_D^3} \quad (7-42)$$

The normalized concentration profile is then given by:

$$C_{PD} = 1 - \frac{3}{\delta_D} \varepsilon_D^* + \frac{3}{\delta_D^2} \varepsilon_D^{*2} - \frac{1}{\delta_D^3} \varepsilon_D^{*3}$$

or, more simply,

$$C_{PD} = \left(1 - \frac{\varepsilon_D^*}{\delta_D}\right)^3 \quad (7-43)$$

Similarly, it can be shown that the normalized concentration distribution ahead of interface for an n^{th} order polynomial profile is given by:

$$\boxed{C_{PD} = \left(1 - \frac{\varepsilon_D^*}{\delta_D}\right)^n} \quad (7-44)$$

From Equation 7-13, the real normalized concentration distribution function is then given by:

$$C_D = \left(1 - \frac{\varepsilon_D^*}{\delta_D(t_{pD})}\right)^{\frac{n}{d+1}} \quad (7-45)$$

The P.D.E. can be converted to an ODE, by integrating both sides of Equation 7-31 over the penetration depth:

$$\begin{aligned} \int_0^{\delta_D} \frac{\partial^2 C_{PD}}{\partial \varepsilon_D^{*2}} \cdot d\varepsilon_D^* + N_{Pe} \int_0^{\delta_D} \frac{\partial C_{PD}}{\partial \varepsilon_D^*} \cdot d\varepsilon_D^* &= \frac{d}{dt} \int_0^{\delta_D} C_{PD} \cdot d\varepsilon_D^* \\ \Rightarrow \frac{\partial C_{PD}}{\partial \varepsilon_D^*} \Big|_0^{\delta_D} + N_{Pe} \cdot C_{PD} \Big|_0^{\delta_D} &= \frac{d}{dt} \int_0^{\delta_D} C_{PD} \cdot d\varepsilon_D^* \end{aligned} \quad (7-46)$$

Each term in the above equation can be obtained from Equation 7-44 and its derivatives, as follows:

$$\frac{\partial C_{PD}}{\partial \varepsilon_D^*} = n \cdot \left(-\frac{1}{\delta_D(t_{pD})}\right) \cdot \left(1 - \frac{\varepsilon_D^*}{\delta_D(t_{pD})}\right)^{n-1} \quad (7-47)$$

$$\Rightarrow \frac{\partial C_{PD}}{\partial \varepsilon_D^*} \Big|_0^{\delta_D} = 0 - \left(-\frac{n}{\delta_D(t_{pD})}\right) = \frac{n}{\delta_D(t_{pD})} \quad (7-48)$$

$$C_{PD} \Big|_0^{\delta_D} = \left(1 - \frac{\varepsilon_D^*}{\delta_D} \right)^n \Big|_0^{\delta_D} = -1 \quad (7-49)$$

$$\int_0^{\delta_D} C_{PD} \cdot d\varepsilon_D^* = \int_0^{\delta_D} \left(1 - \frac{\varepsilon_D^*}{\delta_D} \right)^n \cdot d\varepsilon_D^* = \frac{\delta_D}{n+1} \quad (7-50)$$

Equations 7-48 to 7-50 are substituted into Equation 7-46 to obtain:

$$\begin{aligned} \frac{n}{\delta_D} - N_{Pe} &= \frac{d}{dt_{pD}} \left(\frac{\delta_D}{n+1} \right) \\ \frac{d\delta_D}{dt_{pD}} &= (n+1) \cdot \left(\frac{n}{\delta_D} - N_{Pe} \right) \end{aligned} \quad (7-51a)$$

which can also be written as:

$$\frac{d(\delta_D^2)}{dt_{pD}} = 2(n+1) \cdot (n - N_{Pe} \times \delta_D) \quad (7-51b)$$

The Peclet number is required to solve the O.D.E. and it depends on the rate at which the interface moves. It also remains to solve for the fluid production rate.

7.4. Fluid Flow and Movement of Interface

7.4.1 Fluid Flow Equation

The movement of the interface depends on the flow rate of bitumen out of the interfacial area. The diluted oil flow rate ahead of interface can be expressed using Darcy's Law. The fluid flow is downward and parallel to the interface for the entire mobile fluid (i.e. diluted oil) domain. The flow rate through an element of unit width and parallel to the interface (see Figure 7-1), is given by:

$$dq = Kg \sin \theta \frac{\Delta\rho}{\mu_m} d\varepsilon^* \quad (7-52)$$

where K is the absolute permeability, g is gravitational acceleration m^2/sec , μ_m is the diluted oil viscosity, and $\Delta\rho$ is the density difference between diluted oil and vapour solvent. The density of the vapour solvent is almost negligible and therefore:

$$\Delta\rho = \rho_{mix} - \rho_{vap} \approx \rho_{mix} \quad (7-52a)$$

Equation 7-52 can be written in-terms of the kinematic viscosity of diluted oil:

$$dq = Kg \sin \theta \frac{d\varepsilon^*}{\nu_{mix}} \quad (7-52b)$$

Equation 7-29 is substituted into Equation 7-52b to obtain:

$$dq = KHg \sin \theta \frac{d\varepsilon_D^*}{\nu_{mix}} \quad (7-53)$$

The total flow rate in the diluted oil zone is obtained by integrating Equation 7-53 over the penetration depth:

$$q = KHg \sin \theta \int_0^{\delta_D} \frac{d\varepsilon_D^*}{\nu_{mix}} \quad (7-54)$$

Equations 7-45 and 7-11 are combined to derive the following expression for ν_{mix} :

$$\frac{1}{\nu_{mix}} = \frac{1}{\nu_s} \cdot C_D^m = \frac{1}{\nu_s} \cdot \left(1 - \frac{\varepsilon_D^*}{\delta_D}\right)^{\frac{mn}{d+1}} \quad (7-55)$$

Equation 7-55 is integrated over the normalized penetration depth as follows:

$$\int_0^{\delta_D} \frac{1}{\nu_s} \cdot \left(1 - \frac{\varepsilon_D^*}{\delta_D}\right)^{\frac{mn}{d+1}} \cdot d\varepsilon_D^* = \frac{1}{\nu_s} \cdot \frac{-\delta_D}{\frac{mn}{d+1} + 1} \cdot \left(1 - \frac{\varepsilon_D^*}{\delta_D}\right)^{\frac{mn}{d+1} + 1} \Bigg|_0^{\delta_D}$$

$$\Rightarrow \int_0^{\delta_D} \frac{1}{v_{mix}} \cdot d\varepsilon_D^* = \frac{\delta_D}{v_s \cdot \left[\frac{mn}{d+1} + 1 \right]} \quad (7-56)$$

Total flow rate as function of model height, H , and pseudo time t_{pD} , is obtained by substituting Equation 7-56 into Equation 7-54:

$$q = KHg \sin \theta \cdot \frac{1}{v_s} \cdot \frac{d+1}{nm+d+1} \cdot \delta_D(t_{pD}) \quad (7-57)$$

where, q is the fluid production rate per unit horizontal well length, K is the absolute permeability, g is the gravitational acceleration, θ is the angle of interface to horizontal direction, v_s is the kinematic viscosity of saturated bitumen at the interface. δ_D is the normalized penetration depth, beyond which there is no fluid flow.

Although the concentration profile by Equation 7-45 is different than the exponential profile reported by Dunn et al. (1989) who assumed constant diffusivity, Equation 7-57 has the same form as their fluid rate expression (Chapter 2, Equation 2-23). The only difference between Equation 7-57 and the expression from Dunn (1989) is that the constant m in their equation is replaced by $\left[\frac{mn}{d+1} + 1 \right]$ in our method, $\left[\frac{m}{d} + 1 \right]$ in the Okazawa's 2007 formulation, and $[mn+1]$ in Heidari's model (2008).

7.4.2 Movement of the Interface

A useful equation obtained originally by Butler et al. (1989) and later improved by Okazawa (2007) is the relation between drainage rate and the interface movement. Figure 7-4 shows the position of the interface at an arbitrary time. Consider point X on the

interface. The drained area (shaded zone above Point X in Figure 7-4) is calculated as follows:

$$Area = \int_z^H x(z, t_p) dz \quad (7-58)$$

The bitumen production rate at Point X is assumed to be:

$$q_b(z, t_p) = q \cdot f_b \quad (7-59)$$

where q_b is bitumen volumetric flow rate and f_b is the average bitumen volume fraction in the fluid flow rate, q . The shaded area in Figure 7-4 has been drained due to bitumen production and therefore:

$$Area \times \varphi \times \Delta S_o = \int_0^{t_p} q_b(z, t_p) \cdot dt_p \quad (7-60)$$

Eq 7-58 is substituted into Equation 7-60 to obtain:

$$\int_0^{t_p} q_b(z, t_p) \cdot dt_p = \varphi \cdot \Delta S_o \cdot \int_z^H x(z, t_p) \cdot dz \quad (7-61)$$

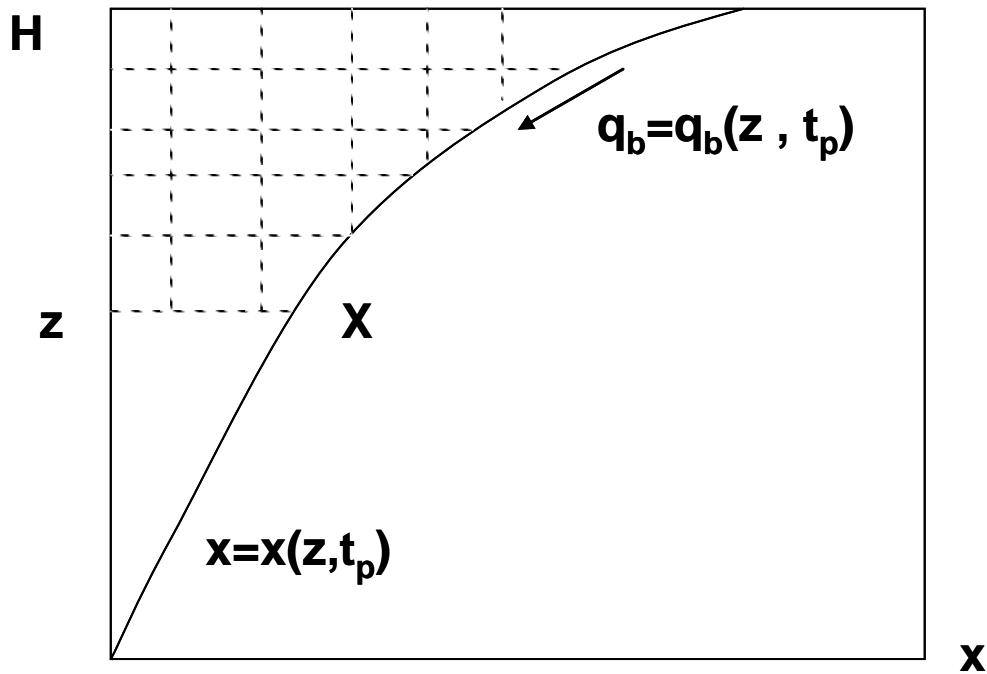


Figure 7-4: Relationship between interface position related and total bitumen produced.

Differentiating both sides of Equation 7-61 with respect to pseudo-time gives:

$$q_b = \varphi \Delta S_o \int_z^H \frac{\partial x}{\partial t_p} \cdot dz \quad (7-62)$$

Both sides of Equation 7-62 are differentiated with respect to depth z to obtain:

$$\left(\frac{\partial q_b}{\partial z} \right)_{t_p} = -\varphi \cdot \Delta S_o \cdot \left(\frac{\partial x}{\partial t_p} \right)_z \quad (7-63)$$

Figure 7-5 shows a material balance on the bitumen fluid flow for a unit width element inside the penetration depth. The material balance simplifies to the difference between the amount of oil that enters an element parallel to the interface and the amount of bitumen that exits the element parallel to the interface:

$$U \cdot \varphi \cdot \Delta S_o \cdot \Delta \eta = -\frac{\partial q_b}{\partial \eta} \cdot \Delta \eta \quad (7-64a)$$

or, rearranging to solve for the rate of interface movement,

$$U = -\frac{1}{\varphi \Delta S_o} \cdot \frac{\partial q_b}{\partial \eta} \quad (7-64b)$$

where η is the coordinate parallel to the interface.

7.4.3 Dimensionless Flow and Interface Movement

To find the dimensionless expressions for the interfacial movement and oil flow, we start with the dimensionless total fluid flow rate, Q , defined as:

$$Q \cdot t_{pD} = \frac{q \cdot t_p}{\varphi \Delta S_o H^2} \quad (7-65)$$

Equation 7-65 shows that the product of dimensionless flow rate with dimensionless pseudo-time equals the dimensionless area of the reservoir that has been drained. The normalized distance along the interface, Γ , is defined as:

$$\Gamma = \frac{\eta}{H} \quad (7-66)$$

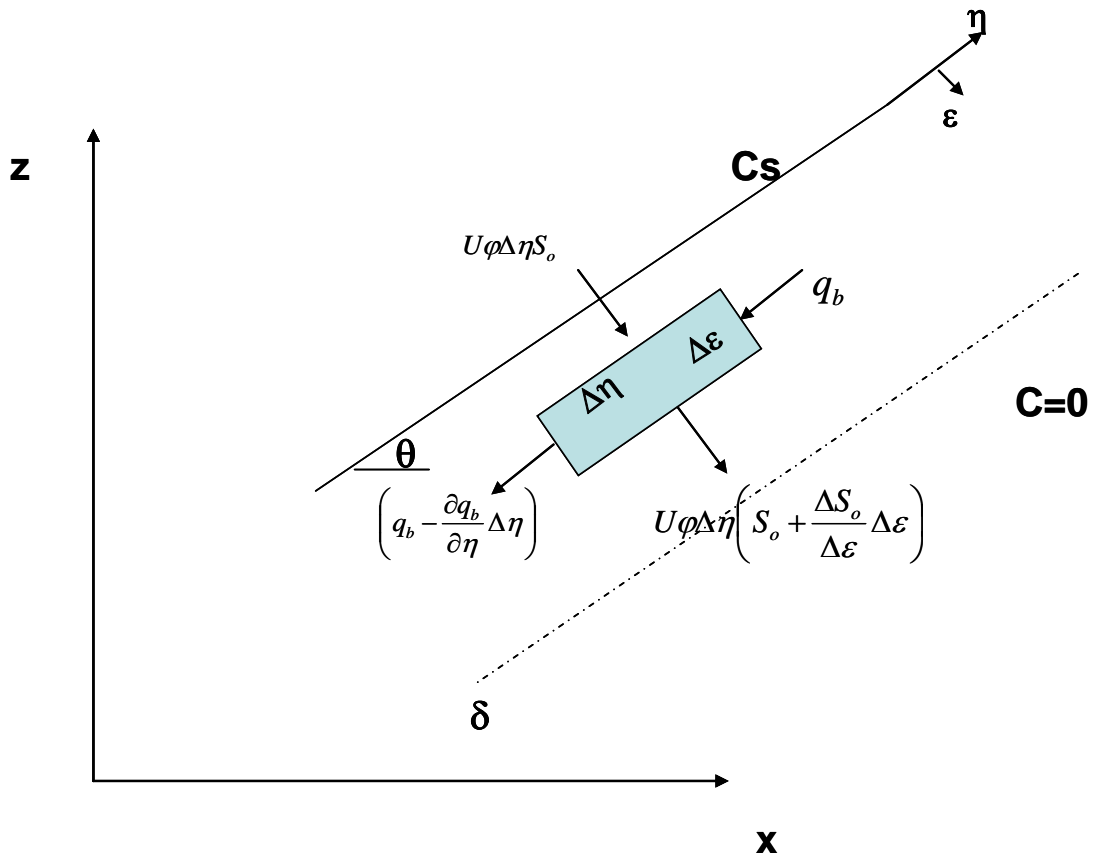


Figure 7-5: Material balance around a unit width element inside the penetration depth.

Equations 7-66, 7-65, 7-59, and 7-30 are substituted into Equation 7-64 to obtain:

$$U = -\frac{\varphi \cdot \Delta S_o H^2}{\varphi \cdot \Delta S_o} \cdot \frac{\partial Q_b}{\partial \Gamma} \cdot \frac{t_{pD}}{H t_p} = -H \cdot \frac{\partial Q_b}{\partial \Gamma} \cdot \frac{D_s}{H^2} \quad (7-67)$$

$$\Rightarrow -\frac{\partial Q_b}{\partial \Gamma} = \frac{UH}{D_s} = N_{Pe} \quad (7-68)$$

Therefore, the change of bitumen flow rate along the interface is equal to Peclet number.

Equation 7-63 can be written in dimensionless form using following dimensionless coordinates:

$$Z_D = \frac{z}{H}$$

$$X_D = \frac{x}{H}$$

The dimensionless form of Equation 7-63 is then given by:

$$\varphi \cdot \Delta S_o \cdot H^2 \cdot \frac{t_{pD}}{t_p} \cdot \frac{\partial Q_b}{H \partial Z_D} = -\varphi \cdot \Delta S_o \cdot \frac{H \partial X_D}{H^2} \frac{\partial t_{pD}}{D_s}$$

$$\Rightarrow \frac{\partial Q_b}{\partial Z_D} = - \frac{\partial X_D}{\partial t_{pD}} \quad (7-69)$$

The interface inclination at each time interval is given by:

$$\tan \theta = \left. \frac{\Delta Z_D}{\Delta X_D} \right|_{X=\hat{X}} \quad (7-70)$$

where \hat{X} is a dimensionless location at the interface.

The position of the interface at the top (i.e. $Z_D = 1.0$) of the Vapex model is calculated from a material balance assuming that the average rate of bitumen drainage from the top section is equal to calculated flow from top element. The fluid flow rate at the top of the model ($Z_D = 1.0$) is zero, and maximum at the bottom of the Vapex model. Since the penetration depth is zero at top and maximum in the bottom at the production well:

$$Q = Q_b = 0.0 @ Z_D = 1.0, t_{pD} \geq 0.0 \quad (7-71)$$

The interface is vertical at initial time and therefore:

$$\sin \theta = 1 @ 0.0 \leq Z_D \leq 1.0, t_{pD} = 0.0 \quad (7-72)$$

In order to prevent the movement of the interface at the bottom, a new boundary condition is applied to keep interface at the production well location:

$$\hat{\varepsilon}_D^* = 0.0 , \quad @ Z_D = 0.0, t_{pD} \geq 0.0 \quad (7-73)$$

The dimensionless parameters are substituted into Equation 7-57 to obtain:

$$q = KHg \sin \theta \cdot \frac{1}{v_s} \cdot \frac{d+1}{nm+d+1} \cdot \delta_D(t_{pD})$$

$$Q \cdot \varphi \cdot \Delta S_o \cdot H^2 \cdot \frac{D_s}{H^2} = KHg \sin \theta \cdot \frac{1}{v_s} \cdot \frac{d+1}{nm+d+1} \cdot \delta_D(t_{pD})$$

$$Q = \frac{KHg}{\varphi \Delta S_o v_s D_s} \cdot \sin \theta \cdot \frac{d+1}{nm+d+1} \cdot \delta_D(t_{pD})$$

$$\boxed{Q = N_{Ra} \cdot \sin \theta \cdot \frac{d+1}{mn+d+1} \cdot \delta_D(t_{pD})} \quad (7-74)$$

where, N_{Ra} is the Rayleigh number. It represents the relative magnitude of gravity drainage to mass transfer by diffusion-dispersion.

7.4.4. Bitumen Flow Rate Equation

Equation 7-74 is the expression for the total flow rate of solvent-bitumen mixture. The flow rate of bitumen through an element of unit width and parallel to the interface will be:

$$dq_b = KHg \sin \theta \cdot \frac{(1-C)}{v_{mix}} d\varepsilon_D^* \quad (7-75)$$

where C is the solvent concentration in the diluted oil. The total bitumen flow rate at any height is the integral of Equation 7-75 over the penetration depth:

$$q_b = \int_0^{\delta_p} dq_b = KHg \sin \theta \int_0^{\delta_p} \frac{(1-C)}{\nu} d\varepsilon_D^* \quad (7-76)$$

Equations 7-5, 7-11, and 7-45 are substituted into the integral term of Equation 7-76 to obtain:

$$\int_0^{\delta_p} \frac{(1-C)}{\nu} \cdot d\varepsilon_D^* = \frac{1}{\nu_s} \cdot \int_0^{\delta_p} C_D^m \times (1 - C_s \cdot C_D) \cdot d\varepsilon_D^*$$

$$\int_0^{\delta_p} \frac{(1-C)}{\nu} \cdot d\varepsilon_D^* = \frac{1}{\nu_s} \cdot \int_0^{\delta_p} \left[\left(1 - \frac{\varepsilon_D^*}{\delta_D}\right)^{\frac{nm}{d+1}} - C_s \cdot \left(1 - \frac{\varepsilon_D^*}{\delta_D}\right)^{\frac{n(m+1)}{d+1}} \right] \cdot d\varepsilon_D^*$$

$$\int_0^{\delta_p} \frac{(1-C)}{\nu} \cdot d\varepsilon_D^* = \frac{1}{\nu_s} \cdot \left[\frac{-\delta_D}{\frac{nm}{d+1} + 1} \cdot \left(1 - \frac{\varepsilon_D^*}{\delta_D}\right)^{\frac{nm}{d+1} + 1} - C_s \cdot \frac{-\delta_D}{\frac{n(m+1)}{d+1} + 1} \cdot \left(1 - \frac{\varepsilon_D^*}{\delta_D}\right)^{\frac{n(m+1)}{d+1} + 1} \right]_0^{\delta_D}$$

$$\int_0^{\delta_p} \frac{(1-C)}{\nu} \cdot d\varepsilon_D^* = \frac{1}{\nu_s} \cdot \left[\left(0 - \frac{-\delta_D}{\frac{nm}{d+1} + 1}\right) - C_s \cdot \left(0 - \frac{-\delta_D}{\frac{n(m+1)}{d+1} + 1}\right) \right]$$

and finally,

$$\boxed{\int_0^{\delta_p} \frac{(1-C)}{\nu} \cdot d\varepsilon_D^* = \frac{\delta_D}{\nu_s} \cdot \frac{d+1}{nm+d+1} \cdot \left[1 - C_s \cdot \frac{nm+d+1}{n(m+1)+d+1} \right]} \quad (7-77)$$

From Equation 7-59, and definition of bitumen fractional flow, we have:

$$f_b = \frac{q_b}{q} = \frac{\int_0^{\delta_p} \frac{(1-c)}{\nu} d\varepsilon_D^*}{\int_0^{\delta_p} \frac{1}{\nu} d\varepsilon_D^*} \quad (7-78)$$

Previously, it has been shown that:

$$\int_0^{\delta_D} \left(\frac{1}{v} \right) \cdot d\varepsilon_D^* = \frac{d+1}{nm+d+1} \cdot \frac{1}{v_s} \cdot \delta_D \quad (7-78a)$$

Therefore, from Equations 7-77 to 7-78a, the bitumen fraction is given by:

$$f_b = \left(1 - C_s \cdot \frac{nm+d+1}{nm+n+d+1} \right) \quad (7-79)$$

The dimension less total flow rate of bitumen at any height over the penetration depth is therefore given by:

$$Q_b = Q \cdot f_b = N_{Ra} \cdot \text{Sin} \theta \cdot \frac{d+1}{nm+d+1} \left[1 - C_s \cdot \frac{nm+d+1}{nm+n+d+1} \right] \cdot \delta_D(t_{pD}) \quad (7-80)$$

From Equation 7-68, the bitumen flow rate at any height is:

$$-\frac{\partial Q_b}{\partial \Gamma} = N_{Pe}$$

but

$$N_{Pe} = -\frac{\partial Q_b}{\partial Z_D} \cdot \frac{\partial Z_D}{\partial \Gamma} = -\frac{\partial Q_b}{\partial Z_D} \cdot \frac{\partial(\Gamma \text{Sin} \theta)}{\partial \Gamma} = -\frac{\partial Q_b}{\partial Z_D} \cdot \text{Sin} \theta$$

and therefore

$$-N_{Pe} \cdot \frac{\partial Z_D}{\partial Q_b} = \text{Sin} \theta \quad (7-81)$$

Equation 7-81 is substituted into Equation 7-80 to obtain:

$$Q_b = -N_{Ra} \cdot N_{Pe} \cdot \frac{d+1}{mn+d+1} \cdot f_b \cdot \delta_D \cdot \frac{\partial Z_D}{\partial Q_b} \quad (7-82)$$

Integration of both sides of the Equation 7-82 gives:

$$\int_0^{Q_b} Q_b \cdot dQ_b = -\int_1^{Z_D} N_{Ra} \cdot N_{Pe} \cdot \frac{d+1}{mn+d+1} \cdot f_b \cdot \delta_D \cdot dZ_D \quad (7-82a)$$

The fluid flow rate is zero at top of the model; therefore Q_b of zero corresponds to Z_D equal to one (i.e. top of the model). It is clear from Equation 7-51 that at any height the normalized penetration depth is a function of time, hence:

$$Q_b = \sqrt{2 \cdot \frac{d+1}{mn+d+1} \cdot N_{Ra} \cdot N_{Pe} \cdot f_b \cdot \delta_D \cdot (1-Z_D)} \quad (7-83)$$

This equation is the generalized dimensionless bitumen flow rate at any normalized height. It includes the effect of gravity drainage, diffusion, and convection on the bitumen flow rate.

7.5. Model Solutions

7.5.1. Pseudo Steady State Condition

At the pseudo steady state condition, from Equation 7-51, the penetration depth can be calculated as:

$$\begin{aligned} S.S. \Rightarrow \frac{\partial \delta_D}{\partial t_{pD}} = 0 &\xrightarrow{Eq.51} \frac{n}{\delta_D} - N_{Pe} = 0 \\ \therefore \delta_D &= \frac{n}{N_{Pe}} \end{aligned} \quad (7-84)$$

Equation 7-84 is substituted into Equation 7-83 to find the bitumen flow rate at pseudo steady state condition:

$$Q_{b.s.s.}|_{Z_D} = \sqrt{\frac{2n(d+1)}{mn+d+1} \cdot f_b \cdot N_{Ra} \cdot (1-Z_D)} \quad (7-85)$$

where, Q_{bss} will be dimensionless bitumen rate in pseudo time scale. Equation 7-15 can be used to scale dimensionless rate in Equation 7-85 to real time as:

$$Q_{b\ s.s.}|_{Z_D} = \left(\frac{v_s}{v_{ss}} \right)^{\frac{d}{m}} \sqrt{\frac{2n(d+1)}{mn+d+1}} \cdot f_b \cdot N_{Ra} \cdot (1-Z_D) \quad (7-85a)$$

where, v_{ss} is steady state kinematic viscosity of the producing oil at Z_D . The values of m , n , and d are required to solve Equation 7-85. Experimental data can be used to obtain the kinematic viscosity power exponent, m (see Figure 7-3). There are experimental data in literature for the solubility of gases in Alberta bitumen. In addition, new viscosity, density, and solubility data for propane, carbon dioxide, and Athabasca bitumen were reported in Chapter 4.

Recall that n is the degree of the polynomial used to fit the concentration profile within the penetration depth. It was reported by Pooladi-Darvish (1999) and later Haidari (2008) that a 3rd degree polynomial function is an adequate approximation for the concentration profile.

The solvent diffusion coefficient at the interface, D_s , and the power, d , are the most challenging unknowns in the Vapex process modeling and design. The intrinsic solvent diffusivity coefficient in bitumen and its functionality to the solvent fraction in the diluted oil is difficult to measure experimentally and rarely reported in the literature (Viera, 1989). However, this information can be obtained from steady state flow data from a Vapex experiment. The fluid production and bitumen rate are stable during the pseudo steady state period of Vapex experiment and from them one can calculate bitumen fractional rate, f_b . Then, Equation 7-79 can be used to calculate the diffusion

power exponent, d , assuming C_s , the equilibrium solubility of solvent in bitumen, is known at the experimental temperature and pressure.

Finally, the Rayleigh number N_{Ra} is calculated from Equation 7-86. The experimental model dimensions, H , porosity, ϕ , permeability, K , kinematic viscosity at interface, ν_s , are all known. The only unknown is solvent diffusion coefficient at the interface, D_s , which can be calculated by Equation 7-88.

$$N_{Ra} = \frac{KHg}{\phi\Delta S_o \nu_s D_s} \quad (7-86)$$

From Equations 7-30 and 7-65, the dimension less bitumen flow rate can be obtained as:

$$Q_b = \frac{q_b}{\phi\Delta S_o D_s} \quad (7-87)$$

Substituting Equations 7-87 and 7-86 into Equation 7-85a, the solvent diffusion coefficient D_s at the interface can be easily calculated by knowing the steady state flow rate of the bitumen (q_{bss}), and its fraction in total production rate (f_{bss}).

$$D_s = \frac{\left(\frac{\nu_s}{\nu_{ss}}\right)^{\frac{2d}{m}} q_{bss}^2}{\frac{2n(d+1)}{mn+d+1} \cdot f_{bss} \cdot \frac{KHg\phi\Delta S_o}{\nu_s} \cdot (1-Z_D)} \quad (7-88)$$

Once D_s and d are extracted from a Vapex experiment(s), then one can obtain the dynamic time dependent solution.

7.5.2. Transient Solution Procedure

Haidari 2008, developed an algorithm for the transient solution of his Vapex mathematical model. This procedure can also be applied for the mathematical model developed in this work. The solvent-bitumen interface is divided into a number of segments in vertical direction. The bitumen drainage rate for each element at specific height is calculated at each time step and the rate is used to estimate the incremental displacement of the interface. The equations to be solved are summarized in dimensionless form in Table 7-1.

To start, a normalized penetration depth, δ_D , is assumed and bitumen production is determined for each element from Equation 7-80. Then, the dimensionless interface velocity is obtained from Equation 7-68 (i.e. N_{Pe}). The new horizontal position (movement) of the interface is obtained from Equation 7-69. The Peclet number obtained from the interface velocity is then used to solve the ODE, Equation 7-51. A new penetration depth and the error are calculated. This procedure is repeated within each time interval (steps) until reasonable convergence will be achieved. Then, the same process is repeated for each new time step. In the case of finite model, with no-flow boundary, when the interface reaches the boundary the inflow rate for the corresponding element will be set to zero and the effective height for drainage will be reduced accordingly.

Table 7-1: Summary of the Vapex mathematical modeling equations.

Equation #	Correlation	Comment
7-45	$C_D = \left(1 - \frac{\varepsilon_D^*}{\delta_D(t_{pD})}\right)^{\frac{n}{d+1}}$	Normalized Solvent concentration ahead of interface
7-51	$\frac{d\delta_D}{dt_{pD}} = (n+1) \cdot \left(\frac{n}{\delta_D} - N_{Pe}\right)$	1 st order ODE to calculate penetration depth ahead of interface
7-11	$\frac{\nu_s}{\nu} = C_D^m$	Variation of the Solvent-Bitumen kinematic viscosity with normalized solvent concentration
7-10	$\frac{D}{D_s} = C_D^d$	Variation of the intrinsic solvent diffusion coefficient with normalized solvent concentration
7-79	$f_b = \left(1 - C_s \cdot \frac{mn + d + 1}{nm + n + d + 1}\right)$	Volume fraction of bitumen

7-74	$Q_b = N_{Ra} \cdot \sin \theta \cdot \frac{d+1}{mn+d+1} \cdot f_b \cdot \delta_D(t_{pD})$	Bitumen flow rate
7-74	$N_{Ra} = \frac{KHg}{\varphi \Delta S_o \nu_s D_s}$	Rayleigh Number
7-32	$N_{Pe} = \frac{UH}{D_s}$	Peclet Number
7-68	$N_{Pe} = -\frac{\partial Q_b}{\partial \Gamma}$	Dimensionless velocity of the interface
7-69	$\frac{\partial Q_b}{\partial Z_D} = -\frac{\partial X_D}{\partial t_{pD}}$	Horizontal movement of the interface
7-70	$\tan \theta = \left. \frac{\Delta Z_D}{\Delta X_D} \right _{x=\hat{x}}$	The interface inclination at each time step
7-71	$Q = Q_b = 0.0 \quad @ \quad Z_D = 1.0, t_{pD} \geq 0.0$	B.C. at the top of the Vapex model
7-72	$\sin \theta = 1 \quad @ \quad 0.0 \leq Z_D \leq 1.0, t_{pD} = 0.0$	Vertical interface at initial time
7-73	$\hat{\varepsilon}_D^* = 0.0, \quad @ \quad Z_D = 0.0, t_{pD} \geq 0.0$	Stationary interface at producer well.

CHAPTER 8 : RESULTS OF VAPEX EXPERIMENTS

This chapter presents the results of physical model experiments for evaluating the effectiveness of carbon dioxide as a non-condensable carrier gas for propane in the Vapex process. Four Vapex experiments were conducted using the annulus type physical model described in Chapter 6. The model was packed with glass beads and the porosity and permeability of the pack were measured prior to each test.

In the previous chapters, the experimental results were reported on the phase behaviour, viscosity and density of the CO₂-propane-Athabasca Bitumen systems. The solvent compositions for the Vapex experiments were selected based on these results. Pure propane and two different mixtures of the carbon dioxide and propane were used as the Vapex solvent with Athabasca bitumen as the oil. These physical model tests were conducted at room temperature and a constant pressure lower than the dew-point pressure of solvent.

The bitumen and solvent production from the physical model along with the cumulative volume of solvent gas injected into the model were measured during the Vapex run. In addition, the stabilized live oil production rate, average fraction of the solvent in the produced oil, density and viscosity of the produced oil at test conditions, and average composition of the produced free gas and solution gas released from produced live-oil were measured.

In this chapter, the experimental results and theoretical analysis of the process are presented, and the applicability of the CO₂ based Vapex process is discussed.

8.1 Experimental Results

Based on the experimental phase behaviour data presented in the preceding chapters for the propane-Athabasca bitumen and CO₂-propane-bitumen, the vapour solvent compositions were chosen in a way that would avoid formation of a separate solvent rich liquid phase along with saturated bitumen, and would minimize the likelihood of asphaltene precipitation at the test conditions. Table 8-1 lists the three solvent compositions evaluated. Table 8-2 shows the solvent compositions and the packed model properties along with the test conditions used in these tests.

Table 8-1: Gaseous solvent composition, and saturation properties at 21°C.

Solvent #	Solvent Comp wt%		T °C	Psat kPa, abs	Pdew kPa, abs	ρ sat Liq kg/m ³	ρsat Vap kg/m ³
	CO ₂	C ₃					
1	59	41	21	4036	2153.6	601.13	50.1
2	78	22	21	4894.4	3719.7	639.1	101.9
3	0	100	21	858.8	858.8	503.4	18.6

Table 8-2: Solvent composition, packed model properties, and Vapex test condition.

Exp#	Inj. Gas Comp		Pavg kPa, abs	Tavg °C	PV m ³ x10 ³	OOIP m ³ x10 ³	Swi	φ	k Darcy	Rec. frac.	Run Time hr
	CO ₂	C ₃									
1	58.79	41.21	1974.1	21.1	1747	1685	0.035	0.357	640	0.373	121.55
2	58.79	41.21	2015.7	20.8	1746	1677.4	0.039	0.357	640	0.387	122.42
3	77.62	22.38	3406.7	20.7	1747	1683.3	0.036	0.357	640	0.536	157.00
4	0	100.00	784.5	20.8	1758	1698	0.034	0.359	640	0.435	48.24

Figures 8-1 to 8-3 show the cumulative production and injection data of each Vapex experiment with different solvents. The second experiment was a repeat of the first test and was carried out to confirm the reproducibility of the results. As it is clear from Figure 8-3, in the case of the pure propane the solution gas amount is higher than the free gas production; therefore most of the injected gas was dissolved in the oil. Actually, in case of a pure component solvent it is possible to run the tests with no free gas production without risking a drastic change in the gas composition in the vapour chamber. However, we ran these tests with some free gas production to ensure that the vapour chamber will extend to the production well and the full drainage height of the system will be available at all times. The symbol points in Figures 8-1 to 8-3 are the experimental data. The solid lines are not directly measured data but they were calculated from the experimental data. For example from each sampling we obtained a value for the solvent fraction; multiplying it by the live oil rate the solution gas rate was calculated. Then the solution gas was subtracted from the live oil production data to calculate the dead oil rate.

The amount of dead oil obtained from first sample, for some Vapex experiments is less than the value calculated from live oil data. As explained in the experimental section the live oil rates were obtained by the level of the produced fluid in the high pressure separator, but when we were discharging it out of the separator for the first time, some of the oil filled the measurement and sampling unit while displacing nitrogen out. Therefore there was an error associated with the volume of live oil being displaced for the first sample.

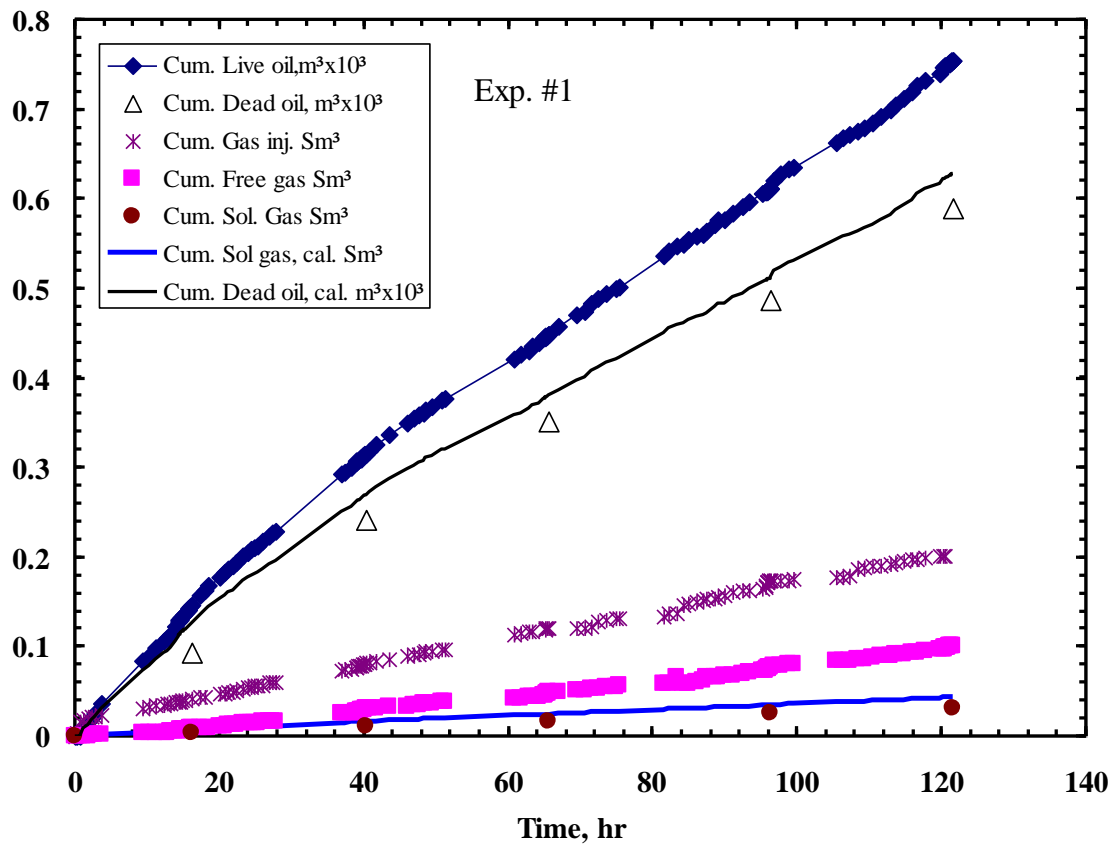


Figure 8-1: The cumulative injection and production data obtained from Run #1.

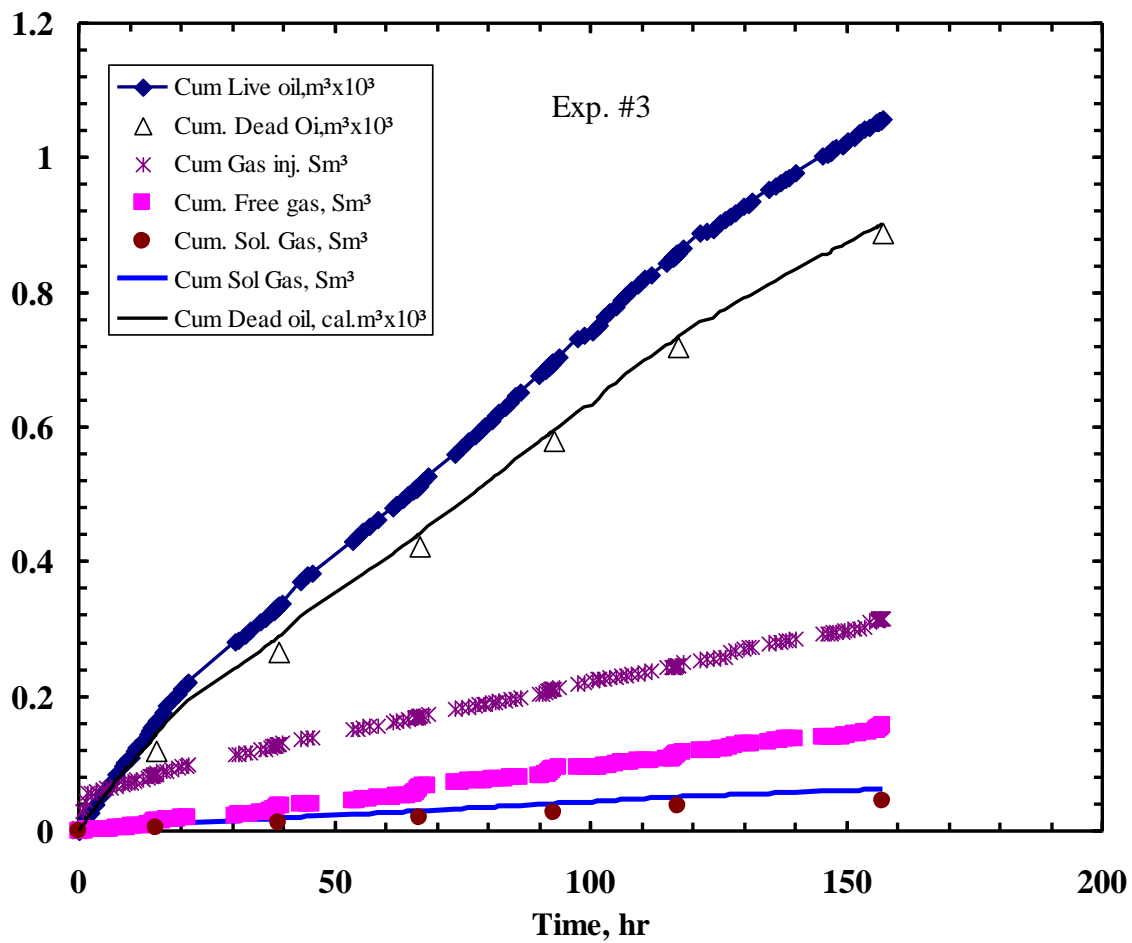


Figure 8-2: The cumulative production and injection data obtained from Run #3.

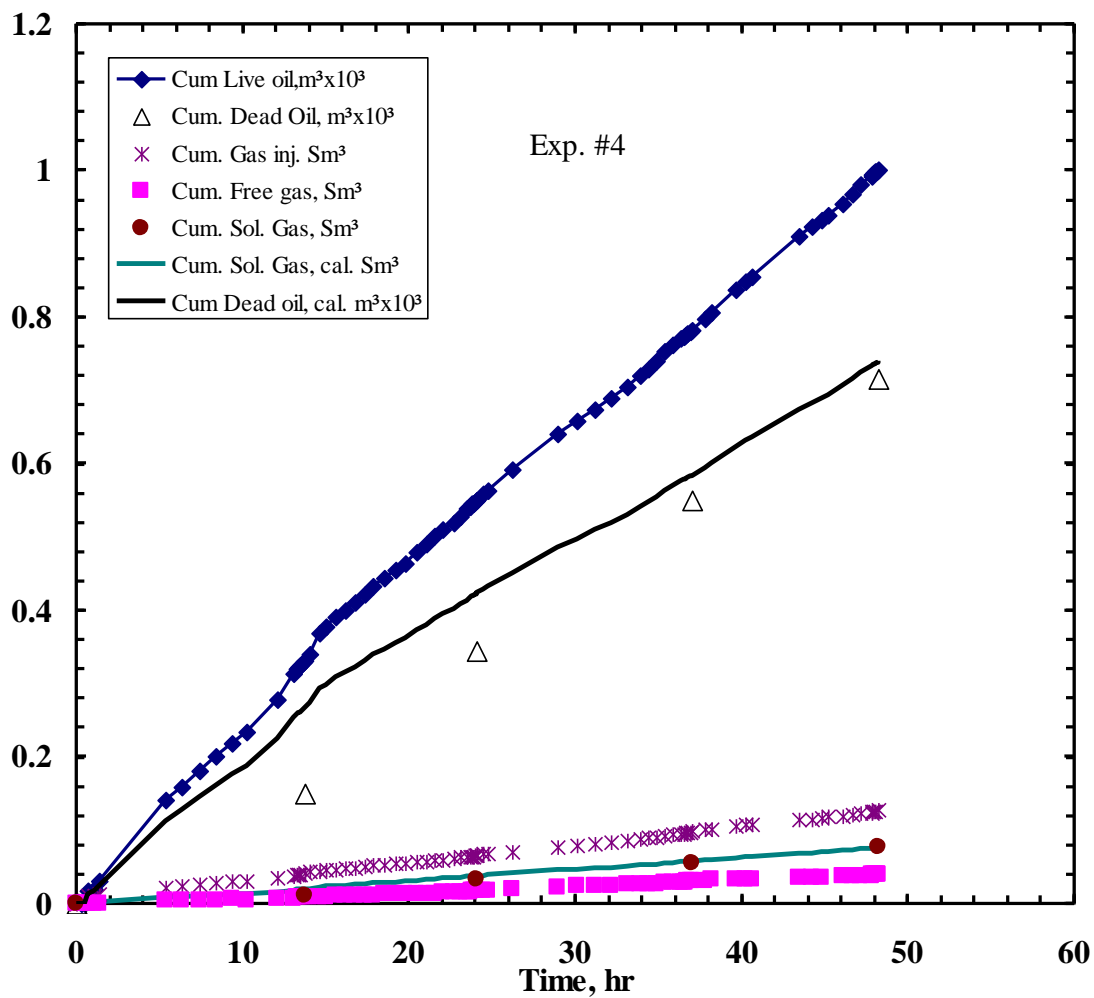


Figure 8-3: The cumulative injection and production data obtained from Run #4.

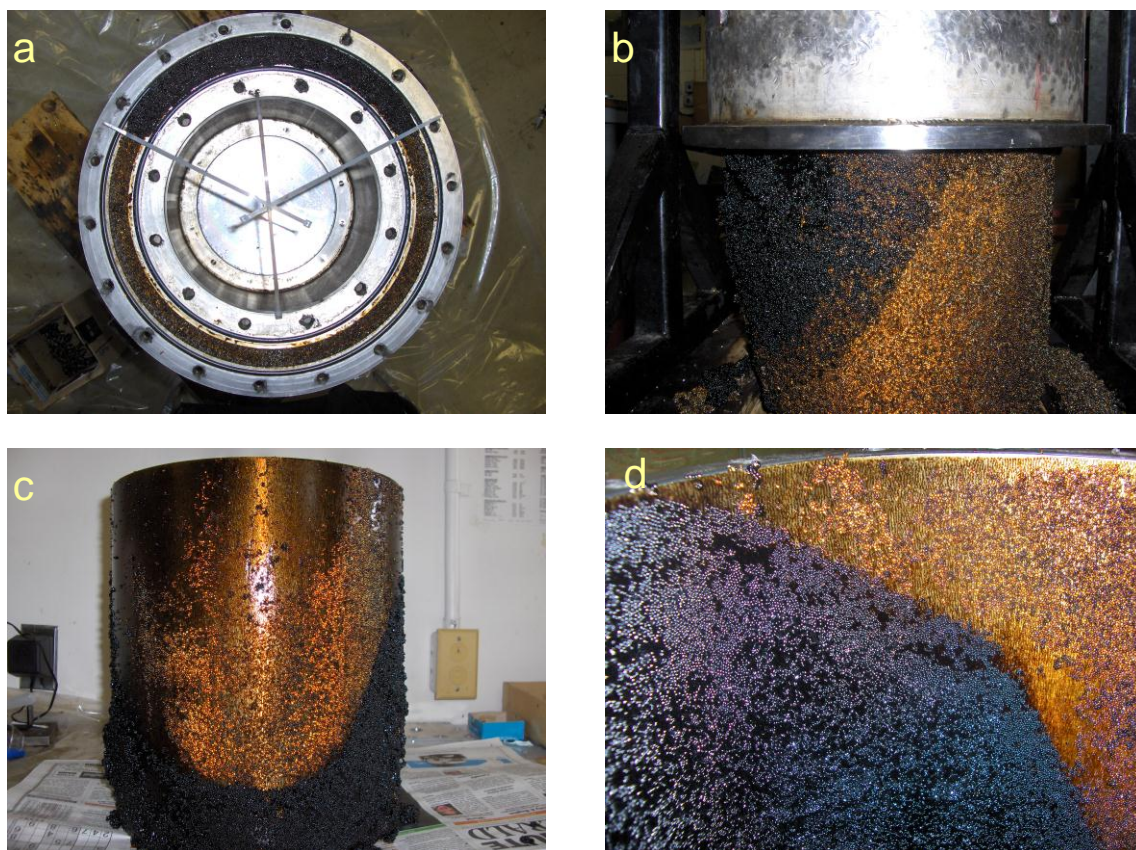


Figure 8-4: Disassembling of the physical model at the end of the Vapex test #1.

Figures 8-4a,b,c,d show photographs taken during disassembling of the physical model at the end of the Vapex test #1. Figure 8-4a was taken after removing top cap from physical model. It shows a symmetric development of the top of vapour chamber. After removing the top cap, physical model was turned upside down, Figure 8-4b shows the inner cylindrical pipe coming out by gravity. As figure 8-4c and d show, there is a clear trace of the developed vapor chamber inside the annulus packed model. No evidence of asphaltene precipitation was observed. The same type of phenomena was seen in all of the experiments.

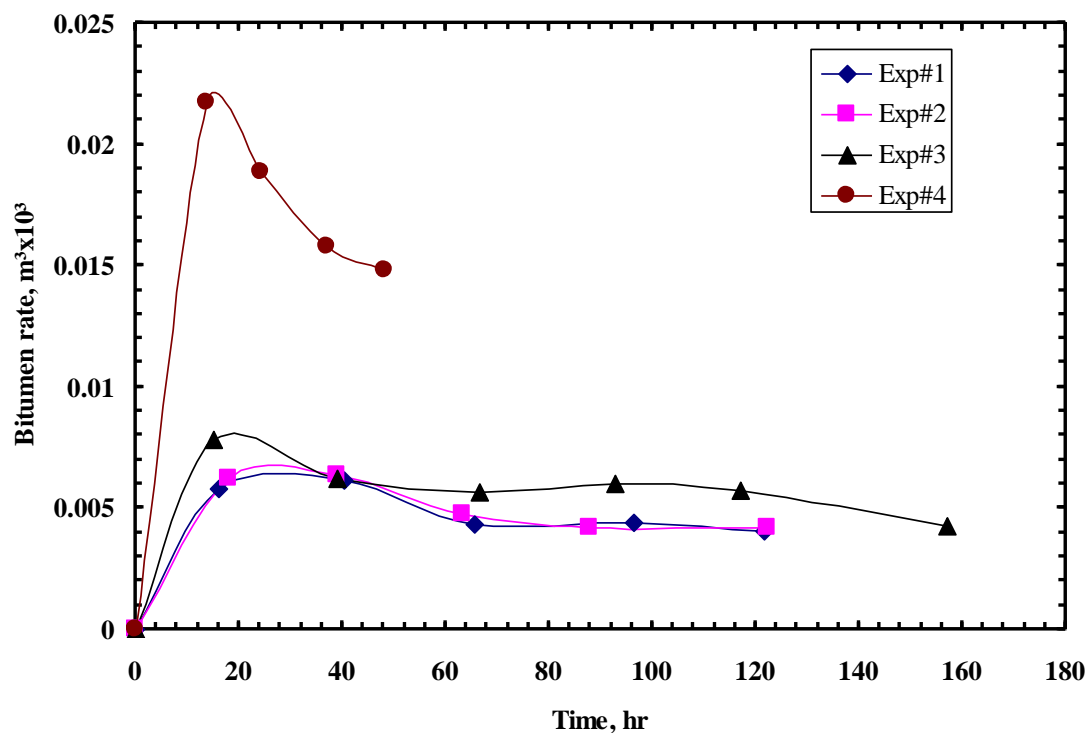


Figure 8-5: Comparing the dead oil flow rate of four Vapex tests.

Figure 8-5 compares the dead oil production rates observed in these Vapex tests. At early time of the experiment there is a high rate of oil production. This rate could be partly due to viscous displacement before break-through time. The other possible cause of this higher rate at early time of the process could be enhanced mixing caused by viscous fingering of the gaseous solvent into the bitumen saturated packed model while pressurizing it from ambient condition to the test pressure. Eventually almost a stabilized flow rate of the bitumen was observed. This represents the spreading and expanding of the vapor chamber. Once the vapor chamber edges from both side of the annulus space reach each other further production would cause reduction in height, therefore the

bitumen production rate starts decreasing. Only in the experiment #3 our test was continued long enough to see this phenomena. It is clear that the presence of the non-condensable gas (CO_2) reduces the bitumen production rate. However, at the higher pressure, due to higher carbon dioxide solubility in bitumen the rate of production is higher than at the lower pressure. This occurs in spite of lower partial pressure of propane in the injected vapour in the higher pressure test, which suggests that at higher pressure CO_2 is no longer acting as a simple carrier of the Vapex solvent. It is now reducing the oil viscosity by dissolving in the oil.

Figure 8-6 shows the results of viscosity measurements of the produced live oil samples during several production intervals of the Vapex tests. It is clear that at early stage of the process the produce live oil has higher viscosity. This is partly due to the mobile oil being displaced under initial pressure gradient during the start-up of the process. There is more time for mixing as the sides of the vapour chamber become more inclined and the viscosity of the produced live oil reduces even further. In cases where it was not possible to measure the viscosity at test temperature due to our viscometer limitations, the viscosity versus temperature profiles for each sample were obtained, and the profiles were extrapolated to estimate the viscosity at the test condition. Using the density data measured by density meter the kinematic viscosity of the produced live oil was calculated. This value represents the average kinematic viscosity for the draining oil in the drainage layer of the Vapex process. This value is higher than the kinematic viscosity at the interface between the vapour chamber and the oil.

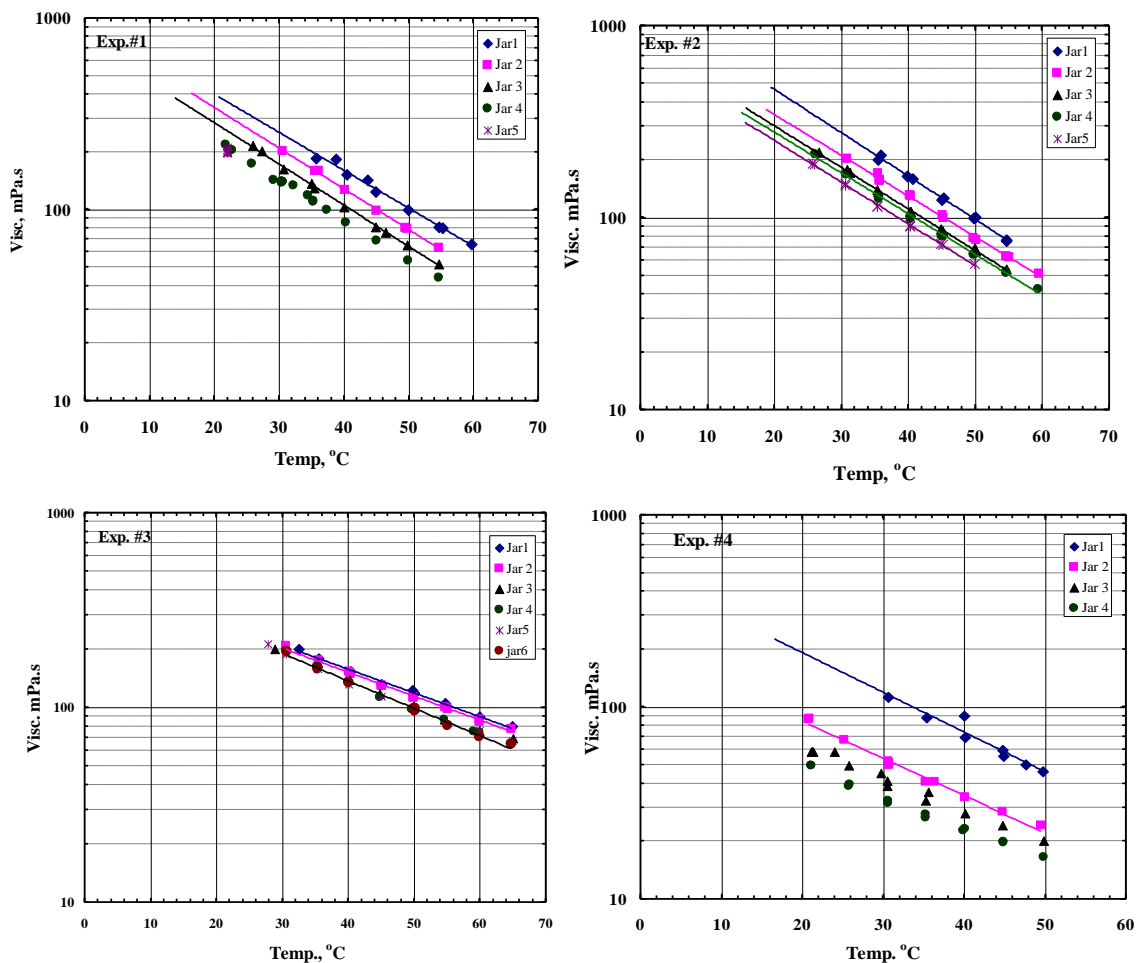


Figure 8-6: Viscosity of the produced live oil sample during the Vapex test 1, 2, 3, and 4.

Figure 8-7 shows the volume fraction of the solvent in produced oil in the four Vapex experiments. To facilitate seeing effect of the Vapex solvent composition on the viscosity of the diluted oil the kinematic viscosity data are shown in Figure 8-8. Also the weight percent of the propane in the vapor chamber, and solution gas during the Vapex experiments are reported in Figures 8-9 to 8-10.

The lowest kinematic viscosity is in the case of pure propane solvent. As the amount of the carbon dioxide increases in the injection gas the viscosity follows an increasing trend. However, an interesting observation is that in the high pressure experiment with 78 wt% carbon dioxide in the injected gas, the kinematic viscosity stabilized at a value lower than the stabilized kinematic viscosity in Experiments 1 and 2. This explains the better performance and higher bitumen production rate in the higher pressure test with lower amount of propane in the injection gas. It is worth noting that the stabilized composition of the gas in the vapour chamber is different than the injection gas composition. There is an increase in the carbon dioxide fraction and decrease in amount of propane (see Figure 8-10).

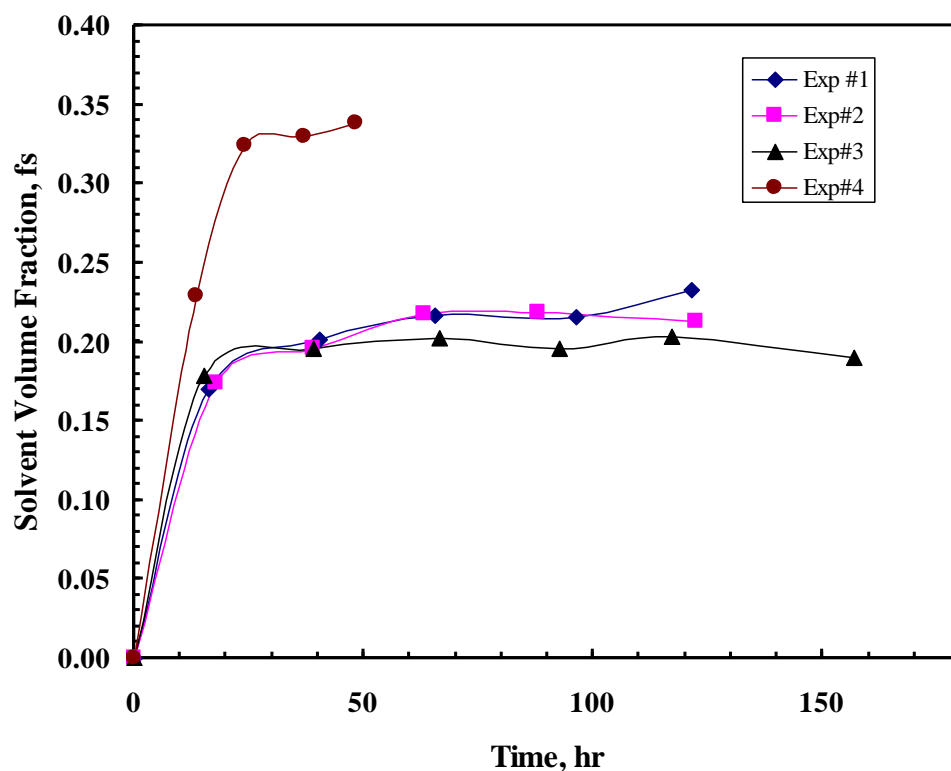


Figure 8-7: Solvent volume fraction in the produced live oil during the several Vapex experiments.

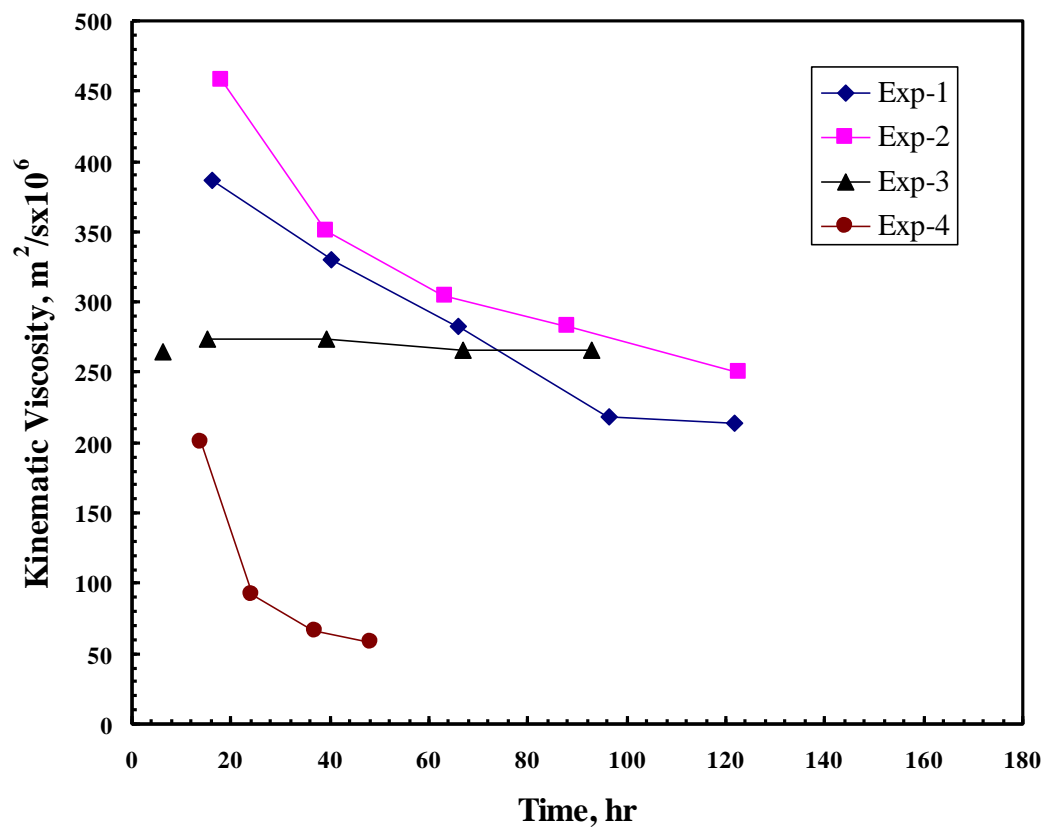


Figure 8-8: Kinematic viscosity of the produced live oil samples during the Vapex experiments.

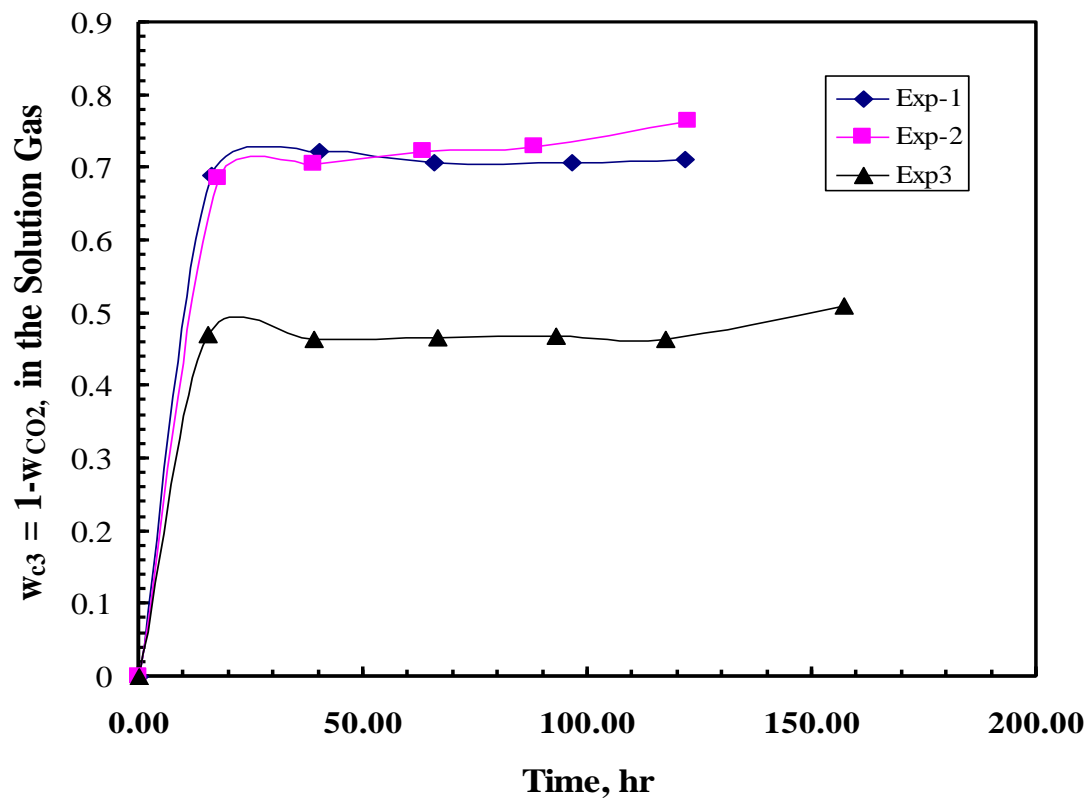


Figure 8-9: Composition of the solution gas during the Vapex experiments.

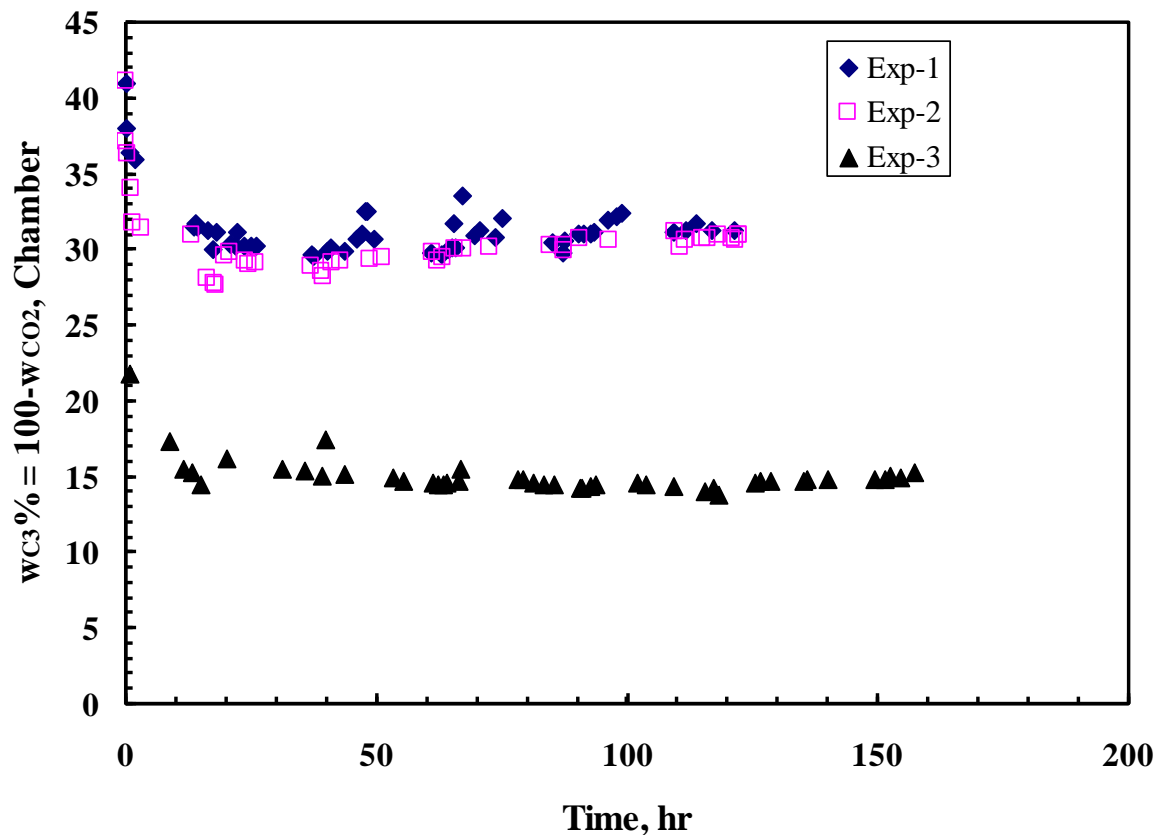


Figure 8-10: Vapor chamber composition during Vapex experiment 1,2, and 3.

Figure 8-7 compares the solvent volume fraction (i.e. solution GOR) for all the Vapex tests. The highest solution GOR is in the case of pure propane as solvent. Based on the viscosity data and solvent volume fraction from Figures 8-8 and 8-7, it is clear that pure propane as the injection solvent results in the highest production rate (see Figure 8-11). But the interesting observation is the better performance of the carbon dioxide at higher pressure in spite of reduced volume fraction of propane. Figure 8-11 compares the dead oil cumulative production data for these Vapex tests.

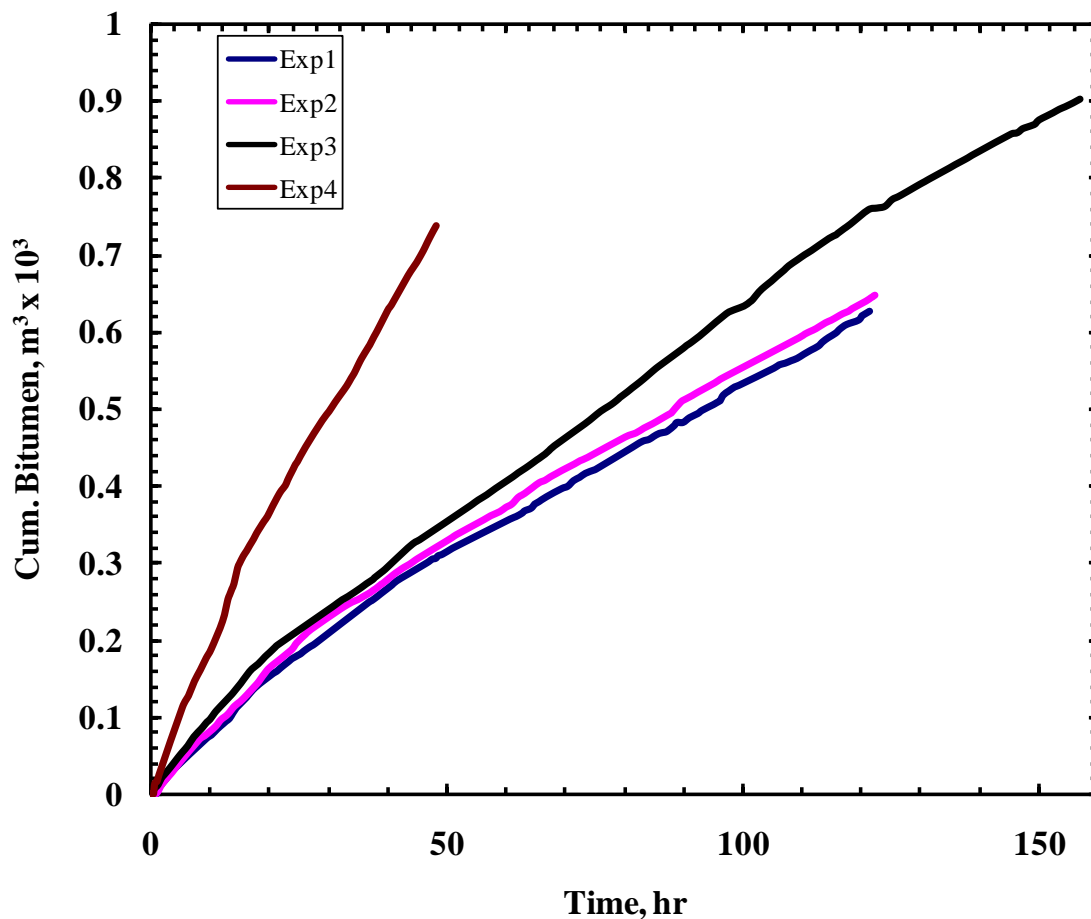


Figure 8-11: comparing the cumulative bitumen production by different solvent composition.

In summary, at high concentration of the CO_2 in the injection gas it was possible to have higher dew point pressure and operate the Vapex test at high pressure and benefit from higher solubility of the CO_2 and its auxiliary effects in viscosity reduction along with propane.

8.4 Phase Behaviour and Compositional Path

We used fixed injected gas compositions in our Vapex tests. Figure 8-10 showed that the vapor chamber composition was different from the injected gas, and that within few hours after the start, it more or less stabilized around a fixed value. To understand the compositional path during the Vapex process we developed an EOS model for mixtures of carbon dioxide, propane, and Athabasca bitumen.

We have previously reported experimental solubility and phase behaviour data for the binary mixtures of Athabasca bitumen with propane and carbon dioxide, and the ternary mixtures of bitumen with both solvents (Badamchizadeh et. al. 2009a, b). These data along with the solubility data for carbon dioxide in Athabasca bitumen reported by Mehrotra et al. (1982) were used to develop an EOS model of the carbon dioxide/propane/Athabasca bitumen phase behaviour. The details of this modeling were presented in the chapter 5. The tuned EoS model was used to predict the ternary diagram for the Athabasca bitumen/propane/carbon dioxide system at the test conditions used in this work.

Figures 8-12 and 8-13 show the ternary diagrams for the oil solvent systems in Experiments 1 and 3 respectively. The composition of the produced diluted oil samples, injection gas, and stabilized vapor chamber are indicated on each plot. When the injected solvent first contacts the bitumen, a vapour-liquid mixture is created with composition on the dilution line connecting the solvent composition and the oil composition. The tie line passing through this point intersects the bimodal curve at the compositions of the

equilibrium vapor and liquid phases. As a result of this contact, the vapor phase has higher CO_2 than the injected gas, and liquid phase has some solvent dissolved in it. When the fixed composition gas enters the chamber it mixes with the existing vapor phase which has higher CO_2 content. Consequently, the gas that contacts fresh oil is richer in CO_2 and the amount of propane that is transferred to the oil becomes lower. If only the diluted oil is removed from the chamber, this process would continue to gradually make the vapor chamber gas leaner in propane. However, in these experiments, some free gas (which has the composition of vapor chamber gas) was continually removed from the system as free gas production with the oil. Since this free gas is richer in CO_2 , its removal counteracts the process causing preferential accumulation of CO_2 in the vapor chamber. At some point the increase in CO_2 fraction in the vapor chamber by preferential dissolution of propane is fully balanced by preferential removal of CO_2 in the free gas and the vapor chamber composition becomes stabilized.

This transition period to reach equilibrium occurred in the early parts of these experiments (see Figure 8-10). Hence, we expect the composition of the liquid phase at interface to be at the liquid side of the bimodal curve along the tie line passing through this vapor composition. However, the composition of the draining oil would be somewhat leaner in the solvent, since the oil in the interior of the drainage layer becomes mobilized without reaching equilibrium concentration of the diffusing solvent. This compositional path is similar to the condensing compositional gravity drainage process described by Dicarlo (2007).

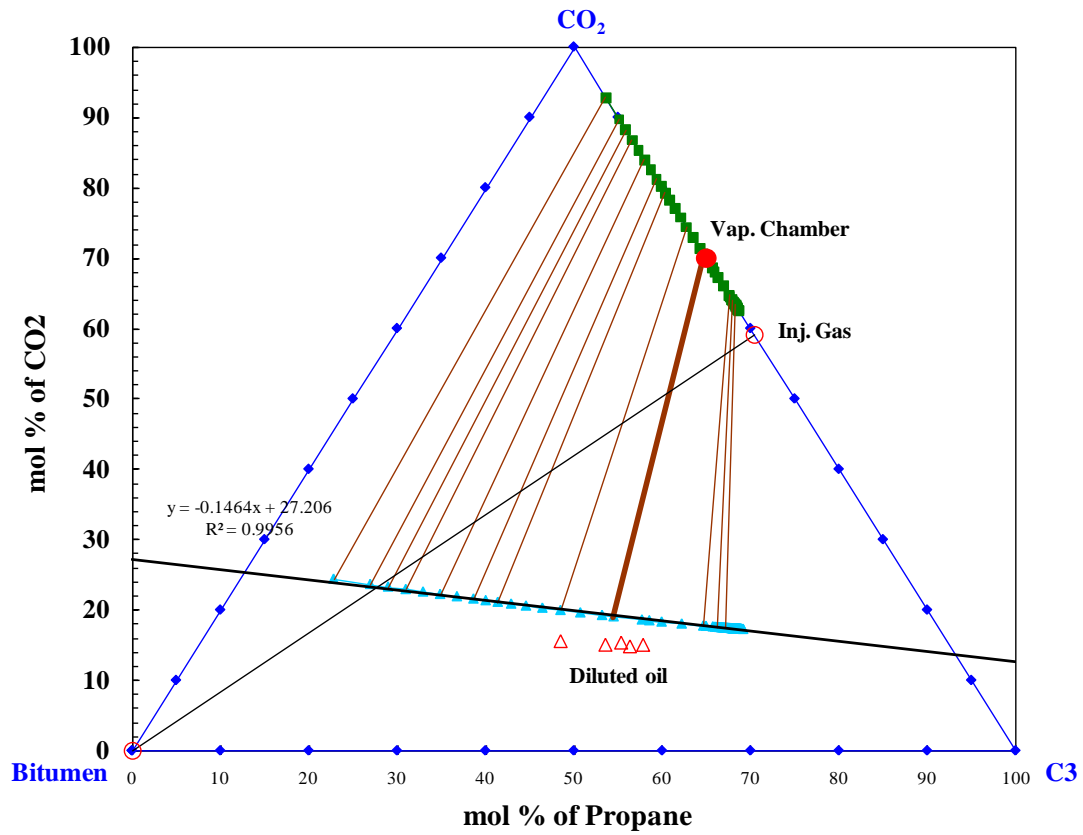


Figure 8-12: Compositional change during the Vapex experiment #1.

the diffusion coefficient. The stabilized bitumen production rate and solvent volume fraction (i.e. $f_{bss} = 1 - f_s$) are extracted from experimental data shown in Figure 8-5 and 8-7 which will be used in Equation 7-79 and 7-88.

The equation of state model and flash calculation were used to calculate solvent mole and volume fraction at interface (saturation condition), bitumen and solvent blend density, viscosity and kinematic viscosity. We assumed that the stabilized gas composition in the vapour chamber (i.e. free gas composition) is in equilibrium with saturated oil at the vapour chamber-oil interface. For the solvent with binary mixture of carbon dioxide and propane, the vapour equilibrium composition was obtained from Figure 8-10 during the stabilized rate (i.e. steady state) period of Vapex experiment. The solvent equilibrium composition in the oil can be obtained from ternary phase diagram Figures 8-12 and 8-13 for solvent with binary mixture of carbon dioxide and propane. It is the composition at the liquid side of the tie line connecting the stabilized vapour composition to the liquid composition at the interface. The equilibrium solvent composition and properties are summarized in Table 8-3.

The solvent and bitumen blend viscosity and density were calculated at each experiment pressure and temperature condition, from saturated composition of solvent down to zero composition of solvent in bitumen. Figure 8-14 and 8-15 show the resulting normalized kinematic viscosity versus normalized volume fraction of solvent with respect to the saturated mixture kinematic viscosity ($\nu_s, m^2/s$) and composition $C_s (m^3/m^3)$. It was used

to obtain the power law trend of normalized kinematic viscosity of mixture to normalized volume fraction of solvent in mixture (i.e. power m).

Table 8-3. Steady State Period of Vapex Experiments data.

Exp#	S.S time hr	Vap. Cham. Comp		Sol. Comp. in Oil		C_s		ρ_s kg/m ³	μ_s m.Pa.s	$f_{bss}=1-f_s$ Fig. 7
		CO ₂	C ₃	CO ₂	C ₃	mol. Frac.	Vol. Frac			
1	40-121	69.73	30.27	25.75	74.25	0.6431	0.2267	910	147.5	0.789
3	39-118	85.17	14.83	51.66	48.34	0.6537	0.2388	932	146.5	0.803
4	15-48	0	100.00	0	100.00	0.7965	0.3866	809	19.5	0.669

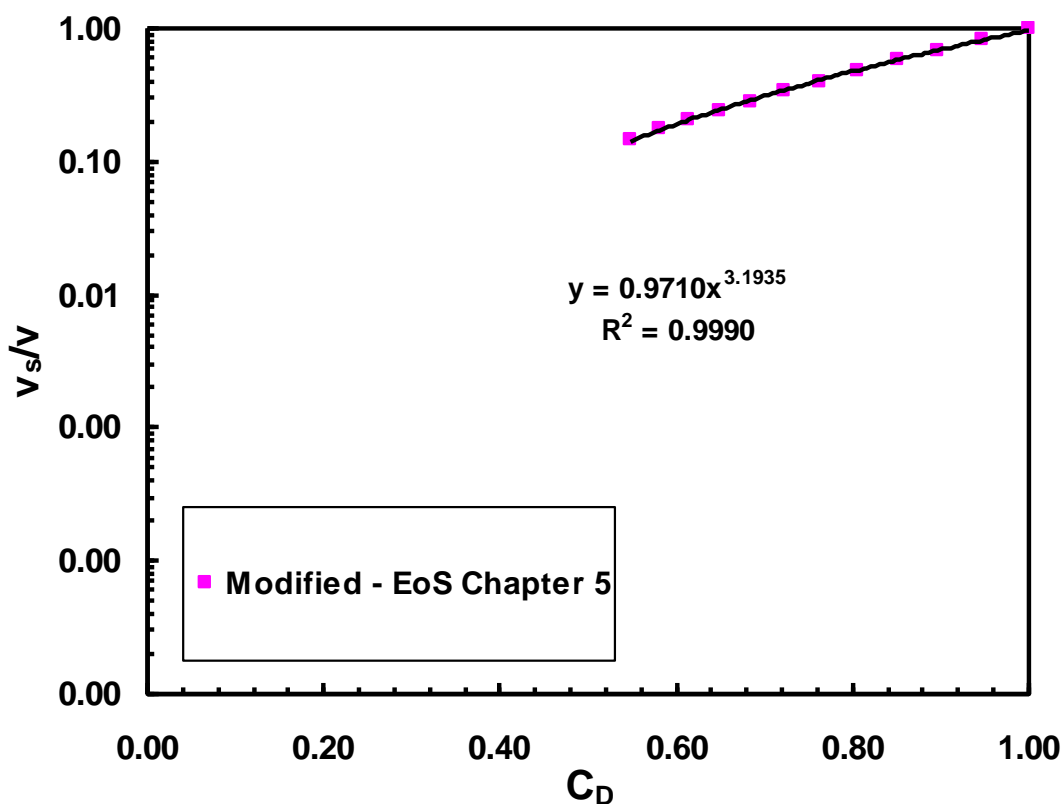


Figure 8-14. Athabasca bitumen – Binary solvent (carbon dioxide and propane) kinematic viscosity calculated by tuned PR EoS model in WinProp at Exp.1 T & P, and fitted to Equation 7-11.

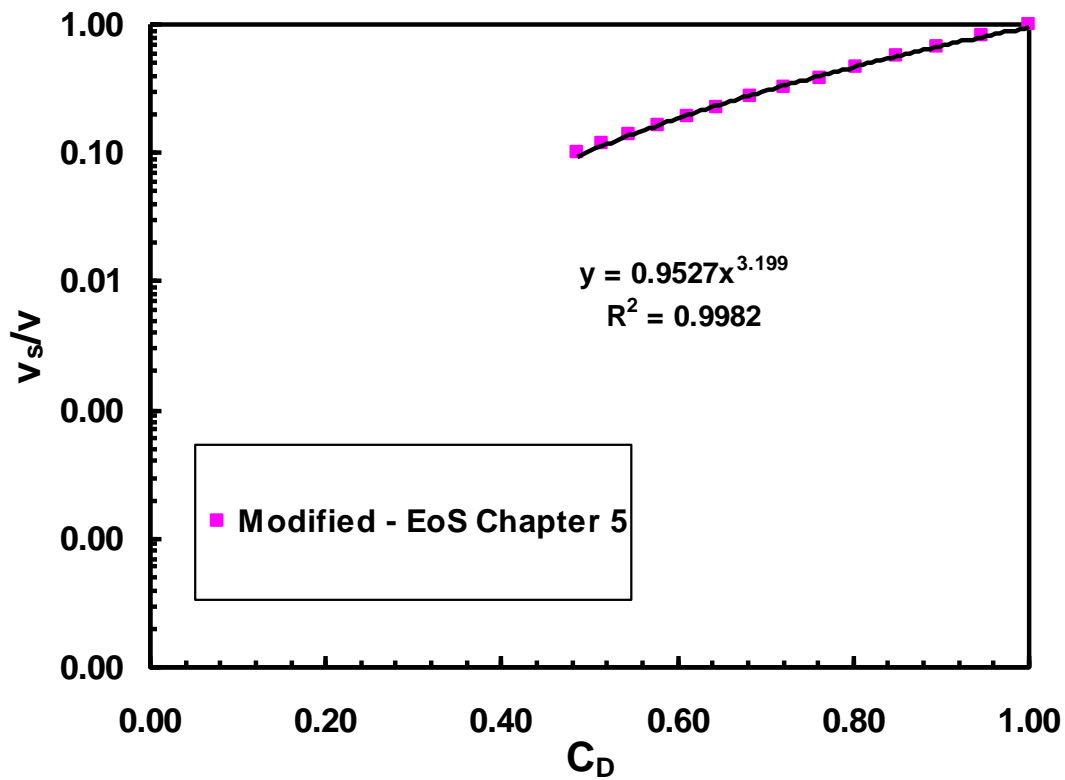


Figure 8-15. Athabasca bitumen – Binary solvent (carbon dioxide and propane) kinematic viscosity calculated by tuned PR EoS model in WinProp at Exp. #4 T & P, and fitted to Equation 7-11.

Haidari et al 2008, and Pooladi-Darvish 1996 have shown that with HIM (Heat-Integral_Method) a polynomial function of third order can sufficiently represent concentration gradient along the penetration depth (i.e. $n = 3$). Table 8-4 summarize the parameters used in Equation 7-79 to obtain diffusion exponent (d), for each experiment.

Table 8-4. Solvent mass diffusion exponent d) calculated by Equation 7-79.

Exp#	f_{bss} Frac	C_s Vol. Frac	m	n	d Calculated
1	0.789	0.2267	3.1930	3	10.00
3	0.803	0.2388	3.1990	3	3.50
4	0.669	0.3866	2.9543	3	7.73

The diffusion coefficient at the interface (D_s) can be calculated by Equation 7-88 using the experimental stabilized volumetric bitumen production rate per unit width of the physical model (i.e. well length). The physical model dimensions, permeability and porosity are summarized in Table 8-5. The porosity and initial water saturation (S_{wi}) data are reported in Table 8-2 for each experiment. The ΔS_o will be equal to the $(1-S_{wi})$. It is the change in the oil saturation during Vapex process.

Table 8-5. Physical Model Properties in SI Units

Permeability, K m²	6.316E-10
Physical Model Height, m	0.3048
Well Length, m	0.0177

Table 8-6 summarize the calculated mass diffusion coefficient of solvent into oil at the interface. It is interesting to notice that carbon dioxide-propane binary mixture at high pressure experiment has higher diffusivity than pure propane. The Rayleigh number N_{Ra} is calculated by Equation 7-86 and reported in Table 8-6. The Rayleigh number is the ratio between characteristic diffusion time to characteristic convection time. For the case

where the angle between gravity vector and diffusion vector is orthogonal diffusion/convection transition occurs for a value $N_{Ra} = 40$ (Montel 1993).

$$N_{Ra} = \frac{KHg}{\phi\Delta S_o v_s D_s} = \frac{H^2/D_s}{v_s H \phi \Delta S_o / Kg} = \frac{\text{characteristic diffusion time}}{\text{characteristic convection time}} \quad (8-1)$$

The larger N_{Ra} means dominance of convective movement of fluid and may result in higher production rate. From Equation 7-85a it is clear that the steady state oil rate in Vapex process has stronger functionality to ratio of the saturated oil to produced oil kinematic viscosity than square root functionality to the N_{Ra} . Table 8-6 shows that the N_{Ra} in case of Experiment 4 is larger than other experiments. Also since pure propane resulted in larger viscosity reduction in the oil mixture the production rate is higher in Experiment 4 than other experiments.

Table 8-6. Solvent apparent mass diffusion coefficient at interface and N_{Ra} .

Exp#	q_{bss} m ³ /(m.sec)	D_s m ² /sec	N_{Ra}	$(v_s/v_{ss})^{(d/m)}$
1	7.3883E-08	2.4288E-10	1.3937E+05	2.1455E-01
3	9.1145E-08	3.7407E-09	9.3398E+03	8.1571E-02
4	2.1267E-07	5.4376E-11	4.1628E+06	5.4013E-01

Das and Butler (1996) proposed the following correlation for the functionality of propane apparent diffusivity in the Peace River bitumen:

$$D_a = 1.306e - 9\mu^{-0.46} \quad (8-1)$$

Using this correlation for the Athabasca bitumen and propane system at the condition of the Experiment 4 where the viscosity at the Vapex interface is calculated by modified Pedersen correlation (Chapter 5) to be $\mu = 19.5 \cdot 10^{-3}$ Pa.s, the apparent diffusivity of propane in Athabasca bitumen will be $3.3 \cdot 10^{-10}$ m²/s, which is one order larger than value reported in Table 8-6.

Yang and Gu (2006) measured the mixture of 70% CO₂ and 30% propane apparent diffusivity in the Lloydminster heavy oil using the dynamic pendant drop volume analysis (DPDVA) method. The apparent diffusivity of this mixture at 23.9°C and pressure 0.9 of the dew point pressure of carbon dioxide and propane was reported $0.8 \cdot 10^{-9}$ m²/s. This vapor mixture composition is same as the vapor chamber composition in the Experiment #1 (see Table 8-3) where the apparent diffusivity at 21°C and same pressure condition is $2.4 \cdot 10^{-10}$ m²/s (Table 8-6). Considering the high viscosity of Athabasca bitumen compared to Lloydminster heavy oil, the apparent diffusivity obtained in this study is comparable to the value reported by Yang and Gu.

CHAPTER 9 : CONCLUSION AND RECOMMENDATION

The preceding chapters presented an experimental and modeling study of solvent (e.g. propane – carbon dioxide) – Athabasca bitumen phase behavior and of its use in the Vapex process. The following conclusions, important observations, and recommendations can be drawn from this study.

9.1 Summary and Conclusions

- Athabasca bitumen and its SARA fractions specific gravity, and molecular weight were measured. The SimDist analysis of the maleten fraction of Athabasca bitumen were also obtained.
- Athabasca bitumen density for temperatures 10 – 50°C and pressure up to 3.5 MPa were measured. An empirical correlation was developed for Athabasca bitumen density as a function of temperature and pressure.
- Athabasca bitumen viscosity was measured at atmospheric pressure and temperatures 103 – 150°C. A linear functionality was verified between the double logarithms of viscosity versus logarithm of the absolute temperature.
- A methodology was developed to measure solubility and phase boundary of VLE, LLE, and VLLE for binary mixture of carbon dioxide and Athabasca bitumen for temperature range of 10 – 40°C and pressure up to 11 MPa.
- An empirical Henry law coefficient correlation for carbon dioxide solubility in heavy oil was developed, which also predicts the solubility and saturation pressure for carbon dioxide and Athabasca bitumen binary mixture in VLE conditions.

- The effects of propane dissolution on Athabasca bitumen density and viscosity were measured for temperatures between 10-90°C and pressures up to 4.9Mpa.
- A modified Raoult's Law was developed which predicts propane solubility and saturation pressure for binary mixture of propane and Athabasca bitumen for temperatures between 10 – 50°C.
- Lobe viscosity mixing rule in its original form was capable of predicting the viscosity of propane – Athabasca bitumen binary mixture.
- Shu viscosity correlation was modified to calculate the viscosity of propane and bitumen binary mixtures.
- The VLE and VLLE phase boundaries were experimentally determined for a ternary mixture of carbon dioxide – propane – Athabasca bitumen. At VLE condition the modified Raoult's law for propane and Henry law for carbon dioxide was able to predict the saturation pressure of the ternary system. Also Lobe viscosity correlation could predict the liquid phase viscosity for the ternary mixture.
- Athabasca bitumen was characterized into four pseudo components based on the SimDist and true boiling point curve obtained experimentally for Athabasca bitumen.
- Peng-Robinson equation of state parameters were modified to calculate the solubility, saturation pressure and density data for binary and ternary mixture of carbon dioxide, propane, and Athabasca bitumen.

- Pederson viscosity correlation coefficients were adjusted to predict the liquid viscosity of binary and ternary mixture of carbon dioxide, propane, and Athabasca bitumen at VLE condition.
- An improved experimental apparatus and procedure were developed to test the performance of the Vapex process in recovering the Athabasca bitumen by injecting a fixed composition of vaporized solvent. This procedure provides experimental data on the compositional changes in the vapor chamber and solution gas. The improved apparatus also enables us to measure the density and the viscosity of produced oil along with its composition.
- Pure propane as a gaseous solvent for Vapex is more effective in recovering Athabasca bitumen. However, the vapor pressure of propane at reservoir temperatures is lower than typical reservoir pressures in Canada. Therefore it is necessary to mix a non-condensable gas with propane to keep the dew point pressure of the injected solvent above the reservoir pressure.
- It is important to have a good understanding of the phase behavior of the solvent and bitumen system at reservoir conditions to select the composition of the injection gas. It is clear from the Vapex physical model experiments that, by controlling the injected gas compositions, it is possible to avoid multiple liquid phase formation.
- The compositional change during the Vapex test was mapped experimentally and theoretically by an EoS model. The compositional path follows a multi-contact immiscible process that can be called condensing compositional gravity drainage.

- A mathematical model of Vapex process was developed in dimensionless format, where the dependency of solvent mass diffusion coefficient on the solvent composition in oil mixture was accounted. The nonlinearity in the moving boundary, diffusion PDE of solvent concentration (Fick's second law) was removed by defining pseudo concentration and pseudo time terms.
- A power law functionality of solvent mass diffusion to solvent concentration resulted in stronger dependence of Vapex process steady-state oil rate to the kinematic viscosity of the saturated oil than the square root functionality to the N_{Ra} .

9.2 Observation

- Binary mixtures of propane and bitumen form a second dense asphaltene-rich phase at propane contents above approximately 20 wt%. Binary mixtures of carbon dioxide and bitumen form a second carbon dioxide rich liquid phase at carbon dioxide contents above approximately 11 wt%. Multiple liquid phases were also observed in a ternary mixture of 13.1 wt% propane, 19.2 wt% carbon dioxide, and bitumen. Only liquid and vapour liquid regions were observed for two other ternary mixtures: 13.5 wt% propane and 11.0 wt% carbon dioxide; 24 wt% propane and 6.2 wt% carbon dioxide.
- The viscosity reduction of Athabasca bitumen by temperature is higher than viscosity reduction by solvents like propane, carbon dioxide, or their binary mixtures at typical reservoir condition.

- Carbon dioxide - propane binary mixture as Vapex solvent is more effective at higher pressure than low operating pressure.
- Vapex is a compositional gravity drainage process where the solvent compositional path appears to follow a condensing drive mechanism.

9.3 Recommendations

- The phase boundary and solubility measurement method developed during the course of this study, should be followed in a PVT cell with higher volumetric capacity. This would make it possible to take samples from the second liquid phase and perform measurements on the composition, density and viscosity of each phase.
- Other forms of the functionality of diffusion coefficient on the solvent concentration than power law, and its effect in the oil rate in the Vapex process should be studied.
- Due to huge viscosity difference between the native oil and saturated oil at the Vapex interface, the solvent mass diffusion functionality to the concentration should not be neglected.
- It is highly desirable to measure the density, viscosity, and solvent volume fraction in the produced oil during the Vapex experiments. It would be near impossible to draw any meaningful conclusion without these measurements from Vapex experimental oil rate, due to the strong dependence of diffusion coefficient on the solvent concentration.

REFERENCES

- Agrawala, M., and Yarranton H. W.: "An Asphaltene Association Model Analogous to Linear Polymerization", *Ind. Eng. Chem. Res.*, Vol. 40, Issue 21, pp. 4664-4672, 2001.
- ASTM D2007 (petroleum Standard): "Standard Test Method for Characteristic Groups in Rubber Extender and Processing Oils and Other Petroleum-Derived Oils by the Clay-Gel Absorption Chromatographic Method", ASTM International, West Conshohocken, PA, 2003, DOI: 10.1520/D2007-11, www.astm.org.
- ASTM Method D2887-97: "Test Method for Boiling Range Distribution of Petroleum Fractions by Gas Chromatography", in *Annual Book of ASTM Standards*, American Society for Testing and Materials, Philadelphia, PA, Vol. 05.02, 1997.
- Badamchi-Zadeh, A., Maini, B.B., and Yarranton, H.W.: "Applicability of CO₂-Based Vapex Process to Recover Athabasca Bitumen", SPE 117855, presented at the International Thermal Operations and Heavy Oil Symposium held in Calgary, Alberta, Canada, 20-23 October 2008.
- Badamchi-Zadeh, A., Yarranton, H.W., Maini, B.B., Satyro, M.A.: "Phase Behaviour and Physical Property Measurements for Vapex Solvents: Part II. Propane Carbon Dioxide and Athabasca Bitumen", *J. Can. Petr. Technol.*, Vol. 48, No. 3, pp 57-65, 2009.
- Badamchi-Zadeh, A., Yarranton, H.W., Svrcek, W.Y., and Maini, B.B.: "Phase Behaviour and Physical Property Measurements for Vapex Solvents: Part I. Propane and Athabasca Bitumen", *J. Can. Petr. Technol.*, Vol. 48, No. 1, pp 54-61, 2009.

- Berkowitz, N., and Speight, J. G.: "The Oil Sands of Alberta", Fuel, 1975, Vol. 54, Issue 3, pp. 138 – 149.
- Bird, R.B., Stewart, W.E., and Lightfoot, E.N.: "Transport Phenomena", 2nd Edition, John Wiley and Sons, Inc., 2002.
- Bishnoi, P.R., Heidmann R.A. and Shah M.K.: "Calculation of the Thermodynamic Properties of Bitumen System", Oil Sands, pp. 248-254, 1977.
- Boustani, A. : "Interfacial Mass Transfer in Vapex", MSc. Thesis, the University of Calgary, 2001.
- Butler, R. M., Mokrys, I. J.: "Recovery of Heavy Oils Using Vaporized Hydrocarbon Solvents: Further Development of The VAPEX Process", J. Can. Petr. Technol., Vol. 32, No. 6, June 1993.
- Butler, R.M., and Mokrys, I.J. : "Solvent Analog of Steam Assisted Gravity Drainage", AOSTRA J. Res., Vol. 5, No. 1, pp. 7-32, 1989.
- Butler, R.M., and Mokrys, I.J.: "A New Process (VAPEX) for Recovering Heavy Oil Using Hot Water and Hydrocarbon Vapour", J. Can. Petr. Technol., Vol. 38, No.1, pp. 97-106, 1991.
- Butler, R.M.: "A New Approach to The Modeling of Steam-Assisted Gravity Drainage", J. Can. Petr. Technol., pp. 42-51, May-June 1985.

Cavallaro, A.N, Galliano, G.R., Sim, S., Singal, A., and Fisher, D.: "Laboratory Investigation of an Innovative Solvent Based Enhanced Recovery and in Situ Upgrading Technique", paper 2005-016, presented at the Canadian International Petroleum Conference (56th Annual meeting), Calgary, Alberta, Canada, 2005.

Chatzis, I. : "Pore Scale Mechanisms of Heavy Oil Recovery Using the Vapex Process", paper 2002-198. Canadian International Petroleum Conference, Calgary, June 2002.

Chueh, P.L. and Prausnitz, J.M: "Vapour-Liquid Equilibria at High Pressures, Calculation of Partial Molar Volume in Non-Polar Liquid Mixtures", AIChE J., Vol. 13, No. 6, pp. 1099-1113, 1967.

Computer Modeling Group, (CMG): "WinProp. Phase Property Program, User's Guide", Version 2004.1.

Cuthiell, D., McCarthy, C., Kissel, G., and Carmeron, S.: "The Role of Capillary in Vapex", paper 2006-073, Canadian International Petroleum Conference, Calgary, June 2006.

Das, S. K. and Butler, R. M.: "Mechanism of the Vapor Extraction Process for Heavy Oil and Bitumen", J. Petr. Sci. Eng., Vol. 21, Issue 1-2, pp 43-59, 1998.

Das, S.K. : " In Situ Recovery of Heavy Oil and Bitumen Using Vaporized Hydrocarbon Solvents", the University of Calgary, PhD Thesis, 1995.

Das., S.K., and Butler, R.M.: "Diffusion Coefficients of Propane and Butane in Peace River Bitumen", Can. J. Chem. Eng., Vol. 74, No. 6, pp. 985-992, 1996.

- DiCarlo, D. A., Jessen, K., and Orr F. M.: “Compositional gravity drainage 1. Equilibrium solution and controlling Bond number for a two-phase, three-component system.”, *Transport Porous Media*, Vol. 69, pp 13-32, 2007a.
- DiCarlo, D. A., Jessen, K., and Orr F. M.: “Compositional gravity drainage 2: experimental measurements using an analog system.”, *Transport Porous Media*, Vol. 69, pp 159-174, 2007b.
- DiCarlo, D. A., Jessen, K., and Orr F. M.: “Simulation of Compositional Gravity Drainage Processes”, SPE – 110077, 2007c.
- Dunn, S.G., Nenniger, E.H, and Rajan, V.S.V.: “A Study of Bitumen Recovery by Gravity Drainage Using Low Temperature Soluble Gas Injection”, *Can. J. Chem. Eng.*, Vol. 67, pp. 987-991, Dec. 1989.
- Eggertsen, F.T., Groennings, S., and Holst, J.J.: “Analytical Distillation by Gas Chromatography”, *Anal. Chem.*, Vol. 32, pp. 904–909, 1960.
- Escobedo, J., and Mansoori, G.A.: “Viscometric Principles of Onsets of Colloidal Asphaltene Flocculation in Paraffinic Oil and Asphaltene Micellization in Aromatics”, *SPE Prod. Facilities*, pp. 116-122, paper # 28729, May 1997.
- EUB Inquiry, “Gas/Bitumen Production in Oil Sand Areas”, March 1998.
- Farouq Ali, S.M., and Thomas, S. :”Enhanced Oil Recovery What We Have Learned”, *J. Can. Petr. Technol.*, Vol. 39, N0. 2, pp. 7-11, Feb. 2000.

Frauenfeld, T. W. J., Kissel, G., and Zaho, S. W.: "PVT and Viscosity Measurements for Lloydminster-Aberfeldy and Cold Lake Blended Oil Systems", paper # 79018, presented at the 2002 SPE/Petroleum Society of CIM/CHOA International Thermal Operation and Heavy Oil Symposium, Calgary, AB, Canada, Nov. 4-7.

Frauenfeld, T., Lillico, D., Jossy, C., Vilcsak, G., Rabeeh, S., and Singh, S. : "Evaluation of Partially Miscible Processes for Alberta Heavy Oil Reservoirs", J. Can. Petr. Technol., Vol. 37, No. 4, pp. 17-24, 1998.

Freitag, N. P., Sayegh, S. G., Exelby, R.: "A New Semiautomatic PVT Apparatus for Characterizing VAPEX Systems", paper # 97783, presented at the SPE/Petroleum Society of CIM/CHOA International Thermal Operation and Heavy Oil Symposium, Calgary, AB, Canada, Nov. 1-3, 2005.

Green, L.E., and Worman, J.C.: "Simulated Distillation of High Boiling Petroleum Fractions", Anal.Chem., Vol. 37, pp. 1620–1621, 1965.

Hayduk, W., and Cheng, S. C., "Review of relation between diffusivity and solvent viscosity in dilute liquid solutions", Chem. Eng. Sci., Vol. 26, Issue. 5, pp. 635-649, 1971.

Hayduk, W., Castaneda, R., Bromfield, H., and Perras, R. R., " Diffusivities of Propane in Normal Paraffin, Chlorobenzene, and Butanol Solvents", AIChE J., Vol. 19, Issue. 4, pp. 859-861, 1973.

- Heidari, M.R., “Mathematical Modeling of SAGD and Vapex Processes”, MSc. Thesis, The University of Calgary, 2008.
- Jacobs, F. A., Donnelly, J. K., Stanislav, J. F., and Svrcek, W. Y.: “Viscosity of gas-saturated bitumen”, J. Can. Petr. Technol., 1980, Vol. 19, No. 4, page 46 – 50.
- Jacoby, R. H.: “Phase Behaviour of Light Hydrocarbon – Heavy Oil or Tar Systems, and Its Application to Recovery Processes”, In Situ, Vol. 11, No. 2&3, pp. 145-167, 1987.
- Jacquín, C., Legait, B., Martin, J.M., Nectoux, A., Anterion, F., and Rioche, M.: “Gravity drainage in a fissured reservoir with fluids not in equilibrium. “, J. Petrol. Sci. Eng. Vol. 2, Issue 2-3, pp. 217–224, April 1989.
- Jhaveri, B.S., and Youngren, G.K.: “ Three Parameter Modification to the Peng-Robinson Equation of State to Improve Volumetric Predictions”, SPE Reservoir Engineering, Vol. 3, No. 3, pp. 1033-1040, August 1988.
- Jiang, Q.: ”Recovery of Heavy Oil Using Vapex Process”, the University of Calgary, PhD. Thesis, 1997.
- Karmaker, K., and Maini, B. B., “Applicability of Vapor Extraction Process to Problematic Viscous Oil Reservoir”, SPE 84034, presented at the SPE ATCE held in Denver, Colorado, USA, 5-8 October 2003.
- Khan, M. A. B, Mehrotra, A. K. and Svrcek, W. Y.: “Viscosity models for gas-free Athabasca bitumen”, J. Can. Petr. Technol., Vol. 23, No. 3, pp. 47-53, 1984.

- Khan, S.A., Pope, G.A. and Sepehrnoori, K.: "Fluid Characterization of Three-Phase CO₂/Oil Mixtures," SPE/DOE 24130, presented at the SPE/DOE Eighth Symposium on Enhanced Oil Recovery, Tulsa, Oklahoma, 22-24 April, 1992.
- Li, Y.K., Nghiem, L.G., and Siu, A.: "Phase behaviour computations for reservoir fluids: effect of pseudo components on phase diagrams and simulation results", J. Can. Petr. Technol., pp.29-36, November-December 1985.
- Lobe, V.M., M.Sc. Thesis, University of Rochester, Rochester, New York, 1973.
- Luhning, R.W., Das, S.K, Fisher, L.J., Bakker, J., Grabowski, J., Engleman, J.R., Wong, S., Sullivan, L.A., and Boyle, H.A. : "Full Scale Vapex Process-Climate Change Advantage and Economic Consequences", J. Can. Petr. Technol., Vol. 42, No. 2, pp. 29-34, Feb. 2003.
- Mehrotra, A. K. and Svrcek, W. Y.: "Measurement and Correlation of Viscosity, Density and Gas solubility for Marguerite Lake Bitumen Saturated with Carbon Dioxide", AOSTRA J. Res., Vol. 1, No. 1, pp. 51-62, 1984.
- Mehrotra, A. K. and Svrcek, W. Y.: "Properties of Cold Lake Bitumen Saturated with Pure Gases and Mixtures", Can. J. Chem. Eng., Vol. 66, No. 8, pp. 656-665, 1988.
- Mehrotra, A. K. and Svrcek, W. Y.: "Viscosity, Density and Gas solubility for Oil-Sand Bitumen. Part I: Athabasca Bitumen Saturated with N₂, CO, CH₄, CO₂, C₂H₆", AOSTRA J. Res., Vol. 1, No. 4, pp. 263-268, 1985a.

Mehrotra, A. K. and Svrcek, W. Y.: "Viscosity, Density and Gas solubility for Oil-Sand Bitumen. Part II: Peace River Bitumen Saturated with N₂, CO, CH₄, CO₂, C₂H₆", AOSTRA J. Res., Vol. 1, No. 4, pp. 269-279, 1985b.

Mehrotra, A. K. and Svrcek, W. Y.: "Viscosity, Density and Gas solubility for Oil-Sand Bitumen. Part III: Wabasca Bitumen Saturated with N₂, CO, CH₄, CO₂, C₂H₆", AOSTRA J. Res., Vol. 2, No. 2, pp. 83-93, 1985c.

Mehrotra, A. K., and Svrcek W. Y.," Correlations for properties of bitumen saturated with CO₂, CH₄, N₂, and experiments with combustion gas mixtures", J. Can. Petr. Technol., Vol. 21, No. 6, pp. 95 104, 1982.

Mehrotra, A. K., Sarkar, M., and Svrcek, W. Y., " Bitumen Density and Gas Solubility Prediction Using the Peng-Robinson Equation of State", AOSTRA J. Res., Vol. 1, No. 4, pp.215 – 229, 1985.

Mehrotra, A. K., "Development of mixing rules for predicting the viscosity of bitumen and its fractions blended with toluene", Can. J. Chem. Eng., Vol. 68, No. 5, pp. 839 848, 1990.

Mehrotra, A. K., "Modeling temperature and composition dependence for the viscosity of diluted bitumen", J. Petr. Sci. Eng., Vol. 5, Issue. 3, pp. 261-272, 1991.

Mehrotra, A. K., "A model for the viscosity of bitumen/bitumen fractions-diluents blends", J. Can. Petr. Technol., Vol. 31, No. 9, pp. 28-32, 1992.

- Montel, F.: "Phase Equilibrium Needs for Petroleum Exploration and Production Industry", *Fluid Phase Equilibria*, Vol. 84, pp. 343-367, 1993.
- Motahhari, H., Satyro, M. A., and Yarranton, H. W., "Predicting the Viscosity of Asymmetric Hydrocarbon Mixtures with the Expanded Fluid Viscosity correlation", *Ind. Eng. Chem. Res.*, Vol. 50, pp. 12831-12843, 2011.
- Nguyen, T.A., Farouq, A.: "Effect of Nitrogen on the Solubility and Diffusivity of Carbon Dioxide into Oil and Oil Recovery by the Immiscible WAG Process", *J. Can. Petr. Technol.*, Vol. 37, No. 2, 1998.
- Oballa, V., and Butler, R.M.: "An Experimental Study of Diffusion in the Bitumen-Toluene System", *J. Can. Petr. Technol.*, Vol. 28, No. 2, pp. 63-69, 1989.
- Okazawa, T., "Impact of Concentration-Dependence of Diffusion Coefficient on Vapex Drainage Rates", *J. Can. Petr. Technol.*, Vol. 48, No. 2, pp. 47-54, 2009.
- Okazawa, T.: "Impacts of Concentration Dependence of Diffusion Coefficient on Vapex Drainage Rate", paper 2007-170, presented at the Canadian International Petroleum Conference (CIPC), June 12-14, 2007.
- Pedersen, K. S., Fredenslund, Aa., Christensen, P. L., and Thomassen, P., "Viscosity of Crude Oils", *Chem. Eng. Sci.*, Vol. 39, No. 6, pp. 1011-1016, 1984.
- Pedersen, K.S., and Fredenslund, Aa.: "An Improved corresponding States Model for the Prediction of Oil and Gas Viscosities and Thermal Conductivities", *Chem. Eng. Sci.*, Vol. 42, No.1, pp. 182-186, 1987.

- Peneloux, A., Rauzy, E., and Freze, R.: "A Consistent Correction for Redlich-Kwong-Saove Volume", *Fluid Phase Equilibria*, Vol. 8, Issue. 1, pp. 7-23, 1982.
- Peng, D.Y., and Robnson, D.B.: "A New Two-Constant Equation of State", *Ind. Eng. Chem. Fundam.*, 1976, 15, pp. 59-64.
- Peramanu, S., Pruden, B. B., and Rahimi, P.: "Molecular Weight and Specific Gravity Distributions for Athabasca and Cold Lake Bitumen and Their Saturate, Aromatic, Resin, Asphaltene Fractions", *Ind. Eng. Chem. Res.*, Vol. 38, pp. 3121-3130, 1999.
- Perry, R.H., Green, D.W., *Perry's Chemical Engineers' Handbook (7th Edition)*, Chapter 2, pp. 2-50, Table 2-6, 1997 McGraw-Hill.
- Plessis, D.: "Alberta's Oil Sands Resources, Production Growth, Products and Market", present at Alberta Economic Development & Alberta Energy Research Institute, Calgary, Alberta, Canada, 18 October 2004.
- Pooladi-Darvish, M.: "Mathematical Modeling of Non-Isothermal Gravity Drainage of Heavy Oil and Bitumen in Porous Media", PhD. Thesis, the University of Alberta, 1996.
- Quail, B., Hill, G. A., and Jha, K. N.: "Correlations of Viscosity, Gas Solubility, and Density for Saskatchewan Heavy Oils", *Ind. Eng. Chem. Res.*, Vol. 27, pp. 519-523, 1988.
- Reamer, H. H., Sage, B. H., and Lacey W. N., "Phase Equilibria in Hydrocarbon System", *Ind. Eng. Chem.*, Vol. 43, No. 11, pp. 2515-2520, November 1951.

Sabbagh, O., Akbarzadeh, K., Badamchizadeh, A., Svrcek, W.Y., and Yarranton, H.W.:

“Applying the PR-EoS to Asphaltene Precipitation from n-Alkane Diluted Heavy Oils and Bitumen”, *Energy & Fuels*, Vol. 20, pp. 625-634, 2006.

Satyro, M. A., and Yarranton, H. W., “Expanded fluid-based viscosity correlation for hydrocarbons using an equation of state”, *Fluid Phase Equilibria*, Vol. 298, pp. 1-11, 2010.

Schmidt, T., Leshchyshyn, T.H., and Puttagunta, V.R.: “Diffusivity of CO₂ into Reservoir fluids”, paper presented at 33rd Annual Technical Meeting of the Petroleum Society of CIM, June 6-9, 1982.

Shelton, J.L., Yarborough, L.: “Multiple Phase Behaviour in Porous Media during CO₂ or Rich-Gas Flooding”, *J. Petr. Technol.*, pp.1171-1178, Sep. 1977.

Shu, W.R.: “A Viscosity Correlation for Mixtures of Heavy Oil, Bitumen, and Petroleum Fractions”, SPE paper 11280, *SPE J.*, pp. 277-282, June 1984.

Simon, R., and Graue, D., “Generalized Correlation for Predicting Solubility, Swelling and Viscosity Behaviour of Co₂ – Crude Oil System”, *J. Petr. Technology*, (SPE # 917), pp. 102-106. January 1965.

Smith, J.M., and Van Ness, H.C.: “Introduction to Chemical Engineering Thermodynamics”, Fourth Edition, © 1987, McGraw-Hill.

Svrcek, W.Y., and Mehrotra, A.K.: “Gas solubility, viscosity and density measurements for Athabasca bitumen.”, *J. Can. Petrol. Tech.*, Vol. 21, No. 4, pp. 31-38, 1982.

Talbi, k. :”Evaluation of CO₂ Based Vapex Process”, MSc. Thesis, the University of Calgary, 2005.

Talbi, K., and Maini, B.B.: “Evaluation of CO₂ Based Vapex Process for The Recovery of Bitumen From Tar Sand Reservoirs”, SPE 84868, presented at the SPE International Improved Oil Recovery conference held in Kuala Lumpur, Malaysia, 20-21 October 2003.

Upreti, S.R., Lohi, A., Kapadia, R.A., and El-Haj, R.: “Vapor Extraction of Heavy Oil and Bitumen: A Review”, Energy & Fuels, Vol. 21, pp. 1562-1574, 2007.

Upreti, S.R., and Mehrotra, A.K.: “Diffusivity of CO₂, CH₄, C₂H₆ and N₂ in Athabasca Bitumen”, Can. J. Chem. Eng., Vol. 80, Issue. 1, pp. 116-125, 2002.

Upreti, S.R., and Mehrotra, A.K.: “Experimental Measurement of Gas Diffusivity in Bitumen: Results for Carbon Dioxide”, Ind. Eng. Chem. Res., Vol. 39, Issue. 4, pp. 1080-1087, 2000.

Virtual Materials Group, “VMGThermo Programmer Manual”, 2007, www.vitualmaterials.com/vmgthermo.

Walter, C., “The Evaluation of Viscosity Data”, Erdol und Teer, Vol. 7, pp. 382-384, 1931.

Wen, Y., Bryan, J. and Kantzas, A.: “Estimation of Diffusion Coefficient in Bitumen Solvent Mixtures as Derived From Low Field NMR Spectra”, J. Can. Petr. Techol., Vol. 44, No. 4, pp. 29-35, 2005.

- Yang, C., and Gu, Y.: “Diffusion Coefficient and Oil Swelling Factors of Carbon Dioxide, Methane, Ethane, Propane, and Their Mixtures in Heavy Oil”, *Fluid Phase Equilibria*, Vol. 243, pp. 64-73, 2006.
- Yarranton, H. W., Alboudwarej, H., and Jakher, R.: “Investigation of Asphaltene Association with Vapor Pressure Osmometry and Interfacial Tension Measurements”, *Ind. Eng. Chem. Res.*, Vol. 39, pp. 2916-2924, July 2000.
- Yarranton, H. W.: “ SARA’s Role in Oil Characterization: Should There be One?” *Petrophase 2009, 10th International Conference on Petroleum Phase Behavior and Fouling*, Rio de Janeiro, Brazil, June 14 – 19, 2009.
- Yarranton, H. W., and Satyro, M. A., “Expanded Fluid-Based Viscosity Correlation for Hydrocarbons”, *Ind. Eng. Chem. Res.*, Vol. 48, No. 7, pp. 3640-3648, 2009.
- Yaws, Carl L.: “Yaws' Handbook of Thermodynamic and Physical Properties of Chemical Compounds.”, Knovel, <http://www.knovel.com>, 2003.
- Yazdani, A., “Physical and Numerical Modeling of Permeability and Drainage Height Effects in Vapex”, PhD. Thesis, the University of Calgary, 2007.